AD NUMBER

AD877137

LIMITATION CHANGES

TO:

Approved for public release; distribution is unlimited.

FROM:

Distribution authorized to DoD only; Administrative/Operational Use; AUG 1970. Other requests shall be referred to Office of Naval Research, Arlington, VA 22203.

AUTHORITY

ONR ltr 29 Aug 1973

PROCEEDINGS OF A CONFERENCE ON HF RADIO PROPAGATION (June 1969)

by
EDWARD W. ERNST, Editor

RRL PUBLICATION NO. 375

August 1970

Technical Report No. 16
Contract N00014-67-A-0305-0002

Supported by
Office of Naval Research

RADIOLOCATION RESEARCH LABORATORY
DEPARTMENT OF ELECTRICAL ENGINEERING
ENGINEERING EXPERIMENT STATION
UNIVERSITY OF ILLINOIS
URBANA, ILLINOIS 61801

PROCEEDINGS OF A CONFERENCE ON HF RADIO PROPAGATION (June 1969)

by

Edward W. Ernst, Editor

RRL PUBLICATION NO. 375

August 1970

Technical Report No. 16

Contract N00014-67-A-0305-0002

Supported by:

Office of Naval Research

Radiolocation Research Laboratory
Department of Electrical Engineering
Engineering Experiment Station
University of Illinois
Urbana, Illinois

UILU-ENG-70-306

TABLE OF CONTENTS

Page

PART I

INTRODUCTION AND AGENDA

1. INTRODUCTION

The conference on "HF Radio Propagation" was held at the Allerton House Conference Center, Monticello, Illinois, on June 2, 3, and 4, 1969. The conference was principally concerned with the propagation of HF radio signals and the effect of the characteristics of the propagation on RDF systems. Planning and operation of the conference were undertaken by the Radiolocation Research Laboratory of the Department of Electrical Engineering, University of Illinois at Urbana/Champaign. The Conference was sponsored by the Office of Naval Research.

The objectives for the conference may be summarized briefly as follows:

1. To assist in delineating those areas of investigation and development which should be emphasized for the future, if significant improvements in the operation of RDF Systems are to be expected.
2. To examine the present status of RDF Systems.
3. To examine the limitations of these RDF Systems which are a consequence of propagation characteristics.
4. To examine the understanding of the ionosphere and HF radio propagation which, it is believed, can contribute to a reduction of the limitations noted in (2) above.

Attendance at the conference was by invitation and included representatives from several agencies of the Department of Defense, ESSA, research organizations conducting investigations in the area included in the conference, and the University of Illinois.

The agenda of presentations and discussion are given on the pages following this introduction. Those presentations for which papers are included in this Proceedings are indicated by two asterisks (**) preceding the title of the paper.

AGENDA

CONFERENCE ON

HF RADIO PROPAGATION

June 2, 3, 4, 1969

Allerton House - Monticello, Illinois

MONDAY, JUNE 2

BREAKFAST	8:00 - 9:00 a.m.
CONFERENCE OPENING	9:00 a.m.
SESSION I. 9:00-10:30 a.m.	Introduction: Survey of RDF and Propagation Research at the University of Illinois. Chairman, E. W. Ernst. "Early History of RDF Efforts at the University of Illinois." E. C. Jordan. **"Recent and Current Status of RDF of the University of Illinois." A. D. Bailey.
COFFEE BREAK	10:30 - 10:45 a.m.
SESSION II. 10:45 a.m. - 12:15 p.m.	Direction of Arrival Studies over a Medium Range Path (452 KM). Chairman, A. D. Bailey. **"HF Direction of Arrival Studies over a Medium Range Path (452 KM)." A. D. Bailey. **"Short and Medium Range Results with a DF Interferometer." P. E. Martin, R. B. Mathews, C. Dodge.
LUNCHEON	12:15 - 1:15 p.m.
SESSION III. 1:30-3:00 p.m.	Direction of Arrival Studies on a Long Range Path. Chairman, A. D. Bailey. **"Direction of Arrival Studies on a Long Path (Summary)." A. D. Bailey. **"The Coordinated HF Propagation Experiment." L. H. Tveten.
COFFEE BREAK	3:00 - 3:20 p.m.

SESSION IV.	Propagation Studies Using Direction of Arrival Data. Chairman, N. N. Rao.
3:20-4:50 p.m.	**"Ray Tracing Simulation of Ionospheric Effects in High Frequency Radiolocation." N. N. Rao.
SOCIAL HOUR	5:00 - 6:00 p.m.
DINNER	6:00 - 7:00 p.m.
VISIT TO THE U. OF I. FIELD STATIONS OR OTHER ACTIVITIES	7:00 - 10:00 p.m.

TUESDAY, JUNE 3

BREAKFAST	7:30 - 8:30 a.m.
SESSION V.	RDF Research by University of Illinois Graduate Students. Chairman, W. R. Flowers.
8:30-10:00 a.m.	"Auroral Backscatter Studies." F. Fahlsing
	**"Short Range High Angle Studies." E. A. Walton.
	**"Aperture Size Effects in a HF Interferometer RDF System " C. R. Talbott.
	"Tracking Mode, CDAA RDF System." H. M. Rice.
COFFEE BREAK	10:00 - 10:30 a. m.
SESSION VI.	RDF Propagation Research. Chairman, A. D. Bailey.
10:30-12:00 noon	**"Interferometer Instrumentation for Propagation Research." D. N. Travers, W. M. Sherill, J. D. Moore.
	**"The Use of Reflectrix Techniques in the Analysis of FM/CW Oblique Ionograms." M. E. Coffey, R. P. McConville (presented by S. M. Bennett).
	**"Review of Small Aperture Investigations at Georgia Tech." H. Jenkins, R. W. Moss.
	"Automatic Radio Phasemeter Technique and High Frequency Direction Finder Concepts." R. Russell.
LUNCHEON	12:00 - 1:00 p.m.
TREASURE HUNT	12:00 - 2:00 p.m.

SESSION VII.	Digital Methods for RDF. Chairman, E. W. Ernst.
2:00-3:30 p.m.	**"Digital Methods for Radio Direction Finding." E. W. Ernst
	**"Digital DF Applications." W. M. Sherrill, T. C. Green, R. Lorenz.
COFFEE BREAK	3:30 - 3:45 p.m.
SESSION VIII.	RDF Systems and Instrumentation for Propagation Research. Chairman, E. W. Ernst.
3:45-5:15 p.m.	**"Elevation Angle Measurements on the University of Illinois Wullenweber Antenna Array." L. J. Miller.
	**"Oblique Incidence Ionosonde Amplitude Data." W. W. Wood.
	**"Wavefront Testing and its Applications." G. A. Smith.
	"Azimuthal Noise Measurements." W. Flowers.
	"System Testing and Maintenance Procedures." W. W. Wood.
SOCIAL HOUR	5:15 - 6:00 p.m.
DINNER	6:00 - 7:00 p.m.
VISIT TO U. OF I. FIELD STATIONS OR OTHER ACTIVITIES	7:00 - 10:00 p.m.

WEDNESDAY, JUNE 4

BREAKFAST	7:30 - 8:30 a.m.
SESSION IX.	The Shape of the Next Generation of RDF.
8:30-10:00 a.m.	
COFFEE BREAK	10:00 - 10:30 a.m.
SESSION X.	Future Directions for RDF Research.
10:30-12:00	
LUNCHEON	12:00 - 1:00 p.m.
CONFERENCE ADJOURNMENT	1:00 p.m.

PART II

PAPERS PRESENTED

A. D. Bailey

Department of Electrical Engineering
University of Illinois, Urbana, Illinois

RECENT AND CURRENT STATUS OF RDF OF THE UNIVERSITY OF ILLINOIS

This is the third conference on RDF to be held at the Allerton House. The first conference was held 2-3-4 June 1959, exactly ten years ago. The second was held 26-29 May 1964, five years ago.

I hope this can be continued and quite possibly we will be meeting together again on or about 3-5 June 1974. Dr. Jordan opened each of the previous conferences and he is hereby respectfully requested to start planning his opening remarks for the next one in five years.

Our emphasis at this meeting is on the use of the RDF systems that we have developed at the University of Illinois in the HF Directional Propagation Research. Such studies are of academic and scientific interest to our University and its Department of Electrical Engineering. The results of these studies are often of interest to the sponsors of the program in RDF at the University. We hope that this arrangement may continue. The research efforts are currently sponsored by ONR and USAECOM. There are two or three other agencies within the DOD who supplement the basic ONR contributions.

The previous conferences were concerned primarily with the work done at the University. In this conference we will hear several papers prepared by other research groups with whom we have cooperated in one way or another. This is as it should be; in the end it has to be some kind of a team effort. Any directional propagation experiment has to have at least two participants, one at each end of the path. Many of the tasks

appear to us to be as enormous as "seeing to the top of Paul Bunyan's upside down mountain," and, as in that case, one needs cooperation.

There will be two visiting periods to the field stations. We will not have much to say about the details of the system per se. Many of your technical questions on our systems can be answered at the time of the field station visits. Tonight the CDAA and the Interferometer sites are open for "knob twiddling"-type inspections. Tomorrow night we will have a propagation experiment going and one can hopefully see real live system operation and, if he wishes, make a comparison of the two systems.

Our program schedule outlines pretty well what we hope to cover. I'm particularly interested in what other speakers have to say so I'll get on to what I'm scheduled to say and let the others have their chance. Accordingly, I'd like to begin talking about the second session material now and get as much of this covered as possible between now and the coffee break.

A. D. BAILEY

Department of Electrical Engineering
University of Illinois, Urbana, Illinois

HF DIRECTION OF ARRIVAL STUDIES OVER A MEDIUM RANGE PATH (452 KM)

1. PHILOSOPHY

DISTINGUISHED GUESTS, COLLEAGUES, CO-WORKERS, STUDENTS AND FRIENDS.

Complementary to the statement of the four general objectives which was carried in the letter of announcement, I would like to add a statement to the effect that, "There is a time for rethinking and that time is now!" I hope that each of us has come to this conference in this spirit. Rethinking is so necessary at this time when Universities and Institutes for Research are looking for ways and means to continue support of our continuing search for the truth and the advancement of the state of the art and science in our disciplines.

Before taking up the subject of this particular session, it is necessary that we review a few definitions and concepts which will provide a basis for arguments and later decisions which we might reach.

Certainly each of us has at some time or another thought about the "two-point problem." Thus, given two separated points A and B, or T and R, or X and Y, etc., one might ask the following:

How to get from A to B.

How to talk between A and B.

How to deliver something from A to B.

How to exploit B from A.

How to destroy B from A.

How to deny to B certain benefits at A.

In Figure 1 I have imbedded points A and B in a coordinate system. The displacement vector $\vec{AB}$ is a function of three variables such as x, y, z or r, θ, ϕ. Thus, a triplet of values is needed to define the position of B relative to A. These could be the range $|AB|$ and the two angles $\angle_{AB}$ and $\angle_{AB}$, respectively.

We will stress that in RDF/RPL disciplines at HF, range and the two angles are needed for completeness.

II. DEFINITION OF SOME GENERAL TERMS

Turning then to a practical aspect of HF directional propagations studies, we next review some definitions as follows:

DEFINITIONS

DIRECTION FINDER -- "A direction finder is a radio receiving device which permits determination of the line of travel of radio waves as received." American Standard Definitions of Electrical Terms. (AIEE).

SENSE FINDER -- "A sense finder is that portion of a direction finder which permits determination of direction without one hundred-eighty degree ambiguity." ASDET/AIEE.

RADIO DIRECTION FINDER -- "A radio direction finder may be defined as a device for determining the direction of arrival of radio frequency energy. It is a receiving system and operates on the energy that it extracts from the passing radio waves." - VHF Techniques, RRL Staff of Harvard University.

NOTES: (1) The word bearing does not appear.

(2) The words direction of arrival as received do appear.

ABOUT THAT FAR

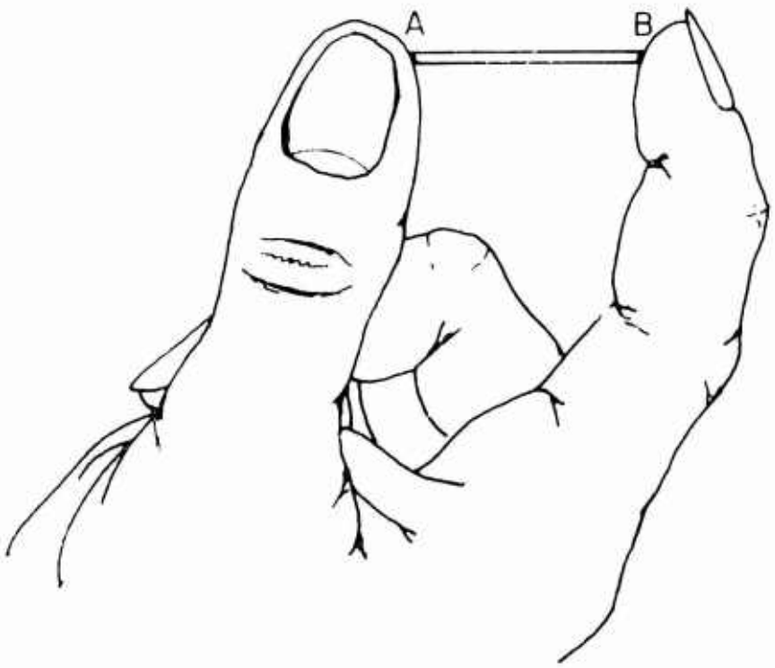

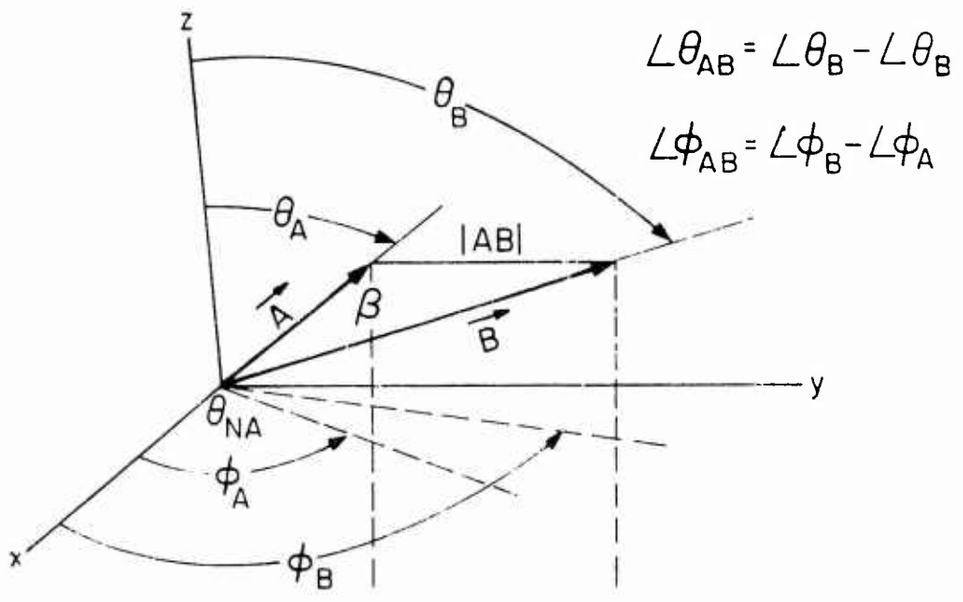

Figure 1 The Two-Point Problem.

(3) Such systems could be active in the sense of the definitions, although at first reading one might infer that RDF systems are passive.

(4) Direction of arrival has two components, e.g., θ and ϕ.

Figure 2 is one representation of a radio direction finder system in functional block form. An observer is necessary to complete the process. It may be a human being or a computer. In any event the human being is still important -- he is the master -- he is the truth seeker.

We next explore briefly some of the applications of the device we have defined.

A radio direction finder has application in at least the following fields:

1. Navigational Aids.
2. Military Surveillance and Countermeasures.
3. Location of Sources of Radio Interference.
4. Directional Radio Wave Propagation Studies.
5. Remote Environmental Sensing, e.g., OTH RADAR at HF.

Next, we should note that the first three are of vital concern to "management." But this latter disciplinary group wants the bearing of the signal and not much else! Hence, we now need more definitions, to wit:

BEARING -- "The situation or direction of one point with respect to another or to the points of a compass."

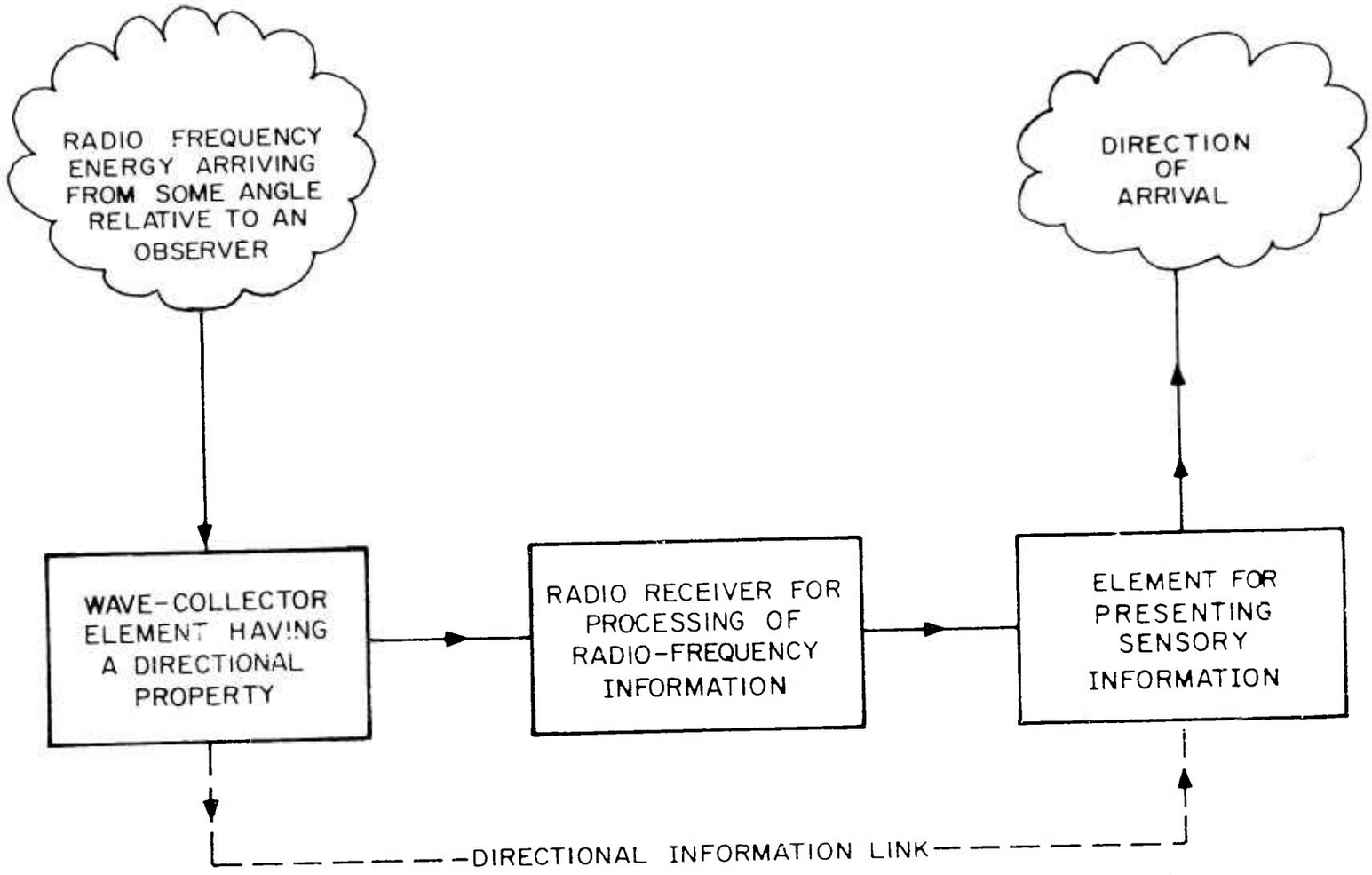

Figure 2. One Functional Classification of a Radio Direction Finder.

GCB -- The great circle bearing of something as it applies to a spherical earth is tacitly understood . It's what the managers want

Our sponsors are often very practical people who are willing to support direction of arrival studies but they really want bearings! In this connection one may recall the classic story of "The Blind Men and the Elephants." The meaning of the word elephant had different sensory interpretations to six different men depending upon where the individual touched the elephant.

Managers are not blind; of course, they need and want the GCB: they buy devices with this need in mind in order to measure the bearing, but the very best that the device can ever do is to measure an apparent angle of arrival as received. It is up to people like ourselves to resolve the dilemma. Also, the bearing can be very elusive in any case other than controlled propagation experiments and cooperative transmitters. When one thinks it through, the bearing of a noncooperative radio source can only be known in the sense of being most probable.

A ship at sea, an airplane in flight, an automobile heading west on Highway 66 are examples of situations where the exact location at any instant is hard to come by, particularly when there is lack of cooperation.

Of course, our motivation here is to find better ways for inferring what is the best estimate of GCB given a set of measurements of angle of arrival as received. Again, the point of all of this was to emphasize the need for more careful use of the word bearing.

We need still more definitions and I next need to talk about RANGE.

It appears necessary, to me, to delineate certain characteristic ranges in radio position finding work. These will be "ball parks" as opposed to the hard, fast, and rigorous.

For reasons that will become evident, it appears to me that one should delineate at least three ranges termed, SHORT, INTERMEDIATE, and LONG. I propose to do this by joint use of the Earth-Ionosphere geometry shown in Figure 3.

First off, we note certain given information;

next,we add two lines to delineate the three sectors;

we discuss the properties of each sector;

we indicate the antenna element types that are appropriate to each sector;

the surface-wave sector is interesting but not very meaningful in the sense of RANGE.

Finally, we stress clustering of rays at extremely high or low angles.

A significant contribution to bearing deviation at the shorter ranges is the effect of lateral and/or longitudinal displacement of the apparent reflection point in the ionosphere. For example, assume that the reflection point is laterally displaced by 5 kilometers. The apparent deviation in azimuthal angle of arrival which occurs as a function of range appears in Table 1.

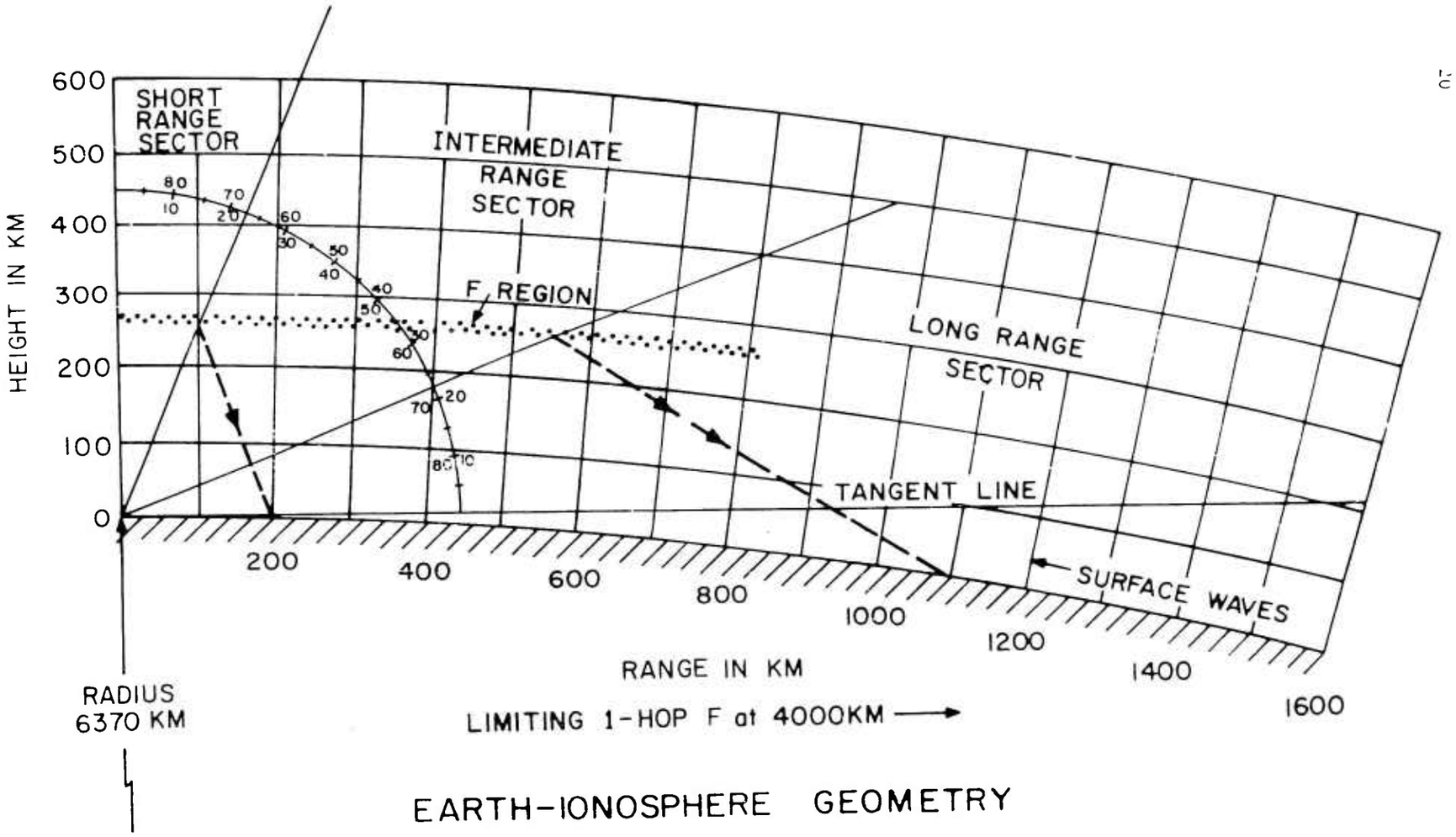

EARTH-IONOSPHERE GEOMETRY

Figure 3. Handout for Active Participation.

TABLE 1

DEVIATION OF ANGLE OF AZIMUTHAL ARRIVAL AS A FUNCTION OF RANGE FOR 5 KILOMETER LATERAL DISPLACEMENT OF REFLECTION POINT.

RANGE (KM)	HALF-RANGE (KM)	DEVIATION
800	400	0.73°
400	200	1.42°
200	100	2.86°
100	50	5.7°
50	25	11.3°
20	10	26.5°
10	5	45°
0	0	90°
0	-5	135°

Again, the significance of RANGE is pointed up by the tabular data. Fortunately, one can improve on this situation by making two corrections. We will see two characteristic deviations of data in later displays. One is due to diurnal and seasonal effects and we believe that it can be corrected by the use of the predictive data supplied in advance by ESSA, for example.

The other characteristic deviation is due to random effective tilting mechanisms but with a quasi-period of approximately 20 minutes. We believe that one can correct for these by using time coincident measurements made upon known sources having frequencies and position

locations close to those of the unknown. Thus, we use additional independent measurements which should reduce the uncertainty. We close this introductory discussion with Figure 4, which illustrates that for very short ground ranges, the slant range line of travel can be long but almost constant and not much different, less than 5 percent from the effective height shown on a vertical incidence ionosonde.

III. DESCRIPTION OF AN INTERMEDIATE RANGE EXPERIMENT

The geometry for the 452 kilometer path E-W directional propagation experiment is shown in Figure 5. It was an example of an intermediate or medium range path. The important subsystem components were the pulsed transmitter located at OSU Columbus, Ohio; the midpath v.i. ionosonde just North of Anderson, Indiana; the triple interferometer receiving site at the Monticello Road Field Station, S.W. of Savoy, Illinois; and the receiving end v.i. ionosonde at the Bondville Road Field Station 3.5 miles N.W. of the receiving site.

The transmitted signals were cosine squared 100 μ sec pulses having a repetition rate of approximately 200 pps. Because of the pulsed nature of the signals, the several gross propagation modes could be identified, separated, and the angle of arrival of each such mode could be determined from the differential phase data obtained with any two of the three interferometers.

All of the reduced data obtained over the 18-month period of observation are contained in an ATLAS.[1]

---

1. A Study of High Frequency Directional Propagation Over a 450 Kilometer East-to-West Path, R.F. Donnelly, D.G. Detert, A.D. Bailey, RRL Publication No. 254, November 1965.

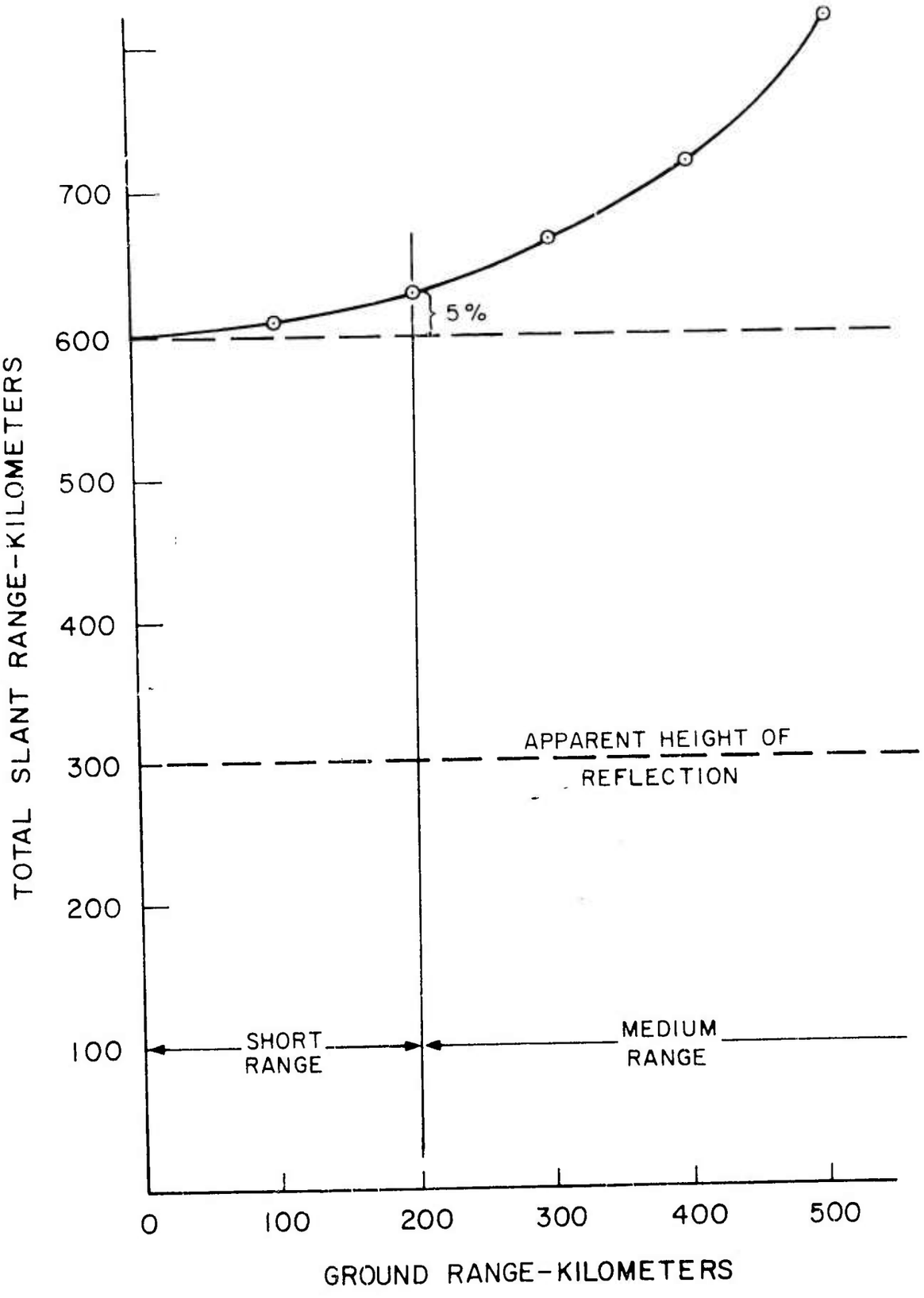

Figure 4. Slant Range vs. Ground Range in the Neighborhood of a HF Receiver.

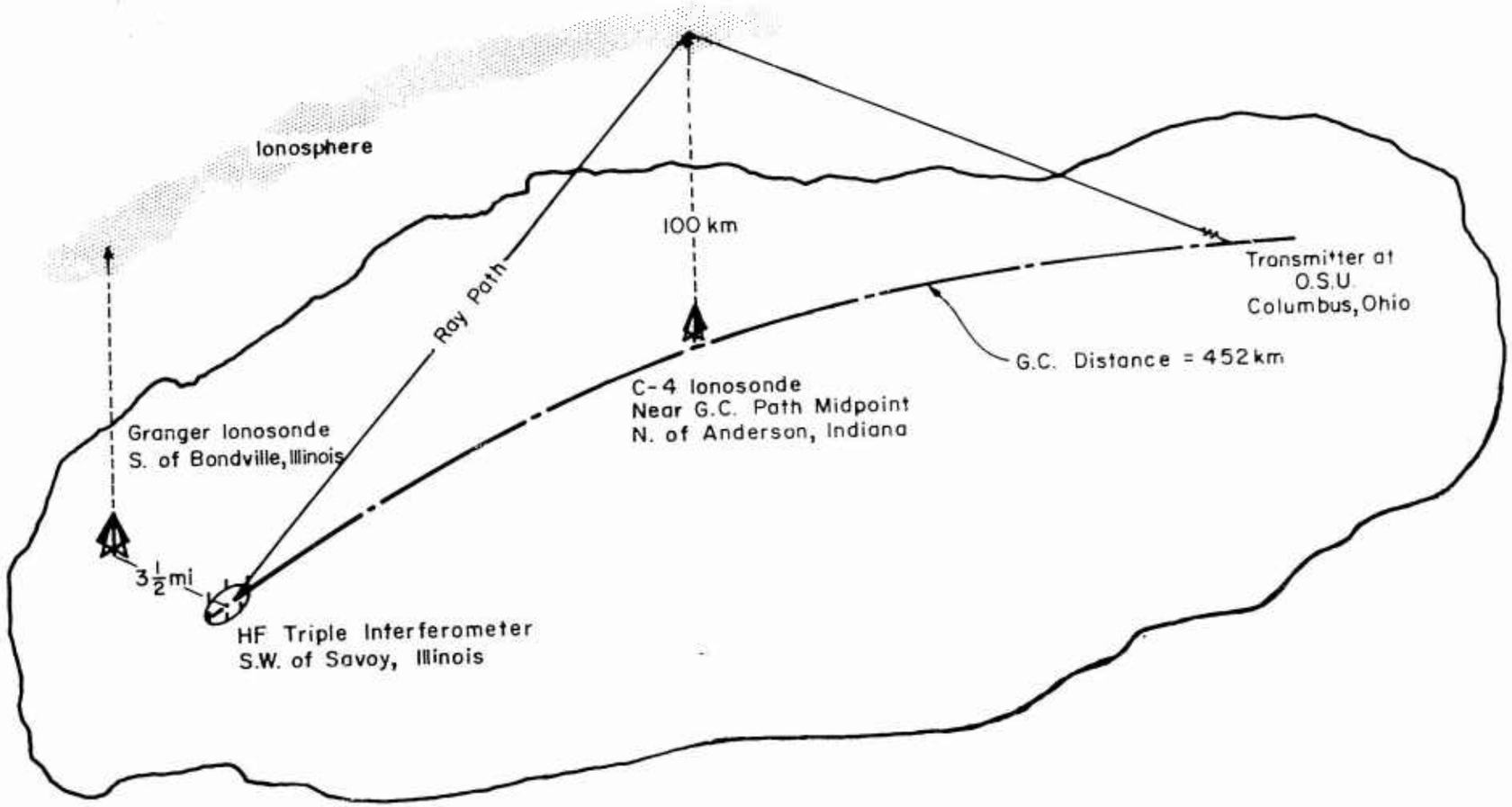

Figure 5. Pertinent to the Geometry of the Columbus-Urbana Directional Propagation Experiment.

I should recognize the contributions of several people. Messrs. Lyle Rocke, Chris McClurg and Gerald Smith developed and operated the systems. Graduate Students Hubert Grush, Richard Donnelly and David Detert did the data reduction. There were many others who also served.

Figures 6, 7, and 8 are examples of the reduced data. In each figure one sees five-time series of data; these are:

a) Azimuthal angle of arrival

b) Incidence angle of arrival as measured by one pair of interferometers (0-120°)

c) Incidence angle of arrival as measured by a second pair of interferometers (0-240°)

d) Predicted incidence angle of arrival obtained from the midpath ionosonde data

e) Predicted incidence angle of arrival obtained from receiving endpoint ionosonde data.

These data permit one to make assessments of the performance of the system as a radiolocation device.

IV. SUMMARY OF THE FINDINGS

There were several important findings from these data that may be listed. The attempts at radio range finding often came out short. Mr. Winkelmann showed that by the use of simple ray tracings using the so-called Booker-Seaton method and taking into account both the underlying E-region and the F-regions he could increase the range.

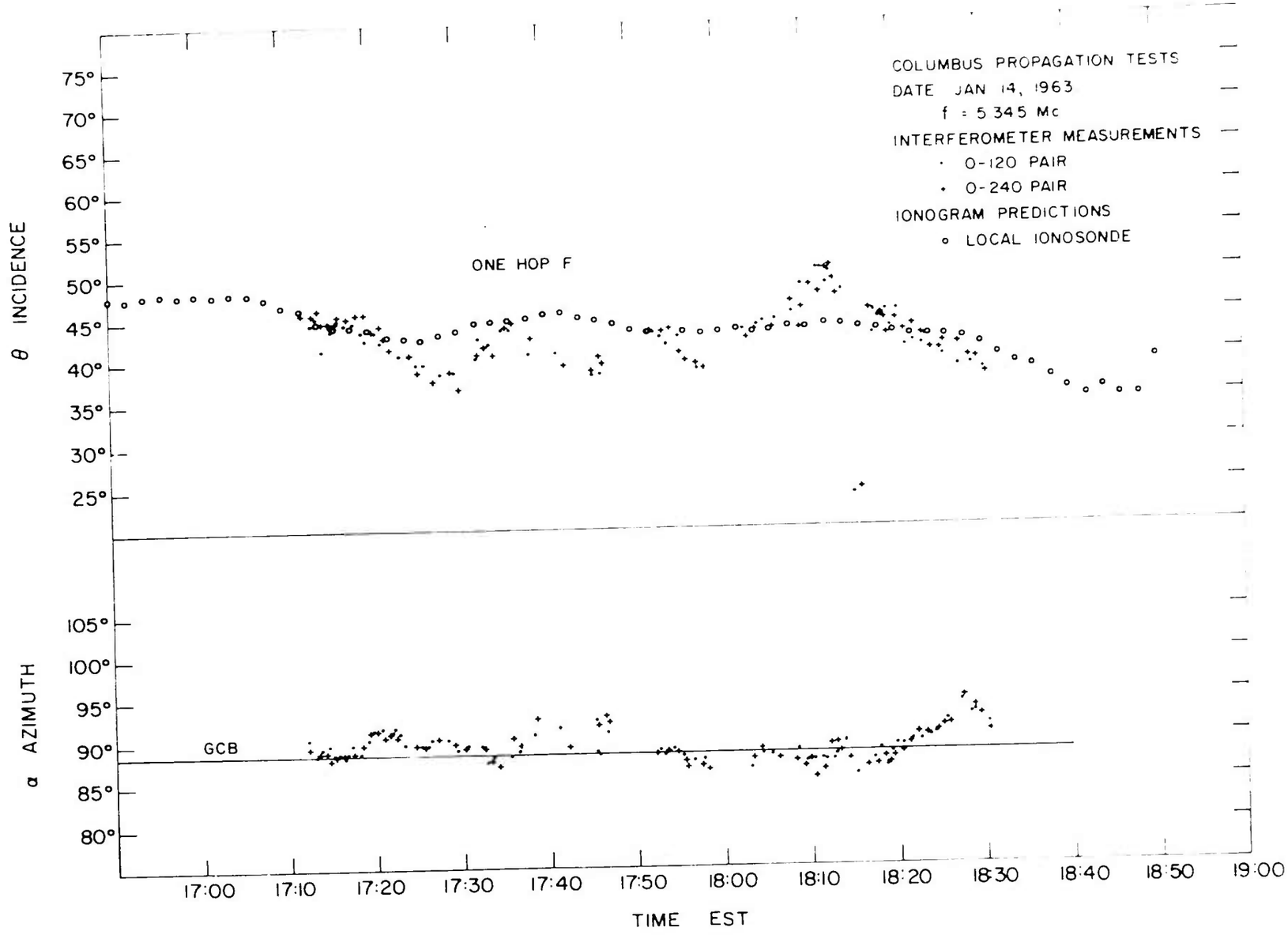

Figure 6. Columbus Propagation Tests, January 14, 1963, 17:00 - 19:00 EST.

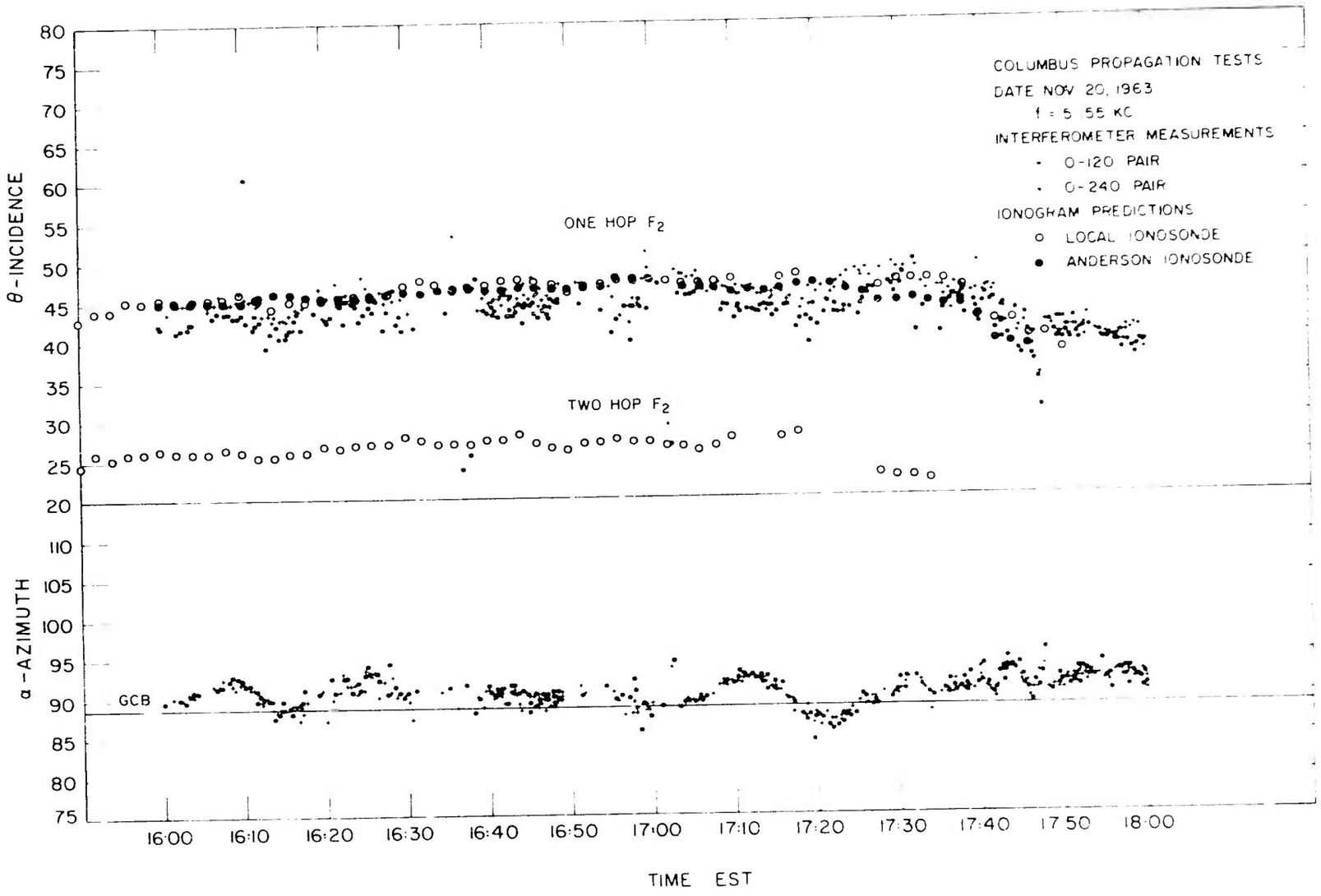

Figure 7. Columbus Propagation Tests, November 20, 1963, 16:00 - 18:00 EST.

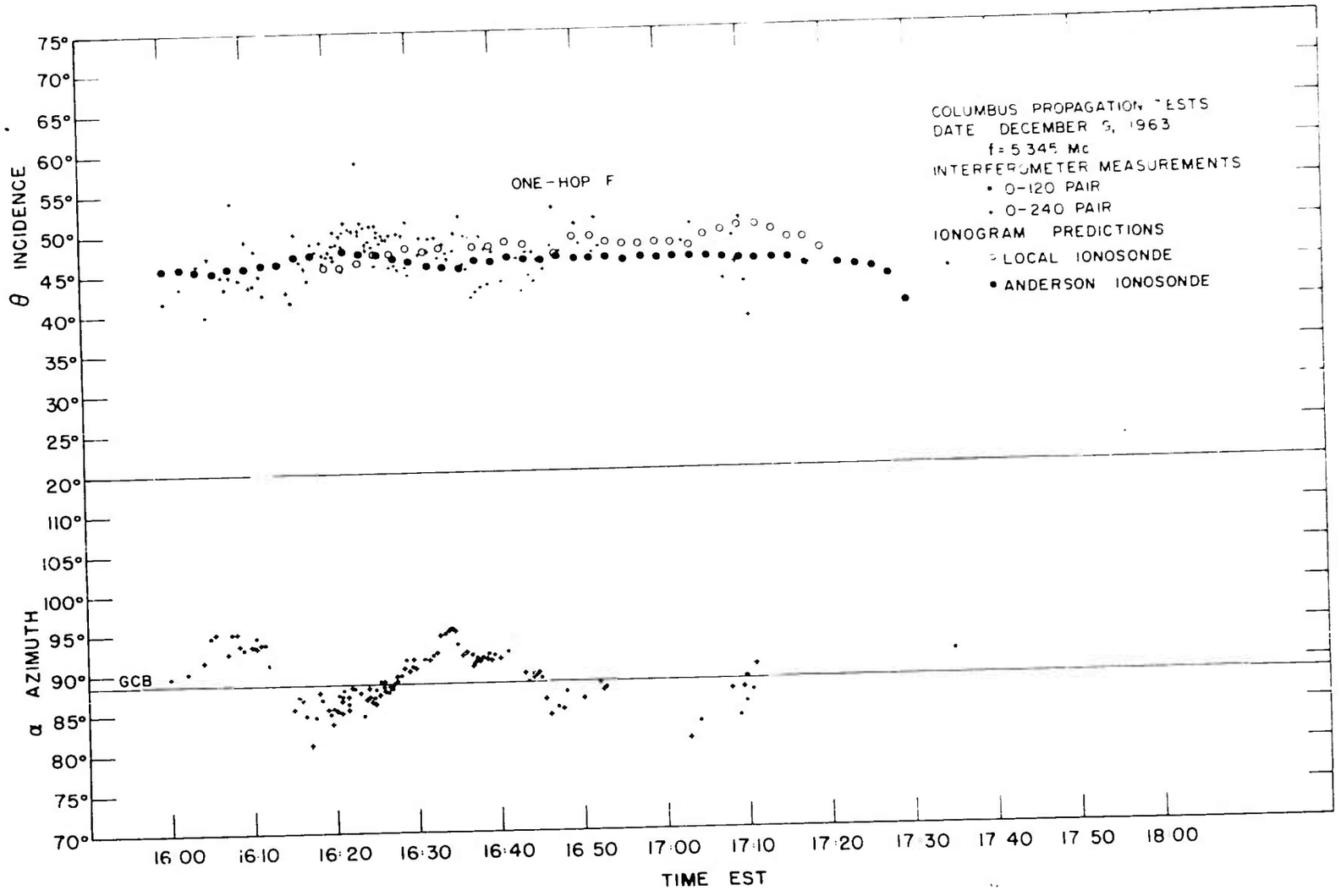

Figure 8. Columbus Propagation Tests, December 9, 1963, 16:00 - 18:00 EST.

Mr. David Detert investigated the use of models of travelling disturbances to explain the variations in incidence angle of arrival He achieved very consistent results with his models

A. D. Bailey showed that there was a very strong correlation between slight but noticeable changes in the effective heights of the midpath ionograms and the lateral deviations in the indicated azimuthal angle of arrival from GCb. This result made a strong impression in the mind of having an ionosonde at the midpoint of the path in any controlled study.

The studies pointed out that the so-called random lateral deviation error could be controlled after all. There are ways and means of getting a handle on it.

Experience with the system proved out its potential promise as a versatile radio direction finding/radio position locating device.

The separation of the modes in the vertical plane was very evident although the azimuthal separation was small. This means that the wave interference fading effects have broader interpretations and an alternate method for determining range now appears feasible.

The lateral deviation error was in evidence in all data at all times of the experiment.

V. SIGNIFICANT CONCLUSIONS

The significant conclusion, in my mind, is the fact that the triple interferometer system as instrumented, for example, at the University of Illinois has proven to be a powerful research tool as well as a practical, true radio direction finder. It is a wide-aperture system measuring differential phase over a large base line and it determines both angles of arrival. Our contribution is not unique; of course, several other investigators have used the interferometer system at HF with similar success.

Of special interest at this time is the article by J. W. Wright of ESSA entitled "Some Current Developments in Radio Systems for Sounding Ionospheric Structure and Motions," Proc IEEE V57, N4, p 481. He discusses a KINESONDE which permits one to measure additional data from a v.i. ionosonde. It appears to me that this is in essence, or can be considered to be, an application of interferometer principles and appears to be one partial solution to an urgent problem that we are attempting to solve here at the radiolocation research laboratory.

P. E. MARTIN, R. B. MATHEWS, C. DODGE

Southwest Research Institute, San Antonio, Texas

SHORT AND MEDIUM RANGE RESULTS WITH A DF INTERFEROMETER

The primary objective of this paper is to describe the angle of arrival performance of a tactical HF phase interferometer using an on-line digital computer to provide azimuth and elevation angle data from signals originating from medium and short range targets.

SYSTEM DESCRIPTION

The interferometer array consists of five elements in an orthogonal arrangement shown in Figure 1. Thirteen meter baselines at the apex of the L-array are used to resolve phase ambiguities on its colinear long baseline of 150 meters. Because the interferometer was required to operate on steeply downcoming signals that include arrival at or near the zenith, the antenna elements are quadrature-summed crossed vertical loops that provide hemispherical response to all polarizations.

A block diagram of the system is also shown in Figure 1. Antenna outputs are each fed to a twin channel phase and gain matched receiver. The relative phase between the IF outputs is measured by a 360° phasemeter. The antenna located at the apex of the array is always connected to one channel and is thus used as a phase reference. The remaining inputs are sequenced through the second channel and the signals compared in phase to the reference. The phasemeter output is multiplexed into the on-line digital computer through an A/D converter along with instructions as to which array baseline is being sampled.

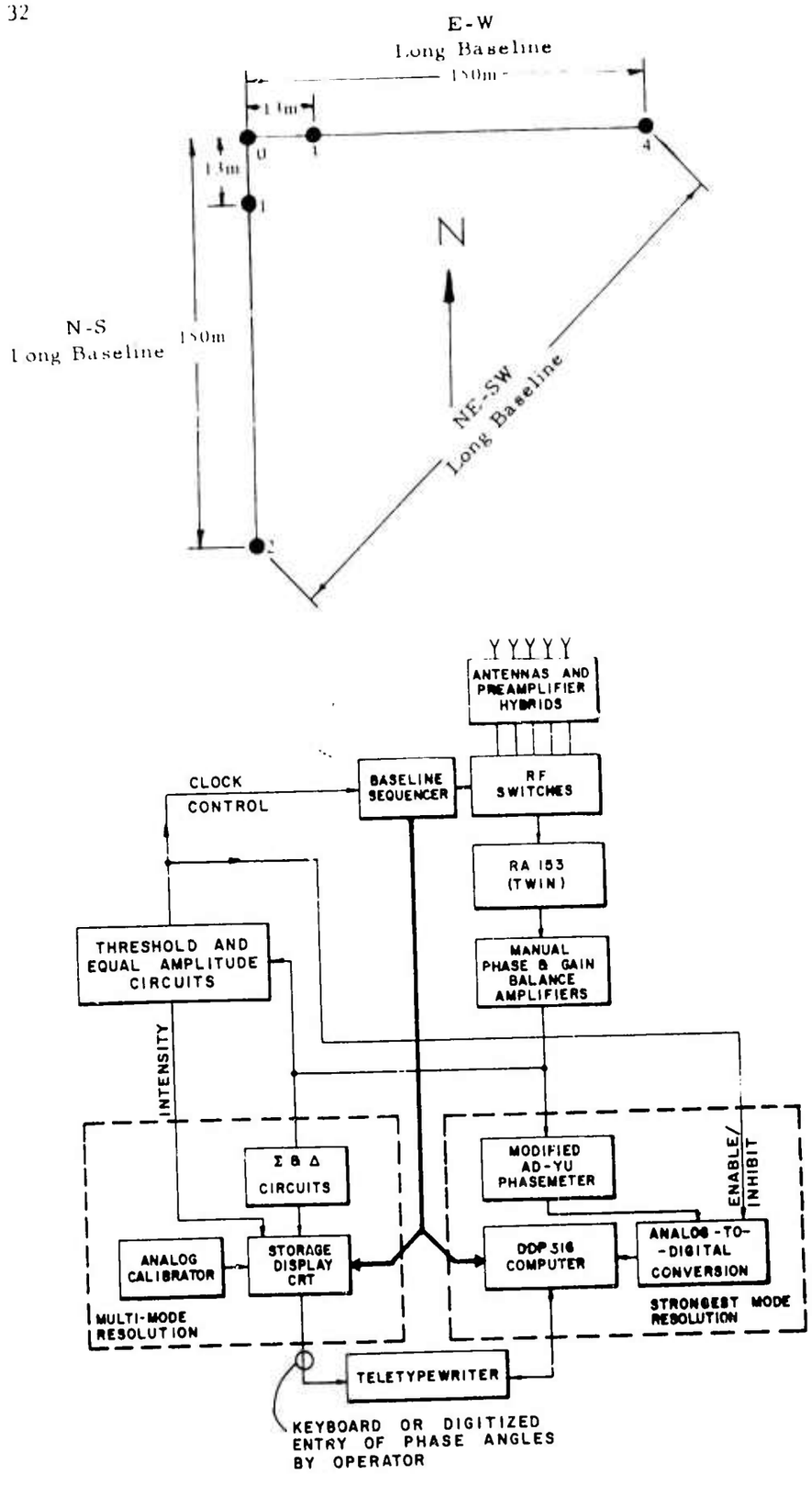

Figure 1. HF Interferometer System.

Enabling logic to sequentially connect the four antennas into the second channel is controlled by a signal analyzer that edits the incoming signal amplitudes to assure they exceed a predetermined threshold level and to assure that the ratio of signal amplitudes in the two channels does not deviate more than a preset amount, say, 1 db (analogous to the so-called plane wave test). The editor also inhibits A/D conversion if either signal input fails to meet threshold or equal amplitude criteri .

In order to save data for off-line analysis, the phase angle data sets are dumped to paper tape (only 150 sets can now be stored in the 5lo's 8K memory due to programming requirements). The results to be described will be from off-line processing. At present, it requires about 100 milliseconds to acquire and process a frame of data; that is, the four baseline phase angles to compute the angle of arrival.

The digital system has been operated on-line for approximately one year; however, the circuits providing threshold and plane wave editing were only recently installed. The results herein were obtained in April and May 1969 and include data before and after the operation of the data editor for medium and short range targets. Two medium range targets are located near Houston, Texas: KLC transmitting A-1 at 8.666 MHz and KA2XTZ transmitting continuous carrier at 8.00 MHz. The transmitters are about 15 miles apart (bearing and range are noted on the histograms).

The remaining three targets are short range: New Berlin, Texas located at 89° azimuth with a range of 48 km; Comfort, 64 km on an

azimuth of 347°; and Bandera, 55 km on an azimuth of 306°. Transmissions were at 8.5 and 6.3 MHz with modulation either A-0 or A-1. Transmitting antennas were resonant 1/2 wave length horizontal dipoles oriented to minimize ground wave. A linear FM CW ionosonde transmitter was colocated at each of the short range targets. The ionosonde receiver was located at the DF site.

II. RESULTS

The capability of the system when the propagating medium is stable is shown in Figure 2. The target is KLC at 346 km range. Mean deviation is 0.18° while the standard deviation is 0.37° for a sample size of 150 frames taken over a period of 2-3 minutes. Subsequent runs show the same stability. Near vertical incidence ionograms predicted E-layer propagation well beyond 8.0 MHz for the path in early afternoon. The elevation histogram is shown in Figure 3. The mean elevation is 60.4° with a standard deviation of 0.27°. Note that we have been using mean deviation and standard deviation very confidently in these examples. However, as suggested later, these normal statistical parameters must be used with care when short range propagation is subjected to ionospheric tilts or other path disturbances.

Figure 4 shows the azimuth histogram for the 55 km target at Bandera at 8.5 MHz about 25 minutes later than the KLC data above. The mean deviation here is 4.19° with a standard deviation of 3.56°. Only threshold editing was used, the plane wave option was off. The distribution appears normal. The elevation histogram in Figure 5 shows a mean elevation angle of 86.13° with a small variance. About 8 minutes

FIGURE 2

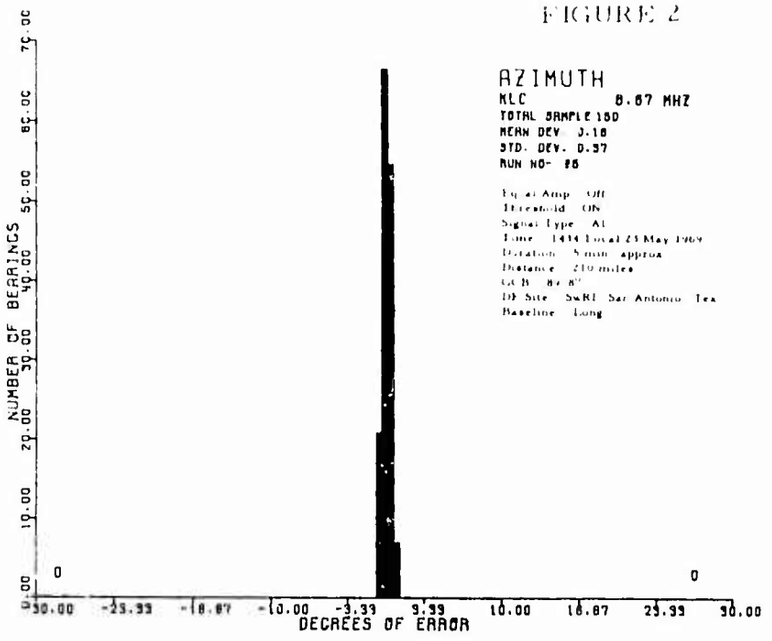

FIGURE 3

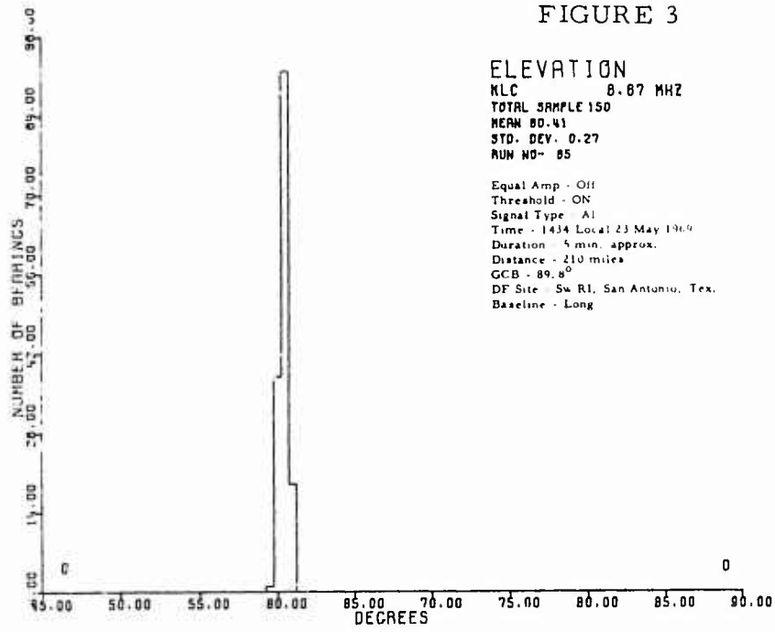

FIGURE 4

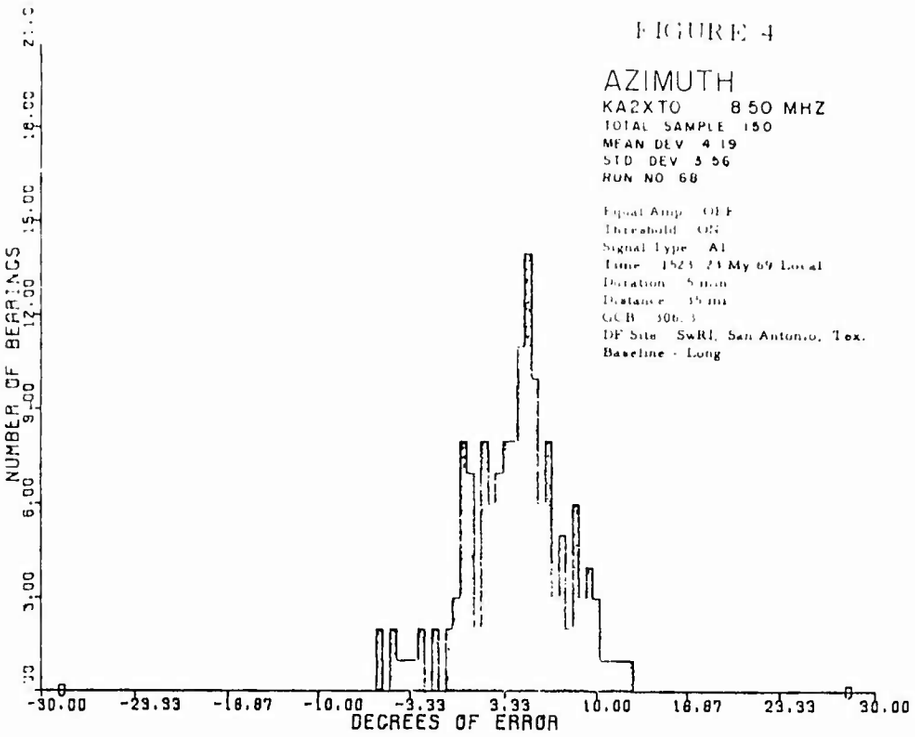

FIGURE 5

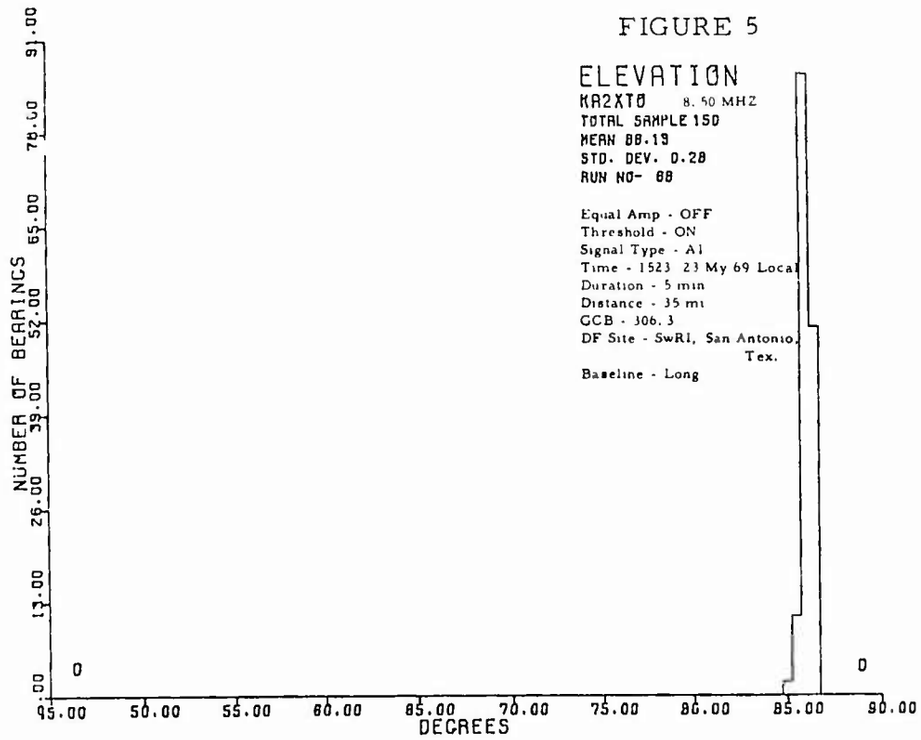

prior to this data set, a similar run was made using the plane wave test option as well as the threshold so that data were taken only when the signal amplitudes were equal at the spaced antenna. Figure 6 shows distinct separation of what appears to be two modes. Although the data sample is the same length and of approximately the same time duration as the last set, an overall mean and standard deviation do not adequately describe what we see here. (For the record, the calculated mean was 0.4° with a standard deviation of 5.5°.) The important characteristic is what appears to be the mode separation. The elevation histogram in Figure 7 shows very little difference from the last sample although the mean elevation is now 84.8° rather than 86.1° which can be significant for target location by vertical triangulation.

The next data sets show performance characteristics for the two medium range targets near 350 km and the short range 64 km target at Comfort. All data were obtained on the evening of 13 May 1969 between 9:00 and 10:30 PM CDT. Only threshold editing was used since the plane wave test option was not instrumented at this time.

The azimuth histogram for KLC Houston at 346 km at 2120 hours is shown in Figure 8. As before, the sample sizes are each 150 frames taken in a 3-5 minute period. As expected, there is more spread in night time data than the earlier example. The mean deviation here is -0.25° with a standard deviation of 1.25°. (In the first series, Figure 4, the mean was +0.18 while the standard deviation was 0.37°.) The elevation data in Figure 9 are uneventful except that it is interesting that the elevation has lowered from the earlier value of 60° to 53°, which suggests that the afternoon propagation was probably two hop E-.

FIGURE 6

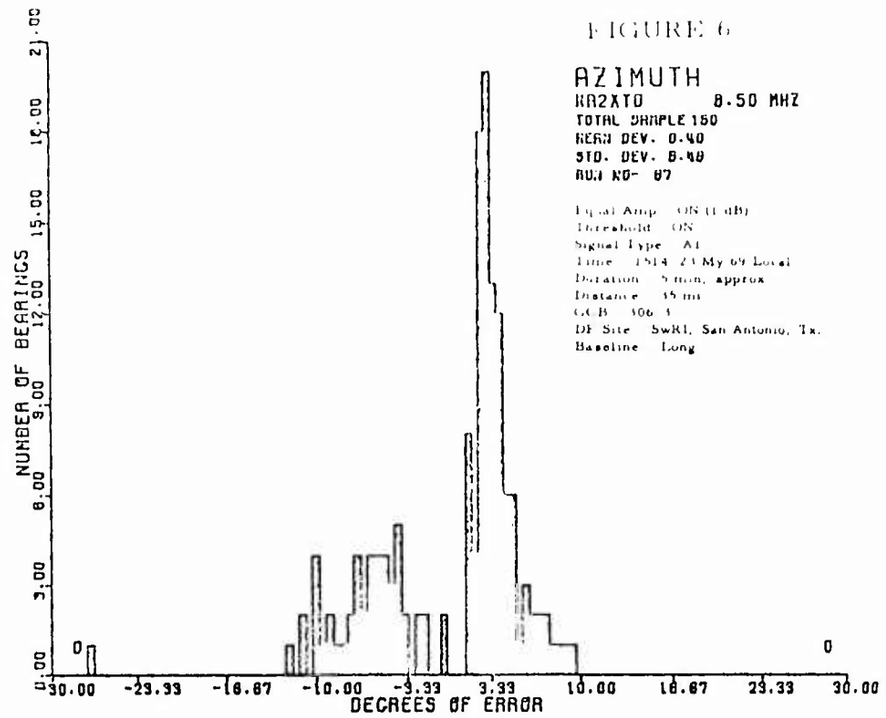

FIGURE 7

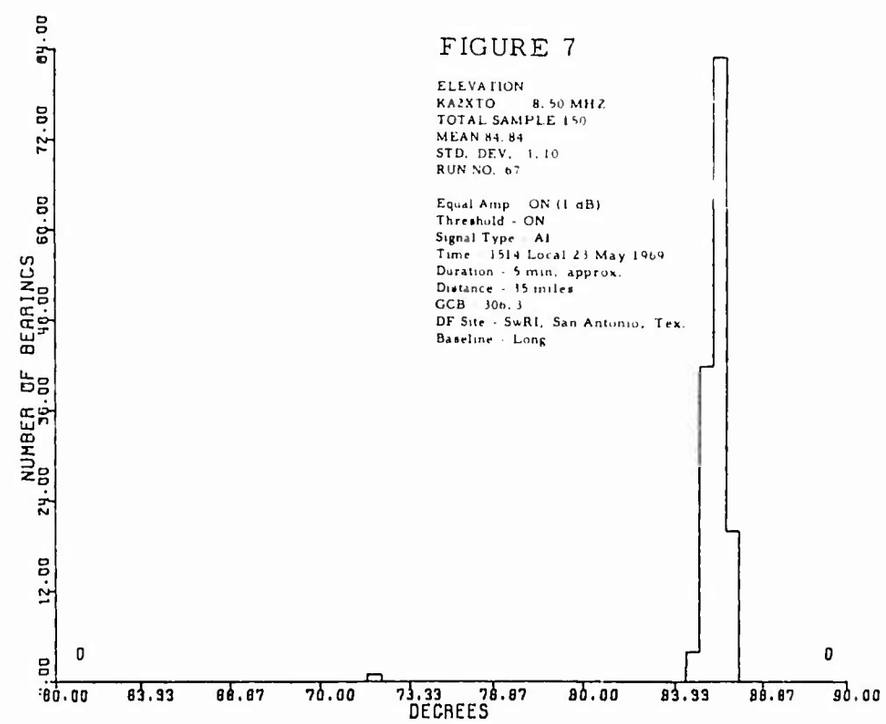

FIGURE 8

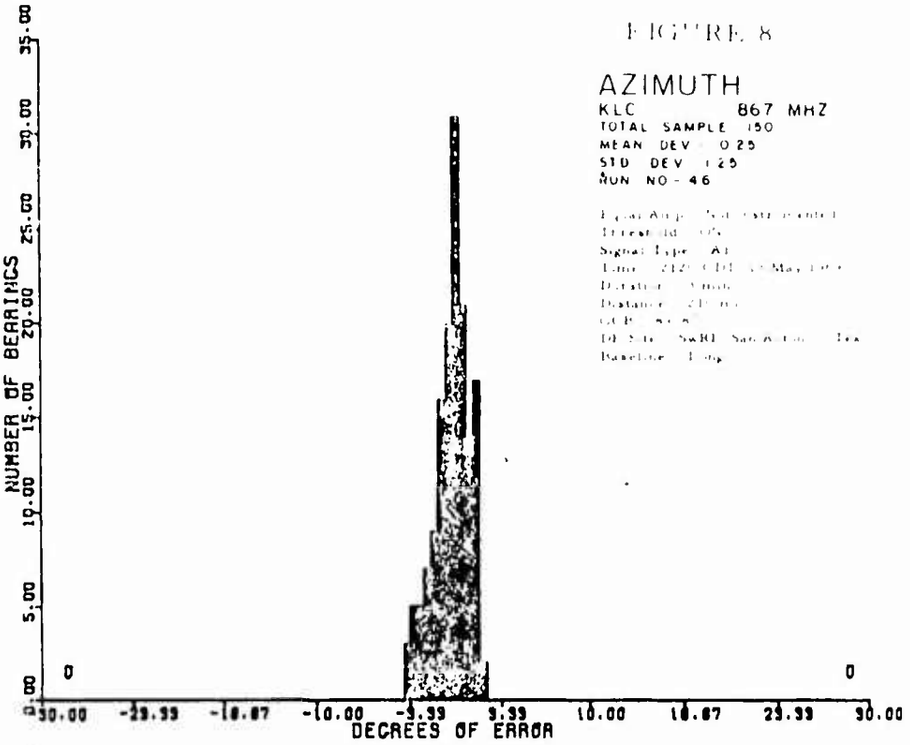

FIGURE 9

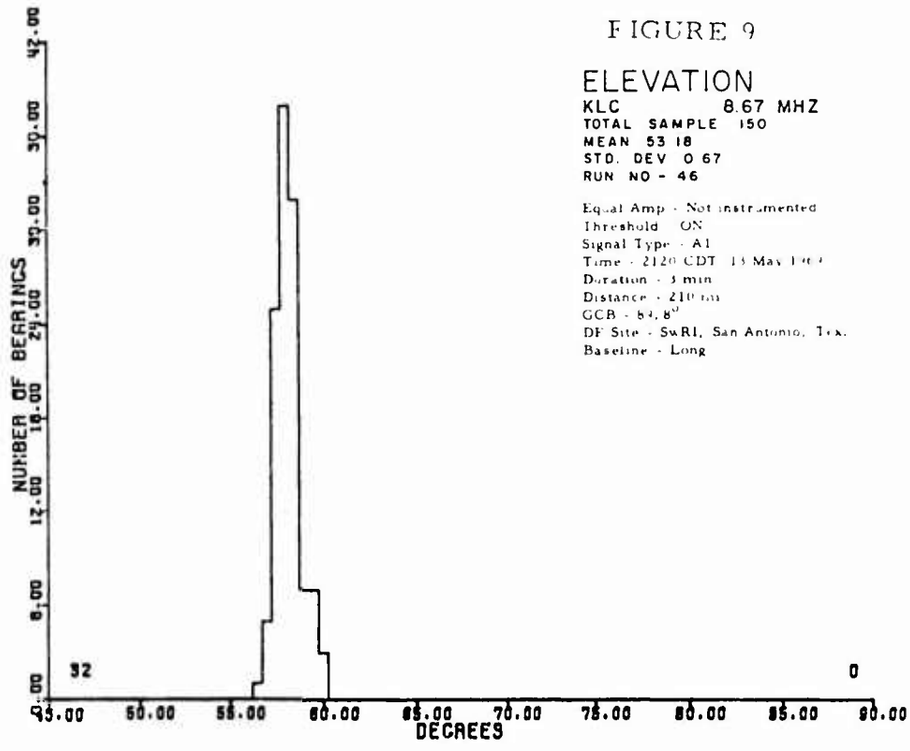

Azimuth data on the University of Houston target--8.0 MHz and 350 km range taken at 2110 just 10 minutes prior to the KLC data just shown--are shown in Figure 10. There is considerably more spread to these data, showing a 4.7° standard deviation. The spread is interesting because the two targets, KLC and KA2XTZ, are separated by not more than 15 miles and 667 kHz in frequency. Transmitting characteristics have not been studied although it is known that we are working off a side lobe of the University of Houston antenna which is directional toward Urbana and that KA2XTZ is transmitting continuous carrier while KLC is ICW.

Before we look at the elevation data, a histogram of this same signal just prior to the path going out an hour later at 2225 hours (Figure 11) demonstrates that comparative statistics on a fixed sample size are no longer relevant since 21 points were cast out on the high side. We do want to emphasize, however, that there is no reason to suspect a deterioration in array performance from those earlier examples. The elevation measurement performances for these two azimuth sets are shown in Figures 12 and 13. The first--well before the path went out--has a mean elevation of 56° while the second just prior to fade out shows considerable deterioration but the mean elevation has gone up to 59°.

Azimuth data for the short range 64 km target at 6.3 MHz are shown in Figure 14, taken around 2210--just 15 minutes before the 8 MHz, 350 km path went out. Conditions are still reasonably stable. The mean deviation is 8.2° while the standard deviation is about 4°, which has been considered extremely good in the past for signals arriving at 82°

FIGURE 10

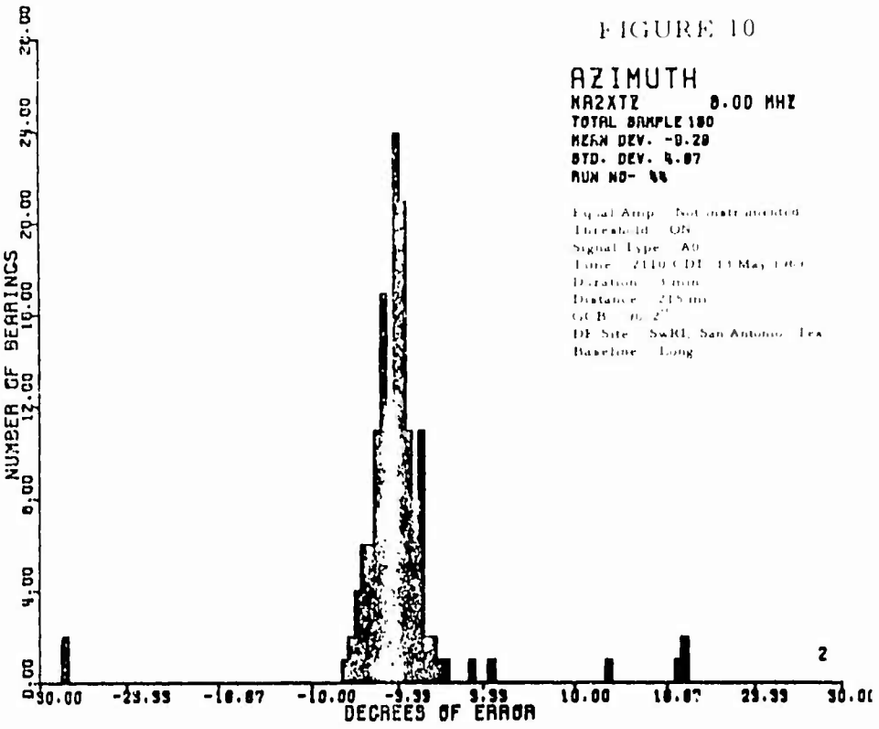

FIGURE 12

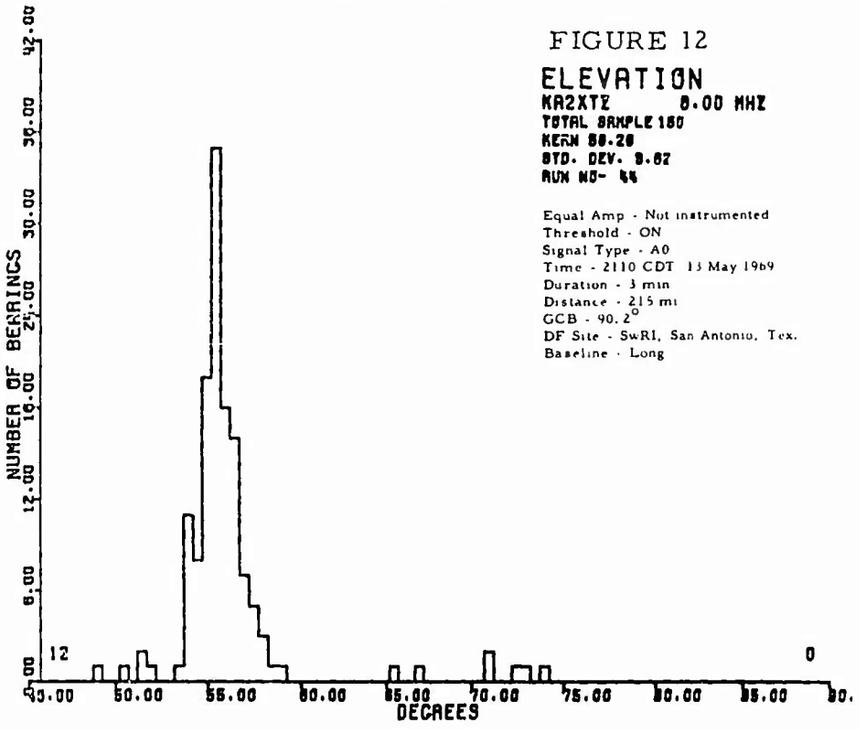

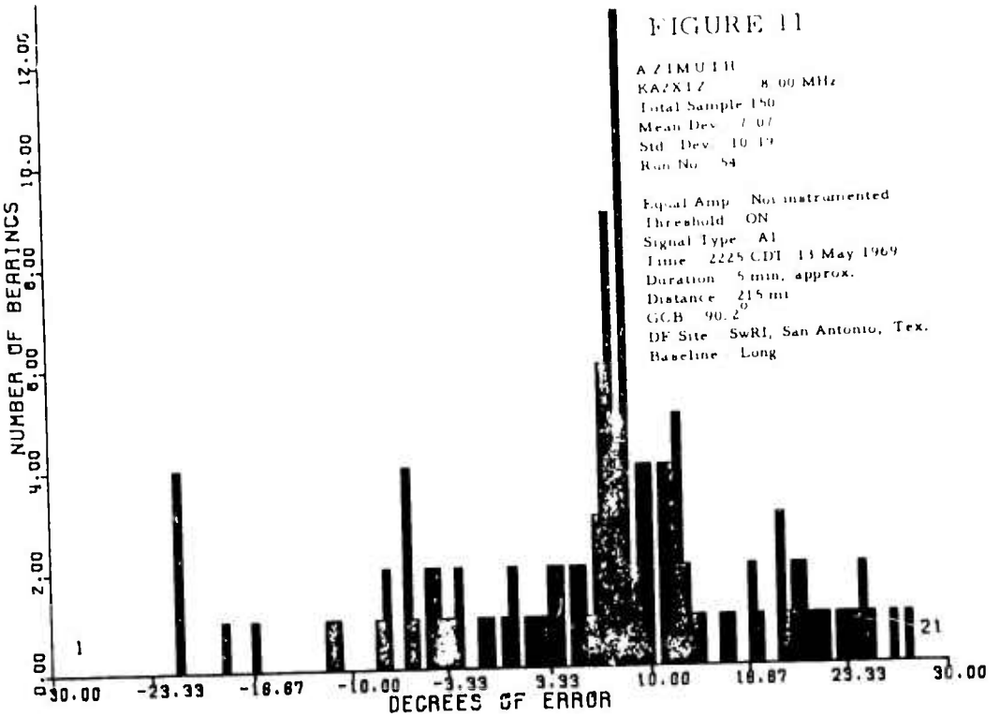

FIGURE 11

AZIMUTH
KA2XTZ 8.00 MHz
Total Sample 150
Mean Dev. 7.07
Std. Dev. 10.19
Run No. 54

Equal Amp. - Not instrumented
Threshold - ON
Signal Type - A1
Time - 2225 CDT 13 May 1969
Duration - 5 min. approx.
Distance - 215 mi
GCB - 90.2°
DF Site - SwRI, San Antonio, Tex.
Baseline - Long

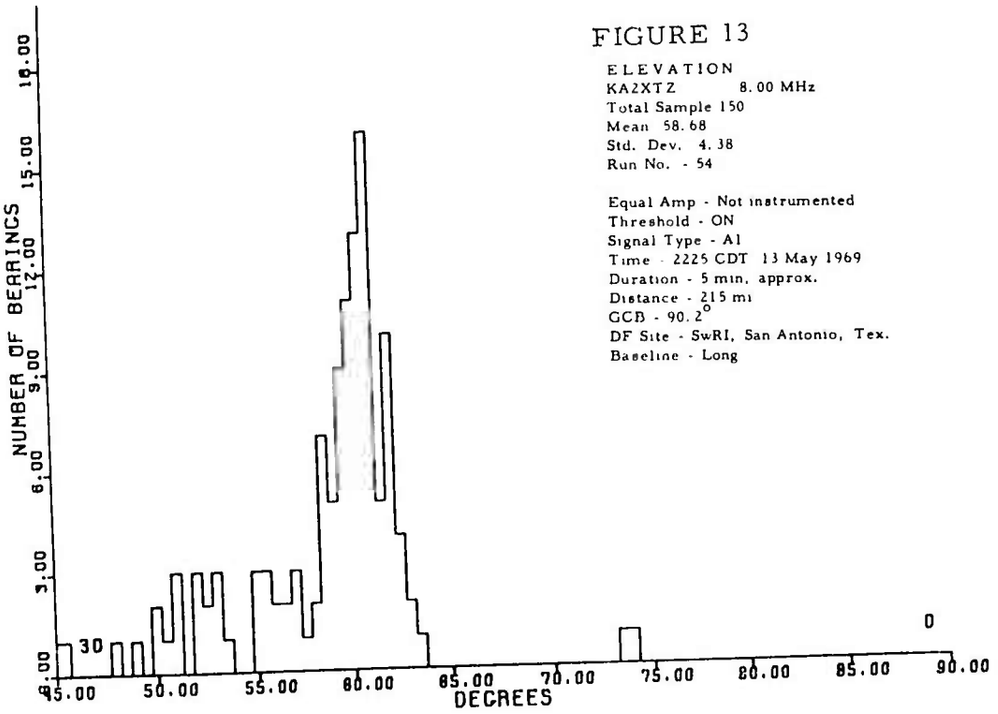

FIGURE 13

ELEVATION
KA2XTZ 8.00 MHz
Total Sample 150
Mean 58.68
Std. Dev. 4.38
Run No. - 54

Equal Amp - Not instrumented
Threshold - ON
Signal Type - A1
Time - 2225 CDT 13 May 1969
Duration - 5 min. approx.
Distance - 215 mi
GCB - 90.2°
DF Site - SwRI, San Antonio, Tex.
Baseline - Long

FIGURE 14

AZIMUTH
KA2XTO 6.30 MHz
TOTAL SAMPLE 150
MEAN DEV. 8.17
STD. DEV. 3.95
RUN NO. 52

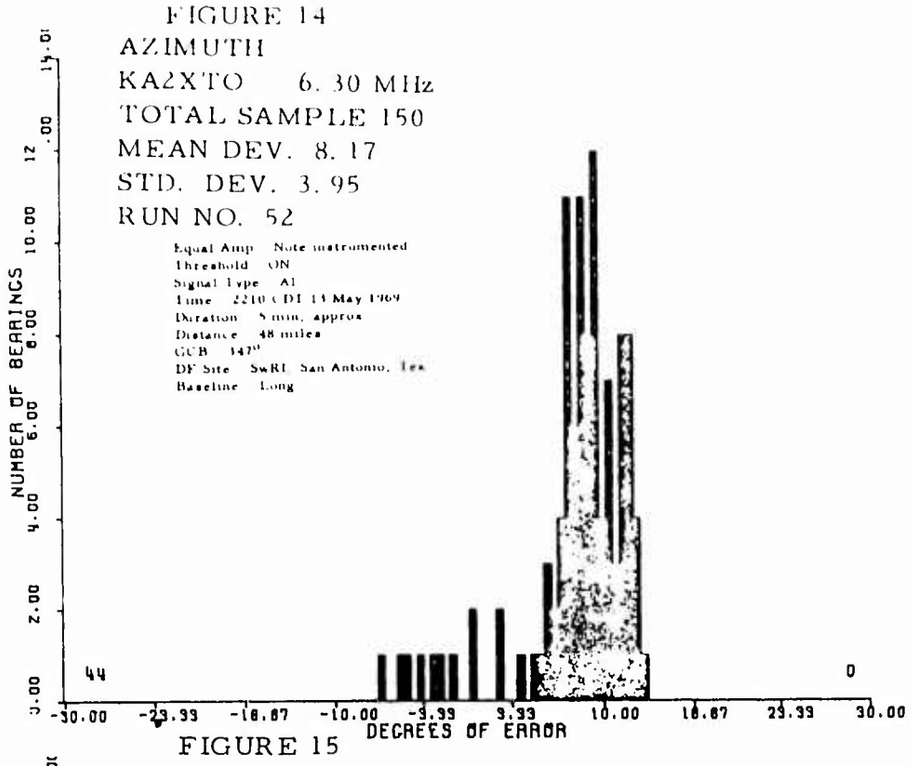

FIGURE 15

ELEVATION
KA2XTO 6.30 MHz
TOTAL SAMPLE 150
MEAN 81.73
STD. DEV 1.56
RUN NO. 52

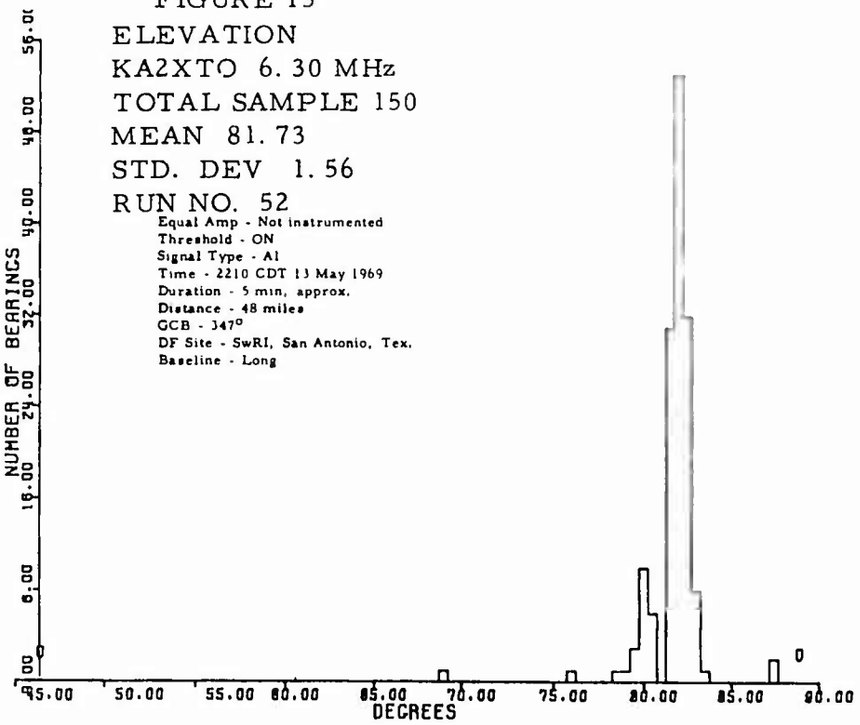

elevation (Figure 15); however, as we said earlier, these numbers can be misleading particularly for steeply downcoming signals and need to be judged with consideration given to the time interval over which the data were taken.

The last sets of data were obtained from the 8.5 MHz, 48 km target at New Berlin on 15 April 1969. These data demonstrate the adverse effects of building histograms or calculating statistical performance data on high angle targets affected by ionospheric tilts or other perturbances. In Figure 16, the mean shown is about -7° while the standard deviation is 9.3°. Compare the data with those of Figure 17, which is a 20 minute sample but beginning about a half hour later. The mean deviation is +8.2° with a standard deviation of 8°. As shown, the data do not appear to be helpful but we've shown these to demonstrate the need for filtering and placing more reliance on a time series type plot.

Filtering is shown in Figure 18. These data, taken between the time intervals of Figures 16 and 17, represent a twelve-minute interval. The azimuth and elevation variations (the top two plots) were obtained by a 50 point sliding average taken 10 frames at a time. The total number of frames is about 800. Note that the overall standard deviation would be relatively large with a mean near zero. However, if we had taken sample sizes of 150 frames as we did in the earlier data, the standard deviation would be low but the mean would vary almost in the manner of the curve shown.

One of the objectives of the HF interferometer research on targets of short and medium range is target location by vertical triangulation. The mechanics of the problem are illustrated in Figure 19. In order to

FIGURE 16

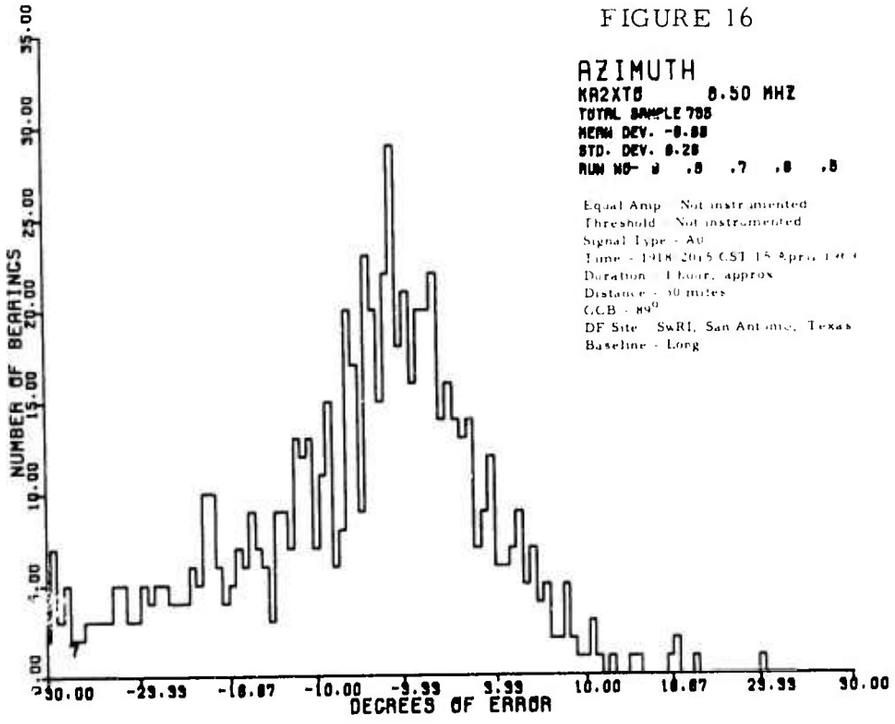
AZIMUTH
KA2XTG 8.50 MHZ
TOTAL SAMPLE 795
MEAN DEV. -0.88
STD. DEV. 8.28
RUN NO- 8 .5 .7 .8 .8
Equal Amp - Not instrumented
Threshold - Not instrumented
Signal Type - AU
Time - 1918-2015 CST 15 Apr
Duration - 1 hour, approx
Distance - 50 miles
GCB - 89°
DF Site - SwRI, San Antonio, Texas
Baseline - Long
NUMBER OF BEARINGS
35.00
30.00
25.00
20.00
15.00
10.00
5.00
0.00
-30.00
-20.00
-10.00
-0.00
0.00
10.00
20.00
30.00
DEGREES OF ERROR

FIGURE 17

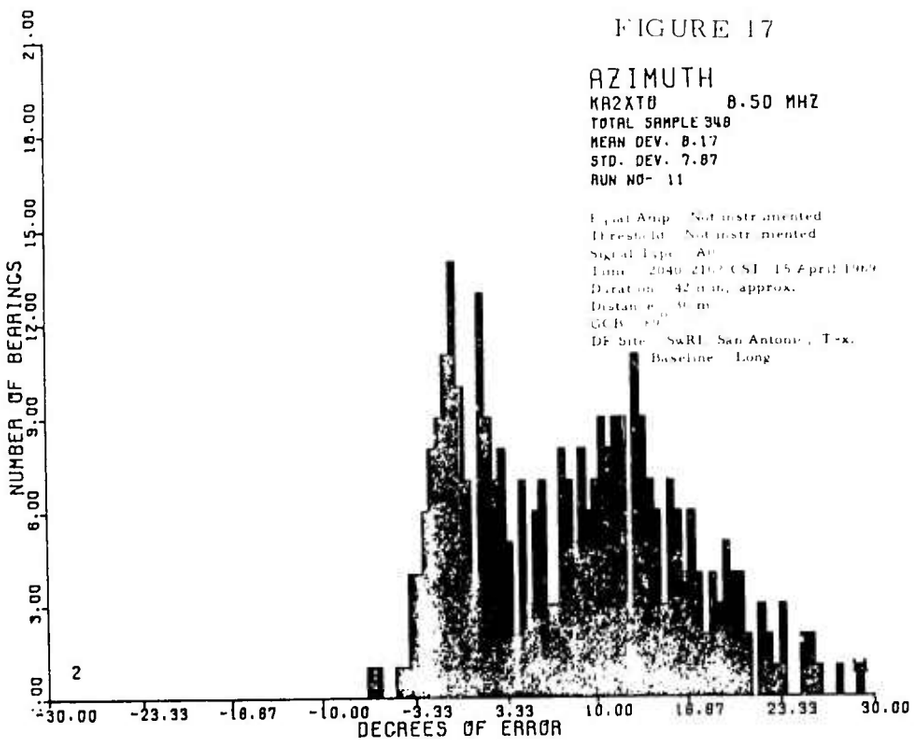
AZIMUTH
KA2XTØ 8.50 MHZ
TOTAL SAMPLE 348
MEAN DEV. 8.17
STD. DEV. 7.87
RUN NO- 11
Signal Amp Not instrumented
Threshold Not instrumented
Signal Type AM
Time 2040-2102 CST 15 April 1969
Duration 42 min. approx.
Distance 40 mi
GCB
DF Site SwRI San Antonio, Tex.
Baseline Long
NUMBER OF BEARINGS
21.00
18.00
15.00
12.00
9.00
6.00
3.00
.00
2
-30.00
-23.33
-16.67
-10.00
-3.33
3.33
10.00
16.67
23.33
30.00
DEGREES OF ERROR

FIGURE 18

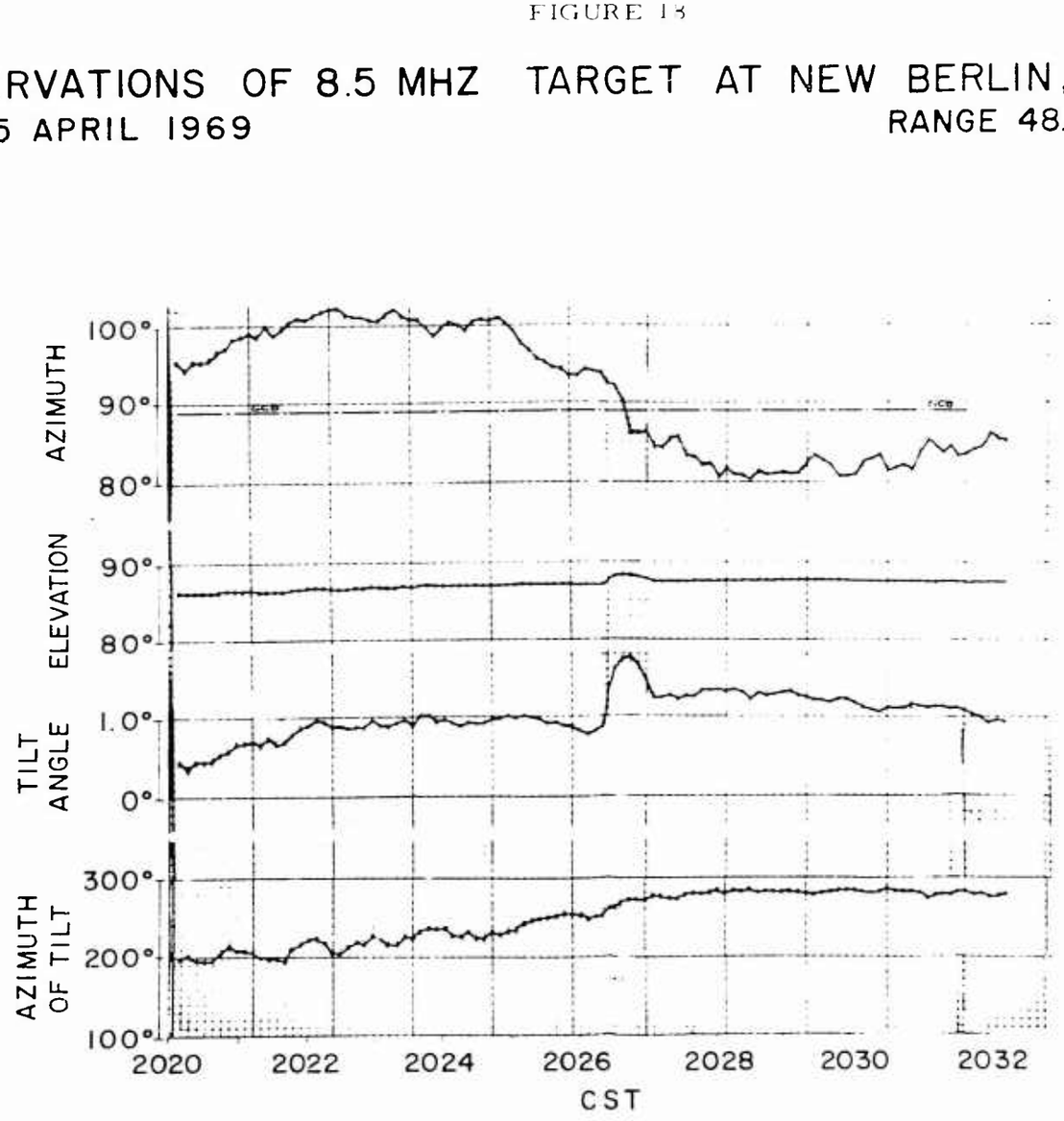

Figure 18. Observations of 8.5 MHZ Target at New Berlin, Texas.

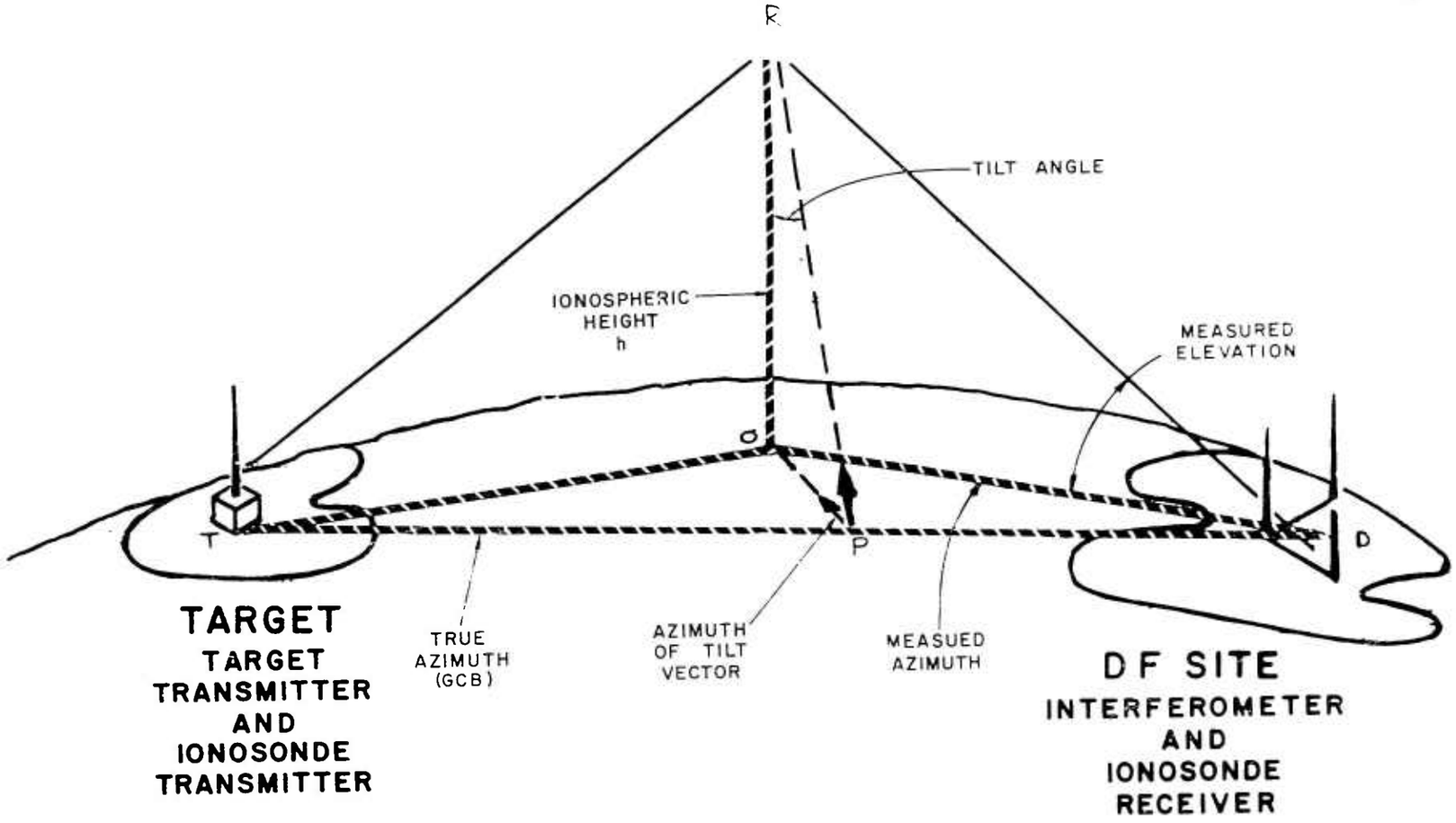

Figure 19. Ionosphere Tilt Effect.

perform vertical triangulation, angle of arrival data must be corrected for ionospheric tilt. The virtual height or the path length must be measured. Other measured parameters are the angles of arrival (azimuth and elevation). If the target location is not known, the tilt angle must be measured by DF'ing on a vertical incidence probe or measurements from a known station can be used as a correction factor applied to azimuth and elevation data of the unknown.

The 12-minute example in Figure 18 demonstrates the calculation of the tilt parameter from the known target at New Berlin -- a 48 km range -- at 8.5 MHz. A linear FM CW ionosonde transmitter colocated with the target enabled the path delay or path length to be measured directly. Data from three ionograms were used to plot the variation of path length shown as a function of time in Figure 20. Data were just after local sunset.

By knowing the deviation from the true azimuth and the elevation angle, along with the path length of the tilt angle, the inclination of the normal to the reflecting surface with respect to the vertical can be calculated, as shown in the third plot of Figure 18. The calculated azimuth of the vertical plane that includes the tilt vector and passes through the midpoint of the GCB line is plotted on the bottom.

As an exercise and to gain insight into the influence of the tilt effect, we assumed the target as unknown and calculated target locations by vertical triangulation using only the measured parameters of azimuth, elevation angle and the near vertical incidence virtual height (assumed plot ionospheric parallel to the earth). The variations in location using data that include the 12-minute sample f Figure 19

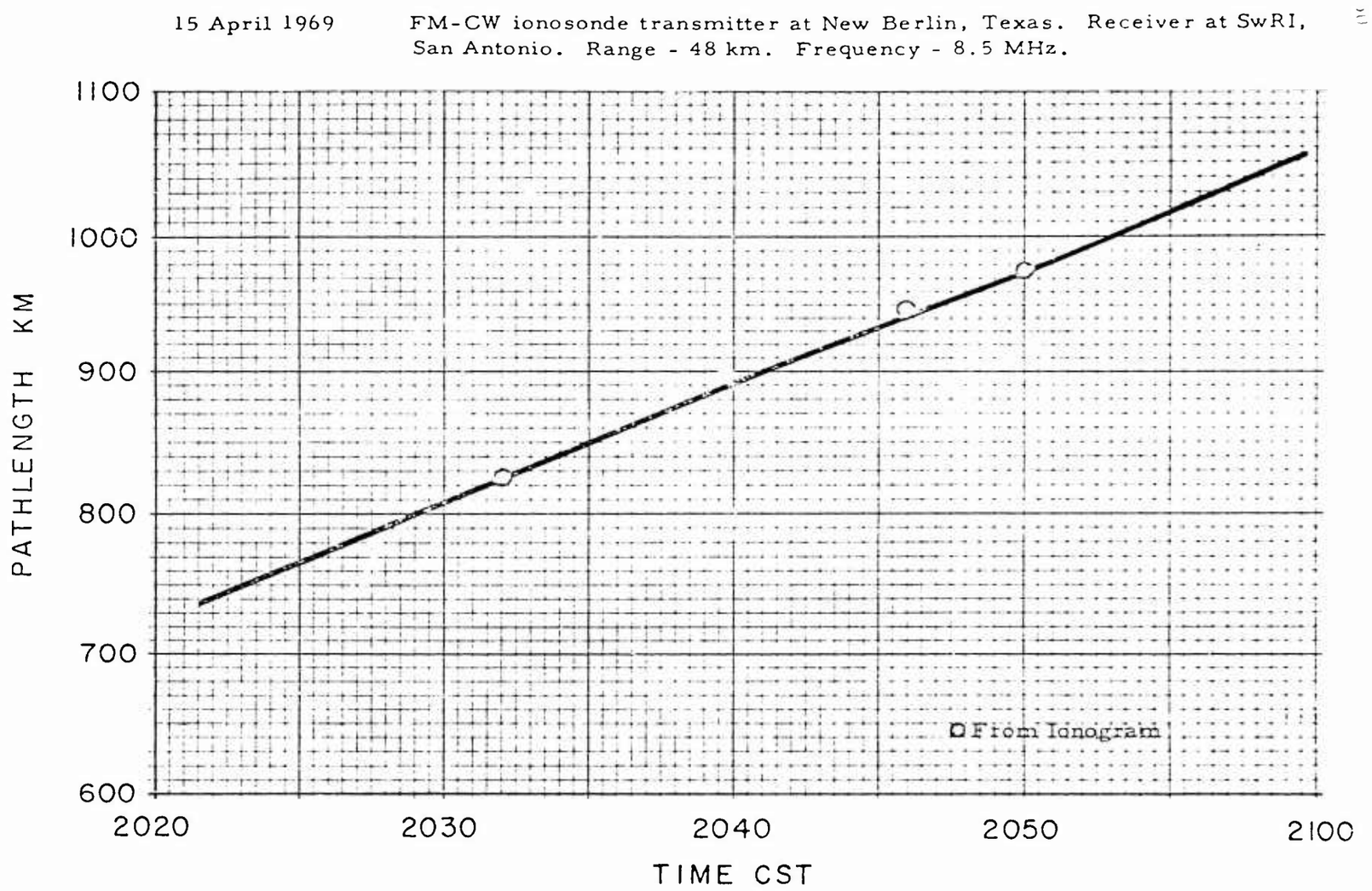

Figure 20. Pathlength versus time - 48 KM Range.

demonstrate that a single tilt correction for a data sample as short as 12 minutes would be of little use for short range targets. The results suggest that tilt parameters are required in real time along with the angle of arrival information. The on-line digital computer with sufficient memory or storage can, of course, handle the chore routinely once the technique of direction finding on a vertical incidence signal, such as a sounder return, is accomplished.

A. D. BAILEY

Department of Electrical Engineering
University of Illinois, Urbana, Illinois

DIRECTION OF ARRIVAL STUDIES ON A LONG PATH (Summary)

Lowell Tveten and I will be presenting some of the results obtained in two series of HF directional propagation experiments over long range paths. Our paths were orthogonal to one another. I've called the experiment a "cooperative" one, Lowell calls it a "coordinated" one I don't believe there was that much difference. To cooperate means "to act or work together with another or others for a common purpose." Coordination implies harmonious adjustment or functioning. From my viewpoint we have had both. The relationship is continuing because there is much left to do with the data that were acquired. We've barely skimmed a small portion of the available data.

The body of the presentation was concerned with information found in the ATLAS of DATA obtained in a cooperative HF directional propagation experiment over a 1330 Kilometer path (March 1967 - March 1968).[1]

Slides were shown which demonstrated:

1. The propagation path geometry
2. The data vector
3. The format for the reduced data
4. An example of a typical page of data.

---

1. "An Atlas of Reduced Data Obtained in a Cooperative HF Directional Propagation Experiment Over a 1330 Kilometer Path (March 1967 - March 1968)" A.D. Bailey, E.W. Ernst, L.J Miller, W.W. Wood. RRL publication No. 344; Radiolocation Research Laboratory, Department of Electrical Engineering, University of Illinois, Urbana, Illinois.

Certain dominant features in the data were pointed out as follows:

1. At night, single (dominant) mode propagation was in evidence and the data represent true angle of arrival as received. The fluctuations in the data are due to the quasi-periodic lateral deviation effects (the "20-minute" or Ross effect) and the diurnal effect. Twenty-minute and 2-hour "moving average windows" brought out the significance of these two deviations.

2. In the daytime, considerable wave interference effects were seen between the two or three modes of propagation when all are of approximately equal amplitudes. These interference effects were removed by the "averaging windows."

3. The importance of the standard deviation of the sample as an immediate indicator of wave interference was pointed out.

4. Also discussed was the dramatic appearance of sidescatter particularly after the main path fails because the frequency is higher than the MUF for the direct path. Of course, the gain of the system had to be increased to see the scatter.

The elevation angle measuring properties of the CDAA were pointed out. These properties, though restricted in elevation, are nevertheless useful at intermediate ranges.

The need for amplitude information in oblique incidence ionograms was stressed.

The need for more rapid sampling of the data (greater than the sampling rate shown) was stressed. In this connection one example of some results obtained from a tracking-type system was shown. This spoke to the need for rapid sampling and indicated in a quantitative

way what one must do if he would have his "druthers" for the cases that appeared to prevail.

The ATLAS shows the way one time series of data may be expected to behave over a twenty-four hour period. It is a conversation with "Mother Nature." If one asks the right questions and is patient, he gets back a lot of answers.

L. H. TVETEN

ESSA, Institute for Telecommunication Sciences, Boulder, Colorado

THE COORDINATED HF PROPAGATION EXPERIMENT

1. ABSTRACT

The general plan and objectives of a coordinated cooperative experiment performed by the University of Illinois and the Institute for Telecommunication Sciences, ESSA Research Laboratories, are discussed. Results so far indicate that it is feasible to use backscatter to assess DF reliability over simple one-hop paths. Until more is understood about the complex interaction between radio waves and the irregular ionosphere, it will not be generally possible to correct DF measurements on the basis of backscatter irregularity patterns. Larger scale tilt determinations by a backscatter mapping technique may ultimately prove useful in DF correction. *

* This paper has not been released for publication by ESSA and should not be referenced.

II. SUMMARY

The coordinated HF propagation experiment was designed to obtain correlations between propagation parameters and direction-of-arrival (DOA) measurements by a multiplicity of observations and observing techniques. The Institute for Telecommunication Sciences (ITS) of ESSA, the University of Illinois, and the University of Houston cooperated in the experiment. The center for the ITS observations was the high-resolution antenna array at Table Mountain near Boulder, shown in Figure 1. The azimuth array forms a beam very narrow in azimuth and wide in elevation. The elevation array forms a beam narrow in elevation and wide in azimuth. The azimuth array has an aperture of 1,392 feet. The elevation array has an effective aperture of 1,000 feet, since it is mounted on a 500-foot tower with the beams formed in such a way that both direct and ground-reflected rays are used. These arrays have a nominal frequency range of 12 to 25 MHz and equivalent beam widths from 1.5 to 3 degrees in the case of the azimuth array, and about 2 to 4 degrees in the case of the elevation array. The effective scan sector for the azimuth array varies between 40 and 90 degrees and the effective scan sector for the elevation beam varies between 22 and 52 degrees, approximately. Figure 2 shows a view of the scan and beam-forming electronics inside the building; not shown are the various recording interfaces and timing systems for the recording and processing of the data.

Figure 3 illustrates some of the types of experiments and experimental observations that were conducted. At Boulder, high-resolution

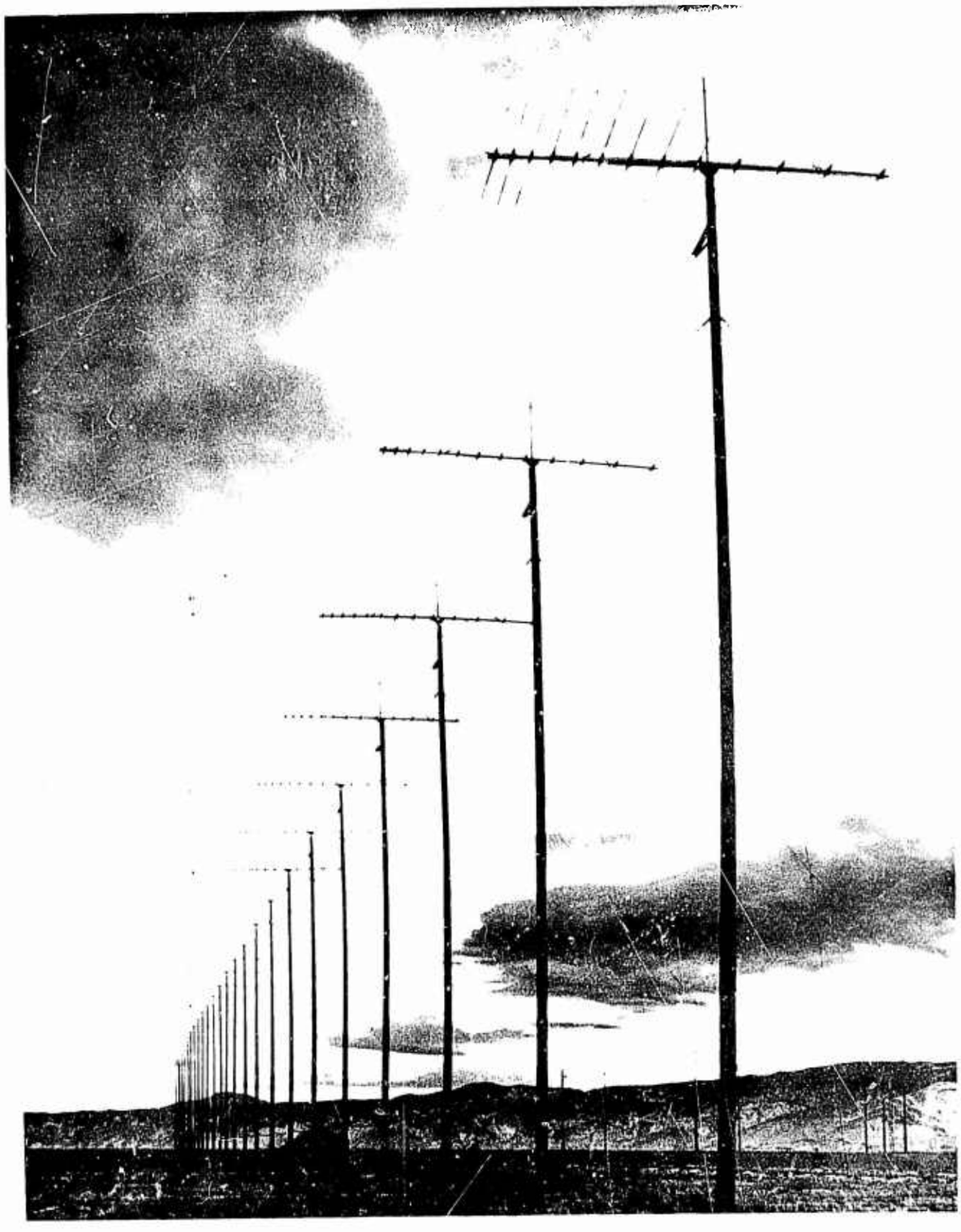

Figure 1. Azimuth and Elevation Arrays at Table Mountain Field Site.

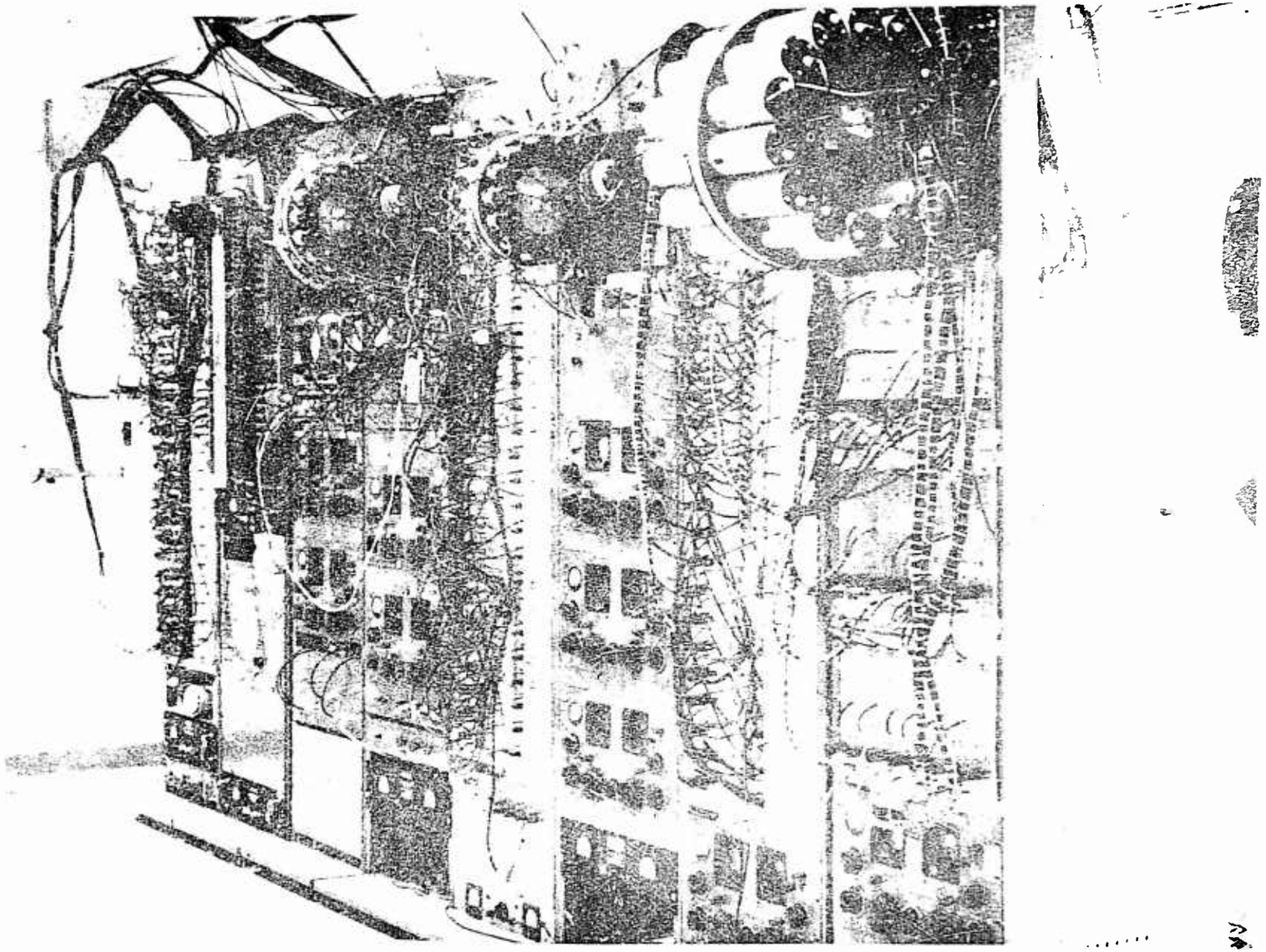

Figure 2. View of Beam Forming and Scanning Electronics for Electronically Scanned Arrays.

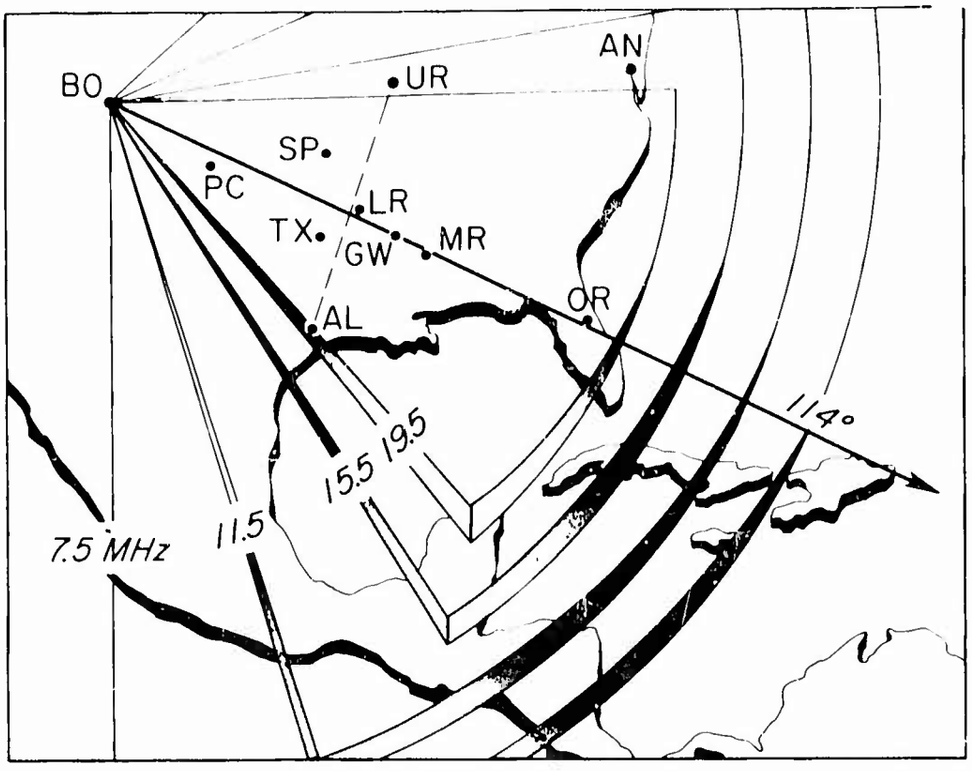

I.T.S.A. HF BACKSCATTER AND
DIRECTION-OF-ARRIVAL INVESTIGATION

Station	Instrumentation
BO-Boulder, Colo.	V-I Sounder, HF high resolution backscatter sounder and receiving system, Granger oblique receiver
PC-Ponca City, Okla.	V-I Sounder
SP-Springfield, Mo.	V-I Sounder & C W Doppler
TX-Texarkana, Ark.	" " " " "
GW-Greenwood, Miss.	" " " " "
UR-Urbana, Ill.	V-I Sounder, DF system, Granger receiver, C W Doppler
AL-Alta Loma, Tex.	Granger oblique sounder
MR-Meridian, Miss.	Transponder
OR-Orlando, Fla.	Transponder
LR-Little Rock, Ark.	Earth currents
AN-Annapolis, Md.	Oblique sounder

Figure 3. I.T.S.A. HF Backscatter and Direction-of-Arrival Investigation.

azimuth and elevation scan backscatter recordings were made on five frequencies. DOA and signal strength for each of two propagation modes from each of two transponders, one located at Meridian, Mississippi, and the other at Orlando, Florida, were made. Vertical sounder stations were located at Ponca City, Oklahoma; Springfield, Missouri; Texarkana, Arkansas; and Greenwood, Mississippi. In addition, steep-incidence phase measuring transmitters were installed at Greenwood, Texarkana, and Springfield and received at Little Rock, Arkansas. The University of Illinois made DOA measurements between Alta Loma, Texas, and Urbana, Illinois. It is obvious the two propagation paths crossed at very nearly right angles. Oblique sounder transmissions from Texas were received at both Urbana and Boulder. Measurements were made 24 hours a day on 5 consecutive days each month from August 1966 to June 1968.

The ITS objectives were: (1) to determine the feasibility of using backscatter for (a) assessing DOA measurement quality or (b) correcting specific DF readings; (2) to check the ITS 3-D ray-tracing program; (3) to identify and measure propagation modes and to obtain experimental data for testing particular processing and analytical techniques; and (4) to study anomalous propagation, specifically sidescatter.

Figure 4 illustrates simultaneous azimuth and elevation scan backscatter records. The horizontal axes are labeled in degrees for both azimuth and elevation; the vertical axis is labeled in milliseconds. As one might expect, the backscatter shows high elevation angles at the smaller delays and lower angles as the delay increases - the classic elevation angle-backscatter delay relationship. The azimuth-versus-delay presentation on the left shows a number of intensifications caused by ionospheric disturbances.

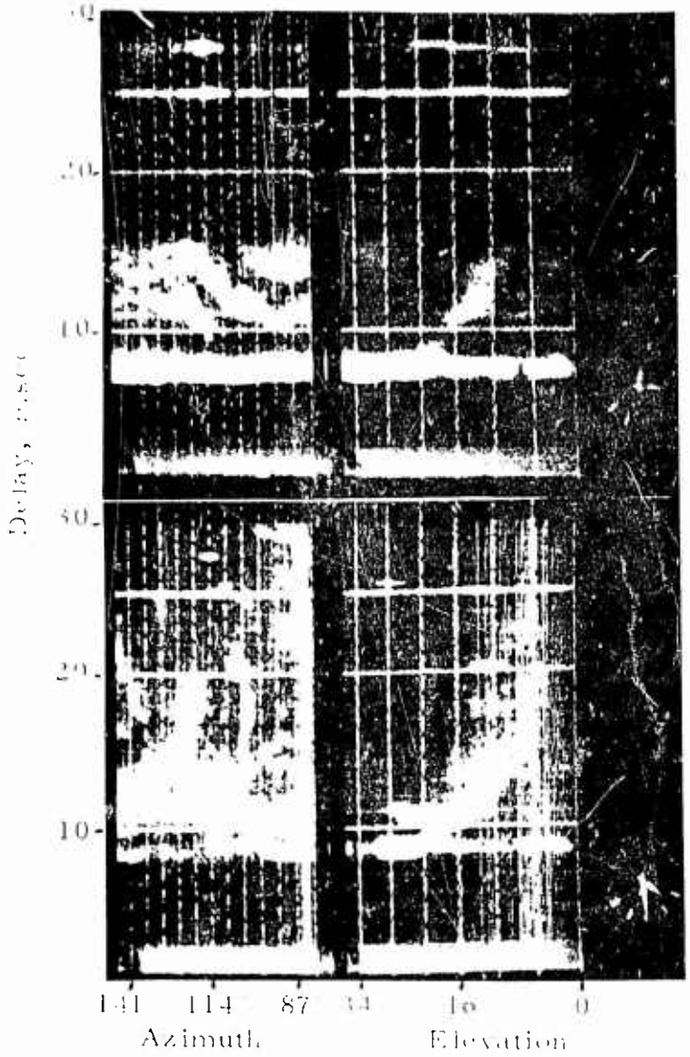

Figure 4. Azimuth Elevation Scan Backscatter Records at 15.67 MHz Taken at 1215 and 1630 MST November 19, 1966. Skip Echoes are Saturated.

To check the feasibility of using backscatter to assess DF quality, the backscatter data for each hour of the day were categorized according to five classifications illustrated in Figure 5. The precise characteristics of these categories are not especially important. They appeared consistently throughout the five months (distributed over a year's time) used in the analysis. DOA data were classified as "bad" if the deviations exceeded one degree during a given hour and as "good" otherwise. Each hour's data were compared with respect to DF quality backscatter category. Results of this comparison are shown in Table 1.

Table 1. Meridian One-Hop F DOA Compared with Backscatter Characteristics

	Backscatter Category				
	A	B	C	D	E
Good DOA, per cent	19	27	37	100	100
Relative occurrence, per cent	19.3	28.9	17.4	20.2	14.2
Order of preferred distributions	4	3	2	1b	1a

The traveling ionospheric disturbance category has only 19 per cent good DF data. Backscatter category E has 100 per cent good data, with a relatively smooth ascending percentage between categories A and E. The next row shows the relative occurrence of the various categories, and we see that the distribution is relatively uniform over the time period. The last row shows the order of preference, if one were to assess the quality of the DOA data with respect to the various backscatter categories.

We therefore conclude that it is indeed feasible to use backscatter to assess DOA measurement quality or accuracy at the same time and in the same general region over simple one-hop F paths.

To actually correct DOA measurements is a bit more complex. One would expect that since the focusing irregularities for backscatter are the same irregularities that cause deviations in DOA, there would be a rather specific relationship between the two. To check this relationship, we examined several months' scan backscatter data and defined the times at which a specific irregularity appeared at the apparent midpoint of the path between Boulder and Meridian, Mississippi. The DOA data were examined for the same time. In general, little correlation was noted except in the December 1967 data, in which the DOA deviated to the south within two minutes of an irregularity over path midpoint in 50 per cent of the cases. The probability of this occurring on the basis of random distributions is extremely small.

To gain insight into the problem, we did some ray tracing with ionospheric irregularity models. Figure 6 is an example of simultaneous azimuth and elevation DOA determined from ray tracing a moving irregularity model. It can be compared directly in Figure 7 with an experimental record taken during December 1967 in which a number of TID's are moving through the area. The two are quite similar; however, one can obtain different relationships in the ray-tracing outputs simply by using the different heights of travel for the disturbance with respect to the ray path geometry, by changing the direction of travel of the disturbance somewhat with respect to the ray geometry, or by changing the type of irregularity from an ionization intensification model to a

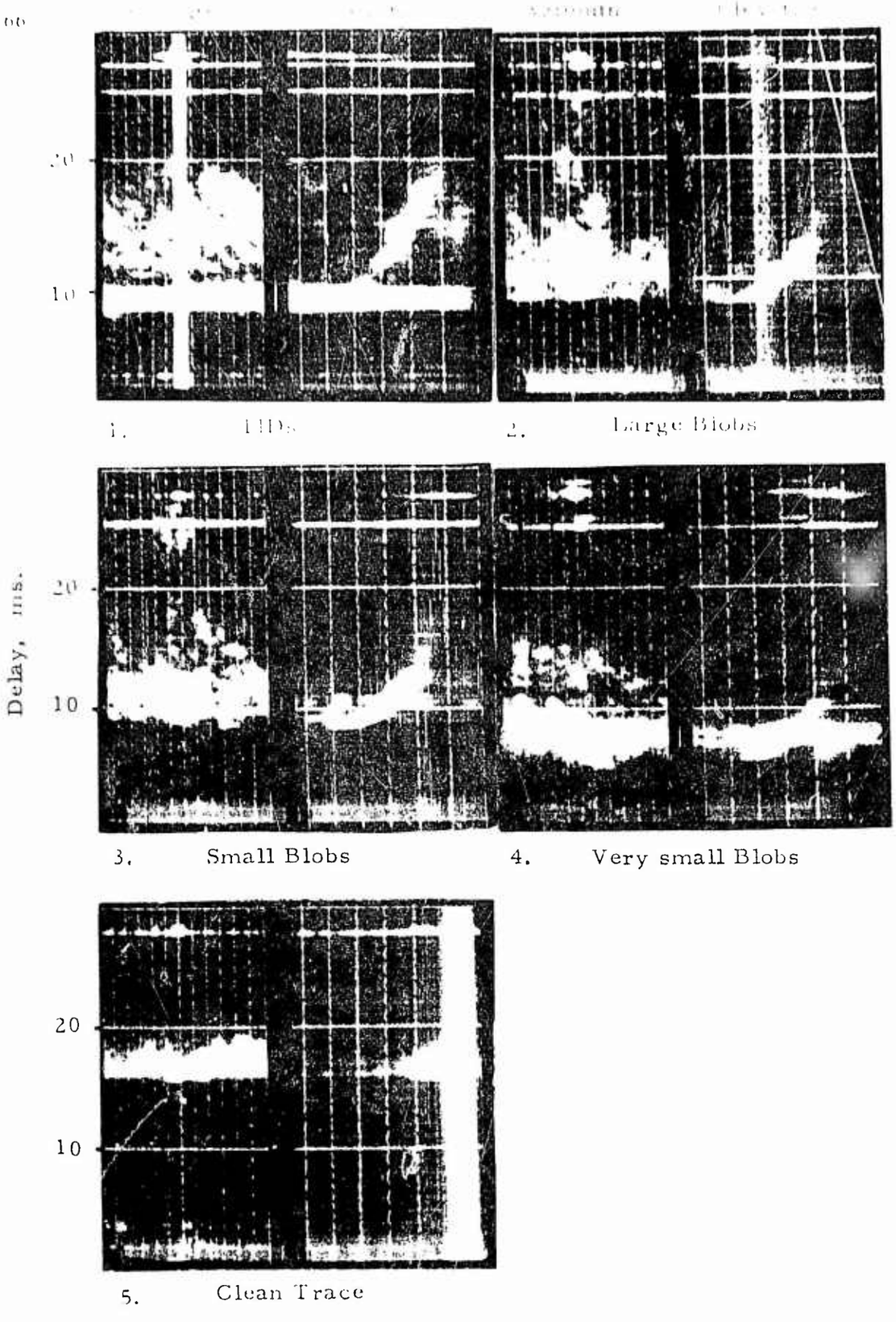

Figure 5. Examples of backscatter Categories.

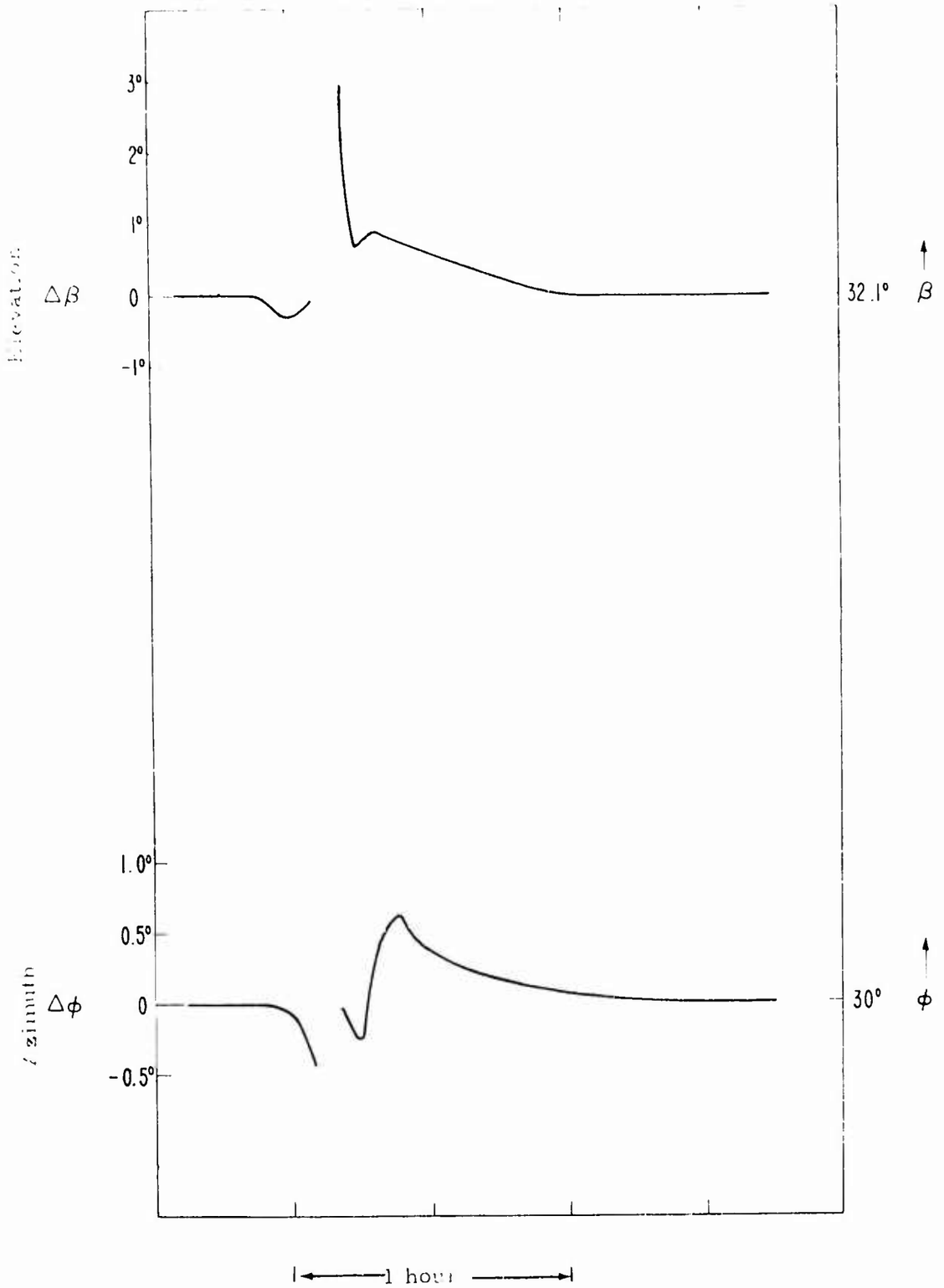

Fig. 6. Azimuth and Elevation DOA with motion of a model ionospheric disturbance traveling at 400 km/h simulated by ray tracing techniques.

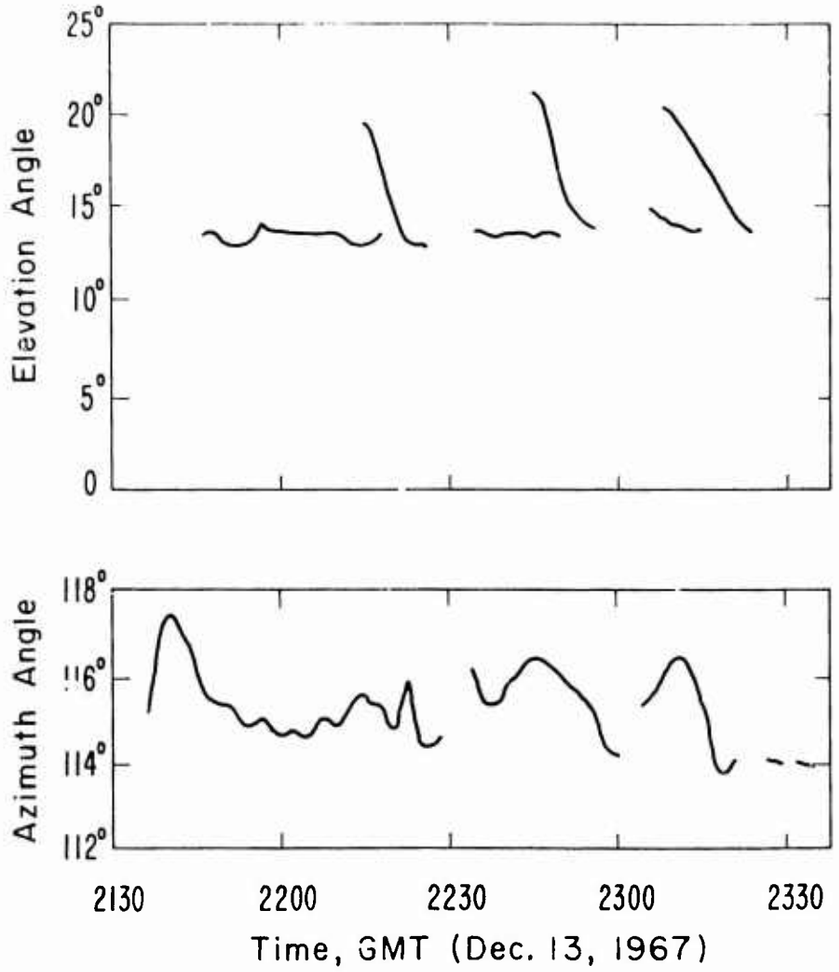

Fig. 7. Azimuth and Elevation angles of arrival on the one-hop F-mode from Meridian, Missippi

rarefaction model. With all these possibilities, it is not difficult to understand why many different relationships can be seen in the actual records when one compares backscatter irregularity structures and DOA behavior and even behavior between the azimuth and elevation angle deviations. On the basis of what we know so far, we conclude that it is not usually possible to make specific DOA corrections on the basis of irregularity positions on backscatter records. Ultimately however, with more knowledge of the mechanisms of interaction, one may be able to go from the backscatter pattern back to the generating ionospheric irregularity and so deduce the correction necessary, but much more work in modeling and ray tracing is required for knowledge of this kind.

The ionosphere may be thought of as being made up of a spectrum of ionospheric irregularities with periods of less than a second to several hours. Another application or possibility for DF correction is to correct for the longer period or larger area tilts. This could perhaps be done by mapping the generalized ionization densities by the backscatter technique. Figure 8 is another azimuth and elevation backscatter record that shows a very classic elevation angle versus delay relationship. From this relationship, in conjunction with transmission curves for an assumed ionosphere model, one can deduce plasma frequencies versus h' at various locations along the path corresponding to the different delays. The use of multiple frequencies allows these plasma frequencies to be determined at different height levels in the ionosphere. With a generalized mapping program, one can map the virtual height versus plasma frequency over a large geographic area to be subsequently used for defining the broad general overall tilts over a rather large area for correction purposes.

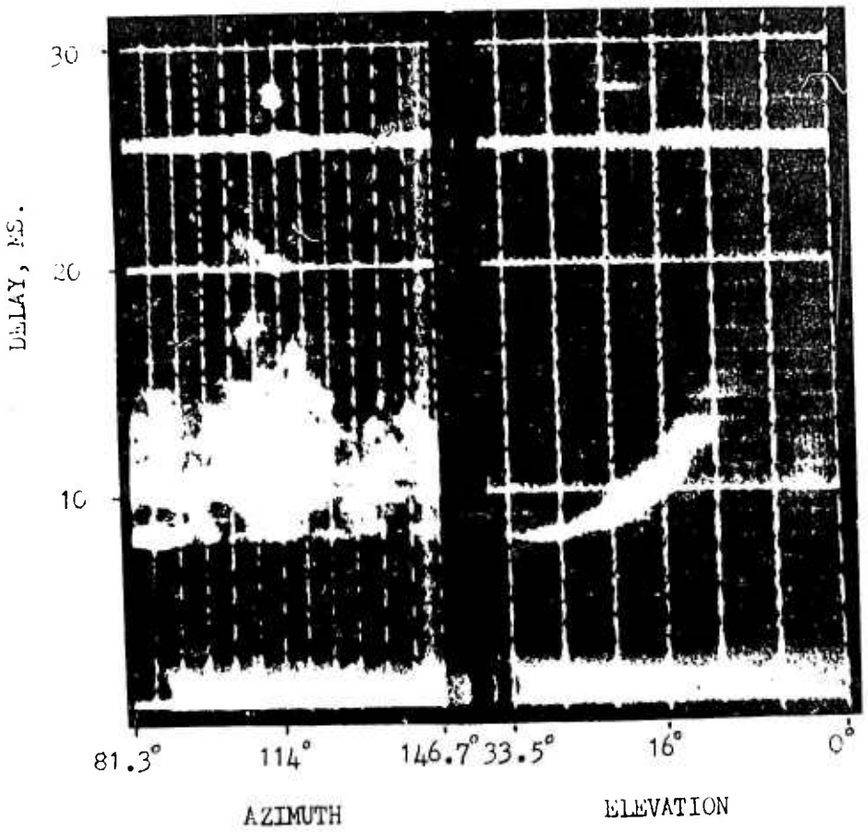

Figure 8. Simultaneous Azimuth and Elevation Scan Display of Backscatter at about 15.5 MHz Taken during a November Day in 1966 at 1405 MST.

For such mapping, one needs azimuthal discrimination for the elevation angle versus delay time response for backscatter, which can be achieved by cross-correlating the azimuth and elevation beam outputs to form an effective pencil beam, a method that has been attempted at ITS It has not proved wholly successful because of our array configuration and spacing, but the addition of a few more elements to the azimuth array on the unoccupied side of the 500-foot tower would we think, bring success.

One could also apply the mapping technique if the transmitting beam were sufficiently narrow. Using a rhombic antenna as an illuminator for transmission, we have made estimates of plasma frequencies versus height from backscatter records and compared them with actual plasma frequencies versus height at particular ionosonde locations. The errors have been on the order of 10 to 15 percent and we believe that with refinement of the technique they can be reduced considerably.

Another objective was to check the 3-D ray-tracing program. This we did by reducing vertical ionosonde data to true height profiles at several locations, connecting them smoothly over the area in question with a generalized mapping program, and ray-tracing through the resulting ionosphere. The directions predicted from the ray-tracing program were compared with the actual measurements made at the same time over the path. Figure 9 is an example of this type of comparison The continuous lines show the measured directional variations of azimuth and elevation, and the dots are the calculated points at the specific times. The agreement is not exact. but, under the circumstances, is considered close enough to validate the ray-tracing program. Other examples have been checked and found to be in reasonable agreement also.

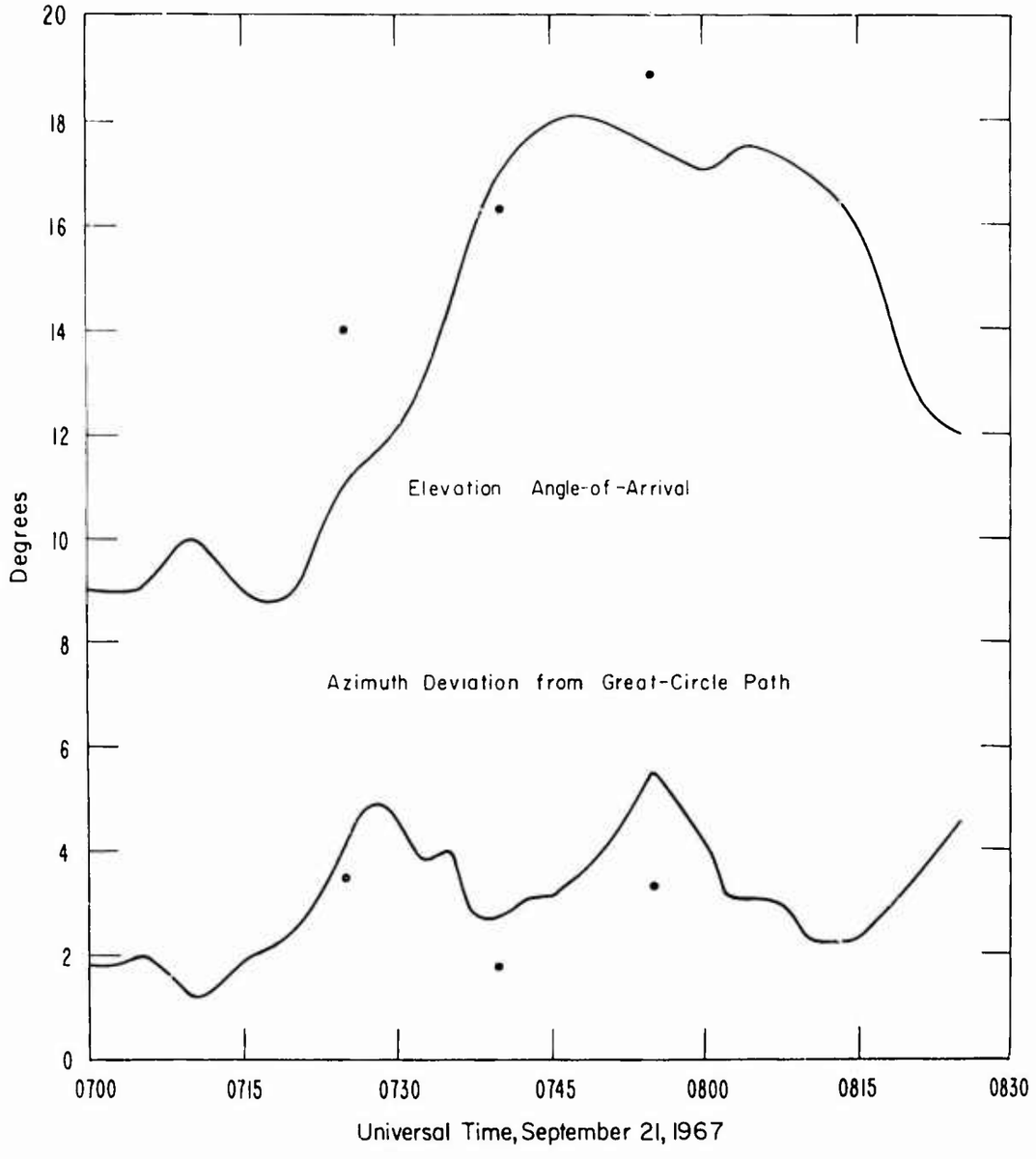

Fig. 9. Comparison of actual direction-of-arrival (continuous curve) and direction-of-arrival determined by ray tracing true height mapped ionosphere from vertical ionograms (dots).

Another area of effort was the determination of propagation modes by elevation angle measurements. The technique for doing this is to generate a large number of ground range-versus-elevation angle curves for different possible propagation modes and combinations of propagation modes. Since the source of transmission must be at one point, a cluster of these modes must indicate a possible source. If, in addition, backscatter data are used to assess the propagation conditions of the ionosphere, a particular range can be chosen. This choice determines the range to the site as well as the identification of the pertinent propagation modes. We compiled a set of data from our transponder locations using elevation angle and backscatter measurements and derived range estimation errors with a standard deviation of about 4 percent. We believe this can possibly be reduced even further and are currently working on an automated computer technique for making these estimates to determine whether we can duplicate the original accuracy.

Figure 10 shows another azimuth-elevation-versus-delay scatter record that, in this case, is sidescatter from the region of the Gulf of Mexico from transmissions originating near Havana, Illinois. At the present time, we are endeavoring to make quantitative measurements of sidescatter parameters.

As useful fallout from this experiment, we are planning to extract DF statistics concerned with mode of propagation and periods of the variations and to perform correlations with various geophysical parameters, etc. We hope to obtain statistics on TID occurrence and to learn much more about the mechanisms of wave interaction with the

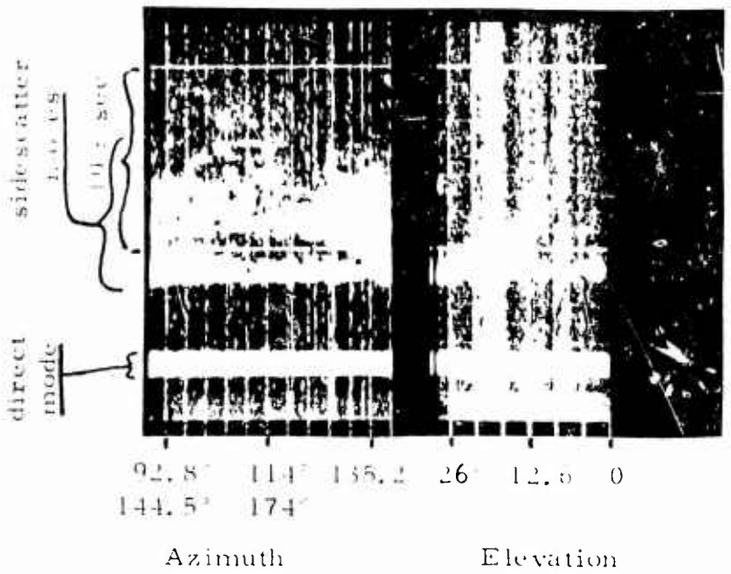

Figure 10. Azimuth and Elevation Record of Direct and Sidescatter Modes Received from Havana, Illinois, at a Frequency of 19.36 MHz at 2250 GMT on March 30, 1967. Left Side of Azimuth Scale is Labeled in Azimuth of First Grating Lobe on the Right as Well as Main Lobe.

irregular ionosphere. Other applications for the data will doubtless arise. Since this experiment covers nearly a 2-year period, the statistics should be fairly useful.

In summary, then, we may say that backscatter can be used to assess reliability or accuracy of DOA measured near the location or area observed by the backscatter. However, specific backscatter irregularity configurations cannot yet be used to correct DOA data. We are optimistic that a general mapping program based on backscatter elevation angle information may be used to correct for large generalized tilts. However, the necessary implementation in the form of a Mills T processing array still requires some further development. The ITS 3-D ray-tracing program appears to be an accurate and useful tool for ionospheric study and it does check well with experimental data. We are hopeful that backscatter and elevation angle information can be used to estimate range rather accurately. Sidescatter has been observed rather extensively, and we expect to define its various characteristics to make it more readily identifiable to DF systems.

Reference

Tveten, L. H. and R. D. Hunsucker (1969), "Remote sensing of the terrestrial environment with an HF radio high-resolution azimuth and elevation scan system." Proc IEEE, 57, No 4 April 1969, 487-493.

N. NARAYANA RAO

Department of Electrical Engineering
University of Florida, Gainesville, Florida

RAY TRACING SIMULATION OF IONOSPHERIC EFFECTS IN HIGH FREQUENCY RADIOLOCATION

1. SUMMARY

Deviation of high frequency radio waves from the great circle plane containing the transmitter and the receiver due to horizontal gradients, irregularities and other effects in the ionosphere is a dominant factor in HF radiolocation. In order to correct for the deviations in the experimentally measured angles of arrival and determine the unknown location of the source, it is first necessary to fully understand the role played by the ionosphere. This is done by the application of radio ray-tracing techniques to signals from sources of known location

The Radiolocation Research Laboratory, in cooperation with the ESSA Research Laboratories, conducted a series of experiments in which the direction-of-arrival observations of high frequency signals transmitted from a site near Houston, Texas, were made continuously for a period of one week per month using the Wullenweber array at the Bondville Road Field Station during the period March, 1967 - March, 1968. This paper is concerned with the ray tracing simulation of certain ionospheric effects observed during this experiment. The bearing deviations obtained from the ray tracing simulation are compared with the measured values during the same period.

Ionospheric effects on the direction-of-arrival of HF signals due to the following phenomena are discussed:

a) Horizontal gradients of electron density due to the sunrise effect, or the "sunrise tilts."

b) Quasi-periodic fluctuations in the tilts with periods of the order of 20 minutes for single mode case.

c) Magnetoionic effect.

Techniques ranging from simple mirror reflection to the most general method using Hiselgrove equations are employed in the simulation. The results presented in this paper have been published (see references) and the reader is referred to those papers for complete details.

REFERENCES

Rao, N.N.,"Ray Tracing Investigation of Direction of Arrival Observations of HF Radio Waves," Radio Science (New Series), Vol. 3, No. 8, pp. 796-802, August 1968.

Rao, N.N.,"Bearing Deviation in HF Transionospheric Propagation, I. Exact Computations for Some Ionospheric Models with No Magnetic Field," Radio Science (New Series), Vol. 3, No. 12, pp. 1113-1118, December 1968.

Rao, N.N.,"Bearing Deviation in HF Transionospheric Propagation, II. Applications of Exact Computations," Radio Science (New Series), Vol. 3, No. 12, pp. 1119-1123, December 1968.

Rao, N.N.,"Bearing Deviation in HF Transionospheric Propagation, III. Ray Tracing Investigation of the Magnetoionic Effect," Radio Science, Vol. 4, No. 2, pp. 153-161, February 1969.

Rao, N.N.,"Direction of Arrival of HF Radio Waves Deduced from Ionospheric Electron Content Gradients," IEEE Transactions on Antennas and Propagation, Vol. AP-17, No. 1, pp. 111-113, 1 January 1969.

ERIC A. WALTON

[illegible]

SHORT RANGE HIGH ANGLE STUDIES

In attempting to perform short-range radiolocation, it is necessary to work with a signal which arrives at the radiolocation site at angles near the zenith (directly overhead). Signals from less than 100 km distant reflecting from an ionosphere at a virtual height of more than 150 km, for example, will have this property. The ray path geometry is shown in Figure 1. This signal will also consist of two independent components, the ordinary component and the extraordinary component.

Also, since a radio signal is polarized in the plane normal to its propagation direction, it will appear horizontally polarized. It is this kind of signal that must be used in short range RDF.

This set of conditions makes several demands on the antennas and indicating equipment. The antennas must be horizontally polarized so that sensitivity is not lost. They should also be circularly polarized so that the ordinary mode (left-hand circularly polarized) and the extraordinary mode (right-hand circularly polarized) do not interfere with each other. Finally, they should be omnidirectional so that signals from all directions will be acceptable.

The expected direction of arrival of the signal also places some special requirements on the indicating equipment. It should display the incidence angle as well as the bearing of the received signal. This incidence angle information can be used to make an estimate of the

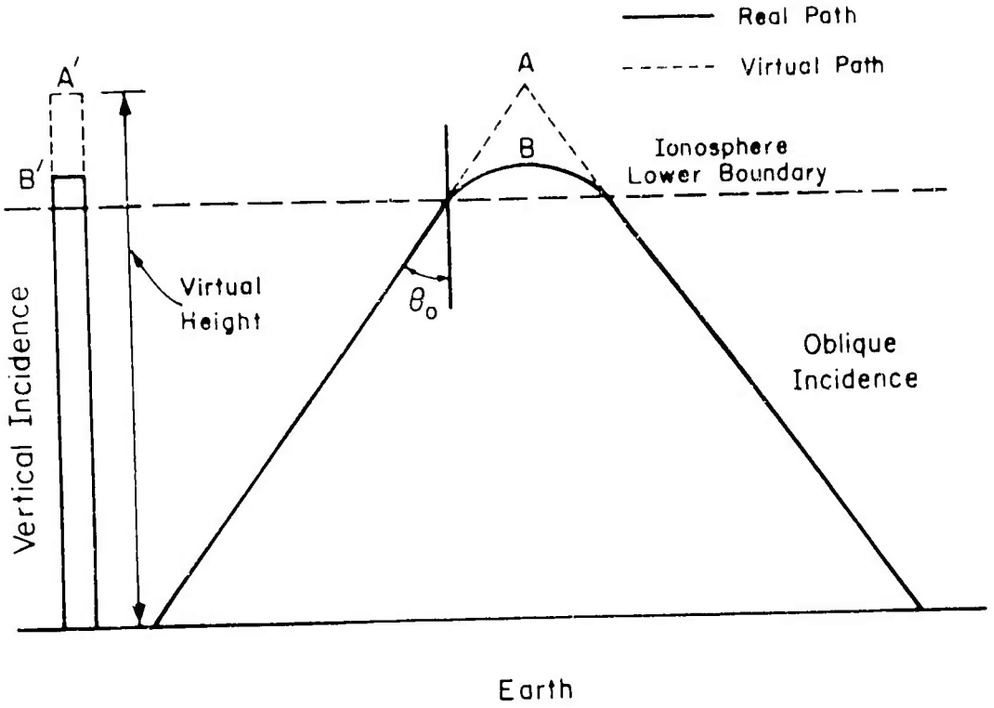

Figure 1. Virtual Ray Path for Plane Ionosphere Model.

range of the transmitting station when coupled with some available ionospheric information.

An example of a system of this kind is shown in Figure 2. This figure is a block diagram of the University of Illinois triple radio interferometer system. A basic set of three antennas is used to give three interferometer pairs. These three pairs of antennas are time-shared by a dual channel receiver and phase display system. The direction of arrival is computed with the available analog computer or by a digital computer using the phase information stored on punched paper tape.

Some more information should be given on the antennas which are used in this system. Each antenna is a pair of crossed loops connected to a quadrature hybrid coupler. The result is a horizontally polarized antenna with two outputs, a right-hand circularly polarized output and a left-hand circularly polarized output. We may thus choose the polarization we want at any time. These antennas are also omnidirectional in bearing angle and nearly omnidirectional in zenith angle. Thus, all of the antenna requirements for radio direction finding at short range and high angles have been met. The physical separation between adjacent antennas is 100 meters.

The signals from these antennas are received as three pairs of signals using time sharing of a dual channel receiver. The three differential phase angles are presented as shown in Figure 2 to an analog system and (via punched paper tape) to a digital computer. These computers solve equations such as shown in Figure 3 and display the angles of arrival of the signal.

To be used subject
to the criterion:

$$1/4 < \frac{d}{\lambda} < 4$$

d = 100 meters

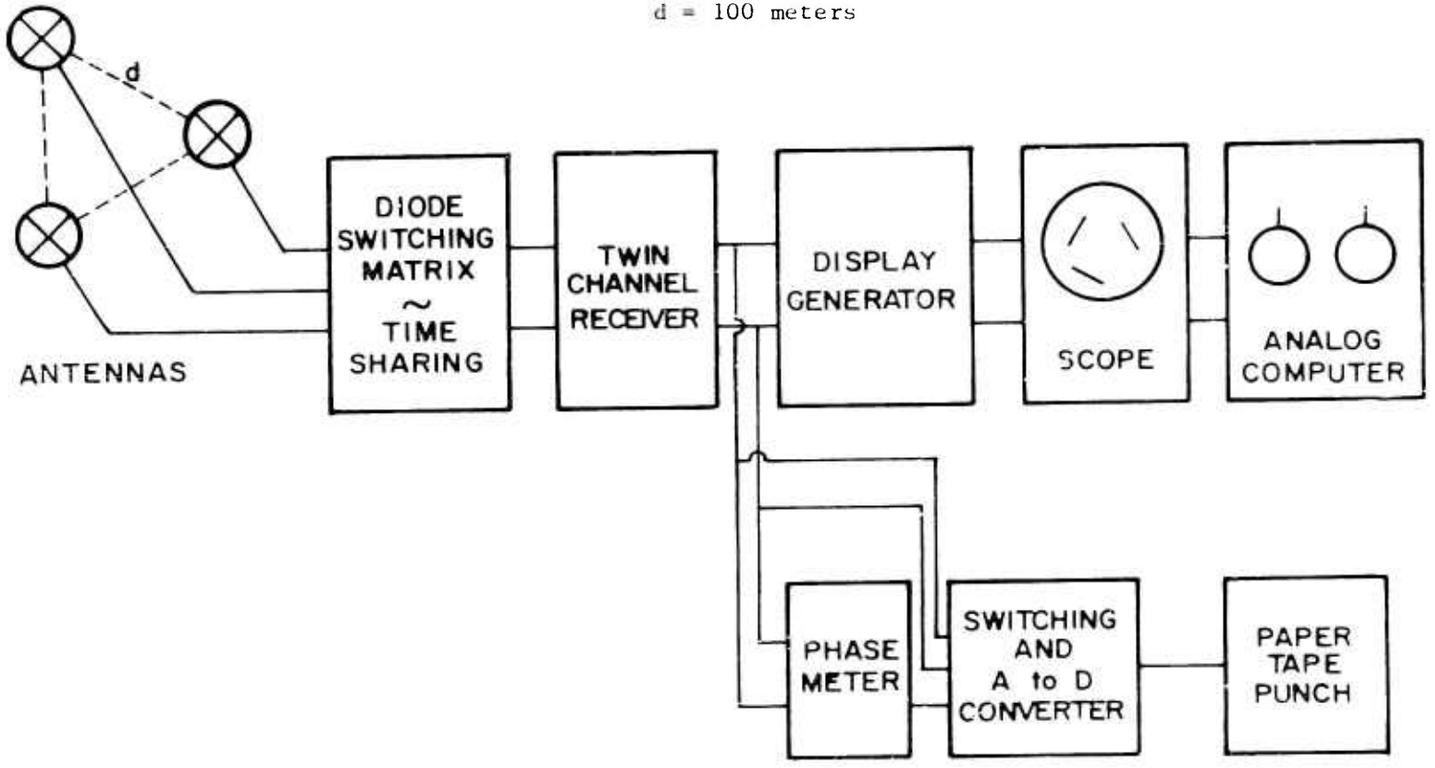

Figure 2. Functional Block Diagram. Triple Interferometer.

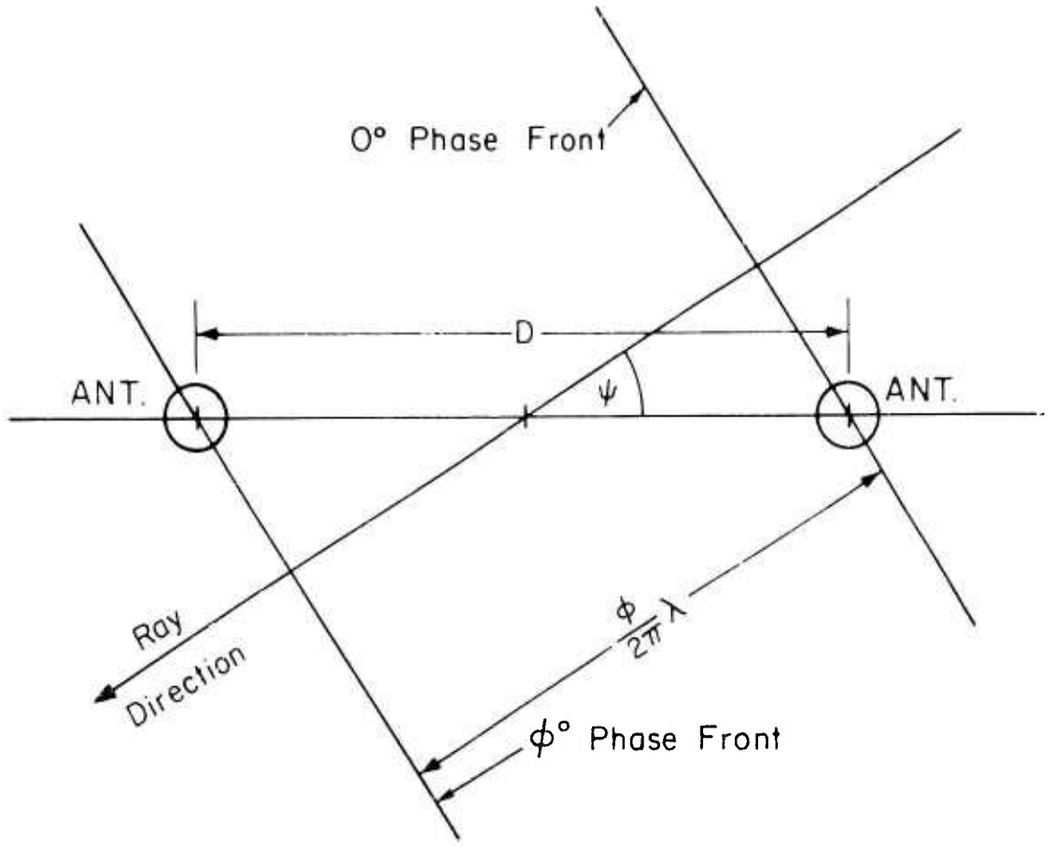

Measured phase ϕ

Wavelength λ

Angle ψ to be measured

$$\psi = \cos^{-1}\left[\frac{\phi\lambda}{2\pi D}\right]$$

Figure 3. Interferometer Pair.

One other piece of equipment is used in the short range studies. Located at the RDF site is a vertical incidence ionosonde. Ionograms are instantly available and also recorded on film for further analysis.

These data can now be used to estimate the range to the transmitter. The first approximation is the so-called "flat ionosphere" model shown in Figure 4. The angle of incidence is used in conjunction with the virtual height for that frequency to find the range using the geometry of Figure 4. The bearing to the transmitter is just the bearing of the signal. We have thus "located" the transmitter using a single RDF site.

More sophisticated techniques may be used, of course, beyond this first approximation. We may go one step beyond the assumption of a horizontal flat mirror-like ionosphere and use a "tilted" mirror. This tilted mirror model can be used, as a first approximation, to absorb all sources of deviation of the signal from the flat ionosphere model if some method of determining the "apparent tilt" parameters of the ionosphere can be found.

Even more sophisticated models are possible. Three-dimensional ray tracing using some method of estimating the lateral as well as vertical electron density distribution would perhaps yield a better estimate of the position of the transmitter.

A typical short range radiolocation experiment was performed on 6 March 1969. Two transmitters were set up as shown in Figure 5. Data were taken at alternating times on the target transmitter and on the beacon transmitter. The flat ionosphere model used on the target transmitter produced the results shown in Figure 6. Note that the average fix is about 18 km from the true position. Next, data from the beacon

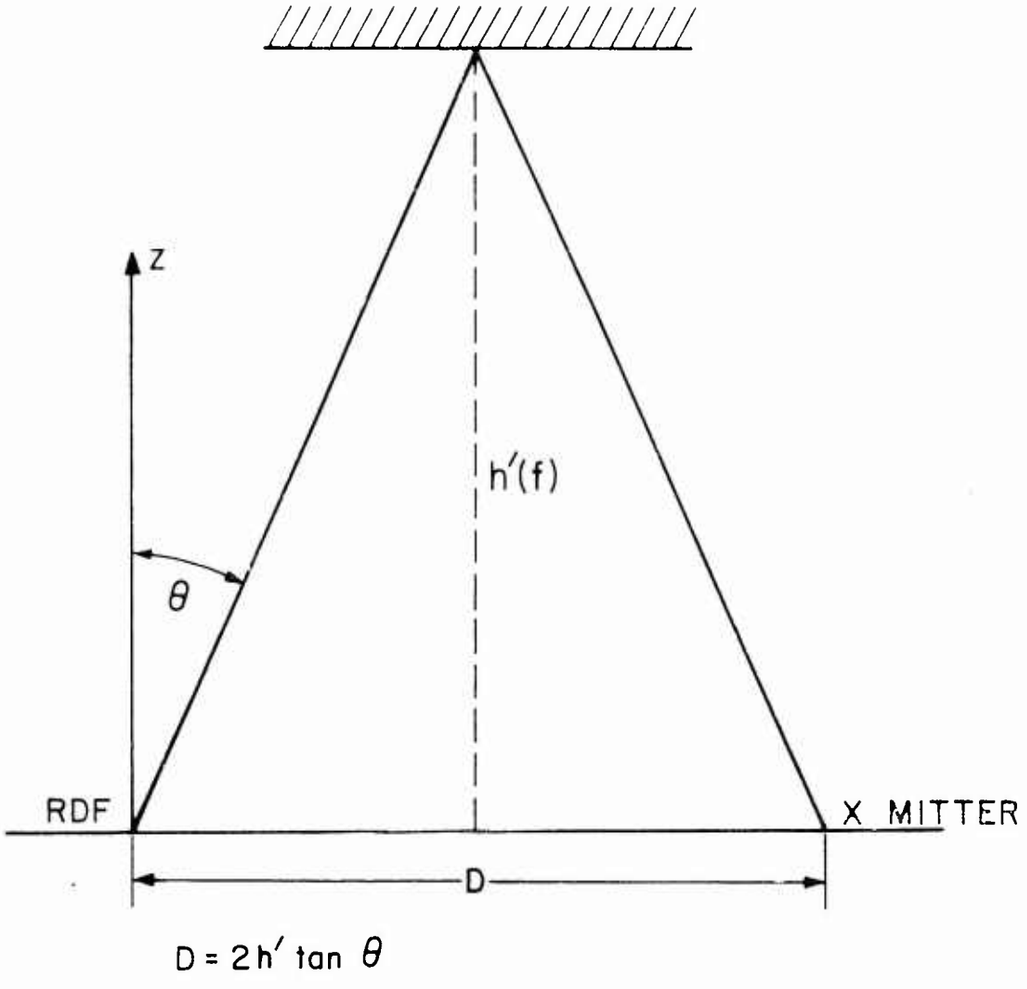

Figure 4. Simple Case.

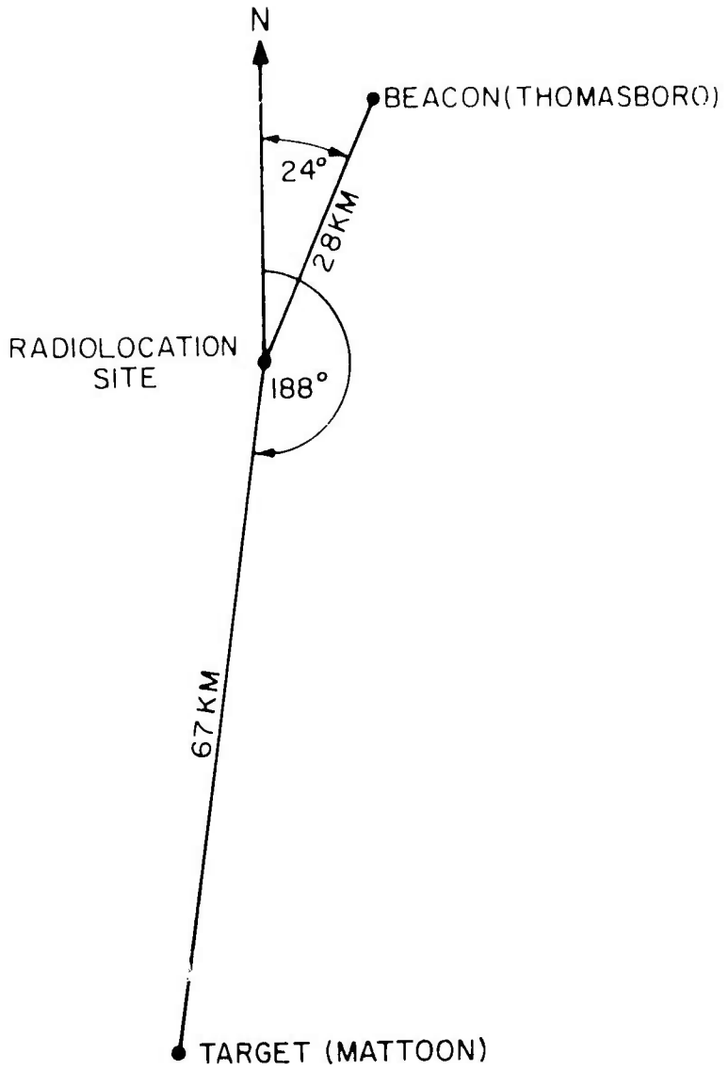

Figure 5. Geometry of Experiment.

FIX ON MATTOON LAKE BEFORE CORRECTION
DATE 3-6-69 11:52 A.M – 12:01 P.M. LT
FREQ. = 4.625 MHz
1 HOP F LAYER

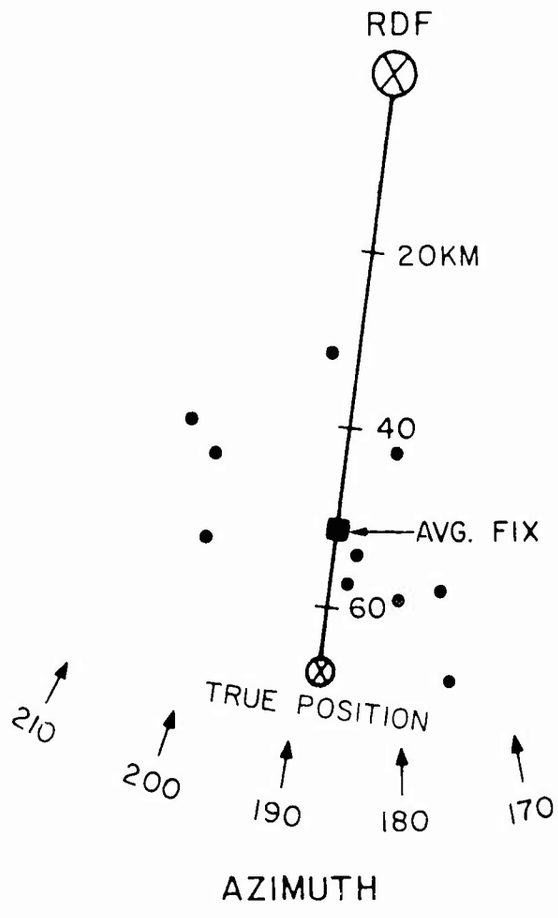

Figure 6. Fix on Mattoon Lake before Correction.

transmitter were used to compute the ionospheric tilt parameters. The tilted ionosphere model is shown in Figure 7. This tilted model was then used to recalculate the position of the target transmitter. The results are shown in Figure 8. Note that the average fix is now only about 5 km. from the true position. Thus, we were able to improve on the flat ionosphere model in this example.

More work of this kind is being done. The tilted ionosphere model and some of the more sophisticated models need to be fully studied if they are to be used in the future.

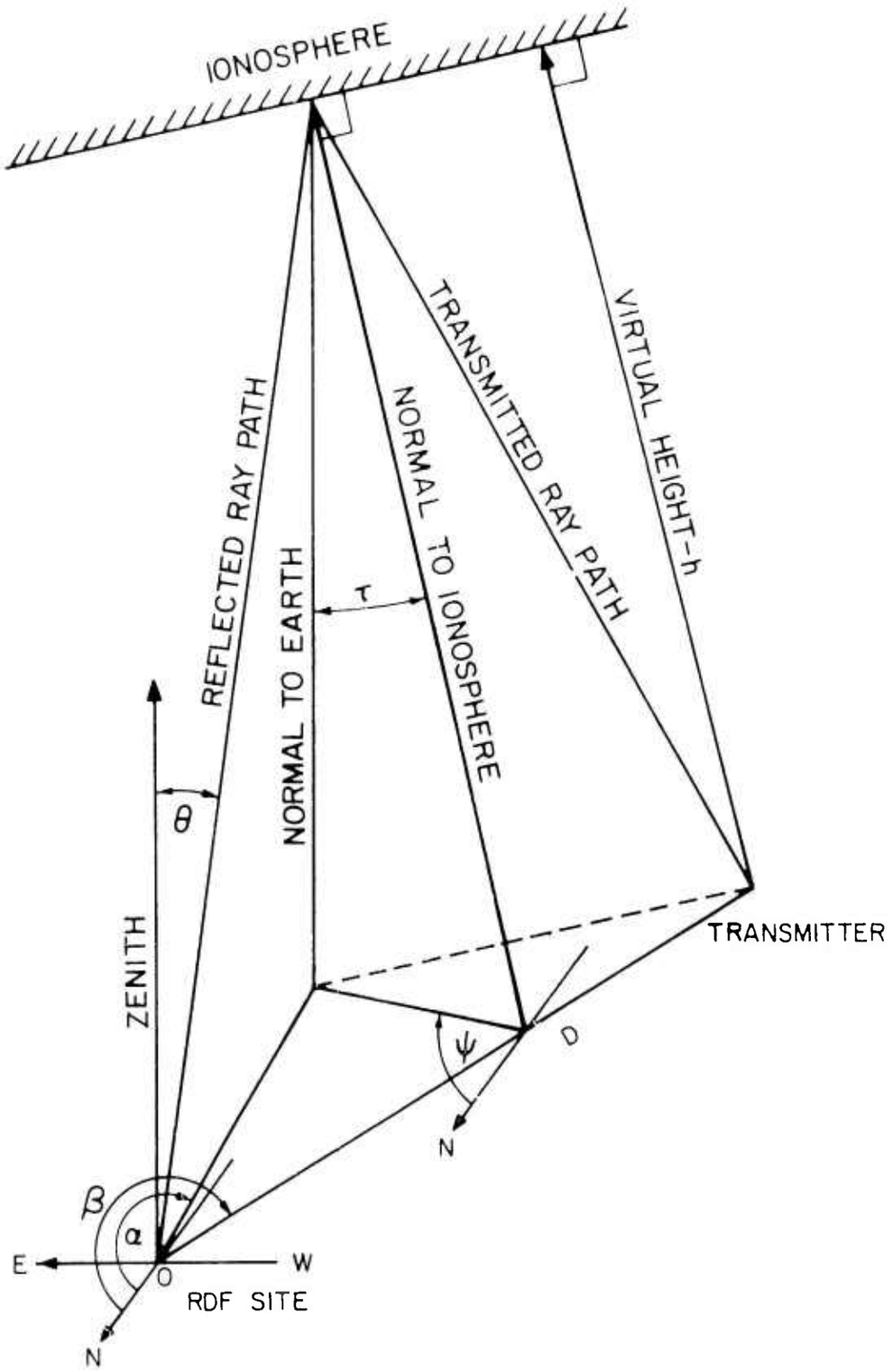

Figure 7. Geometry Pertinent to Calculation of Ionospheric Tilt.

FIX ON MATTOON LAKE AFTER CORRECTIONS
DATE 3-6-69 11:52 A.M. - 12:01 P.M. LT
FREQ. = 4.625 MHz
1 HOP F LAYER

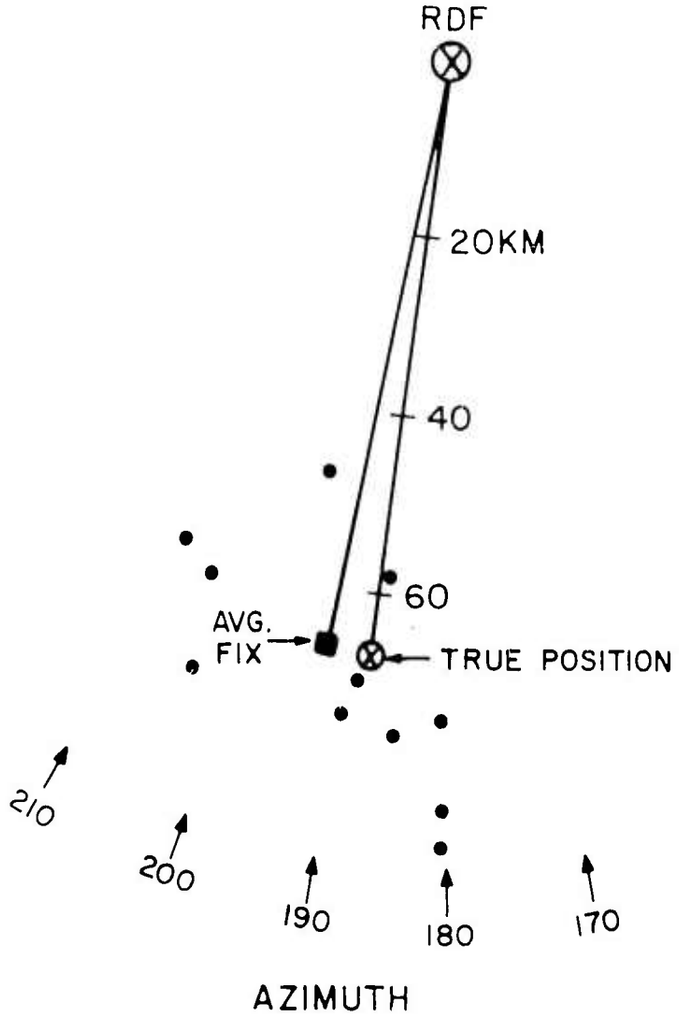

Figure 8. Fix on Mattoon Lake after Corrections.

C. R. TALBOTT

[illegible]

APERTURE SIZE EFFECTS IN A HF INTERFEROMETER RDF SYSTEM*

1. INTRODUCTION

A dual interferometer radio direction finding (RDF) system utilizes both a small aperture and a large aperture antenna array. The distance between the antennas of a small aperture array is less than one-half wavelength over the range of operating frequencies. The opposite is true for a large aperture array. In the past the small aperture (or large aperture) distance was usually dictated by considerations other than those dealing with the relationships between the antenna aperture and the error in the bearing information. The need, therefore, exists to determine this relationship.

This paper is a study of the error generated in the angles of arrival and how it varies with the aperture size of the antenna array. This relationship will be examined under the effects of signal noise, equipment noise, and interference by a secondary wave. A three antenna interferometer system will be simulated using a digital computer. The root mean square (RMS) error of the angles of arrival will be calculated at several aperture sizes ranging from 1/20 wavelength to 5 wavelengths The relationship between the (RMS) error and aperture size will be compared with the relationship obtained from a statistical approach to the problem in order to corroborate the results of both approaches.

The simulation model used in this paper is based on the work by Church[1], which unified and expanded part of the previous works of Creasy[2], Grush[3], and Allen[4].

---

*Submitted in partial fulfillment of the requirements for the degree of Master of Science in Electrical Engineering. Mr. Talbott is currently with TRW, Redondo Beach, California.

TABLE OF CONTENTS

LIST OF FIGURES

CHAPTER 1 -- INTERFEROMETER SYSTEM

The interferometer RDF system studied in this paper uses three monopole antennas located as shown in Figure 1. It will be assumed that two plane waves are incident upon the antenna array. The stronger amplitude wave is designated as the primary wave and the other is called the secondary wave.

The ray path of either wave is defined to be any line which is perpendicular to the phase front of that wave. The azimuthal angle (ϕ) of an incident wave is taken to be the angle between the North reference line and the ground plane projection of the ray path as shown in Figure 1. The azimuthal angle can vary between $\pm \pi$ and is measured positive in the clockwise direction. The incidence angle (θ) is the angle between a normal to the ground plane and the ray path. The incidence angle can vary between 0 and $\pi/2$ and is measured positive from the normal.

The distance (D) measured between antennas 1 and 2 or antennas 1 and 3 is called the aperture size of the interferometer. Although the angle (γ) between antenna pairs (1,2) and (1,3) is assumed to be 60° in this paper, it can have other values.

In general, the directions of arrival of the primary wave and the secondary wave will differ. The direction of arrival is determined by the azimuthal angle and the incidence angle of the wave. The difference in the angles of arrival of the two waves is caused by ionospheric disturbances. Thus, the system sees a secondary wave which travels along a different propagation path than the primary wave. The

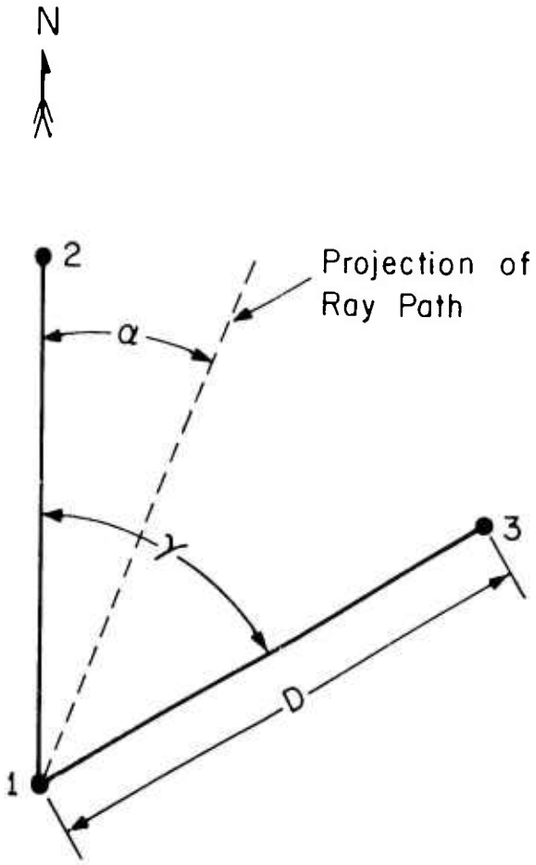

Figure 1 Interferometer RDF Configuration

difference in the propagation paths manifests itself in that the two incident waves have different amplitudes, a relative phase difference (ϕ), and different angles of arrival.

Bailey[6] has shown the relationship between the voltages induced in the antennas by the incident waves and the angles of arrival. If the primary wave phasor is represented as $\overline{E}_o\, e^{jwt}$, and the secondary wave phasor by $h \cdot \overline{E}_o\, e^{jwt}$, the voltages induced in the antennas can be represented as:

$$e_1 = \mathrm{Re}[\overline{E}_o\, e^{jwt} + h \cdot \overline{E}_o\, e^{j(wt + \phi)}]$$

$$e_2 = \mathrm{Re}[\overline{E}_o\, e^{j(wt + NX_p)} + h \cdot \overline{E}_o\, e^{j(wt + \phi + NX_s)}]$$

$$e_3 = \mathrm{Re}[\overline{E}_o\, e^{j(wt + NY_p)} + h \cdot \overline{E}_o\, e^{j(wt + \phi + NY_s)}]$$

where

$$N = 2 \cdot D/\lambda$$

$$X_p = \pi \cos \alpha_p \sin \theta_p$$

$$X_s = \pi \cos \alpha_s \sin \theta_s$$

$$Y_p = \pi \cos (\alpha_p - \gamma) \sin \theta_p$$

$$Y_s = \pi \cos (\alpha_s - \gamma) \sin \theta_s$$

and Re is the real part operator. The other symbols not previously defined are defined as follows:

w = signal frequency, in radians/sec

t = time, in seconds

λ = wavelength, in meters

h = relative amplitude factor, where $0 \leq h \leq 1$.

The antenna voltages can be expressed in phasor notation as follows:

$$\overline{E}_1 = \overline{E}_o + h \cdot \overline{E}_o \, e^{j\phi}$$

$$\overline{E}_2 = \overline{E}_o \, e^{jNX_p} + h \cdot \overline{E}_o \, e^{j(\phi + NX_s)}$$

$$\overline{E}_3 = \overline{E}_o \, e^{jNY_p} + h \cdot \overline{E}_o \, e^{j(\phi + NY_s)}$$

For simplicity let us normalize these phasor voltages by setting $\overline{E}_o = 1$. We obtain:

$$E_1 = [1 + h \cdot \cos \phi] + j[h \cdot \sin \phi] \tag{1-1}$$

$$E_2 = [\cos NX_p + h \cdot \cos(\phi + NX_s)] + j[\sin NX_p + h \cdot \sin(\phi + NX_s)] \tag{1-2}$$

$$E_3 = [\cos NY_p + h \cdot \cos(\phi + NY_s)] + j[\sin NY_p + h \cdot \sin(\phi + NY_s)] \tag{1-3}$$

Creasy[2] determined (using the magnitudes of the phasor voltages and the phasor difference of the voltages at antennas i and j) the phase difference (B_{ij}) between the induced voltages of the two antennas. The phase difference is:

$$B_{ij} = \tan^{-1} \left[\frac{-(|E_i|^2 + |E_j'|^2 - |E_j' - E_i|^2)}{|E_i|^2 + |E_j|^2 - |E_j - E_i|^2} \right] \tag{1-4}$$

where $\overline{E}_j' = \overline{E}_j \, e^{j90°}$.

Equations (1-1) through (1-4) indicate that the phase difference between antenna voltages (B_{ij}) is a function of the phase difference

(ϕ) between the two incident waves. In his investigations Glick[5] assumed that the relative phase could be approximated to be uniformly distributed if the relative phase of the incoming wave is sampled at uniform intervals of time. Applying this assumption Glick[5] showed that the average (with respect to ϕ) phase difference (AVB_{ij}) was a function only of N and the primary angles of arrival. Using Glick's[5] results, Church[1] showed that the average phase difference between antennas is:

$$AVB_{12} = NX_p = N\pi \cos\alpha_p \sin\theta_p \tag{1-5}$$

$$AVB_{13} = NY_p = N\pi \cos(\alpha_p - \gamma) \sin\theta_p \tag{1-6}$$

Solving equations (1-5) and (1-6) for α_p and θ_p yields:

$$\alpha_p = \tan^{-1}\left[\frac{AVB_{13} - AVB_{12}\cos\gamma}{AVB_{12}\sin\gamma}\right] \tag{1-7}$$

$$\theta_p = \tan^{-1}\frac{1}{\left[\left(\frac{N\pi\cos\alpha_p}{AVB_{12}}\right)^2 - 1\right]^{1/2}} \tag{1-8}$$

where α_p in equation (1-8) is that determined in equation (1-7).

CHAPTER 2 -- SIMULATION ANALYSIS OF APERTURE SIZE

The interferometer RDF system has been simulated with a digital computer. The basic structure of the simulation parallels the more rigorous simulation scheme used by Church[1]. The simulation done in this paper was considerably simplified through the use of a priori information. The simulation has a closed loop form in that angles of arrival are used to calculate the same angles of arrival. Any deviations of the angles after simulation from the values before simulation are considered to be errors due to the interferometer system. The simulation of an interferometer system has many parameters all of which have an effect on the final results. Consideration of all of them and their interactions with one another would be difficult. In this paper the primary angles of arrival, aperture size, signal noise, and wave interference are considered to be of major interest, while the secondary angles of arrival, phase meter and system noise, signal frequency, and perturbations of the relative phase between the primary and secondary signals are considered to be of lesser interest.

In the interferometer simulation by Church[1] two problems of considerable importance have to be resolved. The first problem has to do with a "2π" ambiguity which exists between the measured phase difference (BM_{ij}) from the actual antenna voltages and the theoretical phase difference (B_{ij}) obtained from equation (1-4). The relation which exists between these two phase differences can be expressed as:

$$B_{ij} = BM_{ij} \pm k_{ij} \cdot 2\pi, \quad k = 0,1,2,... \tag{2-1}$$

where k_{ij} has to be determined and the pair (ij) can be either (12) or (13). The actual measured phase difference can only vary from $-\pi$ to $+\pi$; whereas, B_{ij} can vary over a much larger range of values. Church[1] described in his paper a method whereby k_{ij} could be evaluated using a dual interferometer system. Since this paper does not focus on this problem, a way is found to avoid it. This method incorporates equations (1-5) and (1-6) which tell exactly what B_{ij} will yield when it is correctly averaged with respect to ϕ. k_{ij} is found with a knowledge of AVB_{ij} from equation (1-5) or (1-6) since it represents the multiple of 2π needed to normalize AVB_{ij} to within the range from $-\pi$ to $+\pi$. The "2π" ambiguity is, thus avoided for the present simulation.

The second problem is that of finding the proper branch cut of the inverse tangent function in equation (1-4) so that the instantaneous B_{ij} will form a continuous distribution. If a branch cut is chosen that makes the B_{ij} distribution discontinuous the correct value of AVB_{ij} will not be obtained when the B_{ij}'s are averaged with respect to ϕ. Allen[4] developed techniques to properly determine the branch cut when real interferometer data are used; however, this problem can also be avoided in the present simulation by using the calculated values of AVB_{ij} from equations (1-5) and (1-6). The correct branch cut can always be found when one knows AVB_{ij}. The relationship between the two can be expressed as:

$$n = AVB_{ij} - 180° \qquad (2-2)$$

where n is the branch cut. It should be emphasized that the AVB_{ij} used in the present simulation to avoid the "2π" ambiguity and branch cut

problems is not available when one uses real interferometer data.

In order that the simulation more closely approximate the real interferometer system, random factors were incorporated into the simulation to account for the perturbations and noise. The random factors were all of the form X·RND(A), where RND(A) is a number taken from a pseudo random number generator that generates values from a Gaussian distribution with a mean of zero and standard deviation of one. X is a scaling factor. The voltage phasor of antenna 1 given by equation (1-1) can then be represented with a perturbation as:

$$E_1 = [1 + h\cdot\cos\ \ + T\cdot RND(A)] + j\ [\sin\ \ + T\cdot RND(A)] \qquad (2\text{-}3)$$

where the scaling factor, T, can be seen to be the standard deviation of the signal noise. The voltages for the other antennas are modified in a similar manner. Phase meter and system noise are included by adding S·RND(A) to B_{ij}. Also a perturbation, PER·RND(A), is added to every ϕ.

Once the B_{ij}'s have been averaged to yield AVB_{ij}, equations (1-7) and (1-8) can be used to find the primary azimuthal angle and the primary incidence angle. The calculated angles of arrival are determined sixteen times for each aperture size (D) in order to obtain the root mean square (RMS) error of the arrival angles. Each of the sixteen calculations would be the same if the same value of RND(A) were used. However, different values of RND(A) are used for each of the calculations. The RMS error can be expressed as:

$$\text{RMS error} = \left[\frac{\sum_{1}^{16} (\text{Calculated angle} - \text{Actual angle})^2}{16}\right]^{1/2} \qquad (2\text{-}4)$$

The results of this analysis are described in Chapter 4 and the programs which were used are listed in Appendix C.

CHAPTER 3 -- STATISTICAL ANALYSIS OF APERTURE SIZE

Equation (2-4) was used to find the RMS error of the angles of arrival. However, the value which was obtained can be considered to be only an estimate of the RMS error based on sixteen samples. The confidence that we have in the estimate is related to the size of the group on which the estimate is based. Ideally we prefer to base our estimate on a group with a very large number of samples.

Sixteen samples were used in the simulation analysis because larger group sizes necessitated the use of an impractical amount of digital computer time. This group size was still able to yield meaningful tendencies in the results of the simulation analysis. Applying statistical techniques we can determine the RMS error based on a very large group size using only a nominal amount of computer time. The tools to be used for the statistical analysis are the standard deviations of both the primary azimuthal angle (σ_{α_p}) and the primary incidence angle (σ_{θ_p}).

Equation (1-7) indicates that α_p is a function of AVB_{12}, AVB_{13}, and γ. The standard deviation of α_p can then be expressed as:

$$\sigma_{\alpha_p} = \left[\left(\frac{\partial \alpha_p}{\partial AVB_{12}}\bigg|_Q\right)^2 \cdot \sigma^2_{AVB_{12}} + \left(\frac{\partial \alpha_p}{\partial AVB_{13}}\bigg|_Q\right)^2 \cdot \sigma^2_{AVB_{13}} + \left(\frac{\partial \alpha_p}{\partial \gamma}\bigg|_Q\right)^2 \cdot \sigma^2_{\gamma}\right]^{1/2} \tag{3-1}$$

where σ^2 represents variance and Q implies that the partial derivative is evaluated with a given set of parameters. In a similar manner equations (1-7) and (1-8) yield:

$$\sigma_{\theta_p} = \left[\left(\frac{\partial \theta_p}{\partial AVB_{12}}\bigg|_Q\right)^2 \cdot \sigma^2_{AVB_{12}} + \left(\frac{\partial \theta_p}{\partial AVB_{13}}\bigg|_Q\right)^2 \cdot \sigma^2_{AVB_{13}} + \left(\frac{\partial \theta_p}{\partial \gamma}\bigg|_Q\right)^2 \cdot \sigma^2_{\gamma}\right]^{1/2} \tag{3-2}$$

Since γ is a constant, σ^2_{γ} is zero.

The partial derivatives needed to evaluate equations (3-1) and (3-2) can be expressed as:

$$\frac{\partial \alpha_p}{\partial AVB_{12}} = \frac{AVB_{13}}{(AVB_{12})^2 \cdot \sin \gamma \cdot X_1} \tag{3-3}$$

$$\frac{\partial \alpha_p}{\partial AVB_{13}} = \frac{-1}{AVB_{12} \cdot \sin \gamma \cdot X_1} \tag{3-4}$$

where

$$X_1 = 1 + \left(\frac{AVB_{13} - AVB_{12} \cdot \cos \gamma}{AVB_{12} \cdot \sin \gamma}\right)^2$$

$$\frac{\partial \theta_p}{\partial AVB_{12}} = \frac{AVB_{12} - \cos \gamma \cdot AVB_{13}}{(N^2 \cdot \pi^2 \cdot \sin^2 \gamma \cdot X_2 - X_2^2)^{1/2}} \tag{3-5}$$

$$\frac{\partial \theta_p}{\partial AVB_{13}} = \frac{AVB_{13} - \cos \gamma \cdot AVB_{12}}{(N^2 \cdot \pi^2 \cdot \sin^2 \gamma \cdot X_2 - X_2^2)^{1/2}} \tag{3-6}$$

where $X_2 = (AVB_{12})^2 + (AVB_{13})^2 - 2 \cdot \cos \gamma \cdot AVB_{12} \cdot AVB_{13}$

The variances of AVB_{12} ($\sigma^2_{AVB_{12}}$) and AVB_{13} ($\sigma^2_{AVB_{13}}$) can be expressed in similar forms. Therefore, the use of AVB_{1j}, where j equals 2 or 3, will considerably simplify the work to follow. Since AVB_{1j} can be represented as:

$$AVB_{1j} = \frac{B_{1j}^{1} + B_{1j}^{2} + \ldots + B_{1j}^{180}}{180}$$

its variance can be written as:

$$\sigma^2_{AVB_{1j}} = \sum_{i=1}^{180} \left(\frac{\partial AVB_{1j}}{\partial B_{1j}^{i}} \bigg|_{Q} \right)^2 \sigma^2_{B_{1j}^{i}}$$

When the partial derivatives are evaluated the result is:

$$\sigma^2_{AVB_{1j}} = \frac{1}{(180)^2} \sum_{i=1}^{180} \sigma^2_{B_{1j}^{i}} \tag{3-7}$$

In order to find $\sigma^2_{B_{1j}^{i}}$ we write equation (1-4) in a simplified form:

$$B_{1j}^{i} = \tan^{-1} \left[\frac{E_{1R} E_{jI} - E_{jR} E_{1I}}{E_{1R} E_{jR} + E_{1I} E_{jI}} \right] \tag{3-8}$$

Using equation (3-8) $\sigma^2_{B_{1j}^{i}}$ can be written as:

$$\sigma^2_{B_{1j}^{i}} = \left(\frac{\partial B_{1j}^{i}}{\partial E_{1R}} \bigg|_{Q} \right)^2 \sigma^2_{E_{1R}} + \left(\frac{\partial B_{1j}^{i}}{\partial E_{1I}} \bigg|_{Q} \right)^2 \sigma^2_{E_{1I}} + \left(\frac{\partial B_{1j}^{i}}{\partial E_{jR}} \bigg|_{Q} \right)^2 \sigma^2_{E_{jR}} + \left(\frac{\partial B_{1j}^{i}}{\partial E_{jI}} \bigg|_{Q} \right)^2 \sigma^2_{E_{jI}} \tag{3-9}$$

Equation (2-3) shows that the variance of the real or imaginary part of the phasor voltage is equal to T^2. Since this is valid for all three antenna voltages, we have:

$$\sigma^2_{E_{1R}} = \sigma^2_{E_{1I}} = \sigma^2_{E_{2R}} = \sigma^2_{E_{2I}} = \sigma^2_{E_{3R}} = \sigma^2_{E_{3I}} = T^2 \tag{3-10}$$

Substitution of the partial derivatives and equation (3-10) into

equation (3-9) gives:

$$\sigma^2_{B^i_{lj}} = T^2 \cdot \frac{(E^2_{lI} + E^2_{lR})(E^2_{jR} + E^2_{jI})^2 + (E^2_{jI} + E^2_{jR})(E^2_{lR} + E^2_{lI})^2}{(E^2_{lR}\,E^2_{jR} + E^2_{lI}\,E^2_{jI} + E^2_{lR}\,E^2_{jI} + E^2_{jR}\,E^2_{lI})^2} \qquad (3\text{-}11)$$

Equations (3-1) through (3-7) with equation (3-11) can be combined to give the standard deviations of the primary angles of arrival as a function of T, the signal noise. The computer programs which applied this analysis are listed in Appendix D. The results of these programs are described in Chapter 4.

CHAPTER 4 -- RESULTS AND CONCLUSIONS

The number of parameters used in the present analysis necessitated that some should be assigned a constant value, which is typical of all the values in its range, and others should be varied over a range of values. The primary incidence angle (α_p), the secondary angles of arrival (α_s, θ_s), gamma, the frequency of the incident waves (f), and the perturbation (PER) of Φ are all assigned typical values. Although α_p is varied, its effect on the bearing error - aperture size relationship is not investigated in depth.

The dependent variables for the present analysis are the bearing errors (the errors in α_p and θ_p). The two major independent variables are the aperture size (D) and the standard deviation of the signal (T). The units of T are volts. The minor independent variables are the wave interference factor (h) and the standard deviation of the phase meter and system noise (S). The parameter h can vary from zero to one and represents the ratio of the amplitudes of the secondary incident wave to the primary incident wave. The parameter S has been described as the phase meter noise; however, in the simulation analysis it was chosen to account for all of the noise produced by the electronic equipment which processed the signals. The units of S are radians.

The data obtained from the statistical analysis and the simulation analysis are listed in Appendix A and Appendix B, respectively. Figures 2 through 13 represent these data in pictorial form; however, the representation is somewhat distorted. Figures 2 through 13 are traces of actual digital computer on-line printer output. The distortion arises

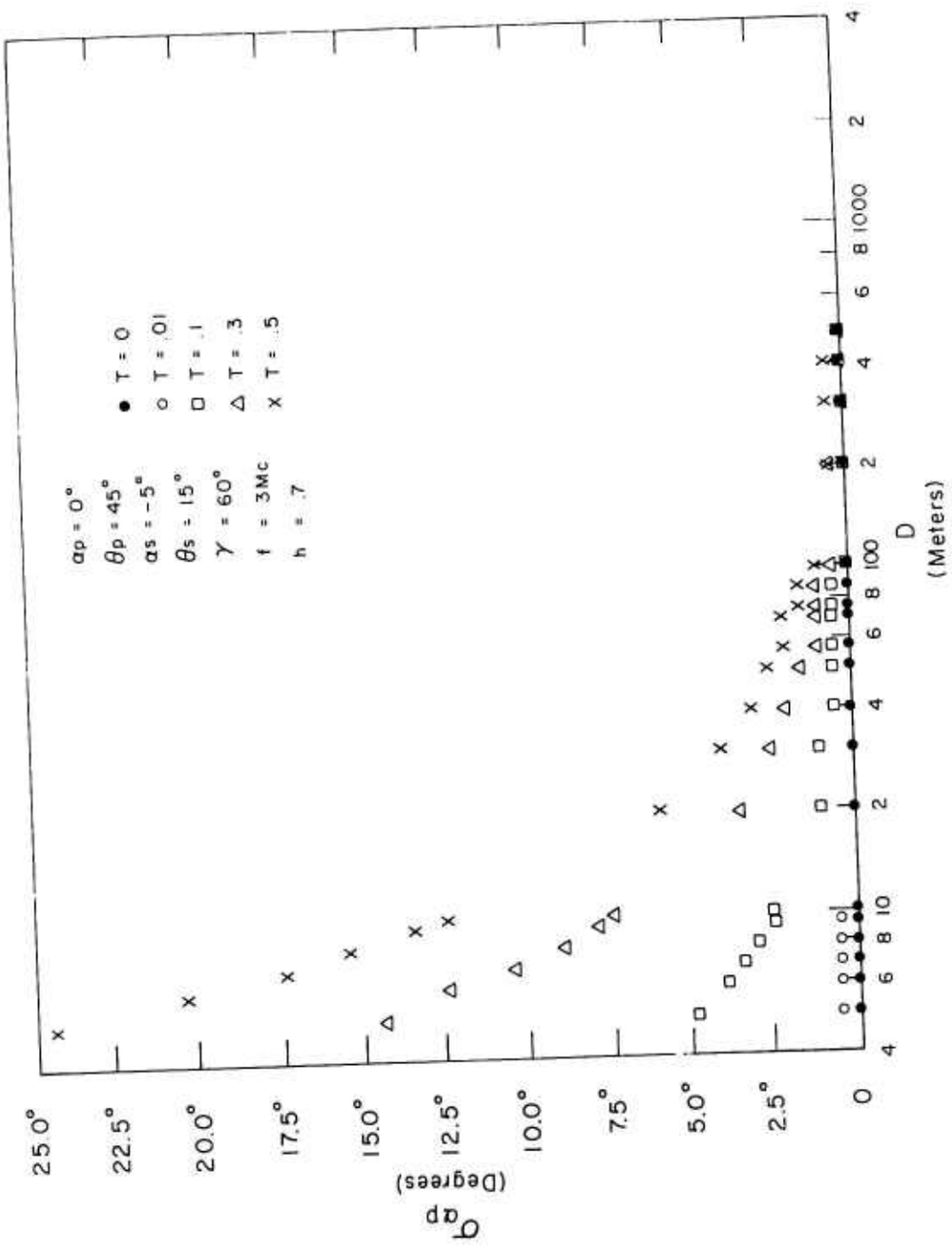

Figure 2 σ_{α_p} vs D

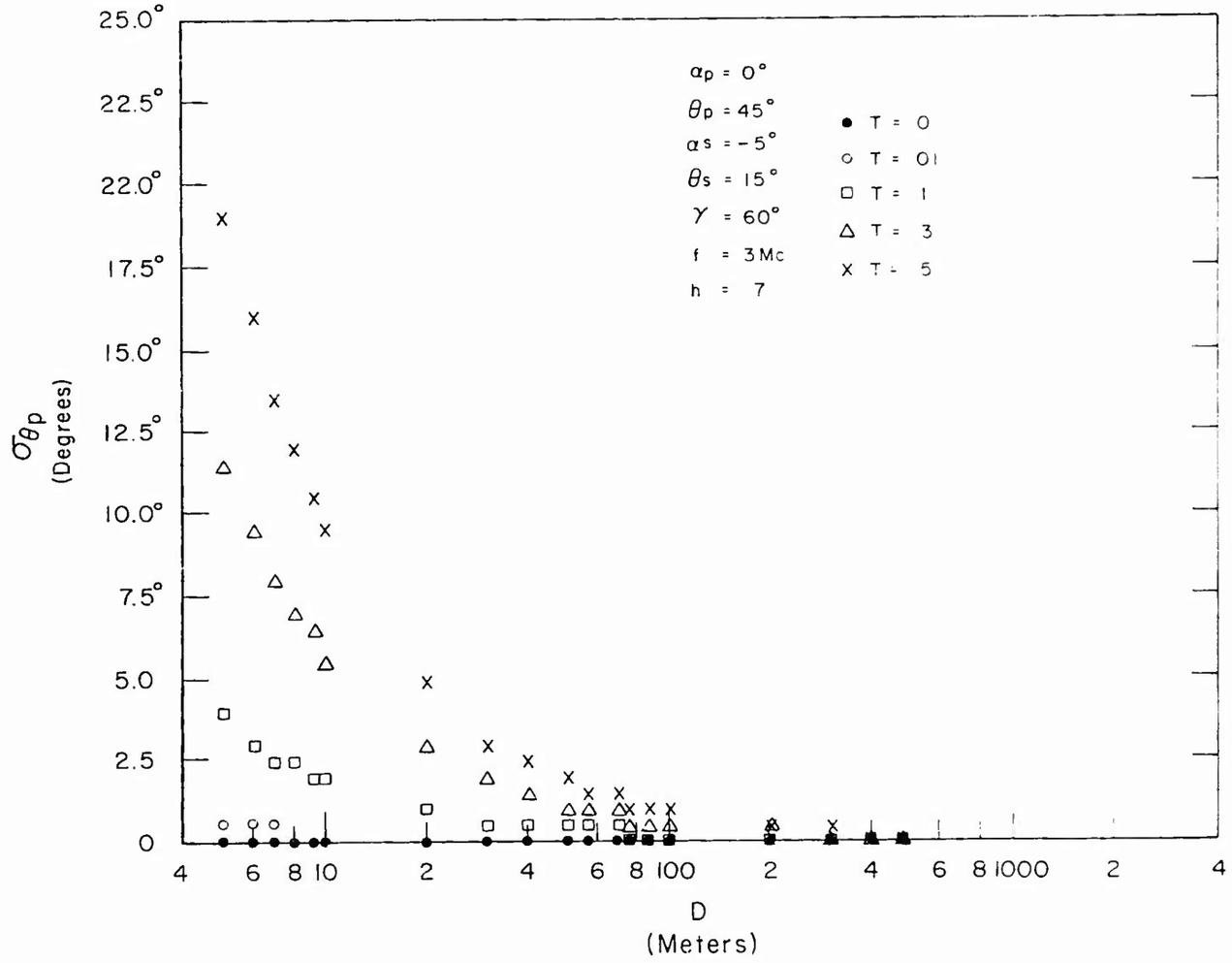

Figure 3 σ_{θ_p} vs D

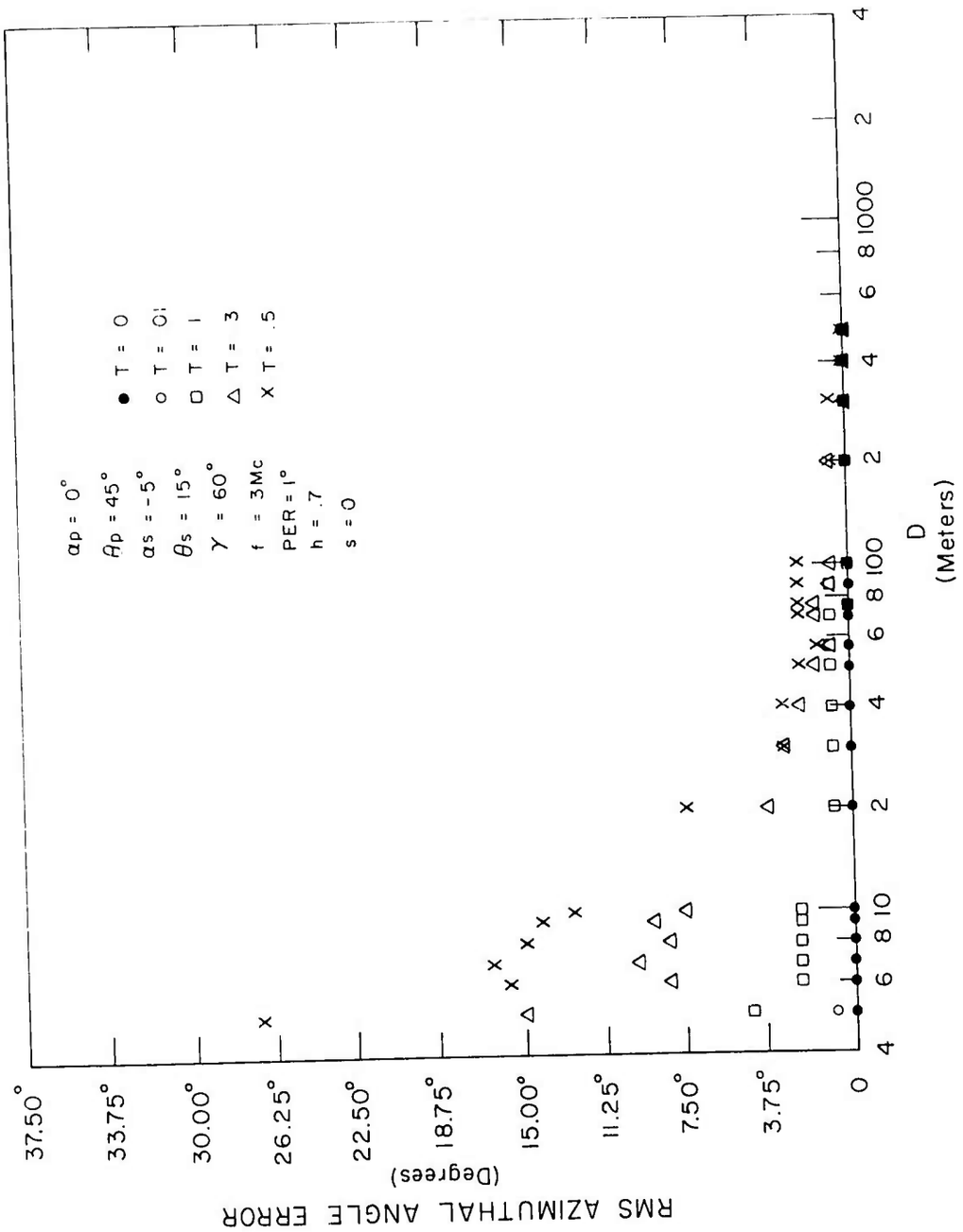

Figure 4 RMS Azimuthal Angle Error vs D -- Parameter T

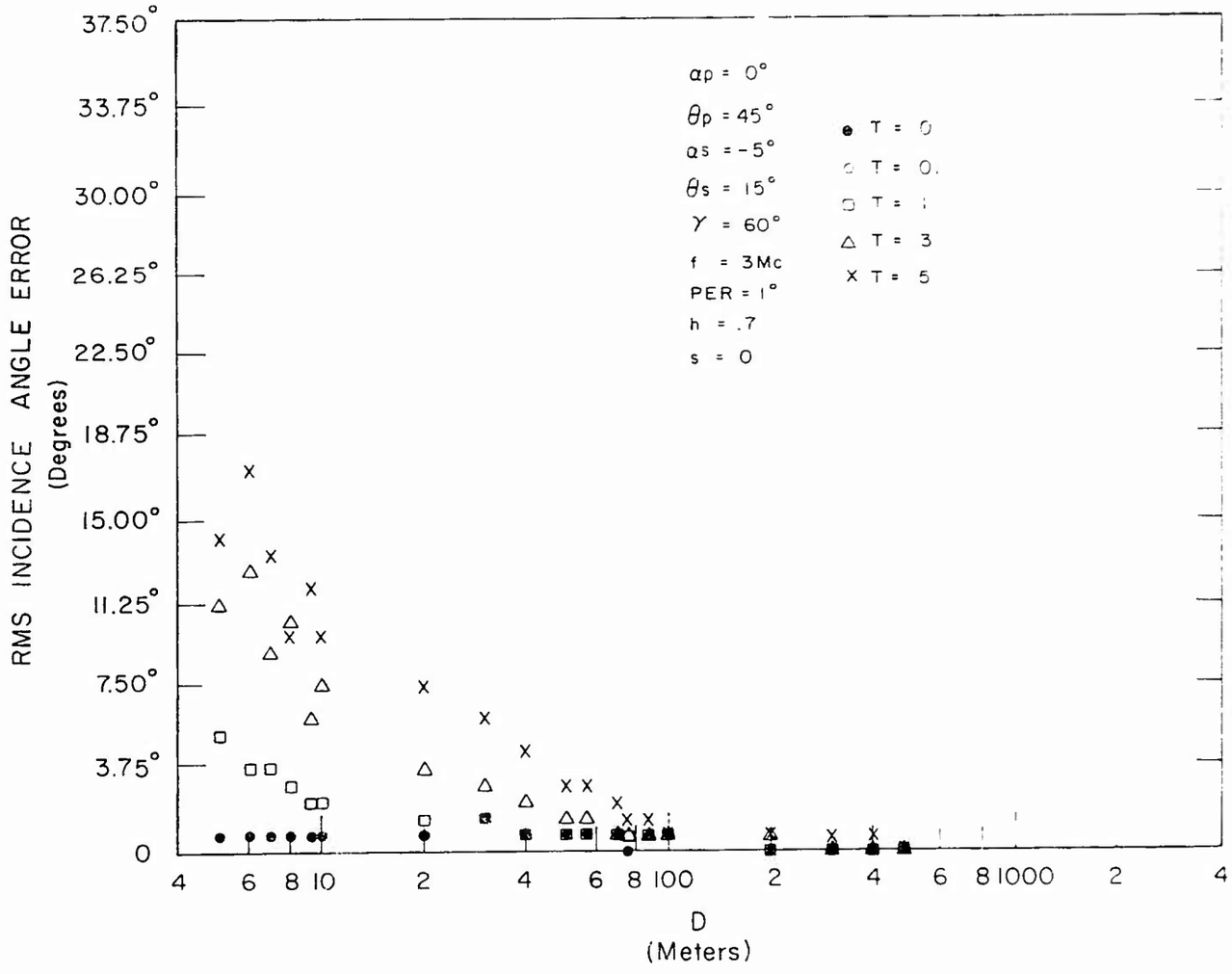

Figure 5 RMS Incidence Angle Error vs D -- Parameter T

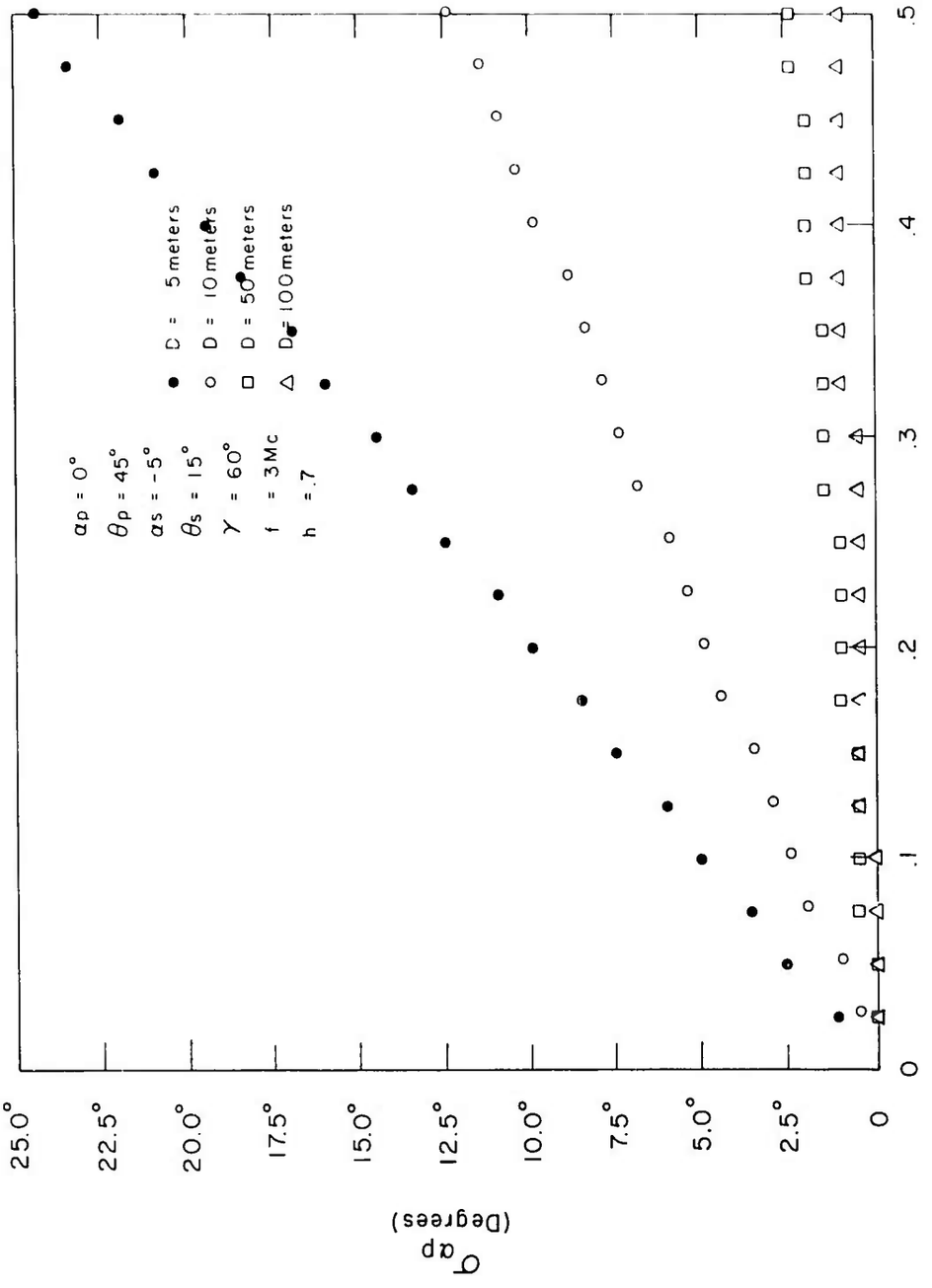

Figure 6 σ_{α_p} vs T

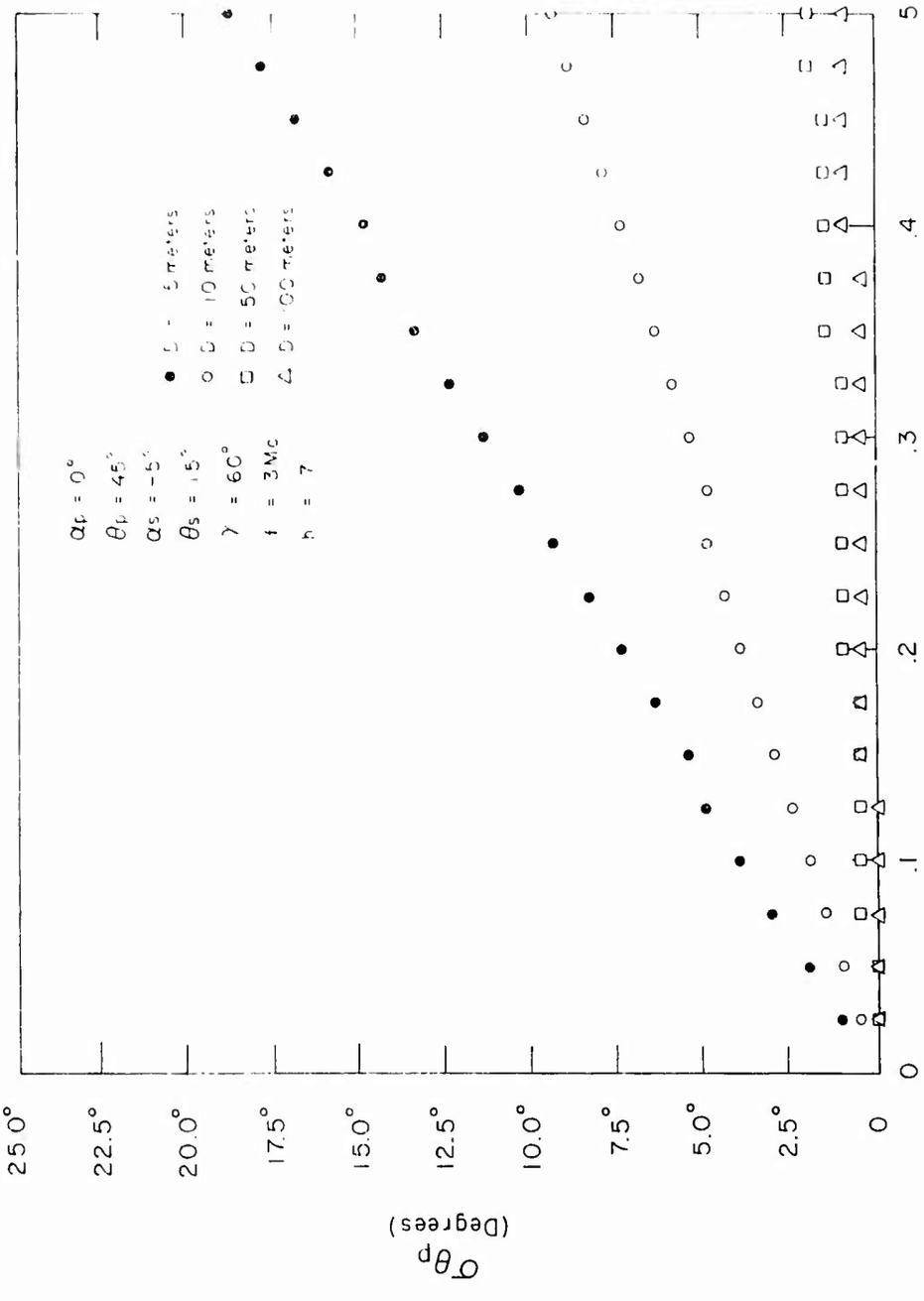

Figure 7 σ_{θ_p} vs T

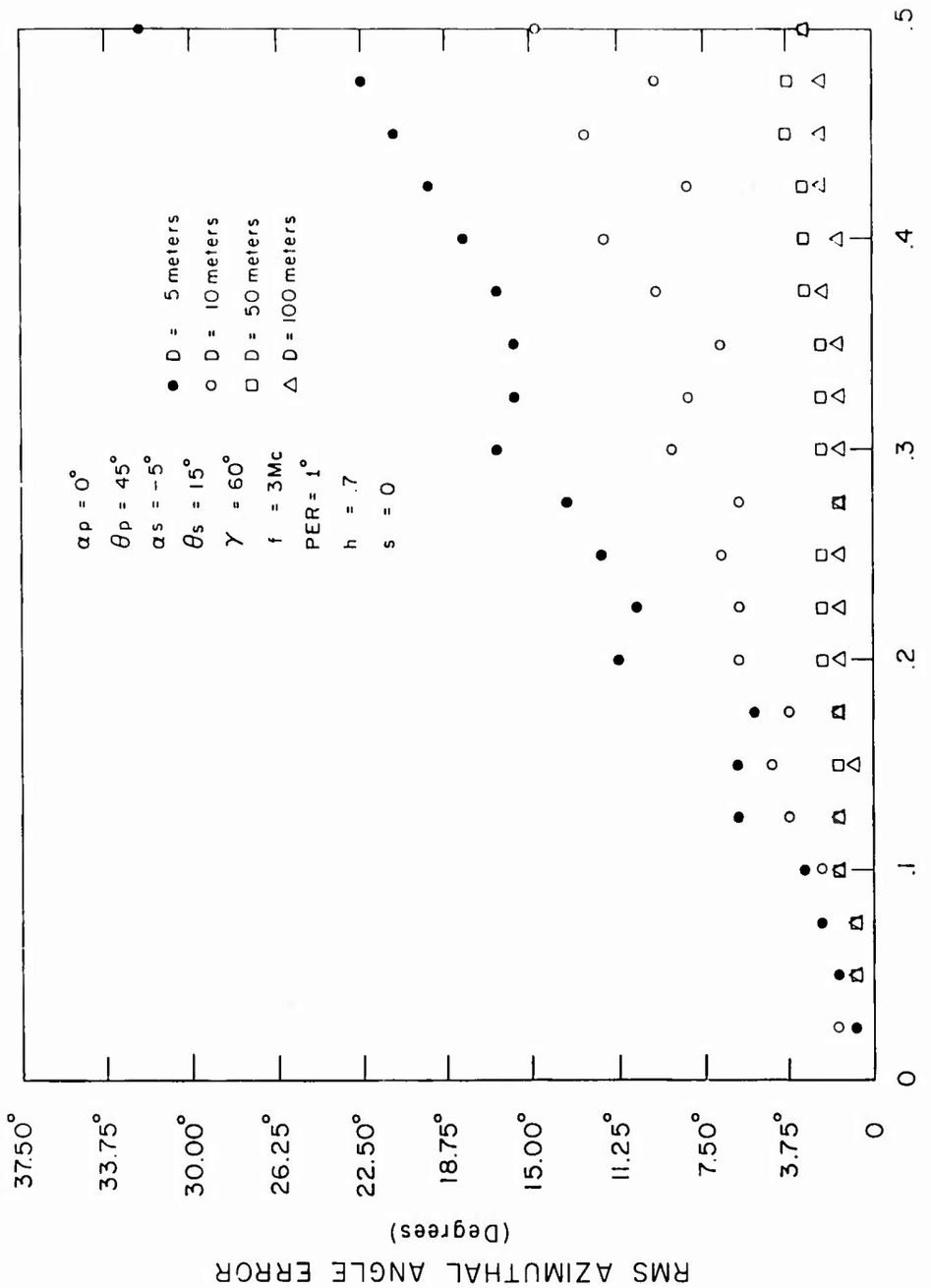

Figure 8 RMS Azimuthal Angle Error vs T -- Parameter D

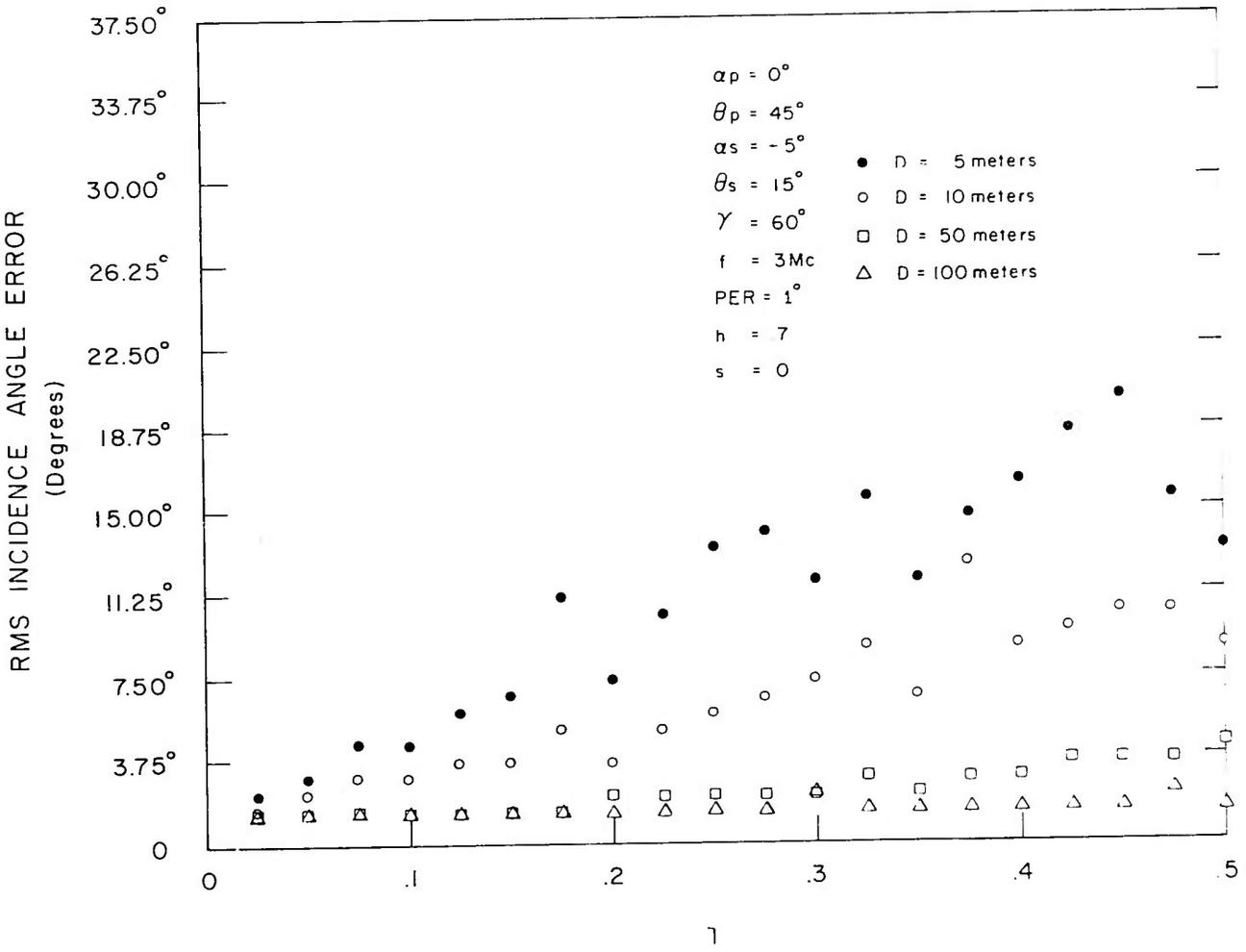

Figure 9 RMS Incidence Angle Error vs T -- Parameter D

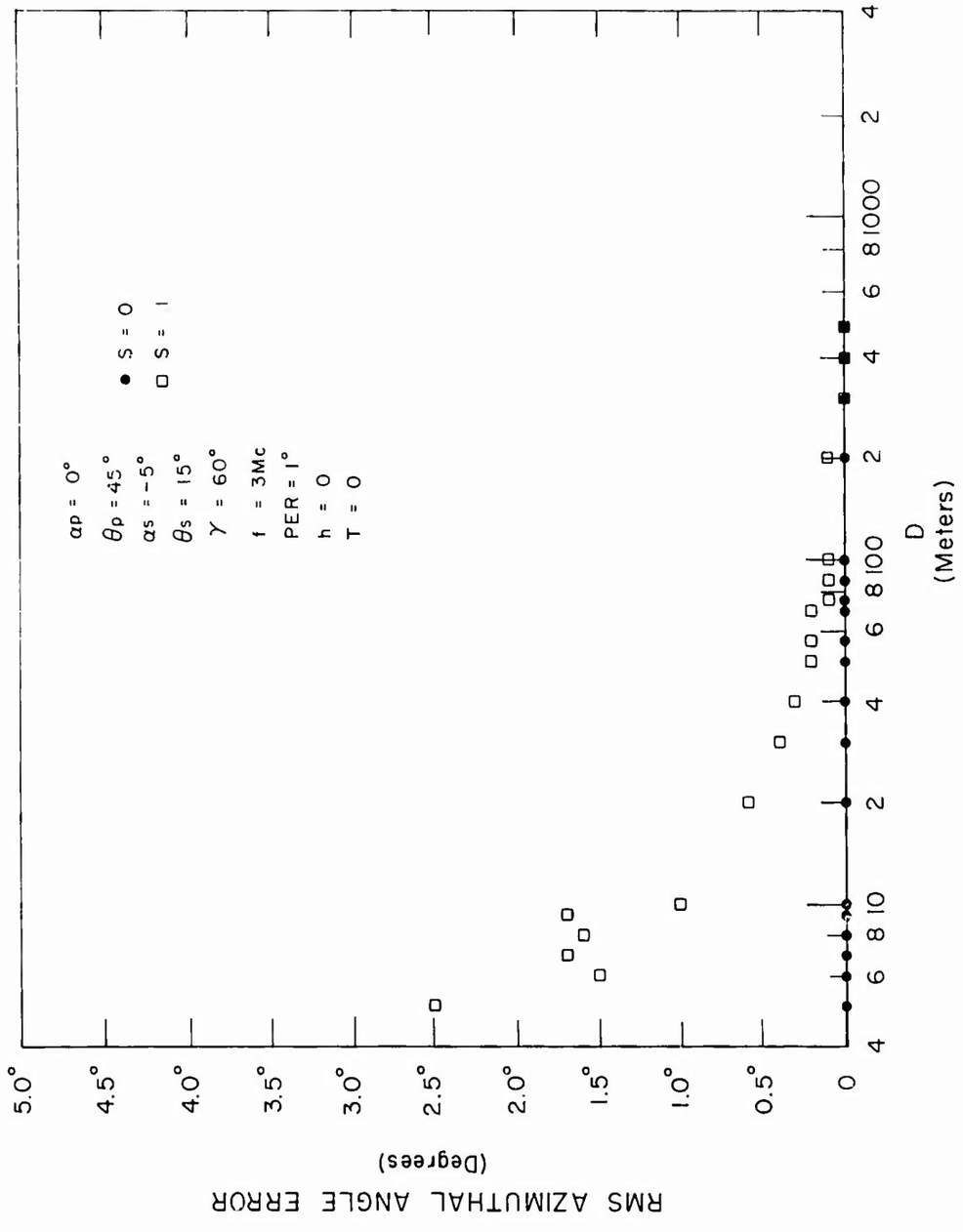

Figure 10 RMS Azimuthal Angle Error vs D -- Parameter S

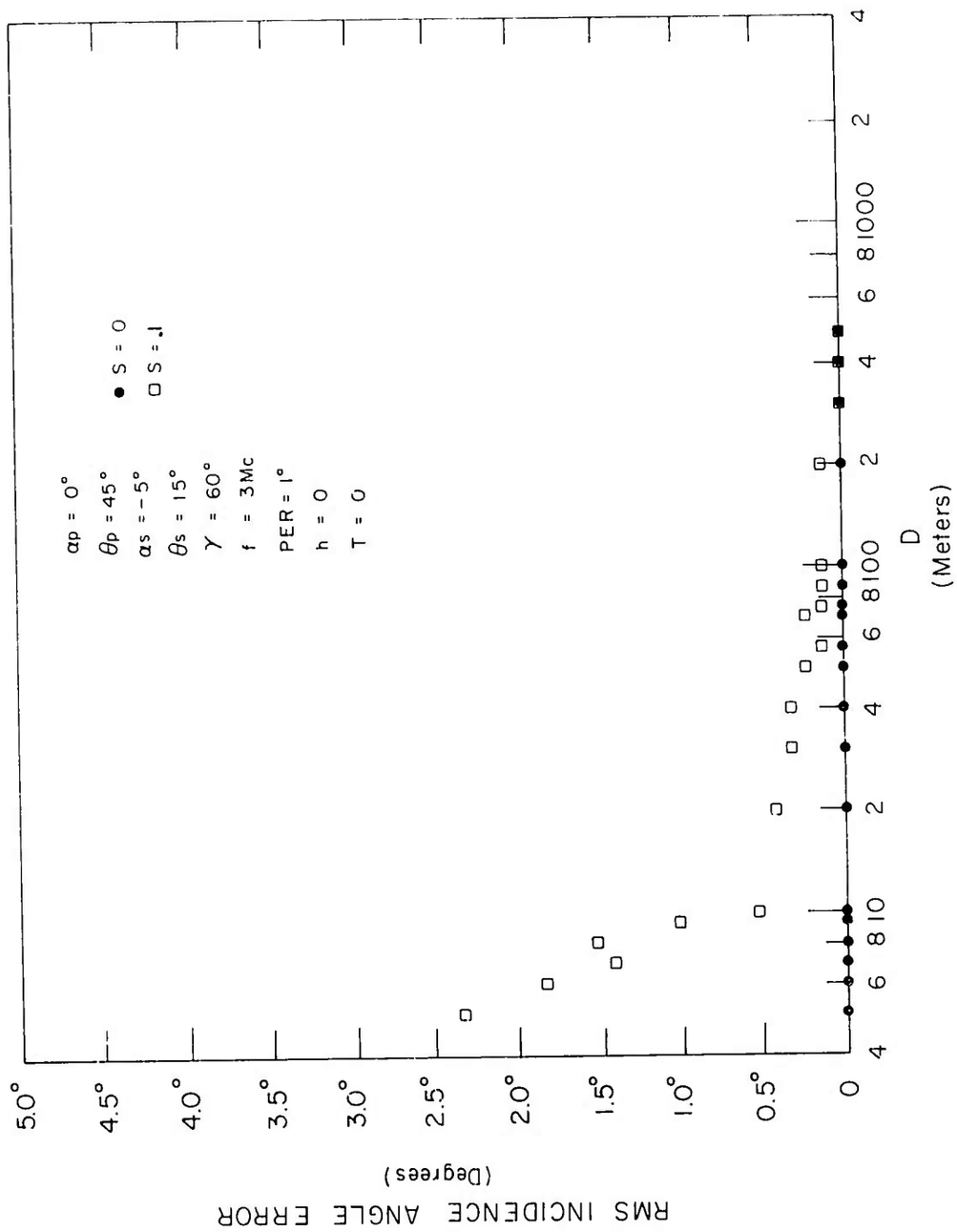

Figure 11 RMS Incidence Angle Error vs D -- Parameter S

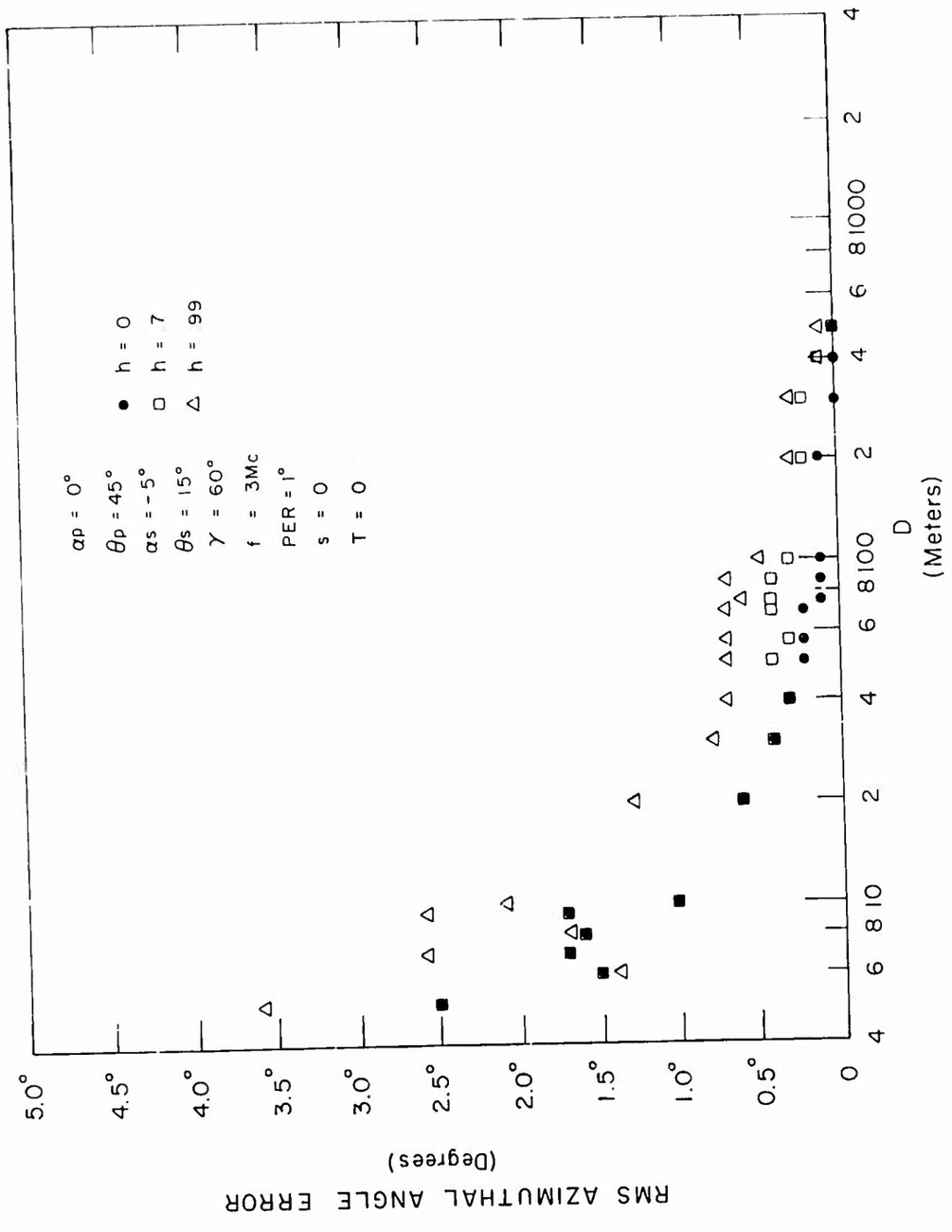

Figure 12 RMS Azimuthal Angle Error vs D -- Parameter h

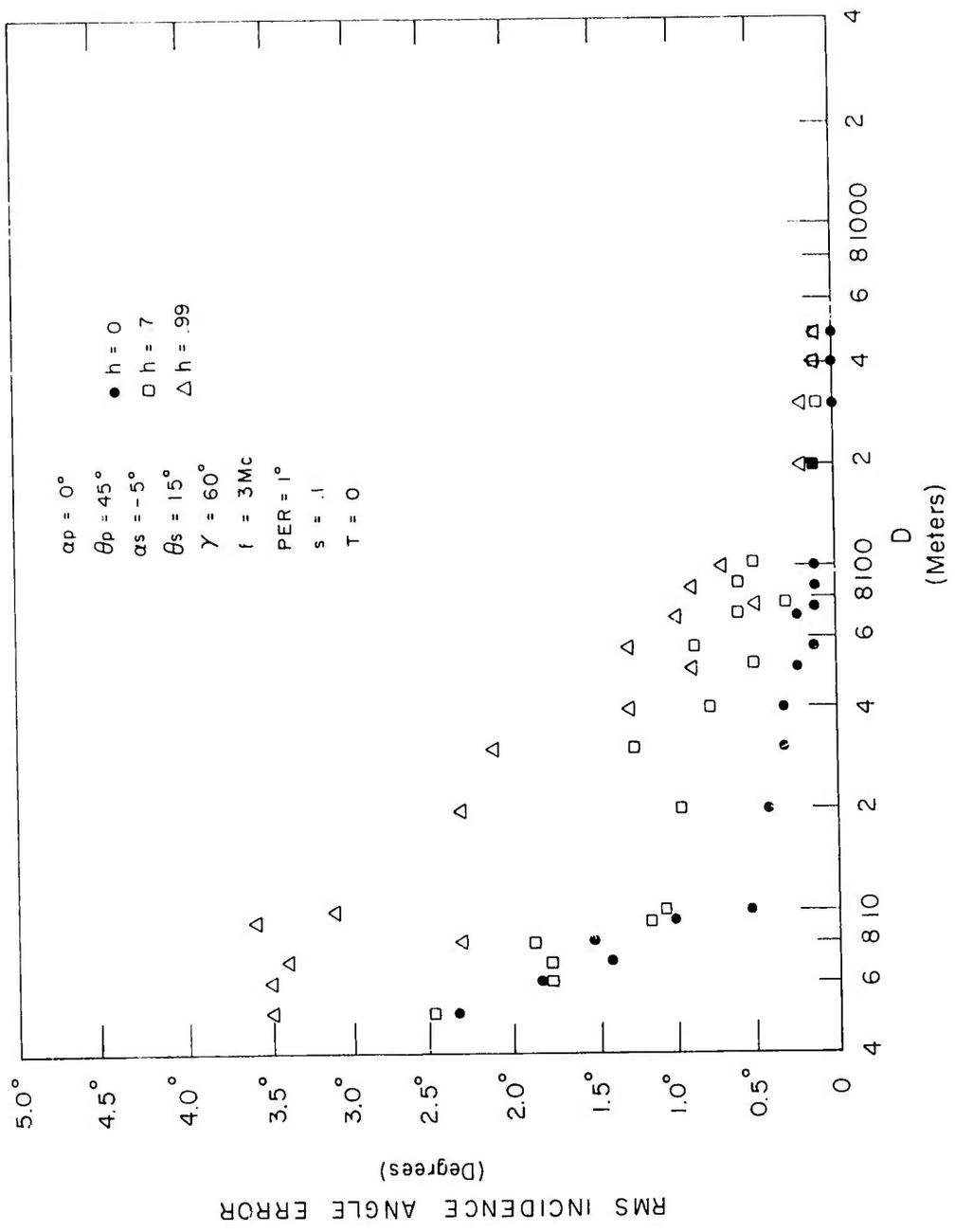

Figure 13 RMS Incidence Angle Error vs D -- Parameter h

because an on-line printer can only plot discrete values of a variable. The distortion introduced by this discrete plotting process, however, does not affect our ability to recognize general tendencies in the data. If a more critical analysis is required reference should be made to the precise tables in Appendix A and B.

For a given set of parameters it is evident from Figures 2 through 13 that the azimuthal angle error and the incidence angle error have the same relative magnitude. It should be pointed out that this condition results from the present choice of parameters. It could have been easily shown, for example, that if the incidence angle was near 90° the magnitude of the incidence angle error would have been larger than the azimuthal angle error.

Figures 2 through 5 show the bearing errors versus D at five values of T. Figures 2 and 3 represent the statistical results and Figures 4 and 5 represent the simulation results. It is seen from these figures that the simulation results approximate the statistical results as they should. At h = .7 and T = .5 volts the simulation analysis shows an azimuthal error of approximately 1° for an aperture size of 100 meters (1λ at 3 Mc.). For the same set of parameters this is exactly what the statistical approach predicts.

Let us assume that the maximum bearing error that we will tolerate is 1°. At T = .5 volts Figures 2 and 3 indicate that the aperture size must always exceed 100 meters (1λ). This result is general though for it implies that for any frequency the aperture size must exceed 1λ. If the signal noise is now decreased to T = .1 volts the aperture must now exceed about 33 meters or 1/3 λ. The previous description is only

one interpretation of the data. The interpretation of the results will depend on particular needs.

Figures 6 through 9 display the same data shown in Figures 2 through 5 in a different form. These figures present the bearing errors as a function of T for different values of D. It is easily seen from these figures that the bearing errors vary linearly with T. As D is increased the bearing errors approach zero as is demonstrated by the decreasing slopes of the plotted lines.

Figures 10 through 13 show the effects of h and S on the bearing errors. Figures 10 and 11 show that at h = 0 and D = 5 meters (1/20 λ. the bearing errors are about 2.5° with S = .1 radian. This represents a relatively small effect for such a substantial noise. With S = .1 radian Figures 12 and 13 show there is no effect on the bearing error when h is changed from 0 to .7. When h is increased to almost maximum, h = .99, the error only changes by 1°. Thus, wave interference is seen to have a relatively small effect on the bearing errors if the differential phase is averaged.

α_p was chosen to be 0° for most of the calculations in this chapter. This value was arbitrarily chosen to represent the complete range of α_p's. Tables 5 and 6 show the variation of bearing errors with D for different values of α_p. The small variation of bearing error with α_p suggests that the results for α_p = 0° may be extended to other values of α_p.

In conclusion the results obtained in the present analysis substantiate our intuitive feelings about the response of the bearing errors to changes in D and T. As D is decreased the errors increase and as T

increases the errors increase. The precise variation is shown in Figures 2 through 13. The agreement between the simulation and statistical approaches to the problem strengthens our belief that this analysis is valid. One area which could be considered for further studies by simulation would be to find the effects of those parameters, which were left constant in this report, on the bearing errors.

It is important to note that the results shown here are derived from a particular model of the interferometer RDF system. Thus, a further experimental study is needed to validate the model used. An investigation of errors in determining angles of arrival for a small aperture size is suggested.

LIST OF REFERENCES

1. Church, J. B., A Digital Bearing Computer For An Interferometer RDF System, Thesis submitted in partial fulfillment of the requirements for the degree of Master of Science in Electrical Engineering, University of Illinois, Urbana, Illinois, 1967.

2. Creasy, J., Digital Techniques For Radio Direction Finding With Interferometer Arrays, Thesis submitted in partial fulfillment of the requirements for the degree of Master of Science in Electrical Engineering, University of Illinois, Urbana, Illinois, June, 1966. RRL Publication No. 309.

3. Grush, H. L., An Investigation of a Digital Bearing Computer for a Small Aperture Radio Direction Finding System, Thesis submitted in partial fulfillment of the requirements for the degree of Doctor of Philosophy in Electrical Engineering, University of Illinois, Urbana, Illinois, June 1965. RRL Publication No. 280.

4. Allen, L. C., Improved Digital Bearing Computer Techniques, Thesis submitted in partial fulfillment of the requirements for the degree of Master of Science in Electrical Engineering, University of Illinois, Urbana, Illinois, June, 1966. RRL Publication No. 314.

5. Glick, M. L., Studies in Time Averaging and Wave Interference in Radio Finding, Thesis submitted in partial fulfillment of the requirements for the degree of Master of Science in Electrical Engineering, University of Illinois, Urbana, Illinois, June, 1966. RRL Publication No. 312.

6. Bailey, A. D. and McClurg, W. C., A Sum-and-Difference Interferometer System for HF Radio Direction Finding, IEEE Transactions On Aerospace and Navigational Electronics, Volume ANE-10, No. 1, March, 1963.

D. N. TRAVERS, W. M. SHERRILL, J. D. MOORE

Southwest Research Institute, San Antonio, Texas

INTERFEROMETER INSTRUMENTATION FOR PROPAGATION RESEARCH

This paper outlines some of the HF propagation capabilities of the DF interferometer instrumentation now in development or in use at Southwest Research.

This review emphasizes the versatility for propagation research provided by the interferometer class of instruments both in amplitude and phase measuring versions. We will briefly describe some propagation work in progress (or soon to be in progress) which supports the Army-sponsored single site location program.

The amplitude interferometer techniques in use today have their origins in the Adcocks and spaced loops of the period before World War II. These early amplitude difference measurements provided an indirect means to obtain phase measurements. The Adcocks, being a relatively easy development, came at an early date; the spaced loop, being a more difficult development, came much later.

There are several references to interferometers in the 1930's. Eckersley in 1938 was probably the first to use spaced loops in research problems which required an interferometric approach. Eckersley measured direction of arrival and estimated visibility functions using the spaced loop as a Michelson interferometer.

After World War II, phase measuring interferometer developments moved toward multiple wavelength baselines as are now in use. The development of rapid phase measuring techniques in the 1950's and small

general purpose digital computers in the 1960's has produced rapid advancement in HF interferometer applications for direction finding and very recently for single site location.

Figure 1 at the top summarizes effects imposed by the ionospheric medium on a target signal which is illustrated by the box on the left. The target signal passes through a propagating medium which establishes a mode structure, alters the polarization, and causes lateral deviation, as illustrated by the box in the center. At the right, we state some major measurements on the emerging signal which are important for propagation research and radiolocation technology.

From the point of view of propagation research, measurements providing directional mode resolution, angular width, and specular to diffracted ratio and others can be interpreted in terms of the ionospheric irregularities which cause them. These measurements yield data on the details of irregularities, effective ionospheric tilts, etc., -- all of importance for understanding the propagation effects.

At the same time, these measurements are significant for radiolocation technology. Directional mode resolution permits reduction of wave interference DF error while knowledge of source angular width and specular to diffracted ratio determines optimum system design including aperture

The interferometer as a direction finder provides a uniquely versatile system for measuring these characteristics. Specular to diffracted ratios are obtained from phase angle distribution measurements. Angular width is obtained by fringe visibility measurements. Directional mode resolution can be obtained by either Σ and Δ polygon displays or

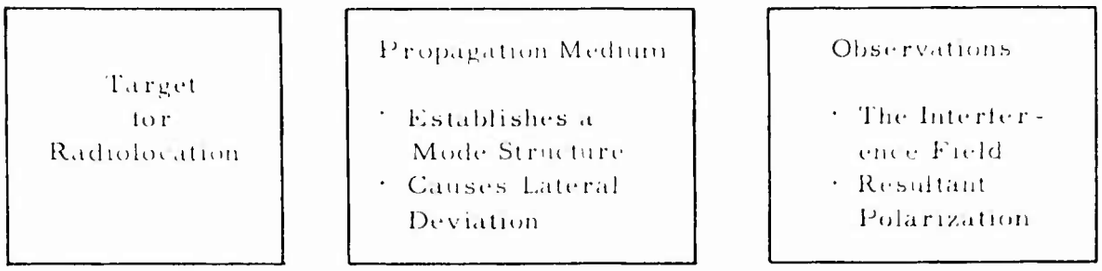

INTERPRETATION OF INTERFEROMETER DATA

Mode Structure Morphology

- Directional Mode Resolution
- Angular Width of Single Mode
- Specular to Diffracted Ratio
- Mode Scintillation
- Mode Amplitudes
- Polarization

Lateral Deviation

- Tilt Vector Slope and Direction
- Tilts on Two Hop Modes

Instrumental Performance

- DF Bearings
- SSL Maps

FIGURE 1

Fourier transform of measured amplitude and phase distributions provided sufficient data samples are available. At the same time, a combination of long and short baseline phase and amplitude measuring interferometers permits separation of polarization from wave interference effects while observing both. We will specifically indicate this capability by examples, but first we will review the instrumentation.

The wide aperture phase measuring interferometer (Figure 2) at SwRI has been previously described. The equipment includes two data readout systems, the digital system shown here and an analog system based on a University of Illinois development and shown in the next figure.

The analog arrangement (Figure 3) permits directional resolution of multiple modes by providing sum and difference phase meter envelope displays in the form of polygons obtained with a storage oscilloscope. Typically the polygon displays are developed when observations are made over intervals on the order of 15 to 30 seconds. Two component signals provide parallelograms, three provide hexagons, etc. The phase angles are measured by the slopes of the sides of the parallelograms. These phase angles may be converted into bearing computations either by feeding the data directly into the computer in a semiautomatic manner or by the use of an analog calibrator (phase angles are slopes of displays).

The four baselines of the interferometer are displayed in four quadrants on the CRT, two short baselines at the top, two long at the bottom. A grating alidade is provided to transfer envelope slopes to the digital computer where bearings are computed after four phase angles have been measured in the proper sequence. Alternatively,

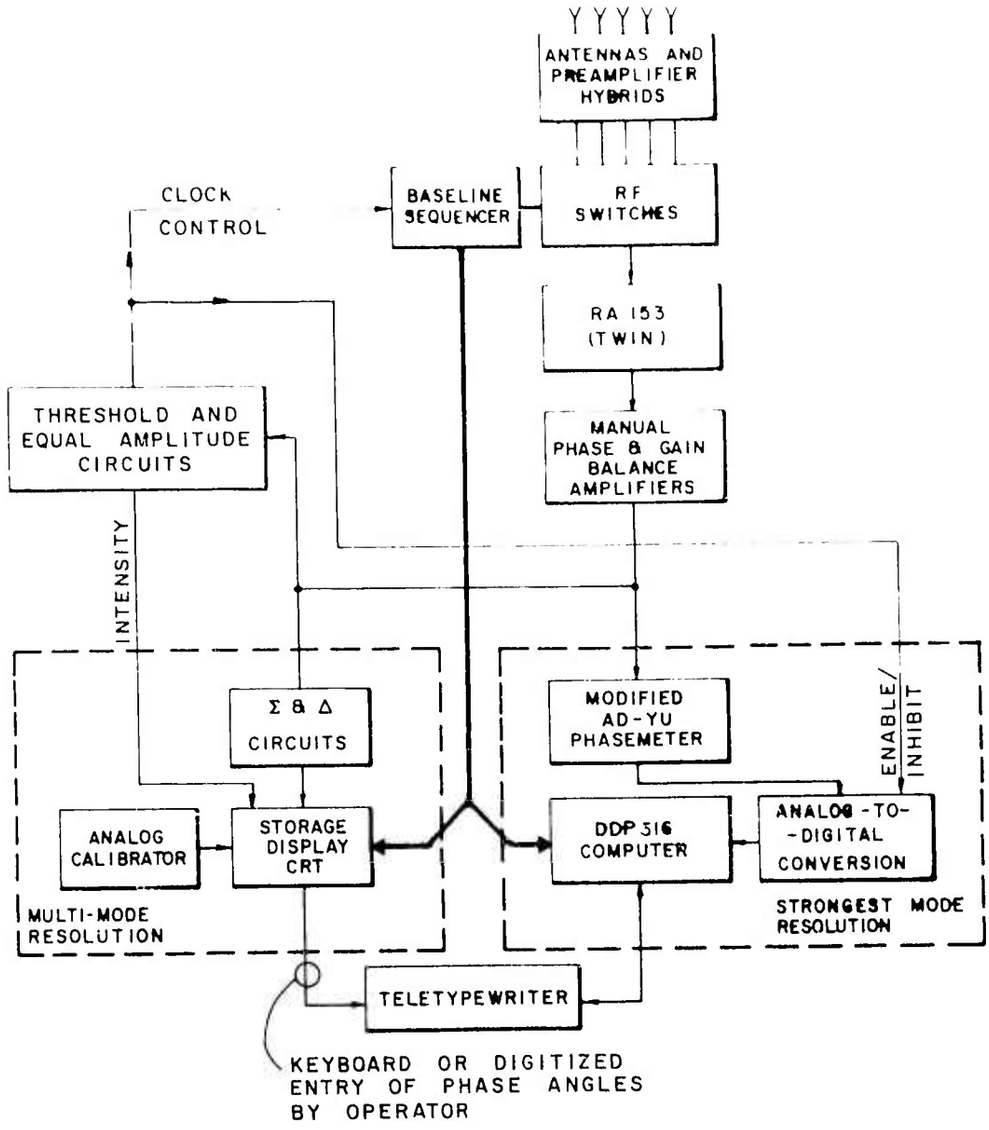

BASELINE EQUATIONS

NS SHORT	$\Phi_{ns} = \beta d_s \cos\phi \cos\Psi$
NS LONG	$\Phi_{ns\ell} + N_{ns}\,360^\circ = \beta d_\ell \cos\phi \cos\Psi$
EW SHORT	$\Phi_{ew} = \beta d_s \sin\phi \cos\Psi$
EW LONG	$\Phi_{ew\ell} + N_{ew}\,360^\circ = \beta d_\ell \sin\phi \cos\Psi$

OBSERVED AZIMUTH

$$\phi = 360^\circ - 180.5^\circ - \tan^{-1}\left[\frac{\Phi_{ew\ell} + N_{ew}\,360^\circ}{\Phi_{ns\ell} + N_{ns}\,360^\circ}\right]$$

OBSERVED ELEVATION

$$\cos\Psi = \frac{\sqrt{(\Phi_{ew\ell} + N_{ew}\,360^\circ)^2 + (\Phi_{ns\ell} + N_{ns}\,360^\circ)^2}}{\beta d_\ell}$$

Figure 2.

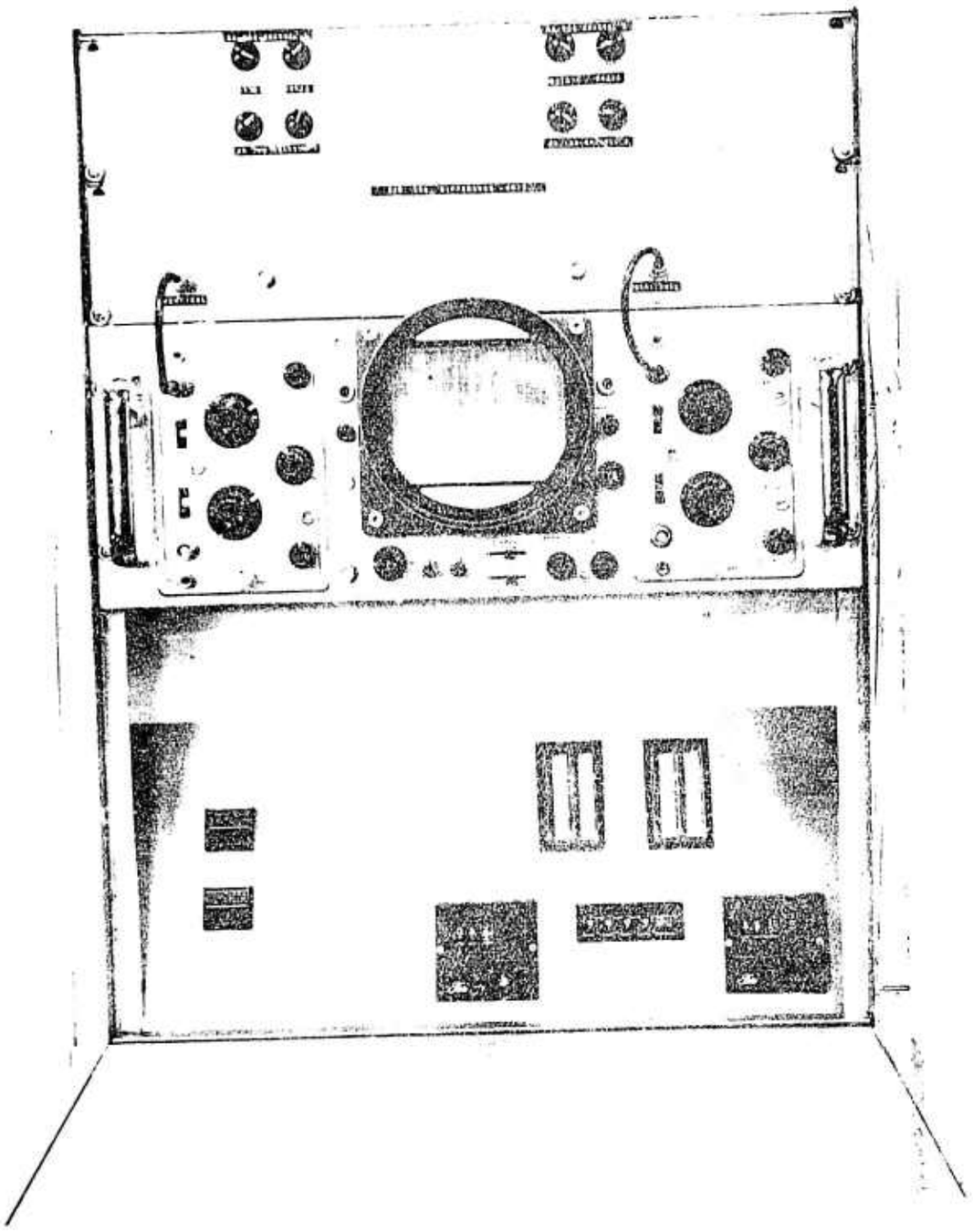

Figure 3.

an analog calibrator which generates electronic strobe lines superimposed over the stored polygons can be used to directly obtain the azimuth and elevation of any one mode. The calibration is shown in the lower part of the figure where separate azimuth and elevation controls are indicated. The calibrator shown is based on a development at the University of Illinois with a number of changes.

In use the procedure is to apply the strobes first to the short baseline displays to obtain rough cuts and then to refine the controls with a second adjustment with the strobes superimposed on the long baseline displays. This procedure eliminates the phase ambiguities and permits the bearing to be obtained without trial and error searching for the proper values since, in general, the short baselines will provide only one answer. This method of obtaining bearings is completely apart from the fully automatic digital system which uses a conventional coincidence type phase meter and computes azimuth and elevation of the strongest mode from phase angles.

Figure 4 shows a two component field near 8.5 MHz. The amplitudes of the two components are evident from the length of the sides of the display.

Figure 5 shows the result of applying plane wave editing to an observed two component signal. It will be noted that the parallelogram display for at least one baseline is replaced with an hour glass figure or so-called bundle of sticks figure which corresponds to a number of instances where equal amplitudes were recognized at the ends of the baseline. Some early test results with plane wave editing have been provided in one of the other papers.

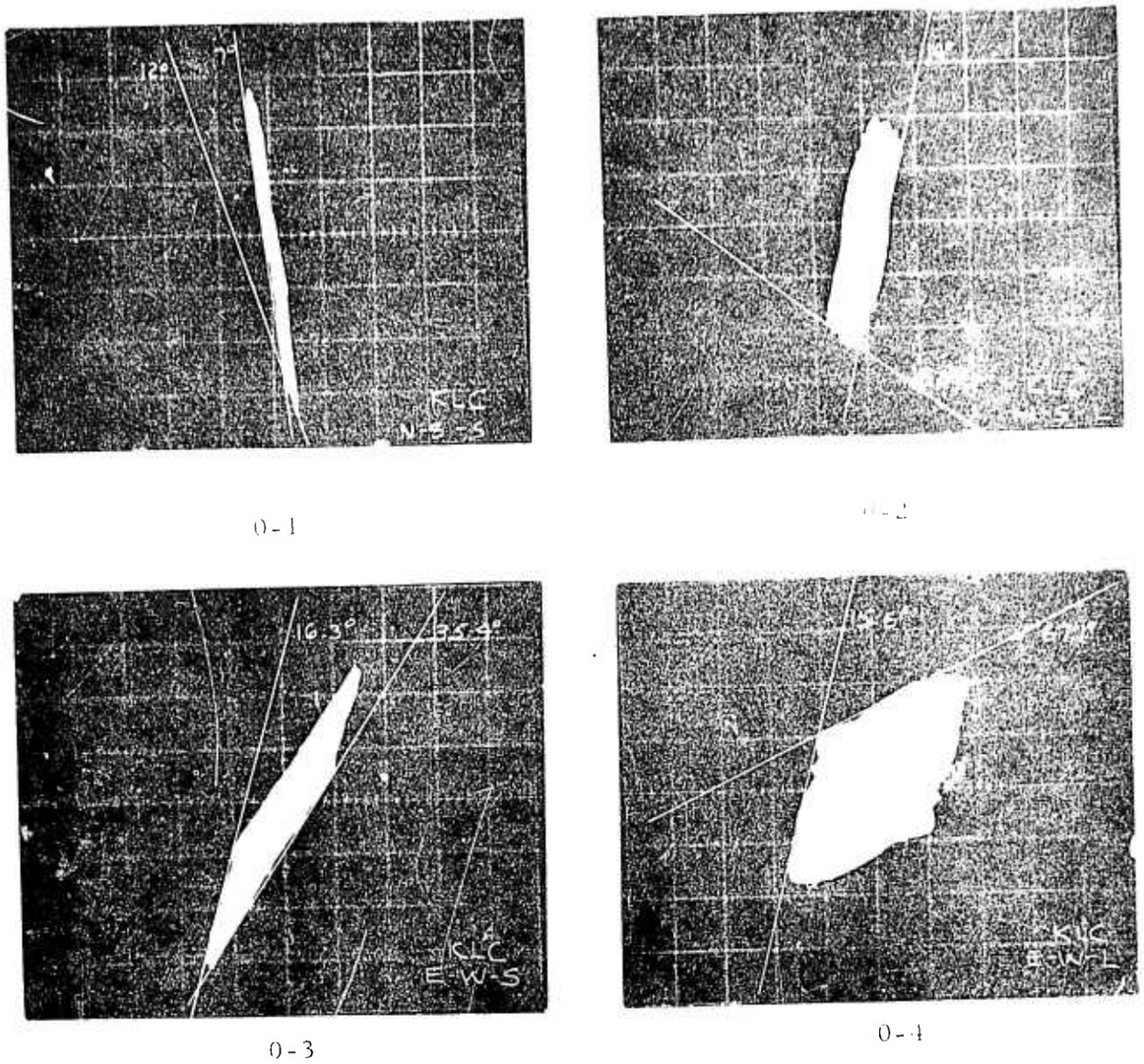

0-1

0-2

0-3

0-4

Figure 4.

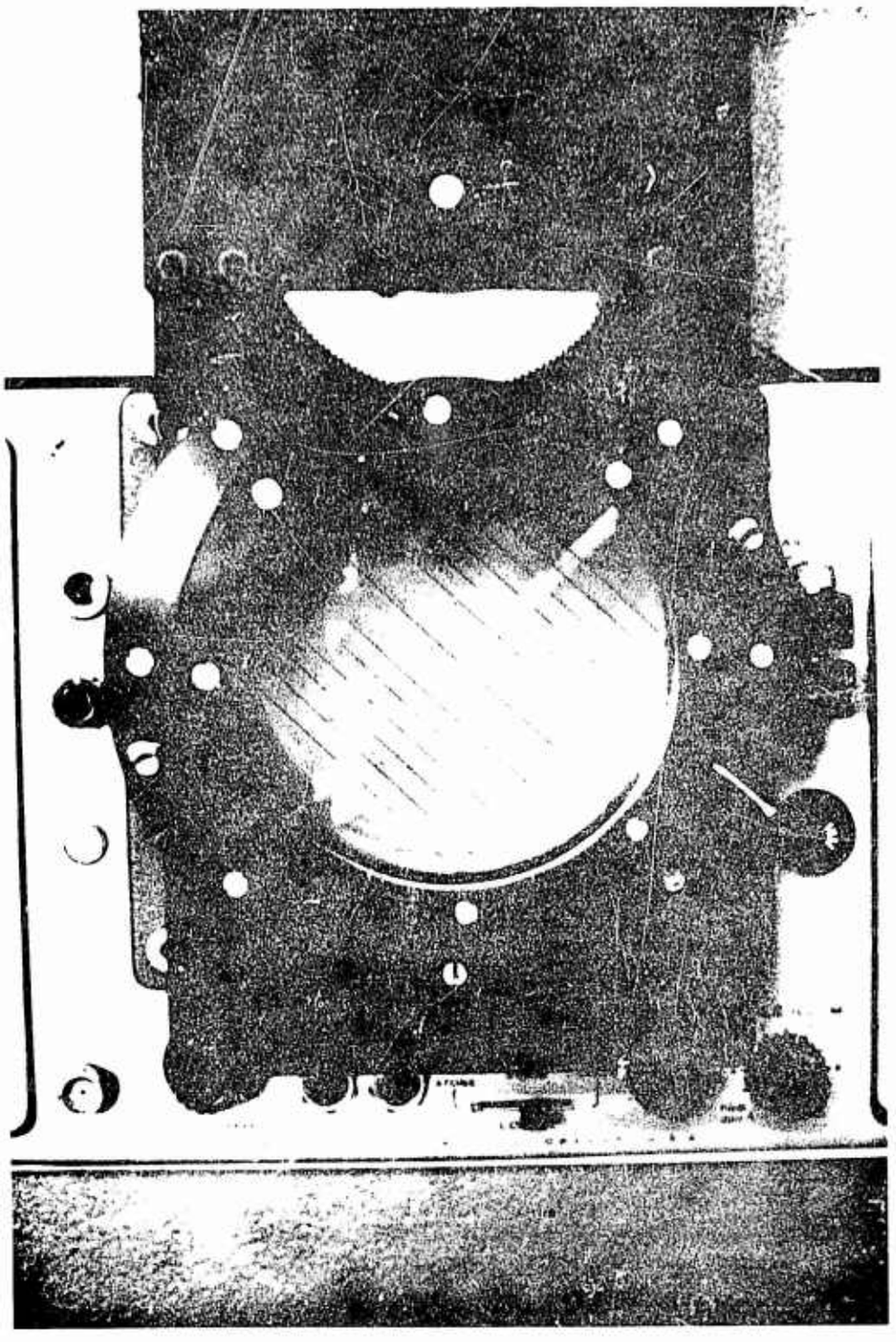

Figure 5.

The spaced loop antenna may be understood from many points of view including that of a rotating baseline amplitude interferometer. Figure 6 shows the external view of a rotating coaxial spaced loop antenna designed for 400 RPM rotation. This is an Army development for tactical applications.

Figure 7 shows the spaced loop indicator and receiver used in the film which follows in a few minutes.

Figure 8 shows calculated spaced loop response patterns for a single signal as a function of polarization at an elevation angle of 45°. The characteristic spaced loop response patterns permit continuous qualitative information on the incident polarization. Thinking of the antenna as a spaced array with loop elements, the array null (or interferometer null) remains fixed on the bearing independent of polarization while the element null (or loop null) rotates and blurs according to the incident polarization. A blurred loop null means elliptical polarization. A sharp loop null indicates linear polarization and rotates with the orientation angle of the incident polarization ellipse. Vertical polarization is on the left, horizontal on the right and circular at bottom center. Equivalent simple loop patterns are shown in some of the patterns as dotted lines. In the film which follows, all of these patterns can be found in varying degrees in combination with wave interference effects. We have not attempted to show here theoretical patterns for the wave interference effects.

As an introduction to rotating spaced loop data, we want to show a sequence of film taken on two typical skywave signals. Varying polarization will be seen on both signals as the film progresses, while the

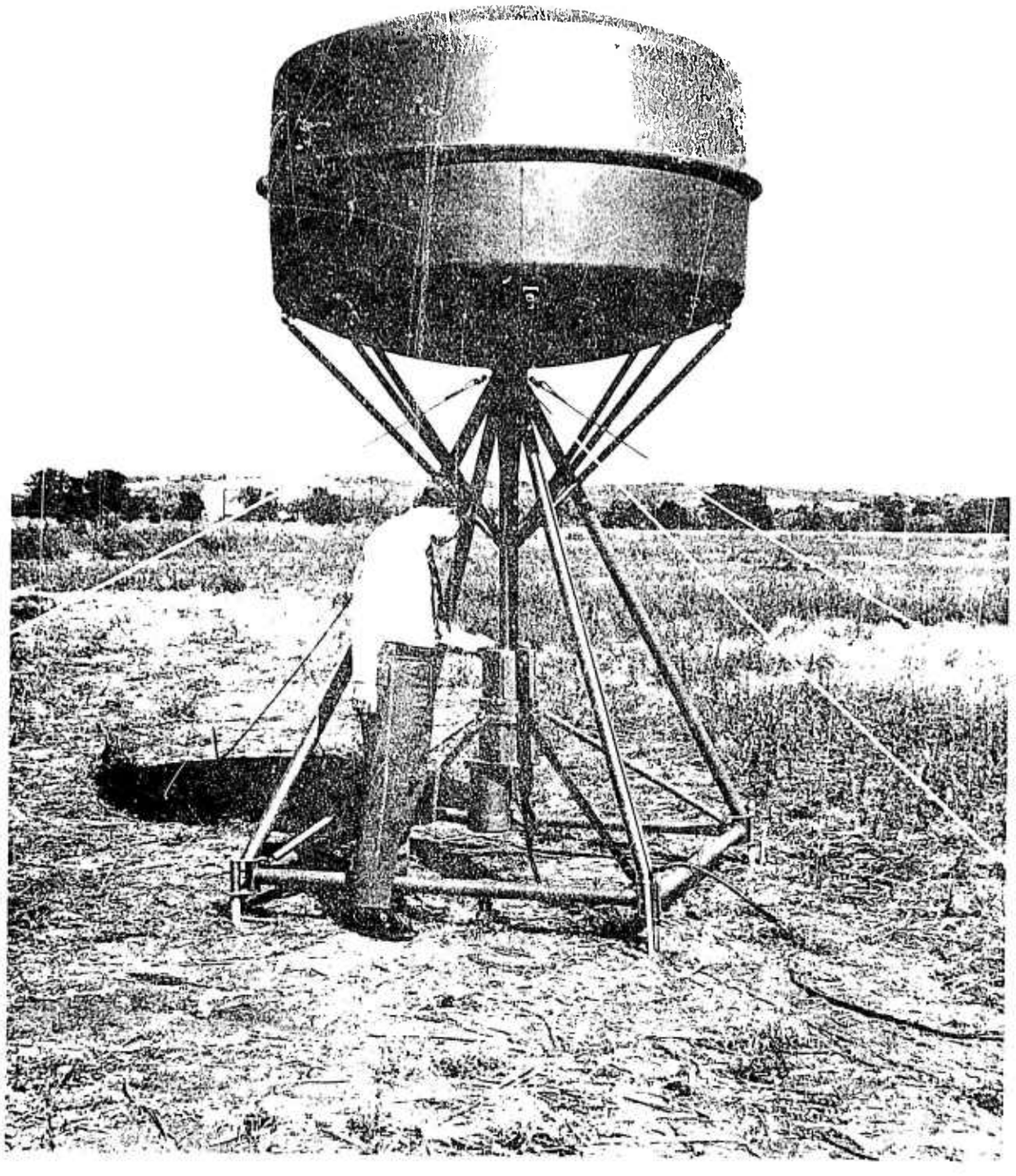

Figure 6.

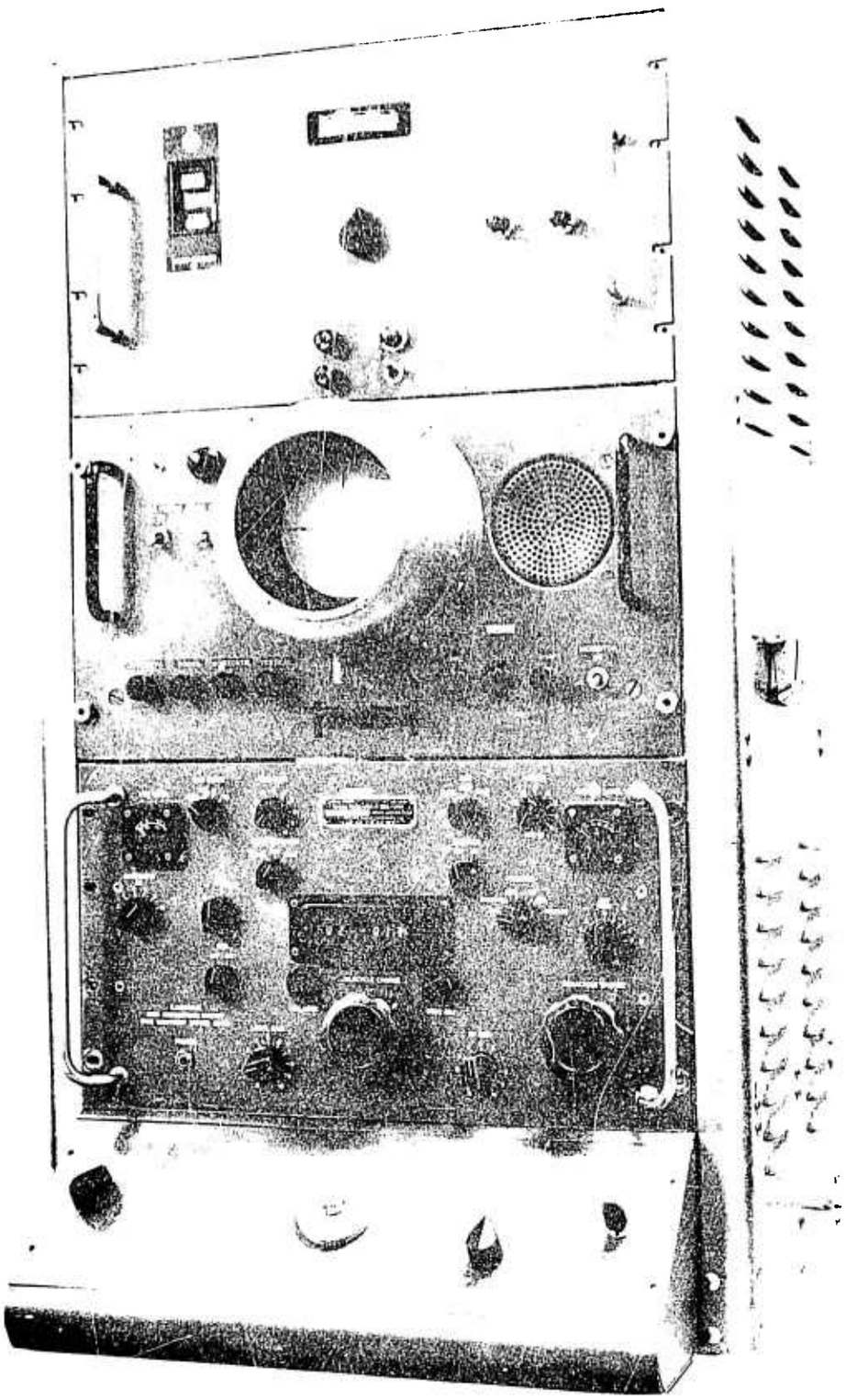

Figure 7.

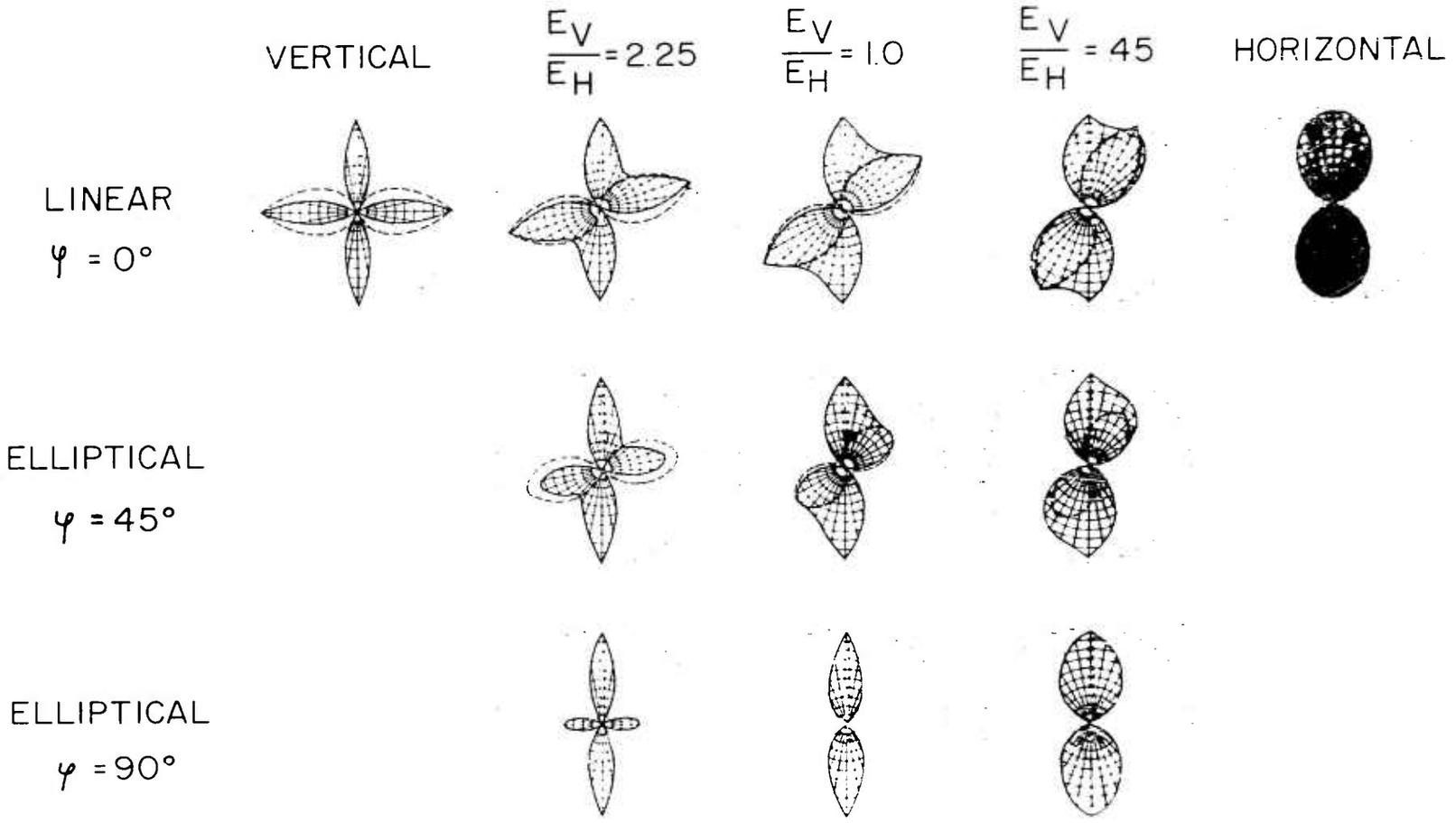
VERTICAL
$\frac{E_V}{E_H}$ = 2.25
$\frac{E_V}{E_H}$ = 1.0
$\frac{E_V}{E_H}$ = 45
HORIZONTAL
LINEAR
φ = 0°
ELLIPTICAL
φ = 45°
ELLIPTICAL
φ = 90°

Figure 8

observed bearing remains nearly fixed depending on wave interference conditions

The first sequence shows WWV at 10 MHz which has a range of approximately 850 miles. This sequence of film shows relatively stable elliptical polarizations as indicated by the depth of the simple loop or element nulls. The photographs were taken with a sequence camera at two frames per second and are being shown at eight frames per second so that there is a factor of four increase in the rate of display. At a number of points in the film, a sudden change in the shape of the pattern accompanied by a loss in symmetry will occur. These patterns provide sense displays obtained by unbalancing the spaced loop (wave interference effects present).

The next sequence will show KLC, an interrupted carrier station at 8.5 MHz, located near Houston, Texas. This station has a range of approximately 215 miles. In contrast to the previous sequence of elliptical polarization, this target shows rotating linear polarization from vertical through horizontal sometimes in the clockwise, other times reversing to the counterclockwise direction. It is important to note that a qualitative measurement of the state of polarization is available at all times making possible a comparison between the polarization information and any wave interference effects which might be present.

One could also compare other direction finders simultaneously to obtain a measure of the degree to which either polarization error or wave interference error are present. It is also important to note that the wave interference or scattering error reduction effect of the spaced loop would provide another means for separating polarization error from

wave interference error such as in the comparison of an Adcock and a spaced loop or a simple loop and a spaced loop.

We now wish to show a comparison of spaced loop patterns with simultaneous sum and difference phase meter displays from the wide aperture phase measuring interferometer. During this sequence, the film will be stopped to show displays frame by frame. One can observe the phase angles and consequent directions of arrival of the components in the incident field, the polarization, and direction of arrival of the resultant. One can also see the number of components present and the signal amplitude of each.

This is a sequence of film obtained on WWV at 10 MHz. The sequence shows the rotating spaced loop pattern on the right and sum and difference phase meter displays from the crossed baseline phase interferometer on the left. The parallelograms on the far left are developed from the phase angles from the long baselines. The parallelograms (which are nearly straight lines) from the short baselines are just to the right of the long baselines. This sequence of data shows elliptical polarizations with rotating orientation angle as indicated by the spaced loop response patterns. The phase parallelograms for each baseline indicate one mode much stronger than the other as determined by the length of the parallelogram sides. The long baseline parallelograms at far left are stable and show greater resolution than the much narrower short baseline parallelograms on the right as expected by the increased resolution of the long baselines. The polarization sequences rapidly change from the elliptical polarizations towards linear. However, similar to the previous WWV sequences, one does not observe much rotation of the orientation angle (simple loop null position).

Finally, it is important to note that in the fully automatic mode the digital computer output is displayed similar to a manner illustrated by the examples shown in Figure 9. This output provides azimuth and elevation angle automatically and repetitively and optionally a variety of other parameters which can be derived from these including the SSL position, ionospheric tilt angle and direction, and all kinds of averaging statistics. In the present display, the azimuth is on the left, elevation next, followed by number of baseline phase sequences and the number stored. The plots to the right were put in by hand to show typical one-minute sequence for three target ranges.

In this example, three time series displays, each about one-minute long, are provided for three targets at different ranges: at the top, WWV; in the center, KLC, the interrupted carrier signal 215 miles to the east; and at the bottom, our own target at New Berlin, Texas, 34 miles east. Relatively stable azimuth data are obtained in the low elevation angle case whereas relatively stable elevation angle data are obtained for the very high elevation angle case. The scale on the azimuth plot is 10°; the scale on the elevation plot is 2°.

Figure 10 shows one more example -- a measured phase angle distribution along both interferometer baselines. These distributions can be interpreted in terms of specular to diffracted ratios. Our data show variations from .1 to 1.

We emphasize in closing that the capability of the computer-instrumented and analog readout interferometer systems can now be fully exploited for propagation research. Basic rigorous interference techniques are available for obtaining new quantitative data for radiolocation technology and propagation research.

Az.	El.		
[illegible]	32.0	10	150
330.0	31.3	10	150
[illegible]	[illegible]	10	150
[illegible]	34.7	10	150
[illegible]	[illegible]	10	150
[illegible]	[illegible]	10	150
333.6	32.7	10	150
[illegible]	[illegible]	10	150
[illegible]	[illegible]	10	150
[illegible]	31.3	10	150
[illegible]	[illegible]	10	150
[illegible]	[illegible]	10	150
327.5	-1.0	10	150
[illegible]	[illegible]	10	150
[illegible]	[illegible]	10	150
[illegible]	31.6	10	150
333.8	32.5	10	150
333.9	31.5	10	150

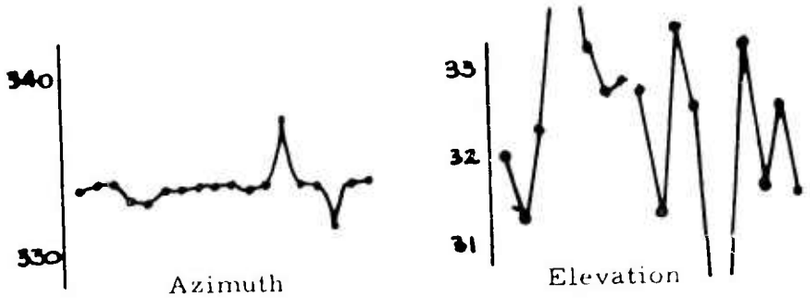

Long Range Target, WWV, 10 MHz, Range 858 miles

89.2	58.0	1	28
89.5	58.6	1	29
88.9	58.3	1	30
89.9	58.2	1	31
89.9	58.6	1	32
89.4	58.4	1	33
89.5	58.6	1	34
89.4	58.6	1	35
89.5	58.5	1	36
89.4	58.6	1	37
89.9	58.6	1	38
88.5	58.4	1	39
89.1	58.6	1	40
89.8	59.1	1	41
88.7	59.0	1	42
90.2	58.6	1	43
89.9	58.9	1	44
89.8	58.9	1	45
90.3	58.9	1	46

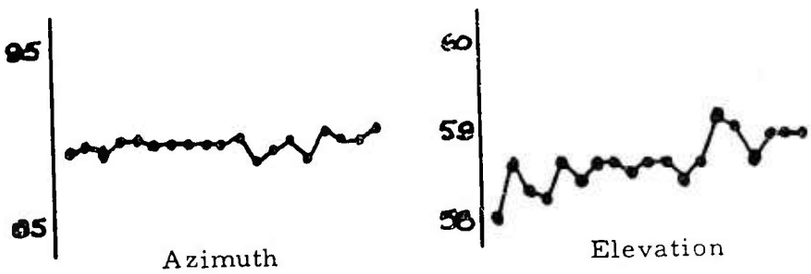

Medium Range Target, KLC, Houston, Texas
Range 215 miles

86.2	87.1	10	10
89.0	87.1	10	20
84.6	87.1	10	30
90.9	87.0	10	40
86.6	87.1	10	50
88.2	86.9	10	60
86.5	87.1	10	70
84.3	87.2	10	80
88.1	87.0	10	90
86.0	87.0	10	100
84.9	87.1	10	110
89.5	86.9	10	120
84.6	87.0	10	130
85.5	87.1	10	140
91.8	87.0	10	150

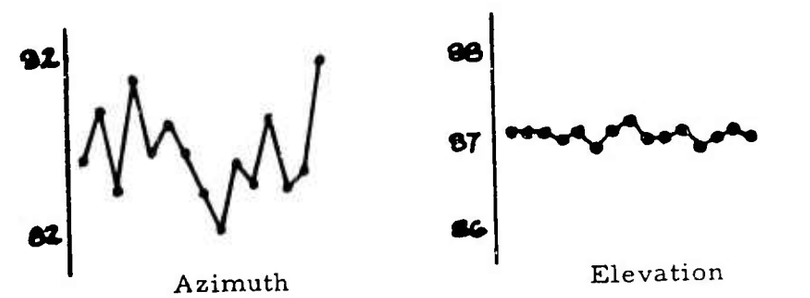

Short Range Target, New Berlin, Texas
Range 34 miles

FIGURE 9

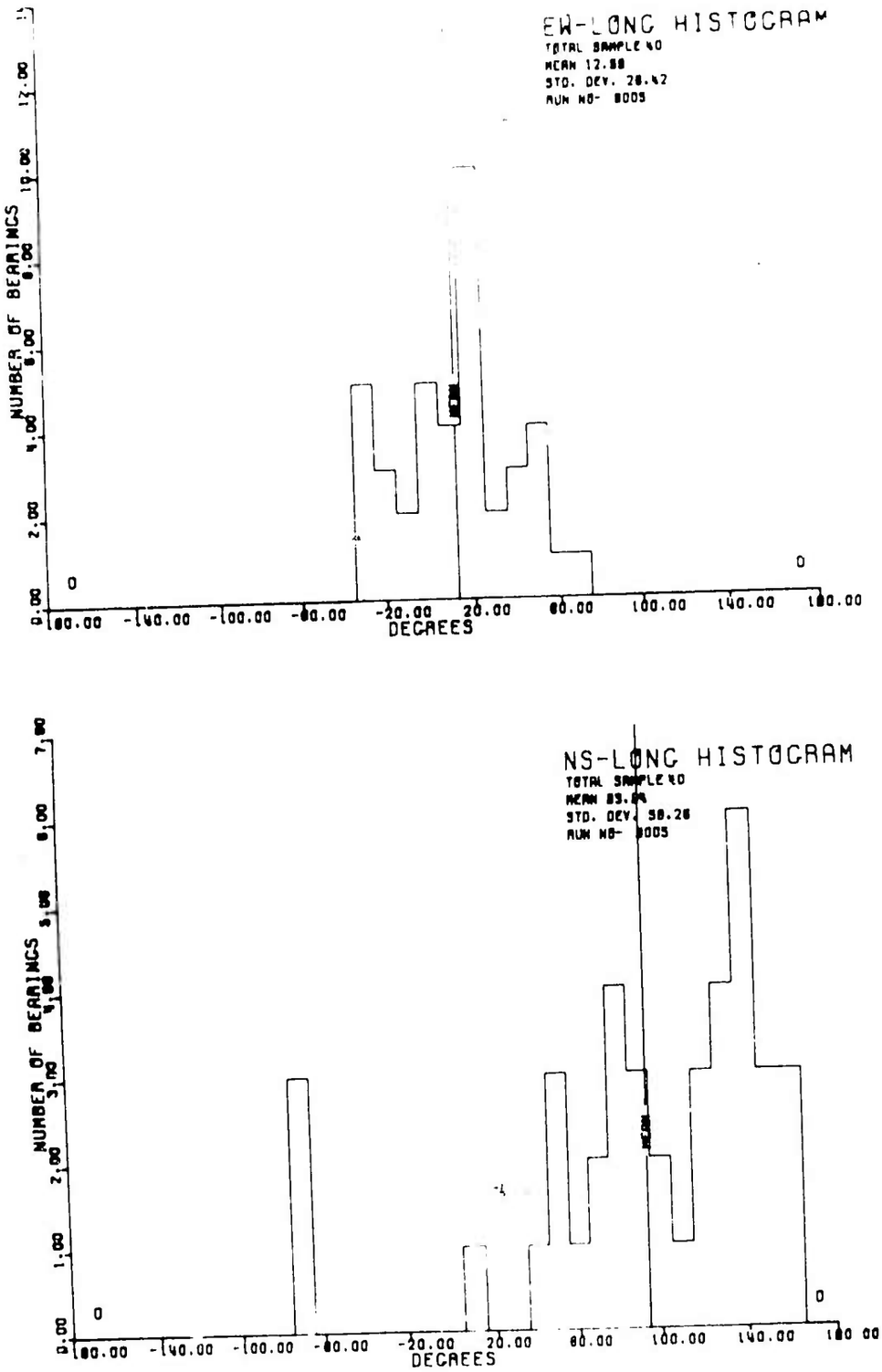

WWV 10MHz

FIGURE 10

M. E. COFFEY, R. P. McCONVILLE
(Presented by S. M. Bennett)

AVCO [illegible], Systems Division, Wilmington, Massachusetts

THE USE OF REFLECTRIX TECHNIQUES IN THE ANALYSIS OF FM/CW OBLIQUE IONOGRAMS*

A study has recently been conducted by Barnum of the Stanford University Electronics Laboratory (SEL) with FM/CW ionograms taken over a 1900 km path from Texas to Stanford, for which an absolute time delay scale was available for each ionogram.[1] As a test of the procedures developed by Avco for calculating absolute time delay scales for oblique incidence ionograms from the inter-mode time delays evident in the data, the method was applied to the SEL Texas to Stanford ionograms, and the resulting time scale compared with the known time scale. The Avco computer generated time delay versus virtual height plots were used in this analysis; the Texas to Stanford plot is shown in Figure 1. The lowest order pure F mode for this path should be the 1F mode. For the ionograms where no E mode was present, the time scale was determined by using the relative time delays between the pure F modes.

The time delay scales determined by using the computer plots without regard to the time delay axis of Barnum's records were usually within 0.03 milliseconds of the absolute delay time scales given on the data, which had been determined by two calibrated cesium clocks. For one case the time scales differed by 0.06 milliseconds, and this was the maximum deviation obtained for the ionograms scaled.

---

*Work Sponsored by RADC under Contract F30602-69-C-0096

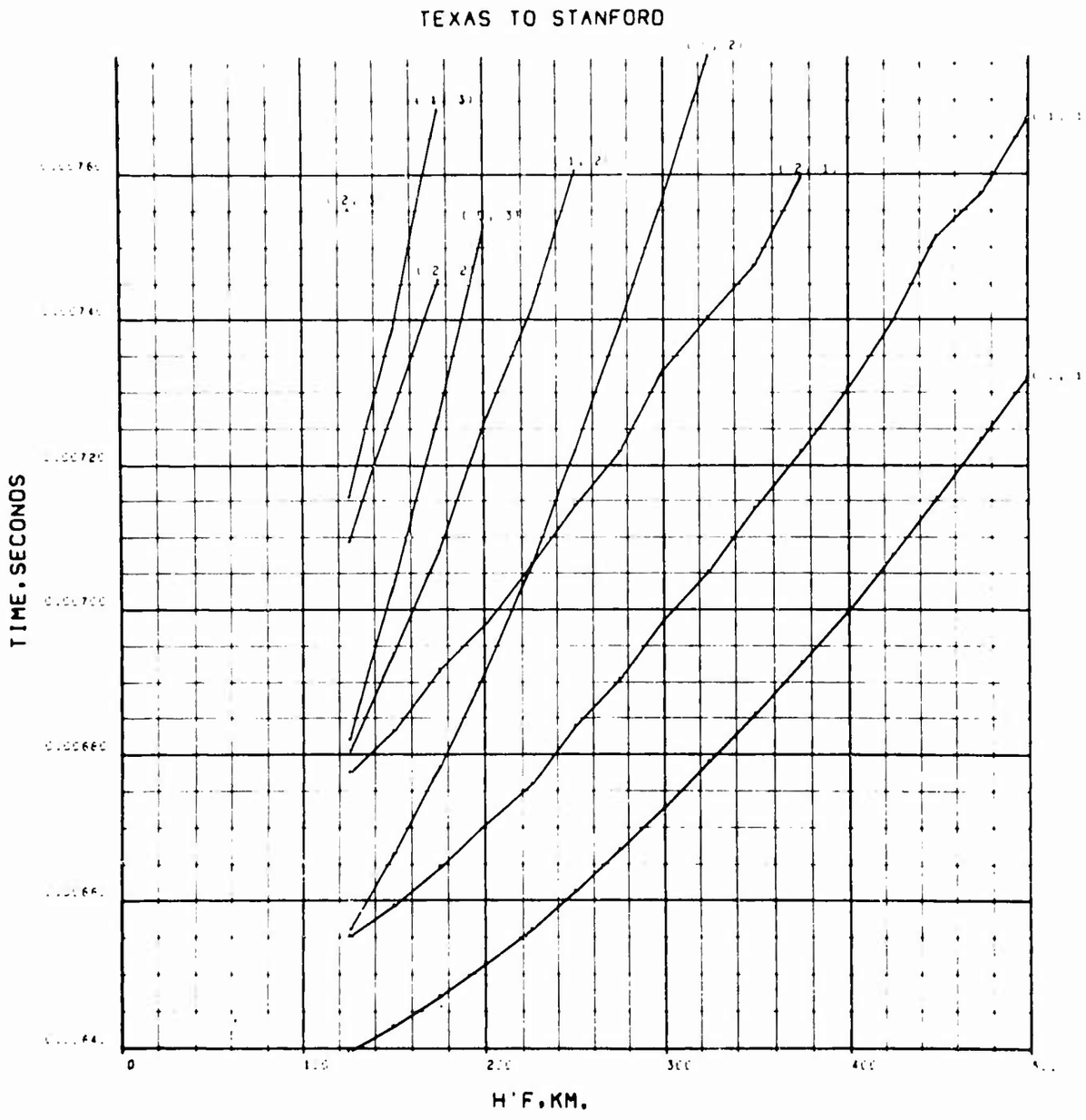

Figure 1. Computer Plot: Mode Delay Time Versus Virtual Height of F for Pure F and Mixed Modes.

In Barnum's work the 1F mode trace was used to estimate a model ionosphere (electron density profile) through which to ray trace and simulate the 1F mode trace. Corrections to the model ionosphere were made in order to minimize the difference between the measured and calculated 1F mode trace. When a satisfactory simulated 1F trace was obtained, the other mode traces were simulated with the same model ionosphere.

It was our purpose to see if the reflectrix method[2] could be used directly to generate mode traces, i.e., to go from the measured 1F trace to a reflectrix, and then to whatever other mode trace is desired, such as the 2F, without any iterative procedure or costly ray tracing. The Avco reflectrix program converts an oblique incidence ionogram into an equivalent midpath vertical incidence ionogram and then plots virtual height versus ground range, parametric in frequency, for various takeoff angles. The program also allows one to superimpose a function of virtual height and ground range onto the reflectrix plots for the purpose of calculating ranges to critical reflection regions. The points of intersection of the reflectrix curve and this function are printed out for each frequency.

One of the oblique incidence ionograms from Barnum's report (see Figure 2) was used to generate a 2F mode from the actual 1F mode. First the time delays versus frequency for the 1F mode were read off the ionogram. These were inverted into the equivalent midpath vertical incidence ionogram shown in Figure 3 and then transformed into the reflectrix curves shown in Figure 4. The total path range and the ground range to the first reflection point of a 2F mode were then read in as data. The program determines the points of intersection of this vertical

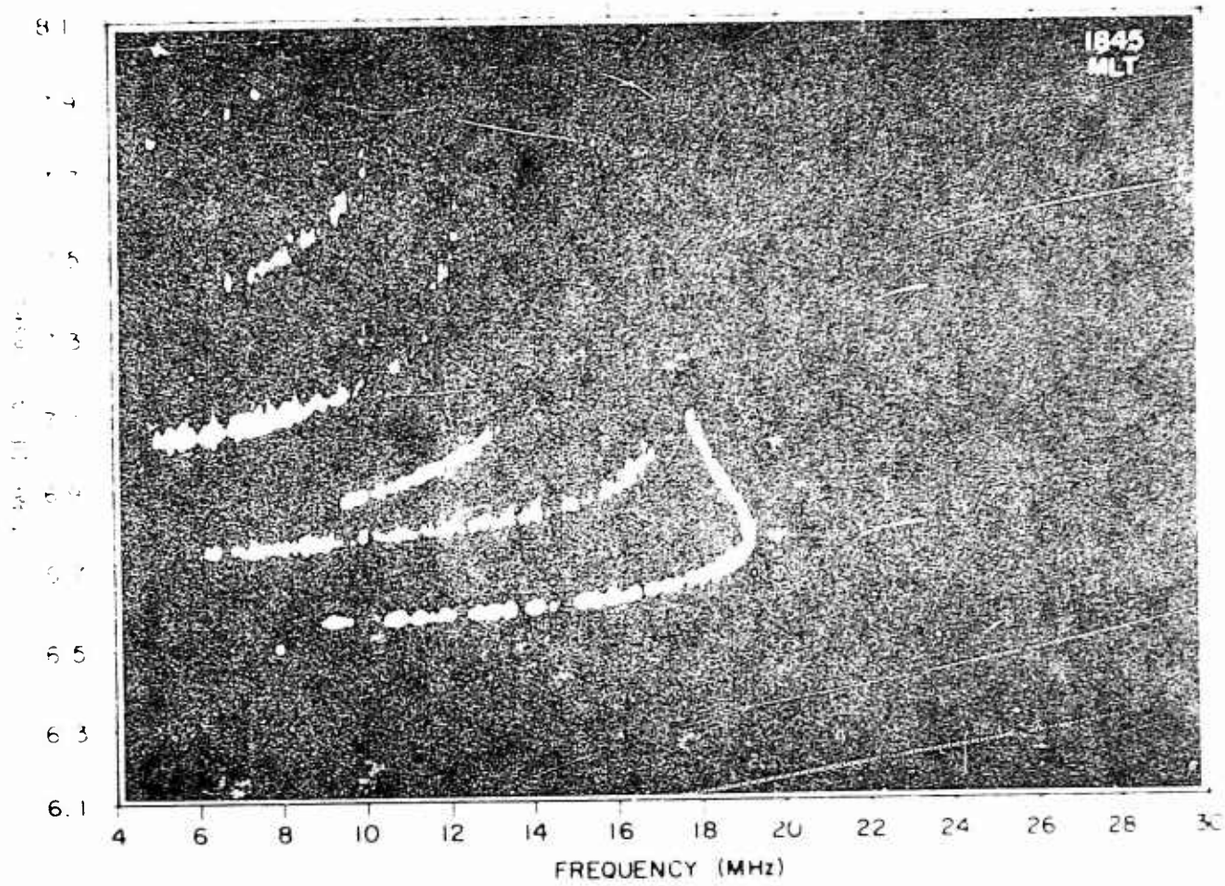

Figure 2. Copy of Figure 9

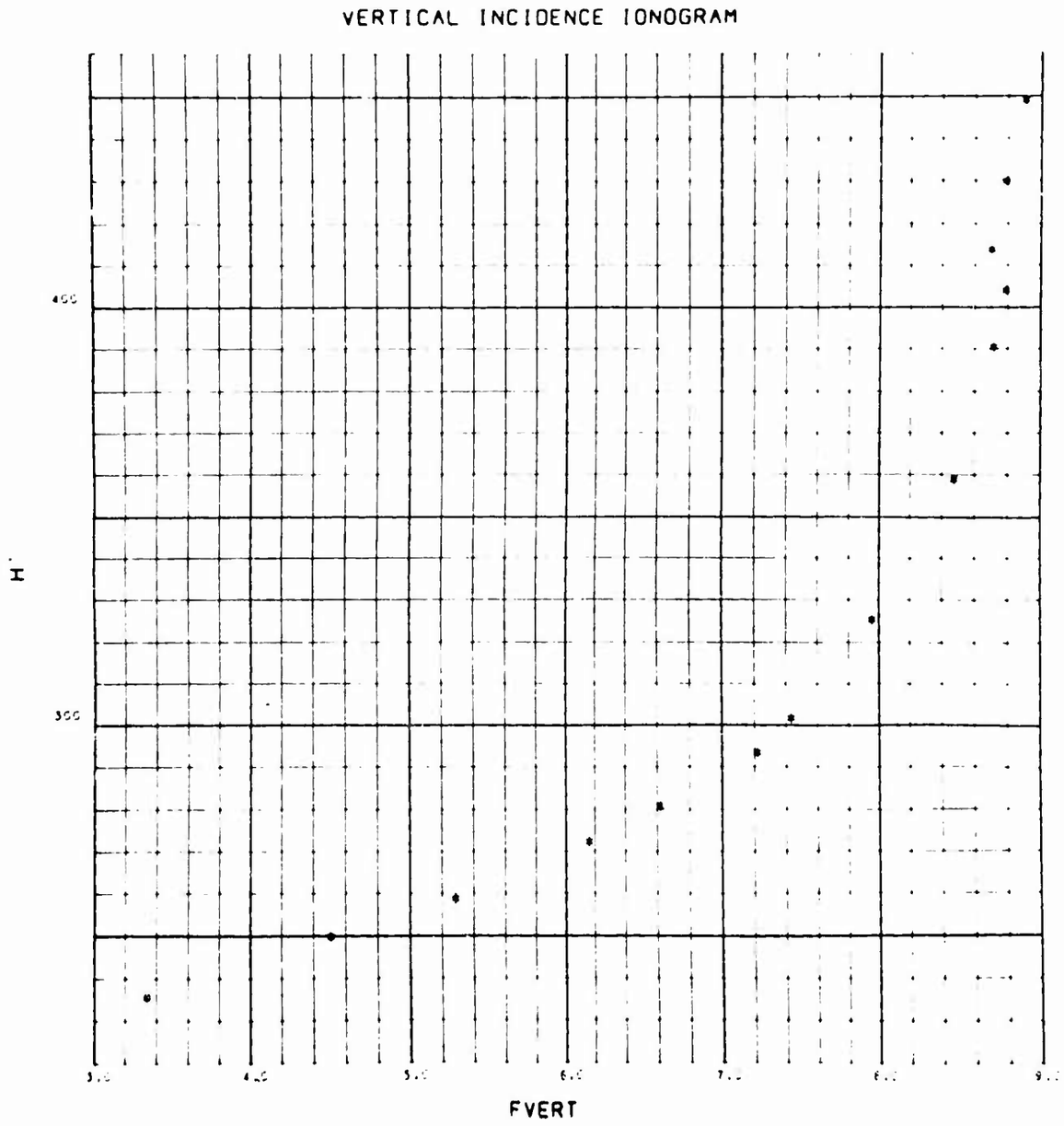

Figure 3. Equivalent Midpath Vertical Incidence Ionogram Inverted from Mode Identified Ionogram.

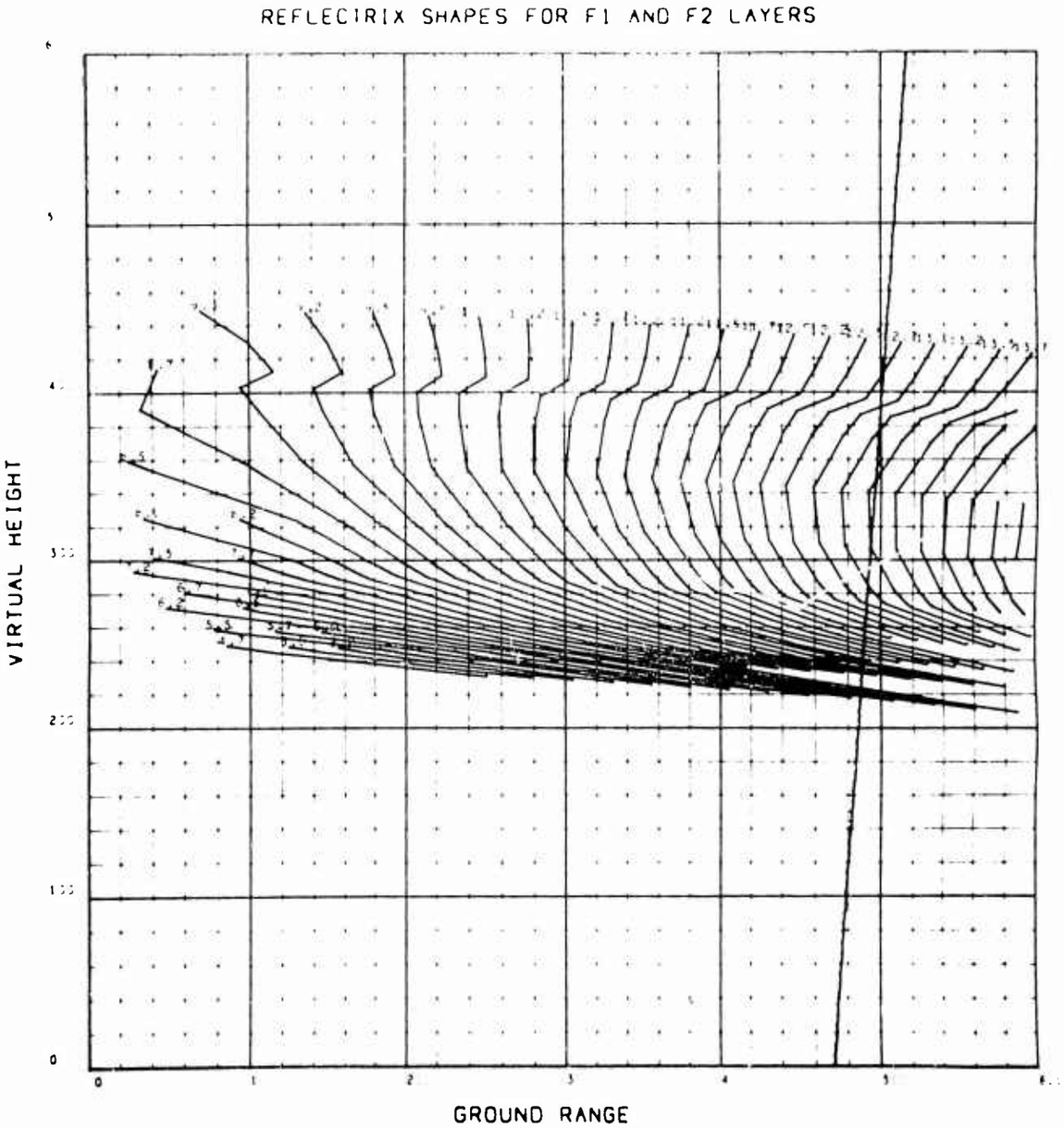

Figure 4: Reflectrix Curves With the Ground Range Plotted. The Coordinate System is a Rectangular Coordinate System Tangent to the Earth's Surface With x = 0, y = 0 at the Receiver

line, with the reflectrices, and calculates the ray path distance from the transmitter to the point of reflection. From this, by assuming equal and symmetrical hop configurations, it is possible to obtain the time delay for a given frequency for the 2F mode simply by multiplying the distance computed above by 4/c for each frequency. Figure 5 shows a tracing of the original ionogram with the 2F trace points calculated in this fashion from the 1F data. While the calculated times are not precisely on the line drawn along the bottom of the 2F trace of the actual ionogram, they easily fall within the spread of the experimental trace at the lower frequencies (i.e., they are all within 0.02 milliseconds of this line). The biggest discrepancy (up to 0.06 milliseconds) occurs at the upper frequency end of the 2F mode, where a discontinuity in the original data trace seems to indicate the presence of a more complicated layer shape or irregular region.

References

1. Barnum, J.R. "Mixed-Mode Oblique Ionograms: A Computer Ray-Tracing Interpretation," Stanford University Radioscience Lab Tech. Report No. 148, December 1968.

2. Croft, T.A. "HF Radio Focusing Caused by the Electron Distribution Between Ionospheric Layers," JGR 72, 2343 (1967).

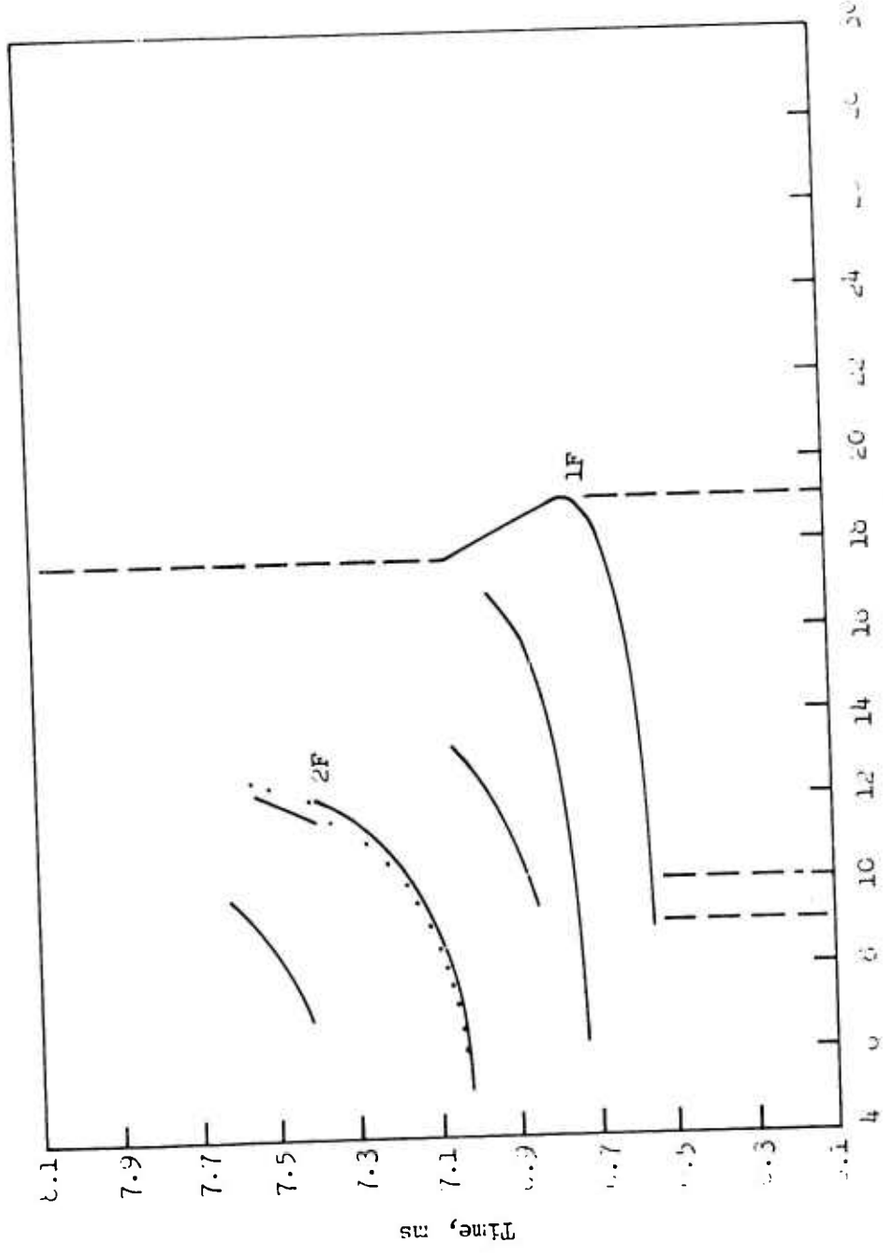

Figure 5. Tracing of Figure 9 from Barnum with Calculated 2F Trace (Dotted Points).

H. H. JENKINS and R. W. MOSS

Georgia Institute of Technology, Electronics Division
Atlanta, Georgia

REVIEW OF SMALL-APERTURE INVESTIGATIONS AT GEORGIA TECH

I. BACKGROUND AND INTRODUCTION

The HF/DF work at Georgia Tech, which has been sponsored by the U. S. Army Electronics Command, is directed toward reducing bearing errors in small-aperture simple loop HF direction-finders, especially when used for ionospherically-propagated signals. Also, as a result of the error reduction work, techniques have been developed to improve sensitivity and display characteristics. The capability of obtaining a measure of elevation angle-of-arrival with a simple loop has been developed.

A major consideration is the tactical nature of simple loop DF systems requiring that all the techniques be amenable to tactical usage. Techniques must be simple and operate in real-time without the benefit of ancillary data processing or computer devices. Weight, volume, and power consumption must be minimized; hence, all circuitry is solid state except the receiver and displays, which are GFE.

The techniques were developed, implemented in a complete exploratory HF/DF system, and operationally evaluated in a realistic tactical environment using both cooperative and uncooperative transmissions from a wide variety of locations and distances.

The following will describe: (1) the sources of bearing errors in loop DF systems; (2) the fundamental approaches to error reduction; (3) a general description of the specific techniques for error reduction;

(4) the functional block diagram of an exploratory HF/DF system; (5) a detailed description of the error reduction techniques; and, (6) the test results obtained from operational evaluations of the exploratory system.

II. SOURCES OF BEARING ERRORS

Large bearing errors are usual when conventional HF loop direction-finding (DF) systems are used for ionospherically-propagated signals. The inaccuracies are primarily determined by the characteristics of the incident signal which, unfortunately, change constantly as a function of time [1]-[6]. The ionosphere not only affects signal parameters such as amplitude, polarization, and phase, but also introduces multipath propagation modes [7]-[10]. Real-time, instantaneous bearing error is a function of the real-time, instantaneous state of the incident signal; hence, as the signal characteristics vary, bearing errors vary [12]-[14]. However, at certain times the signal state is such that minimum bearing errors can be expected.

There are two major error-producing effects in loop DF systems: signal depolarization caused by Faraday rotation and wave interference caused by multipath propagation modes.

Polarization Errors

Loop DF accuracy depends upon the existence of a correct and constant relationship between the direction of propagation and the polarization of the E-field vector. The correct polarization occurs when the incident E-field contains no horizontal components perpendicular to the direction of propagation. In this case, which generally occurs with

ground-wave signals, no polarization error exists, and the measured bearing will be the true great-circle bearing (GCB). However, any E-field polarization tilt creating horizontal components perpendicular to the direction of propagation produces bearing error for sky-wave signals [2].

A signal propagated via the ionosphere is depolarized into a time-variant, elliptically polarized form [15]. Polarization tilt introduces voltages in the loop that are not zero when the plane of the loop is perpendicular to the GCB. As the loop is rotated, the resulting null indicates a bearing which is incorrect. Such bearing errors are a function of the elevation angle-of-arrival, ϕ, and polarization tilt angle, ψ. The general expression for the total induced voltage, V, in a small, vertical loop (diameter less than about 0.1λ) located in freespace is given by

$$V = KE\,[\sin\theta\cos\psi - \cos\theta\sin\phi\sin\psi] \qquad (1)$$

where

$K = \frac{2\pi}{\lambda}$ x (area of loop) x (number of turns),

θ = azimuth angle between direction of propagation and the normal to the plane of the loop,

λ = wavelength,

ψ = polarization tilt angle or the angle between the E-field vector and the vertical plane normal to the plane of the loop,

ϕ = elevation angle between direction of propagation and the normal to the plane of the loop,

and E = the electric field strength in volts/meter.

If θ is not zero when a minimum value of V is obtained, a bearing error results. It can be shown from (1) that the bearing error, θ, is

given by

$$\theta = \tan^{-1} (\sin \Psi \tan \phi) \tag{2}$$

when the loop is rotated until the receiver output is zero. Figure 1 depicts θ as a function of ϕ for various selected values of Ψ and clearly shows that any nonzero value of ϕ produces a bearing error with $\Psi \neq 0^\circ$. A maximum error of 90° occurs with $\Psi = 90^\circ$ for all elevation angles-of-arrival. θ is a function of both Ψ and ϕ; hence, bearing accuracy can vary as the elevation angle-of-arrival changes even though polarization tilt is constant. The time variations of bearing errors caused by polarization rotation are a function of elevation angle-of-arrival and the polarization rotation rate. If the tilt angle Ψ varies linearly as a function of time, (2) becomes

$$\theta(t) = \tan^{-1}(\sin \phi \tan Kt) \tag{3}$$

where t is time in seconds and K is the time-rate-of-change of Ψ. The time derivative of (3) is

$$\frac{d\theta(t)}{dt} = K \left[\frac{\sin \phi}{\cos^2 Kt + \sin^2 \phi \sin^2 Kt} \right]. \tag{4}$$

This function is plotted in Figure 2 for selected elevation angles-of-arrival. Figures 1 and 2 indicate that continuous, uniform polarization rotation which occurs during polarization fading causes continuous changes in bearing error and rate-of-change and that these variations are determined by both ϕ and Ψ. Each elevation angle produces different θ and $\frac{d\theta}{dt}$ curves.

The time-rate-of-change of θ is smallest when Ψ is near 0° or 180°,

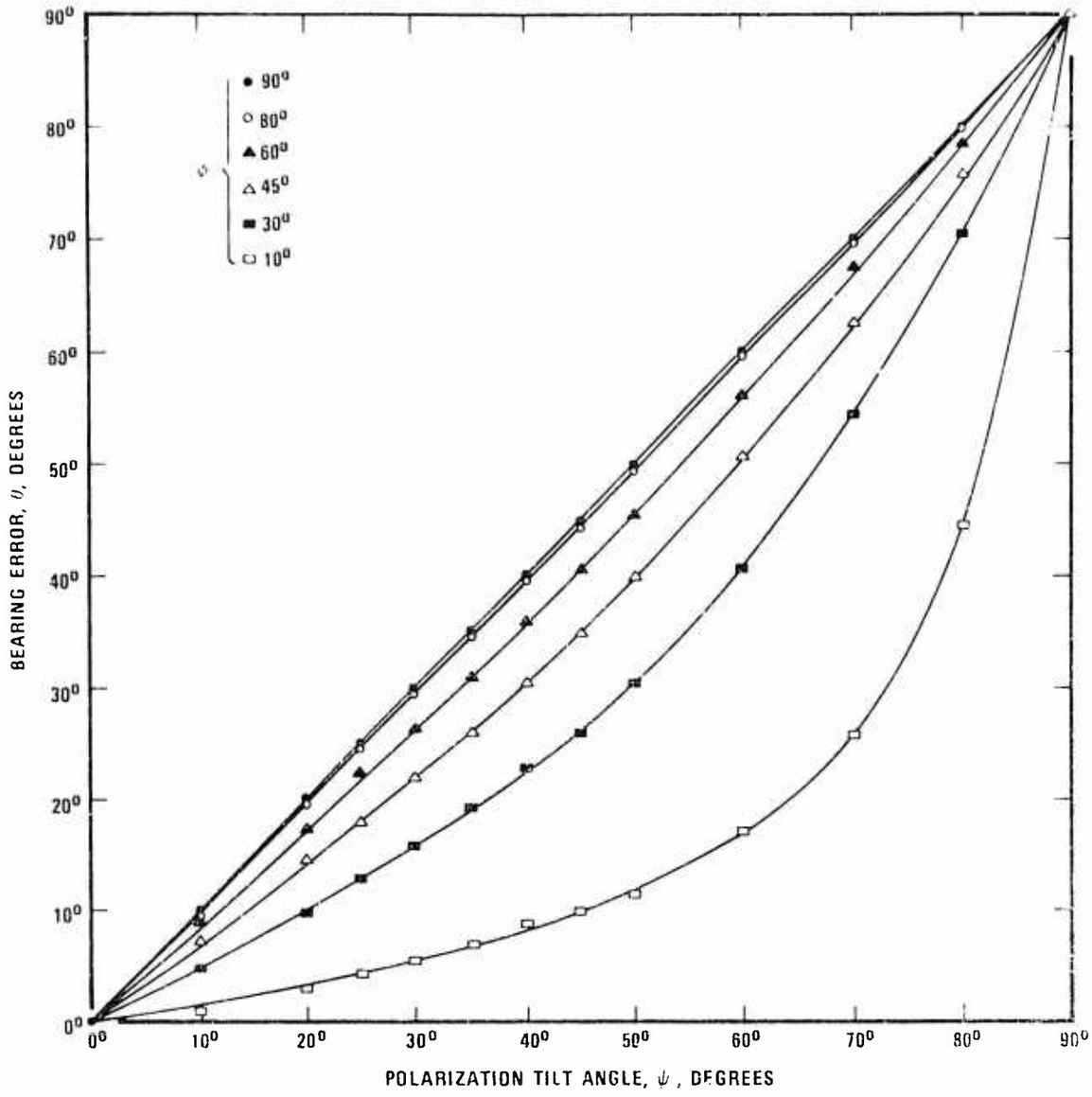

Figure 1. Bearing Error vs. Polarization Tilt Angle.

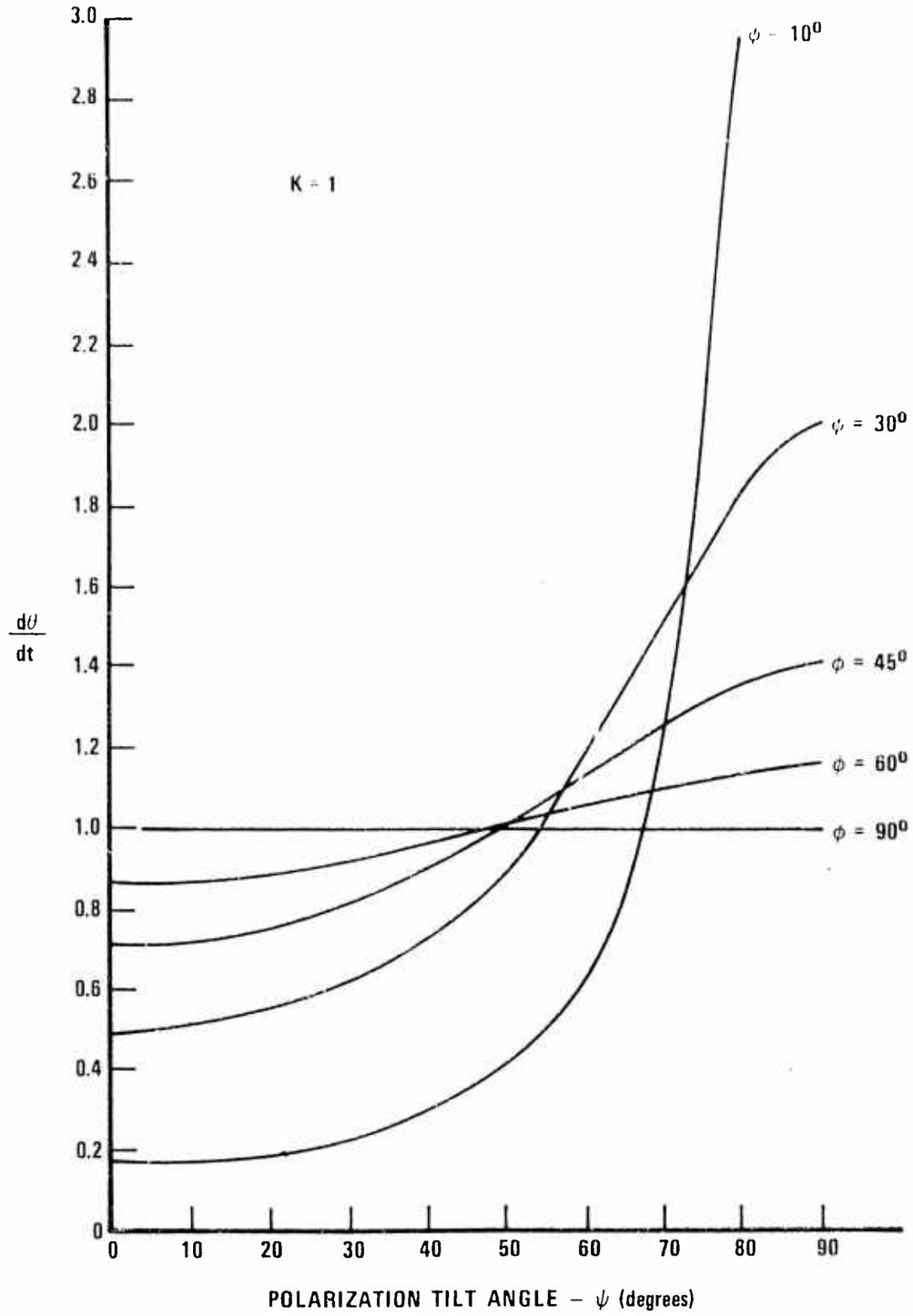

Figure 2. Bearing Swing Rate vs. Polarization Tilt Angle.

which corresponds to minimum bearing error polarization, and largest when τ is near 270° or 90° which corresponds to maximum bearing error polarization. For low elevation angle signals ($0° \leq \Delta \leq 45°$) the variations in $\frac{d\tau}{dt}$ are very pronounced as τ rotates over 360°; signals arriving at the higher elevations angles produce less change in $\frac{d\tau}{dt}$ as τ rotates over 360°. For the case $\Delta = 90°$, the bearing rotation rate is constant implying that the true bearing cannot be defined using $\frac{d\tau}{dt}$ as a measure.

Polarization tilt also decreases the sharpness or distinctness of the bearing null by decreasing the time-rate-of-change of the induced voltage as the antenna rotates through the null. The change in sharpness is much greater for the lower elevation angle signals. Higher elevation angle signals (60° - 90°) have less than a 15 percent decrease in the time-rate-of-change of induced voltage.

Polarization errors are particularly prevalent when the sky-wave signal is experiencing Faraday rotation in the ionosphere and when multipath effects are minimal. This normally occurs near the MUF, especially on a one-hop path. Faraday rotation leads to time-decorrelated fading between the vertical and horizontal components of the incident signal with typical fade rates in the order of several per minute.

To summarize, bearing polarization rotation errors can be as large as ± 90° from the GCB. Inaccurate bearings are evidenced by swinging bearings and display broadening with the slowest swing and minimum broadening near the GCB. However, as the elevation angle increases, the swing rate and bearing display characteristics become more uniform over a complete rotation cycle.

Wave-Interference (Multipath) Errors

Polarization errors are an inherent inadequacy of a loop antenna and can be reduced by using an entirely different DF antenna system, such as spaced loops [16] or an Adcock [17]. However, wave interference errors have their sources entirely external to the loop and are a source of bearing error for all DF systems. The loop is more susceptible to wave interference (or multipath) errors because it is a small-aperture device.

In practice, more than a single wave front at the same frequency is incident on a DF antenna. In fact, most of the energy is normally contained within discrete modes that arrive from many horizontal and vertical angles. The results of investigations using wide-aperture, special-purpose antennas (such as the Wullenweber array) have delineated the complex, multimode structure of an ionospherically-propagated signal [3]. These studies have indicated that the discrete modes in the incident multimode signal are not only often of comparable amplitude, but also arrive at different bearing angles. Also, the relative phases between the modes are time-variables. The resultant of all these variations is a corrugated phase front whose pattern is changing as a function of time. With a small-aperture loop antenna, the observed bearings at any instant will be normal to the phase surface at that point. Therefore, under multipath effects, the bearings are constantly shifting and swinging. A small-aperture loop follows every corrugation and shift of the equiphase surface since the aperture size is too small for significant averaging across corrugations. Also, large ($\pm$ 90°) bearing error can occur due to multipath propagation even though no horizontal components exist in the incident field.

Multipath propagation produces a variable amplitude (fading) signal, and there exists a relationship between the amplitude variation and bearing swing rate and error. Maximum bearing error and swing rate occur at the fade null; minimum bearing error and swing rate occur on the fade crest.

In general, multipath propagation creates time-correlated fading between the E-field vertical and horizontal components whereas polarization rotation produces time-decorrelated fading. However, in both cases, minimum bearing error and swing rate occur on the maximum of the vertical E-field component of the fading signal.

Multipath fading is the more common type; however, the effects of polarization fading are worse for a loop DF system since a rotating bearing is displayed with little or no pattern change.

III. FUNDAMENTAL APPROACH TO ERROR REDUCTION [18-21]

The fundamental approach to error reduction was based on the determination of the specific characteristics of the incident signal that produce minimum bearing errors and the development of techniques for using these characteristics to either (1) restrict or unblank the display of bearing information to only those conditions that produce minimum bearing error, or (2) create distinct and interpretable differences between accurate and erroneous bearing displays.

IV. SPECIFIC APPROACHES

For both multipath and polarization errors, minimum bearing errors occur when the vertical E-field component is at a maximum. The fade crest detection method of error reduction uses a dual-channel receiver

One channel is used as a conventional loop DF; the other uses a vertical probe to sense the magnitude of the vertical component and supply display unblanking pulses at or near the fade crests.

For both multipath and polarization errors, minimum bearing errors occur when the bearing swing rate is a minimum. The swing rate discrimination method measures the bearing swing rate and unblanks the display as a function of the time rate-of change of the bearing swing. This technique can be used with a single-receiving channel.

Conventional loop DF systems display all bearings and the operater rejects or accepts bearings based on subjective evaluations; the fade crest detection and swing rate discrimination described above remove the more erroneous bearings from the operator's view and display only the more accurate bearings.

The tilted loop technique for bearing error reduction does not use unblanking but creates distinct and interpretable differences between accurate and erroneous bearing displays. Also, the technique can be used to obtain a measure of elevation angle. This technique can also be used with a single-receiving channel.

V. FUNCTIONAL BLOCK DIAGRAM

Figure 3 is a functional block diagram of the final version of the exploratory system. (The swing rate discriminator is not shown, having been replaced by the tilted loop technique which performs essentially the same function.) Figure 4 is a front panel view of the post-IF signal processor which includes all the post-IF circuitry except the display and sine/cosine potentiometer.

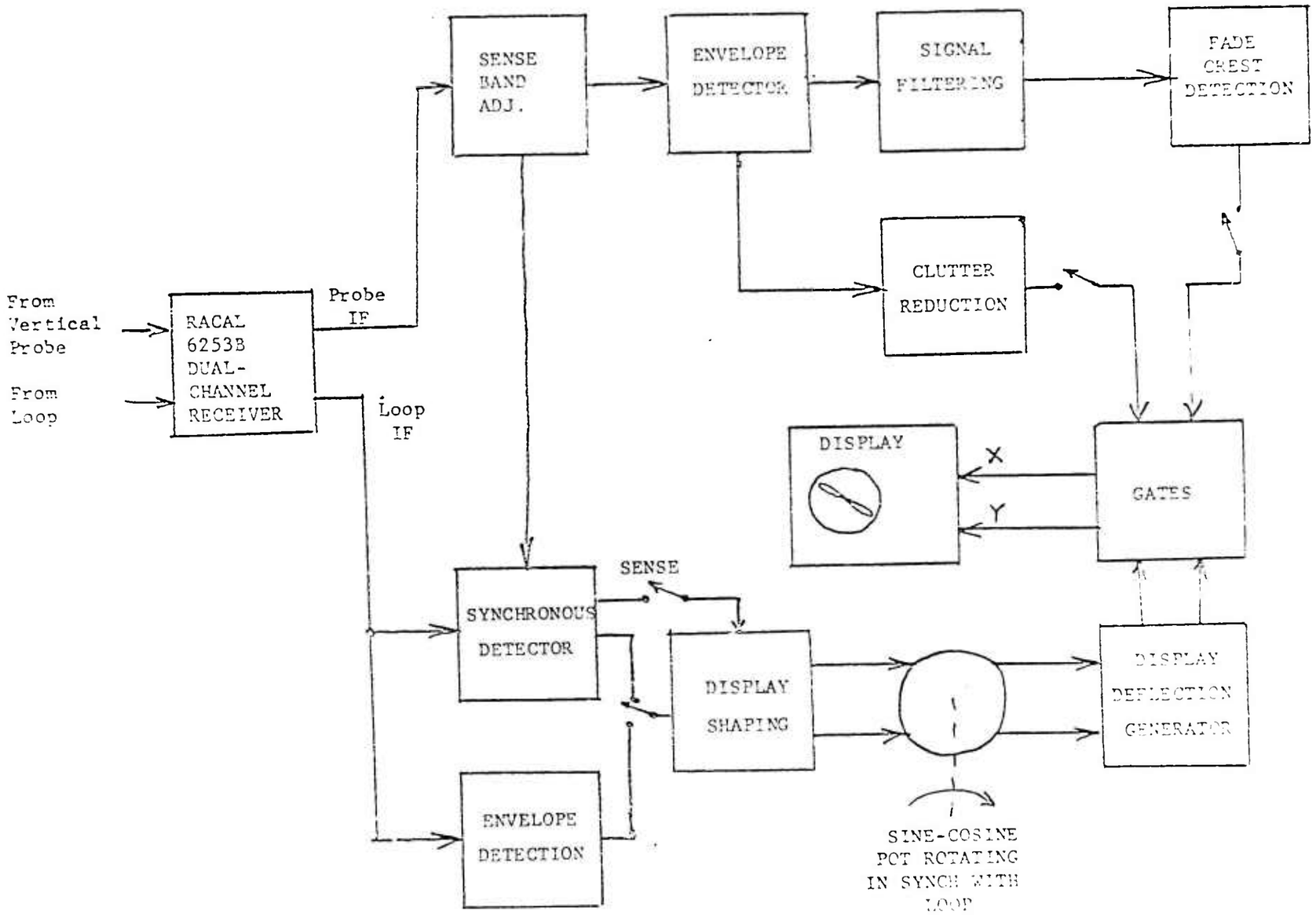

Figure 3. Simplified Functional Diagram of Post-IF Circuitry.

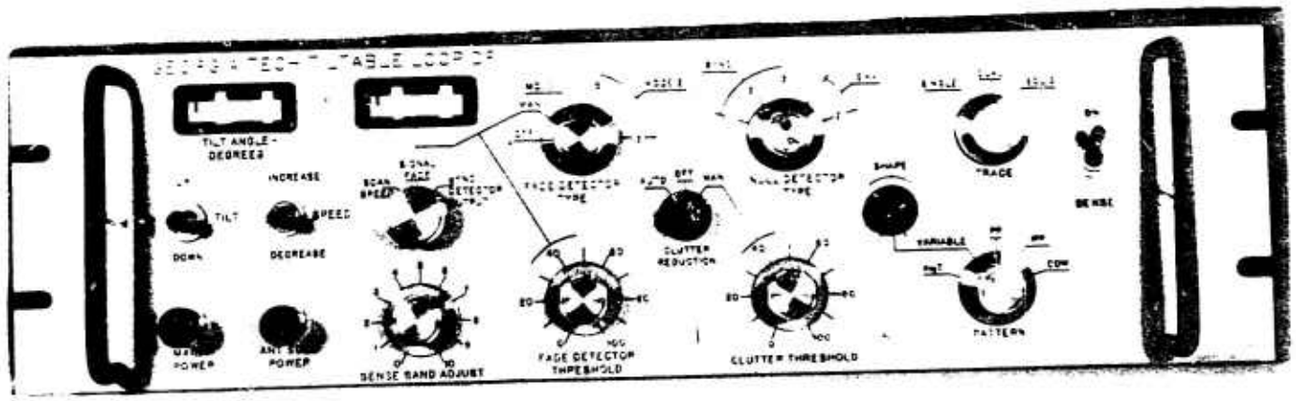

Figure 4. Front-Panel View of Post-IF Signal Processor.

Two antennas are used: a loop (2.25 ft^2 area) for Channel 1 of the RACAL 6253b, and a vertical probe for Channel 2. Figure 5 is a functional diagram of the antenna assembly; Figure 6 is an overall view. The loop is mechanically rotated, scan rate is continuously variable from 0 to 250 rpm. The loop plane can be continuously tilted from 0° to 90°, about a horizontal axis. Tilt rate is 6° per second. The vertical probe is 9 inches long and is mounted directly in the center of the loop. The effective heights of the loop and probe were experimentally matched at 10 MHz to avoid excessive cross-coupling problems.

The loop IF signal contains the scan modulation which can be either envelope or synchronously detected.

Conventional, single-channel loop DF systems use incoherent detection of the loop scan modulation by an envelope detector. Envelope detection has several disadvantages for DF applications. One, the output signal represents the magnitude of the scan modulation and is, hence, unipolar with a high harmonic content. The low-pass filtering following the envelope detector must have a frequency response much greater than the basic scan fundamental in order to pass higher-order harmonics and, hence, preserve the integrity of the bearing nulls. This wide bandwidth adds noise. Two, the envelope detector further deteriorates low SNR signals, e.g., an envelope detector input SNR of -10 dB yields an output SNR of about -14 dB. Three, the envelope detector contains a 180° ambiguity in the bearing information in that a bearing null at θ_1, for example, cannot be distinguished from a true null at $\theta_1 + \pi$. Four, the envelope detector has a limited dynamic range and saturation effects degrade the bearing display.

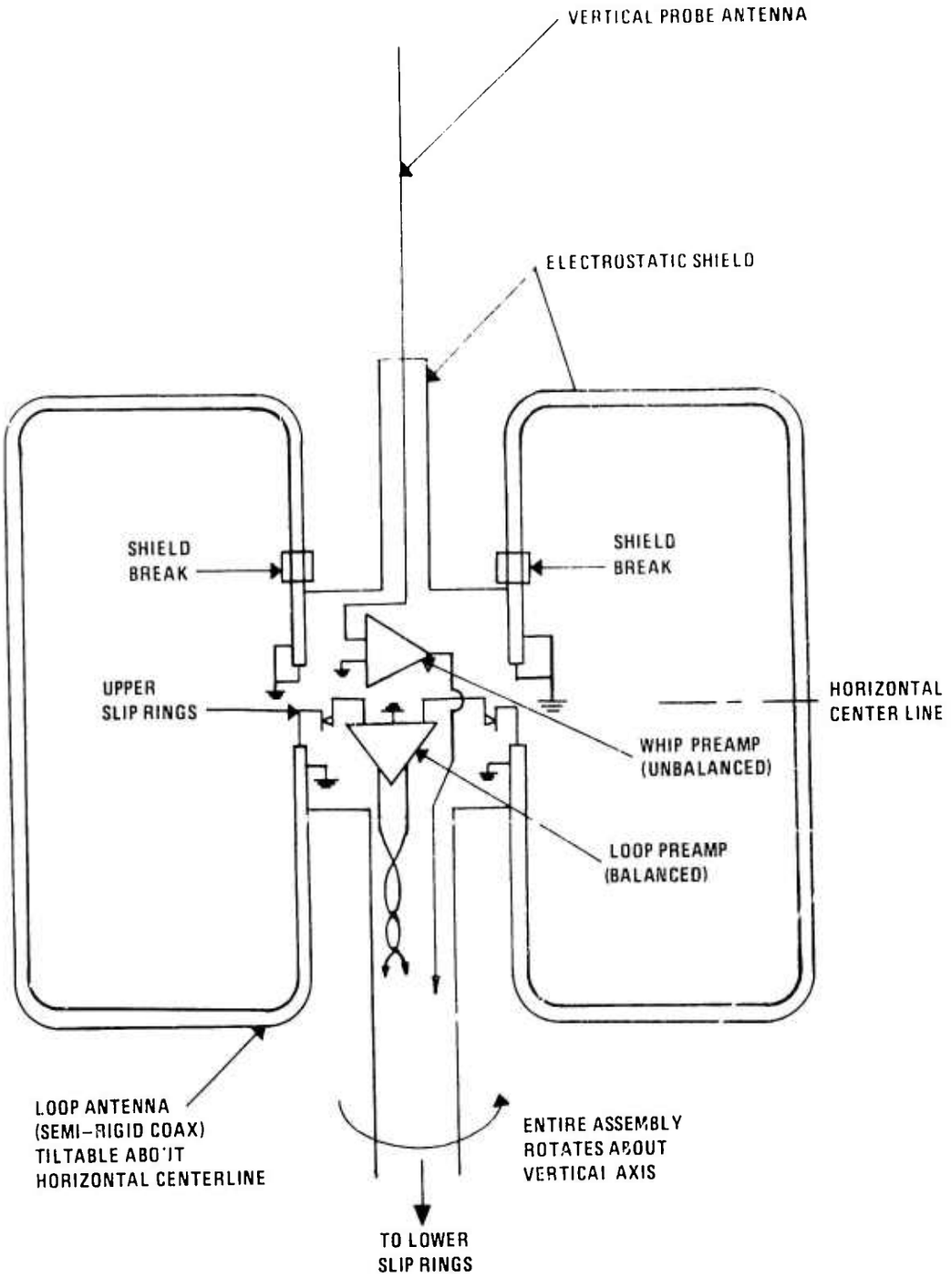

Figure 5. Basic Electrical and Mechanical Configuration of Tiltable Loop Antenna System.

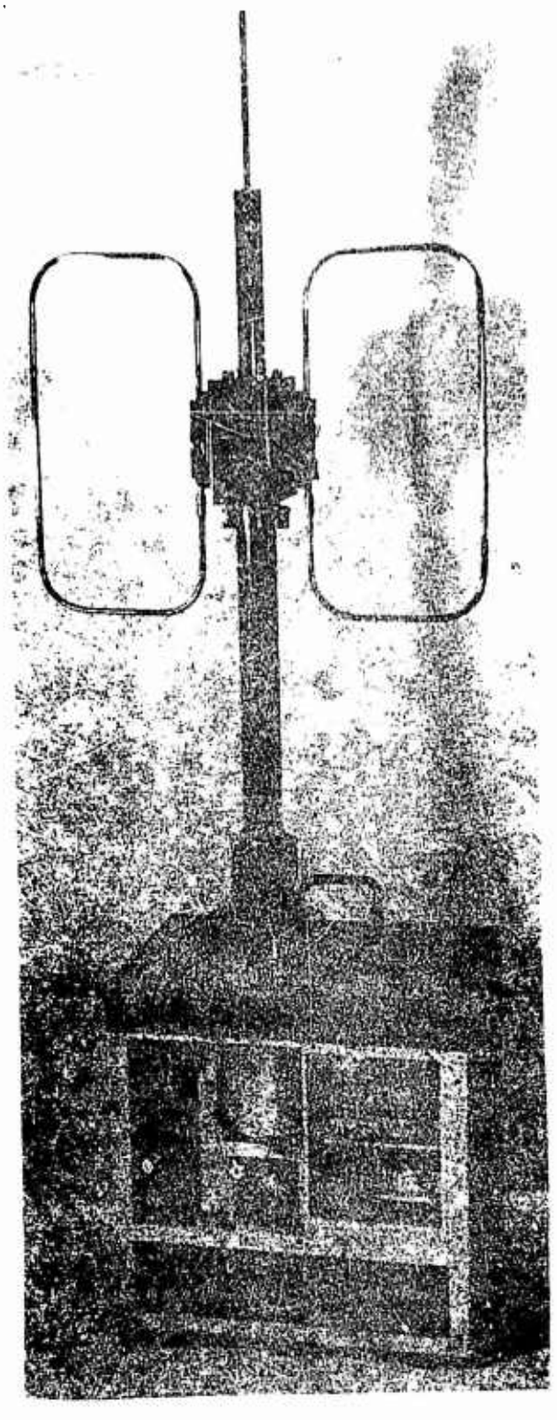

Figure 6. Overall View of Antenna Assembly.

Synchronous (coherent) detection reduces the disadvantages of envelope (incoherent) detection and was a natural addition to the system due to the presence of the channel 2 output. This output is coherent (or can be made coherent) with the loop channel output except for the desired scan modulation containing the bearing information. The channel 2 output is used as a coherent demodulation signal for the synchronous detector.

The synchronous detection output is a sinusoid, bipolar signal with the zero-crossings containing the bearing information. Resultant advantages over the envelope detection are: (1) narrow-band post-detection filtering can be used to improve SNR since the synchronous detector output is a simple sinusoid at the antenna scan fundamental; (2) low SNR signals are not degraded; (3) sense information is inherent in the bipolar signal; and (4) dynamic range is improved.

In the exploratory system, synchronous detection improved the sensitivity by about 10 dB. Figure 7 illustrates the improvement in sensitivity and display characteristics compared to envelope detection.

The IF output of channel 2 is modulated by fading. The fading envelope is detected by a conventional envelope detector and low-pass filter circuitry and applied to the fade crest detectors, where a positive gating pulse is generated at the fade crest. For optimum detection, two types of fade crest detectors may be selected depending upon the type of fading (polarization or multipath) encountered. One type, the averaging and comparison technique, was designed primarily for polarization fading conditions where a good signal-to-noise ratio and reasonably periodic fade cycles exist. The other, the peak sample and hold technique, was

ENVELOPE DETECTOR
BEARING DISPLAYS

SYNCHRONOUS DETECTOR
BEARING DISPLAYS

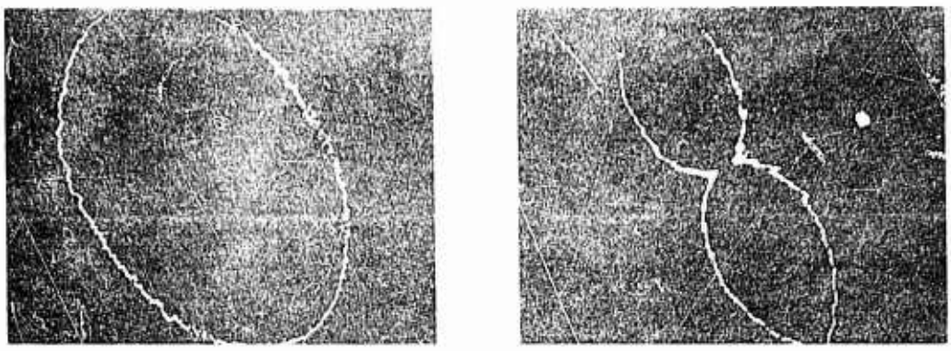

INPUT AT REFERENCE LEVEL

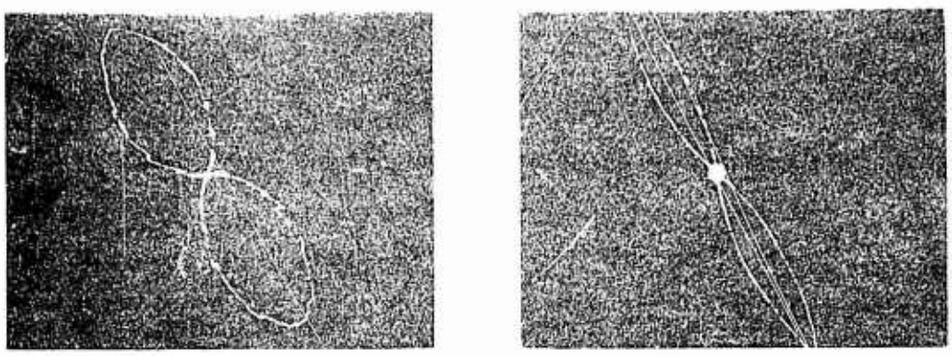

RF REFERENCE PLUS 10dB

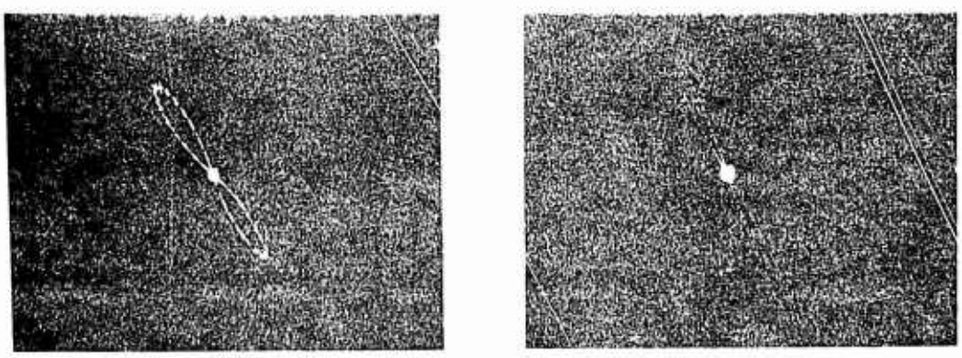

RF REFERENCE PLUS 20dB

Figure 7. Bearing Displays Comparing Synchronous and Envelope Detection.

designed primarily for multipath fading conditions with low signal levels and irregular, erratic, nonperiodic amplitude variations.

The channel 2 detected signal is also supplied to clutter reduction circuitry that removes display clutter due to on-off transitions of the carrier.

The circuitry uses the output of channel 2 as a gating signal to allow only the true bearing nulls to be displayed and gate-out the false bearing nulls due to carrier interruptions. Channel 2 output does not contain the loop scan modulation but does contain the on-off modulation; channel 1 output contains both scan and modulation nulls. Clutter reduction is based on the simple concept that true bearing nulls occur only when the channel 2 output is high and the channel 1 output is simultaneously low, i.e., in a null. The clutter reduction circuitry applies deflection voltages to the bearing display only when the channel 2 output is above an established threshold and, hence, carrier on-off transitions are removed from the display leaving only the true bearing null. Figure 8 illustrates the effects of clutter reduction.

In the loop channel, the post-detection circuitry (display shaping and deflection generator) processes the bearing information for display on the storage scope (HP141A with variable persistence). The display drive signals are applied through gate circuits prior to the scope. Conventional sensing techniques require display deflection plate switching; however, the synchronous detection sensing technique obviates the need for deflection plate switching allowing for more flexibility in the selection of displays.

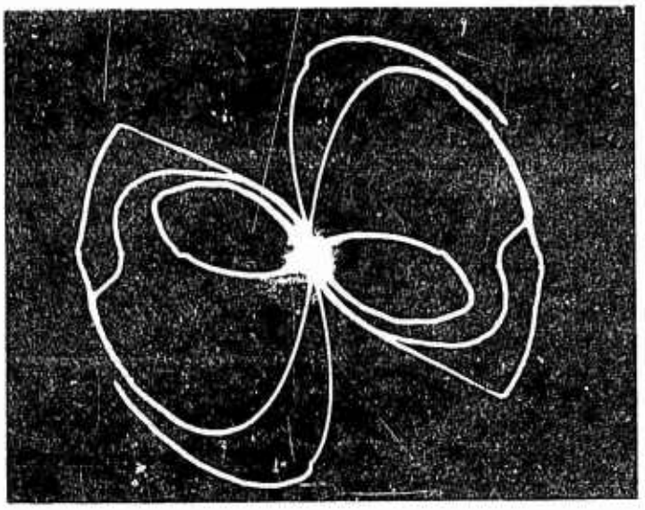

WITHOUT CLUTTER REDUCTION

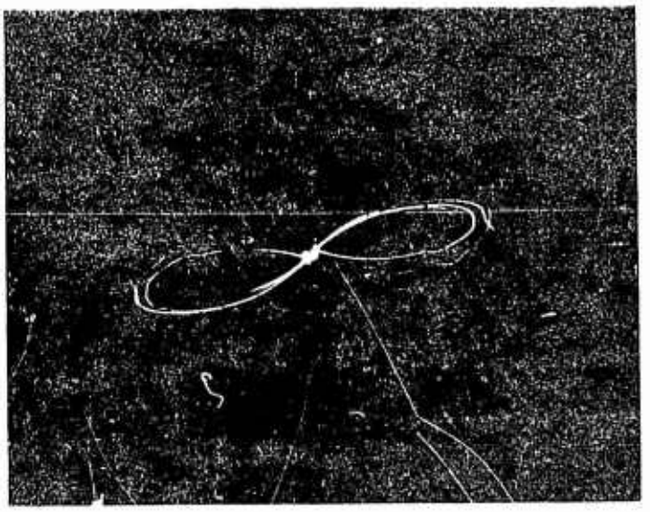

WITH CLUTTER REDUCTION

Figure 8. Effect of Clutter Reduction on ICW Bearing Displays.

VI. DETAILED DESCRIPTION OF ERROR REDUCTION TECHNIQUES

Fade Crest Detection

The averaging and comparison mode (Figure 9) operates by (1) averaging the fading envelope, and (2) comparing the average value with a weighted envelope. An output occurs only if the weighted input exceeds the average value. The weighting factor, called the fade margin, determines how far above the average value the input must rise before an output occurs. For example, with a 3 dB fade margin, an output occurs when the input is 3 dB or greater above the average.

An averaging time of approximately 15 seconds was chosen based on an assumed minimum rate of four fade cycles per minute. The averaging time must be at least equal to the fade period since it requires at least one fade cycle to indicate short-term behavior.

The fade margins of 0, 1, 3, 6 and 10 dB were based on the anticipated range of the maxima relative to the average for both multipath and polarization fading. Multipath may be characterized by a Rician distribution [10] which allows for the finite probability of having a fade crest of infinite amplitude. However, 10 dB was chosen as a practical upper limit since the percentage of time that this level is exceeded for Rician statistics is less than 0.01%. Based on theoretical considerations, 3 dB was considered to be about the highest fade margin that could be reliably used for polarization fading. (Operational evaluation proved this to be true.) Figures 10 and 11 illustrate the fade detector input (bottom) and output (top) waveforms for fade margins of 0 to 5 dB, respectively. The time base was 2 sec/cm. (The 5 dB was later changed to 3 dB.)

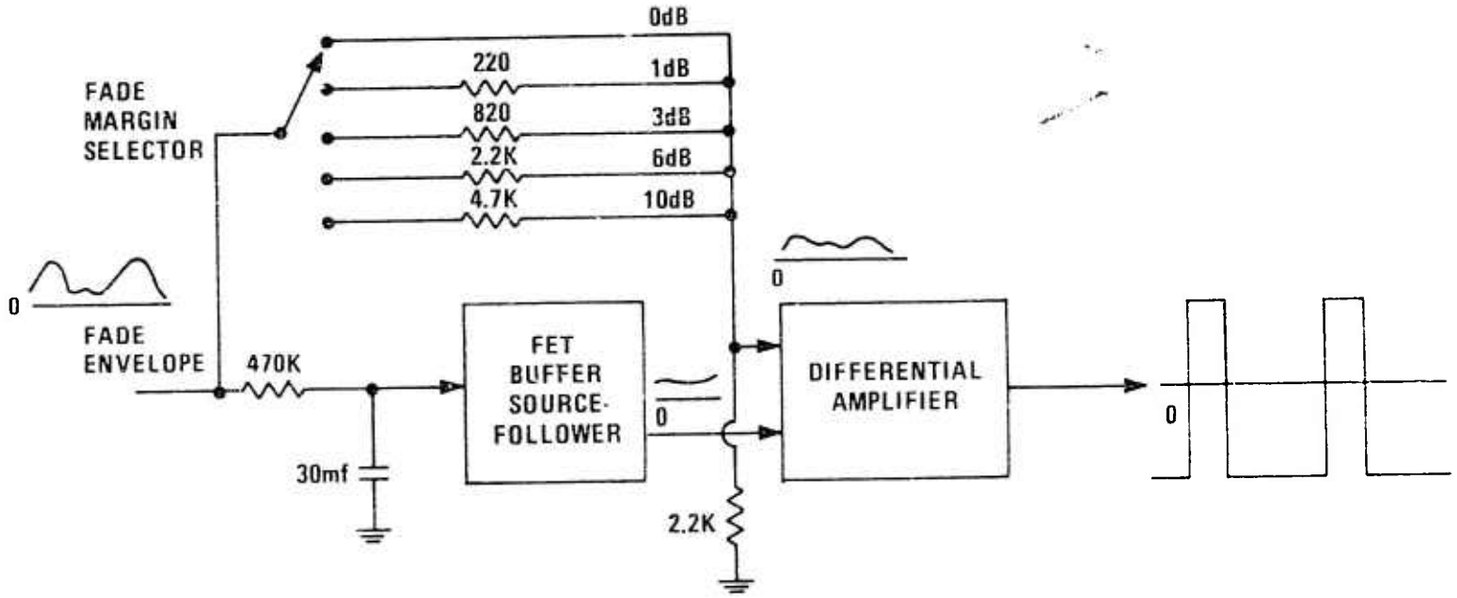

Figure 9. Fade Detector--Average and Comparison with Selectable Fade Margin.

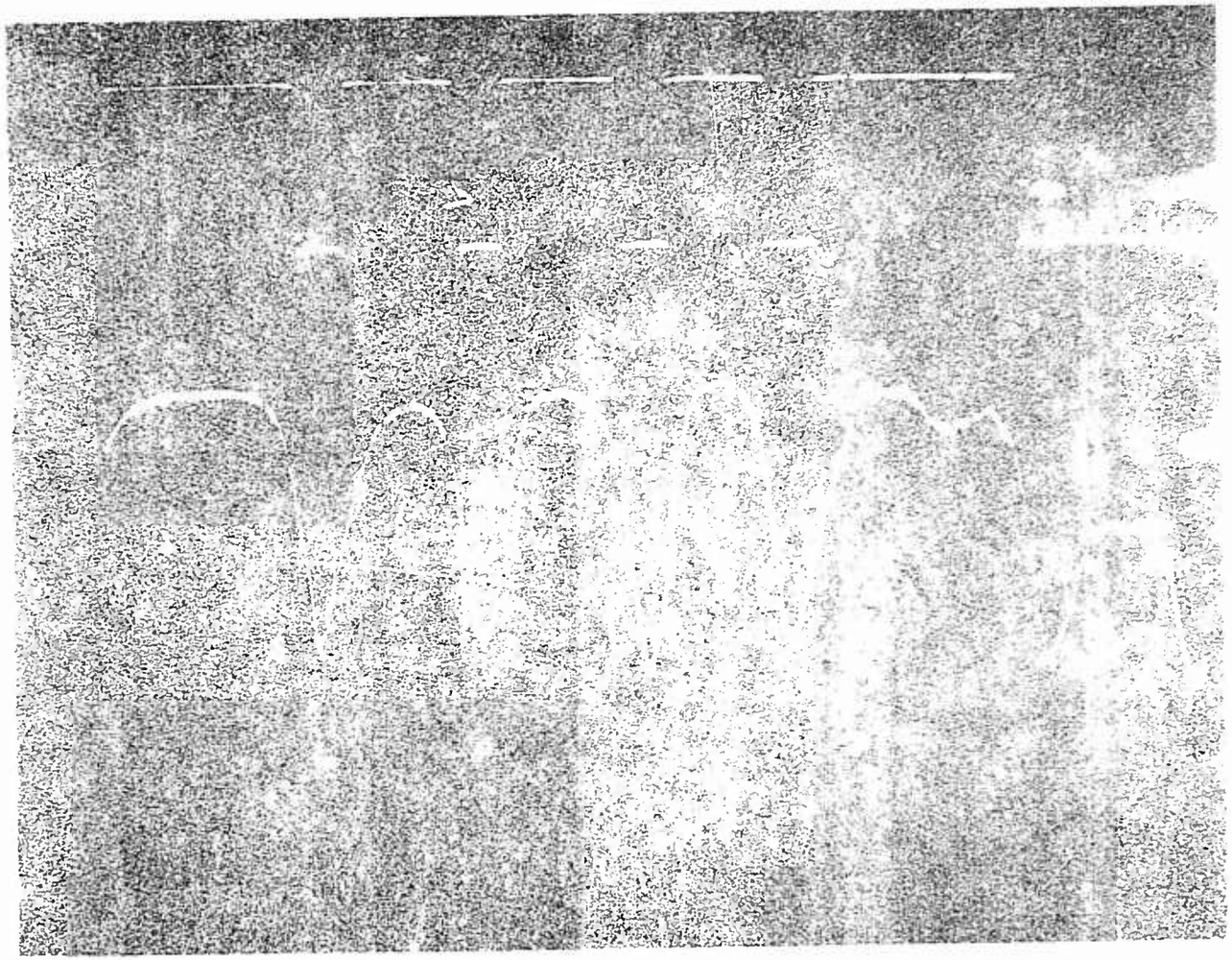

Figure 10. Average and Comparison Fade [illegible]
9.[illegible] v/cm) and Output (Top Trace [illegible]).

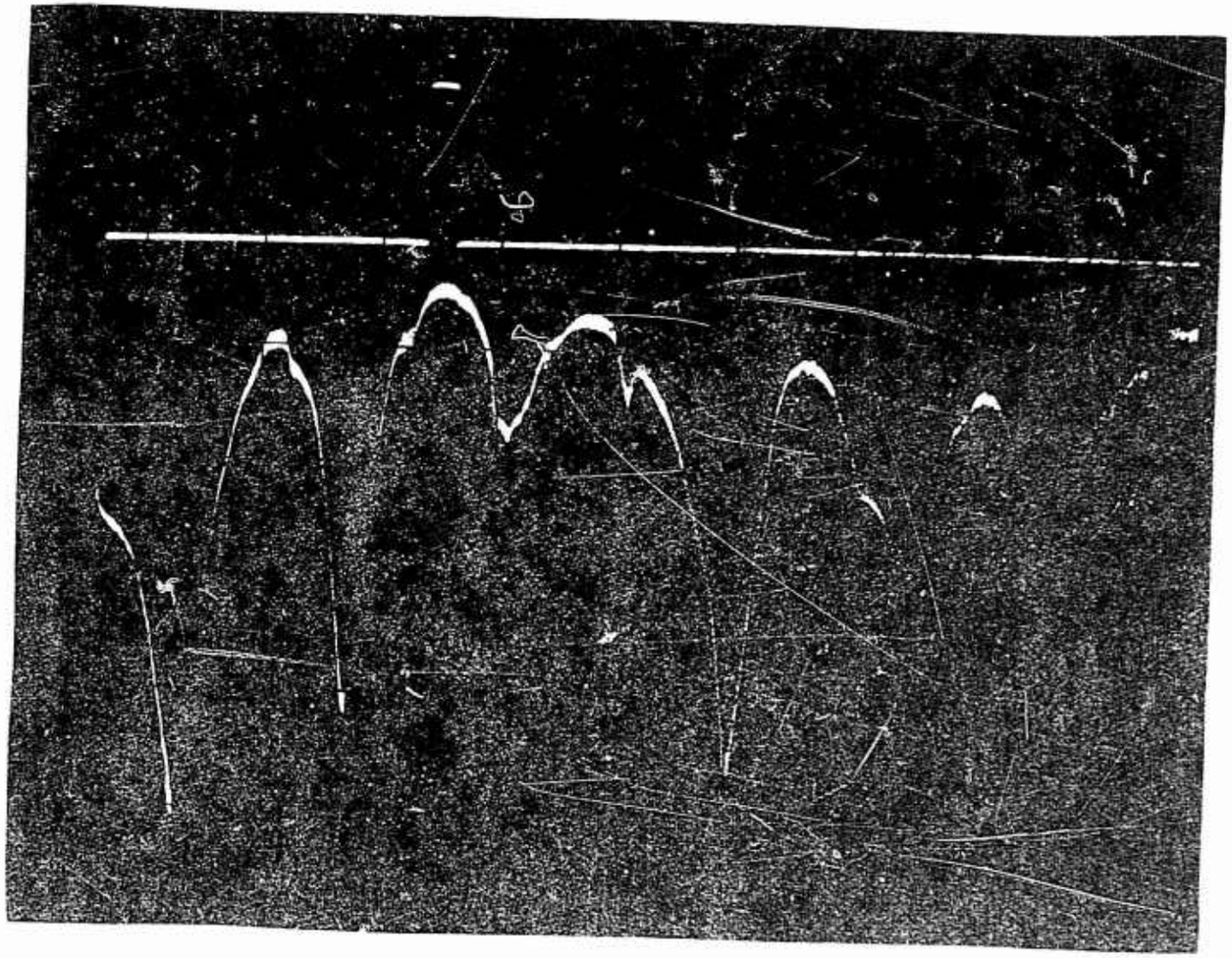

The peak sample and hold sweep (Figure 12) operates on the signal peaks directly and does not depend upon the average value. This is desirable when (1) irregular amplitude fading is present and no consistent average value can be maintained; and (2) the signal-to-noise (or interference) ratio is small with the desired signal consistently peaking-up out of the noise or interference. This technique operates in the following manner. When the input is applied the 30 mfd capacitor charges to the peak value of the first fade cycle and is then allowed to slowly discharge. When the next fade crest arrives and exceeds the level on the holding capacitor, a discontinuity in the differentiator input signal level results and a pulse is produced at the differentiator output. This pulse is amplified and used for unblanking. The 52 second discharge time constant was chosen to be much greater than a fade cycle rate of 10 seconds which was considered to be a typical minimum for multipath fading. This technique unblanks before the fade crest maxima on the positive-going portion of the fade cycle when the signal-to-noise ratio is increasing; unblanking during decreasing signal-to-noise ratio is reduced. Tests showed that restricting displays to periods of increasing signal-to-noise ratios reduced the number of spurious bearings and increased accuracy, especially when the maximum signal-to-noise ratio is low. Operation is depicted in Figure 13 with a time base of 2 sec/cm. It may be noted that the unblanking time is proportional to the magnitude of the fade crest amplitude. The larger the fade crest level the longer unblanking occurs providing automatic amplitude weighting for the unblanking technique.

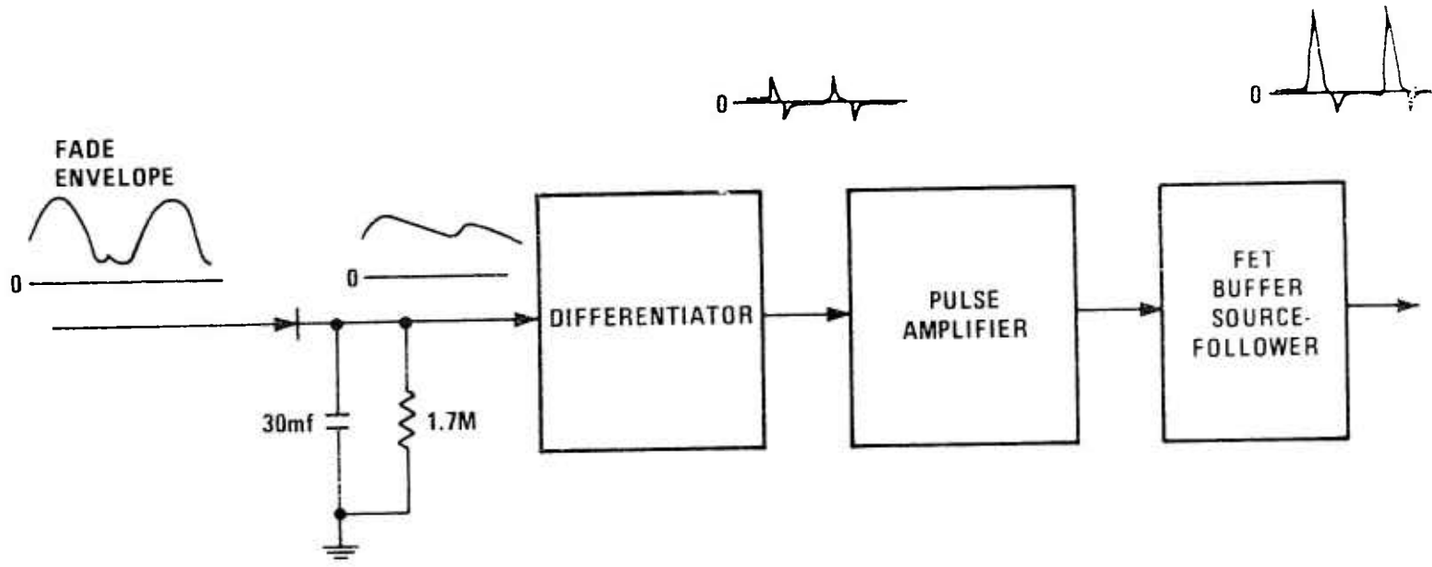

Figure 12. Fade Crest Detector--Peak Sample and Hold Technique.

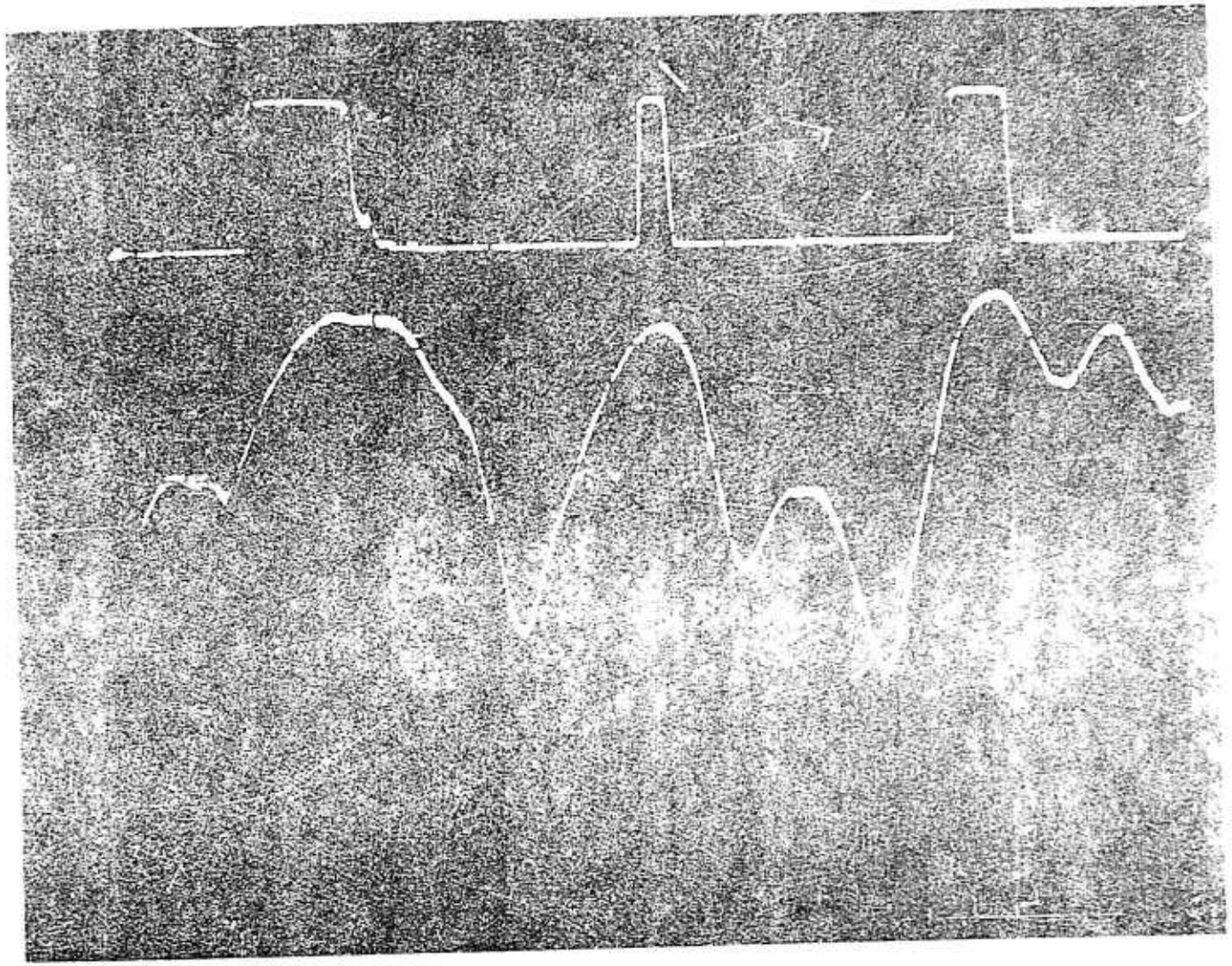

Figure 13. Peak Sample and Hold Fade Crest [illegible]
0.5 v/cm) and Output (Top Trace [illegible]

VII SWING RATE DISCRIMINATOR (SRD)

The SRD, Figure 14, unblanks the display depending on the time-rate-of-change of the bearing swings. The bearings are converted to digital form, i.e., a pulse occurs at each bearing null. As the bearing swings, the time interval between the bearing pulses varies; a steady bearing produces a constant time interval between pulses (about 100 msec for a 5 rps loop scan). When a predetermined number (eight in the exploratory system) of consecutive bearing azimuths occurs within a preset number of degrees from one another, the SRD unblanks the display. The preset allowable swing region can be varied from about 5° to 20°. The SRD converts the bearing pulses, which are in the form of a pulse-position modulated signal, to a DC analog form with the DC level indicating the bearing in degrees relative to reference azimuth. The bearing pulses sample a ramp pulse which also starts a timer. The DC level corresponding to the first bearing pulse is stored and compared with the DC level of seven succeeding bearing pulses. If no comparisons are out of the voltage range corresponding to the allowable bearing swing rate, the timer completes its 2.6 second cycle and the next bearing display is unblanked. If excessive swing occurs, the timer and sampling circuits are reset to start another comparison sequence.

VIII. TILTED LOOP TECHNIQUE

A major problem with loop DF systems is that the bearing null information and consequently the display for both accurate and inaccurate bearings remain essentially unchanged -- except for bearing shift -- as polarization changes. Hence, the ability to separate accurate from

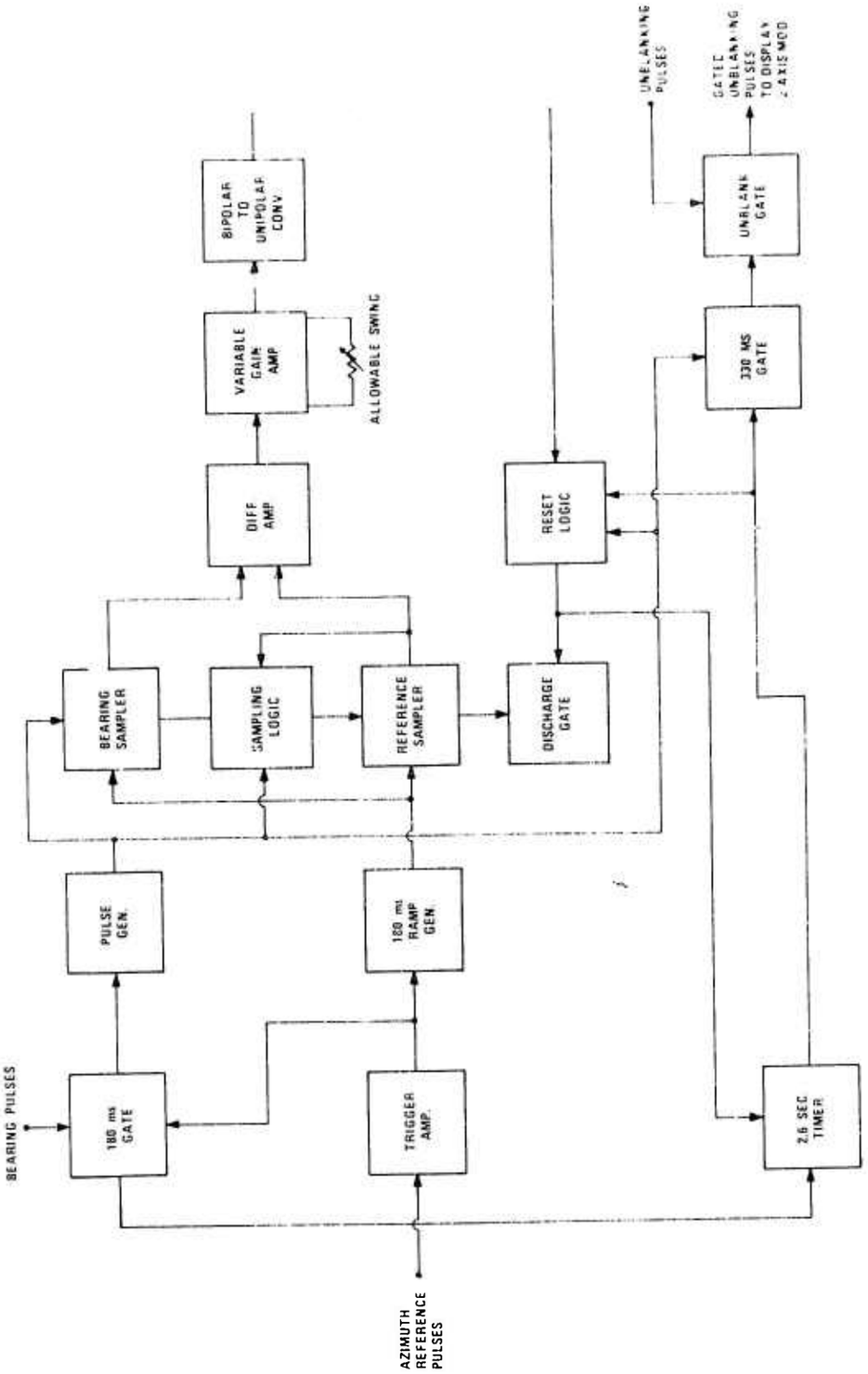

Figure 14. Block Diagram of the Swing Rate Discriminator.

inaccurate bearings based on display characteristics does not exist in conventional systems. The exploratory system developed by Georgia Tech uses a tilted loop technique that creates distinct and interpretable differences between accurate and erroneous bearing displays. Also, the technique can be used to obtain a measure of the elevation angle of the incident sky-wave signal. The following describes how this is accomplished.

The expression of the free-space induced voltage, E_L, in a small loop rotating about a vertical axis is given by

$$E_L = K \left\{ \cos \Psi \sin \theta - \sin \Psi \sin \Phi \cos \theta \right\} \tag{5}$$

where K = a constant that is a function of loop area, frequency, and number of turns,

Ψ = the incident signal polarization tilt angle relative to vertical,

θ = the angle between the direction of propagation and the normal to the plane of the loop,

and Φ = the elevation angle of the incident signal referenced to the horizontal.

Equation (5) can be simplified to

$$E_L = KA_o \left[\cos (\theta - \delta)\right] \tag{6}$$

where $A_o = \sqrt{A_1^2 + A_2^2}$,

$A_1 = \cos \Psi$,

$A_2 = -\sin \Psi \sin \Phi$,

and $\delta = \tan^{-1} \left(- \frac{A_1}{A_2} \right)$.

Equation (5) shows that the response is a function of both signal

depolarization and elevation angle, and (6) indicates that the response as a function of θ is a sinusoidal, figure-eight response for all combinations of Ψ and Φ. Accurate bearing indications are obtained only whenever $E_L = 0$ and $\theta = 0°$ or $180°$. It can be seen from (5) that this condition occurs only when $\Phi = 0°$ or $180°$. Then

$$E_L = K \sin \theta. \tag{7}$$

For nonzero values of Ψ and Φ, (6) indicates two inaccurate but symmetrical nulls 180° apart. The null locations, however, do not occur at the correct bearing along the direction of signal propagation. Unfortunately, these inaccurate bearings exhibit the same shape and null symmetry as accurate bearings. Figure 15a illustrates the type of bearing display obtained from a vertical loop. The tips of the lobes correspond to the null locations. A double-nulled, symmetrical response occurs for all signal conditions, but the bearing display rotates as the polarization rotates and will indicate an accurate bearing only when $\Psi = 0°$ for sky-wave signals.

Tilting is performed by positioning the plane of the loop at a tilt angle α relative to horizontal while maintaining rotation about the vertical axis. Figure 16 depicts the relationship between α and Φ. The tilt angle α is variable from 0° to 90°. The free space induced voltage, E_{Lt}, for the tilted loop is

$$E_{Lt} = K \left\{ \cos \Psi \sin \theta \cos \alpha - \sin \Psi \sin \Phi \cos \theta \cos \alpha + \sin \Psi \cos \Phi \sin \alpha \right\} \tag{8}$$

which can be reduced to

(a)

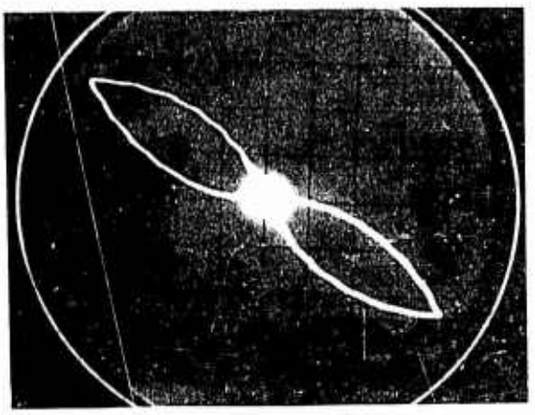

(b)

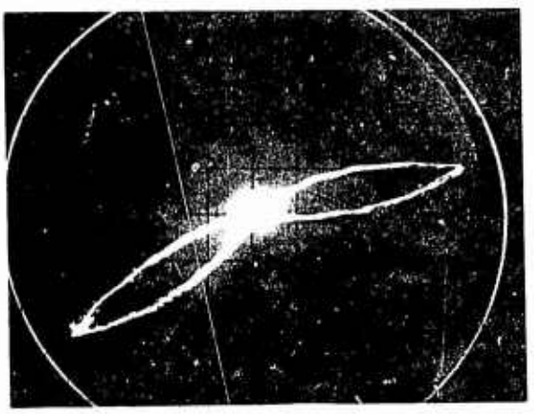

(c)

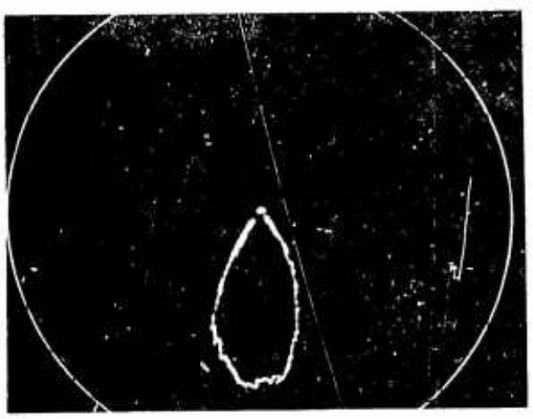

Figure 15. Bearing Displays Illustrating (a) Double-Nulled Symmetrical, (b) Double-Nulled Asymmetrical, and (c) Single-Nulled Responses.

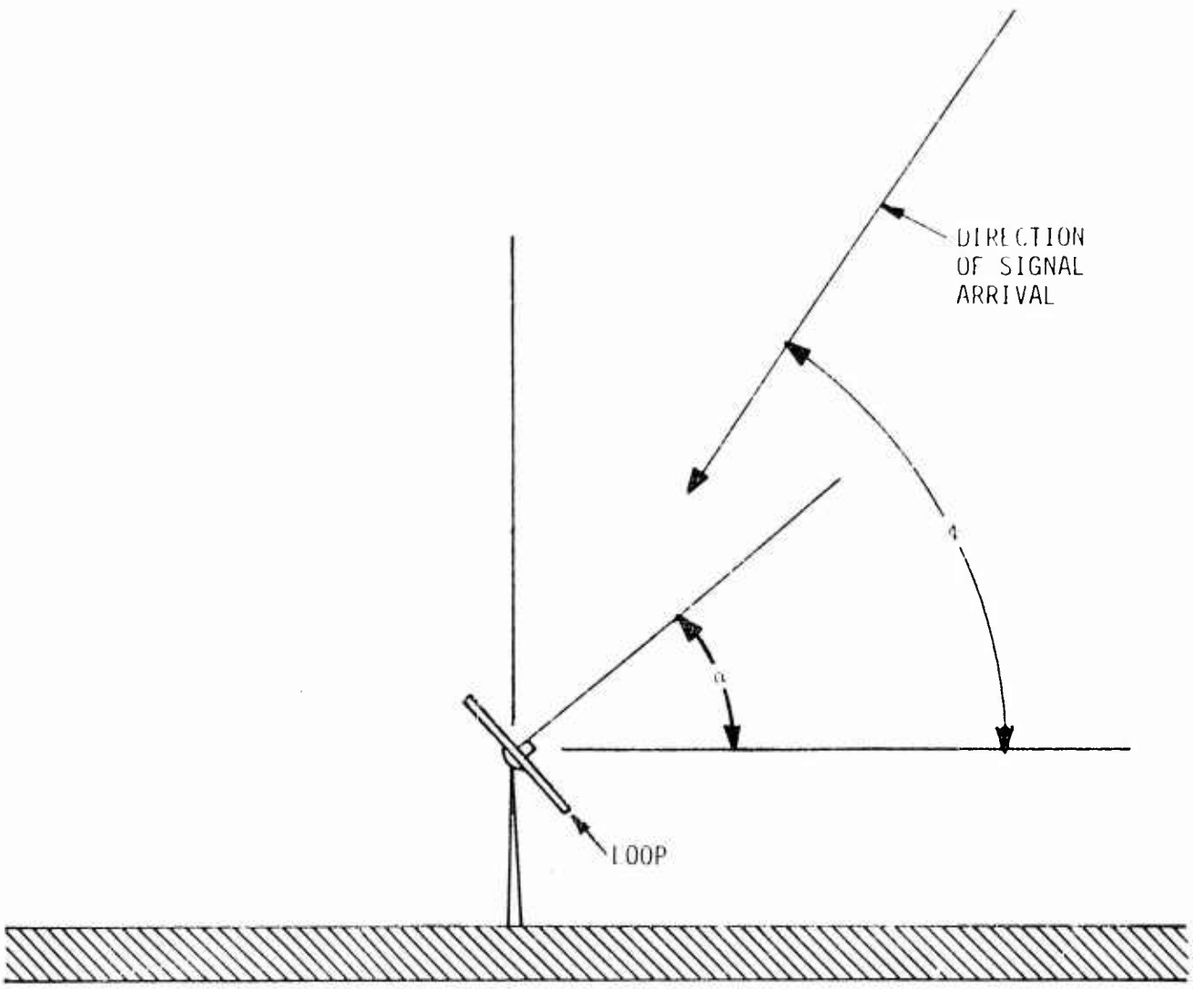

Figure 16. Diagram Depicting Loop Tilt Angle and Signal Elevation Angle-of-Arrival.

$$E_{Lt} = K\left\{B_1 \cos\left(\theta - \frac{\pi}{2}\right) + B_2 \cos \gamma + B_3\right\}$$

$$= K\left\{B_0 \cos(\theta - \gamma) + B_3\right\} \quad , \tag{9}$$

where $B_0 = \sqrt{B_1^2 + B_2^2}$,

$B_1 = \cos \Psi \cos \alpha$,

$B_2 = -\sin \Psi \cos \alpha \sin \Phi$,

$B_3 = \sin \Psi \cos \Phi \sin \alpha$,

and $\gamma = \tan^{-1}\left(-\frac{B_1}{B_2}\right)$.

Equation (8) shows that the tilted loop response is also a function of γ and Ψ; but (9) indicates that the response is a figure-eight pattern providing accurate bearings only when the incident sky-wave signal is vertically polarized ($\Psi = 0°$). If $\Psi \neq 0°$, the response is not a figure-eight pattern due to a nonzero B_3 value. The response nulls are separated by less than 180°, and the bearing display exhibits asymmetrical patterns indicating inaccurate bearing information. Hence, accurate bearings can be separated from erroneous bearings using the symmetry of the bearing display.

The effect of tilting on display characteristics is illustrated by Figure 15. If α is much less than Φ, the display is as shown in Figure 15a with the bearing rotating as Ψ rotates. In (9), B_3 is much less than B_0 and the response is, for all practical purposes, a symmetrical figure-eight pattern for any Ψ value. As α is increased and approaches Φ, the display continues to rotate with Ψ rotation but develops discernible

asymmetry for nonzero values of α as illustrated by Figure 15b. With $\alpha \neq 0°$, B_3 in (9) increases as α increases and begins to affect the response as $\alpha \to 1$. Since B_3 is a function of α, the degree of symmetry is a function of α. When $\alpha = 90°$, asymmetry is largest. When $\alpha = 0°$, there is symmetry, thus indicating an accurate bearing. (The above is true for any tilt angle.) Since $\alpha \neq 1$, B_3 is always less than B_0, and the response is double nulled. However, with $\alpha = 1$ note from (8) that one of the response nulls remains fixed while the other null rotates with α, and the two nulls merge to form a single null when $\alpha = 90°$ as illustrated by Figure 15c. Here $B_3 = B_0$ and a cardioid response results. Single-nulled responses occur only when $\alpha \geq \Phi$. It has been experimentally determined that the best tilt angle for the collection of bearing information is with $\alpha \doteq \Phi$.

The transition from a double-nulled to a single-nulled response as α is increased also allows for a measure of elevation angle-of-arrival For $\alpha < \Phi$, a double-nulled response occurs for any Ψ value. For $\alpha = \Phi$, a single-nulled response occurs as Ψ rotates through 90°. Hence, Φ can be estimated by increasing α until a single-nulled response is obtained at $\alpha = 90°$. In practice, most ionospherically-propagated signals experience depolarization as large as 90°. In fact, many signals undergo cyclic polarization rotation. Therefore, an estimate of elevation angle of arrival can be obtained on many ionospherically-propagated signals

Another method of analyzing the tilted loop response is to resolve the tilted loop into two components - one vertical and one horizontal The horizontal component produces the third term (B_3) in (8). The first and second terms in (8) are due to the vertical component. Signal

pickup in the horizontal component, which occurs only when γ is nonzero, combines with the vertical component pickup to produce a response with asymmetrical nulls. When $\gamma = 0°$ and the incident signal is vertically polarized, the horizontal component signal pickup is zero, and symmetrical nulls occur defining an accurate bearing situation. The horizontal and vertical components result from the same physical loop and, hence, have the same constant K in the response equations. If separate loops were used for the horizontal and vertical components, the constants in the response equations may not track as a function of frequency.

IX. OPERATIONAL EVALUATION - FADE CREST DETECTION

Test Methods

Field tests were conducted over a five-month period during the winter of 1966-67. All tests were performed on short-wave broadcast stations of known bearing over propagation paths ranging from 600 km to 8600 km. Essentially all the tests were taken on transmissions at or below the calculated F2MUF. The nominal test period for each test was five minutes.

Three-hundred and eighty-four tests were performed using sixty-seven different frequencies in the 5-20 MHz range originating from twenty-three separate locations. Two-hundred and thirty-six of the tests were performed during the 1100-1500 GMT (dawn) and 2200-0200 GMT (dusk) periods of relatively high ionospheric variation.

The test phase included an operational comparison of the exploratory systems performance with that of the AN/PRD-5 HF/DF system.

Data Reduction

The bearing data from each test were reduced to the following statistical parameters:

- $\Delta\theta$: The average bearing deviation from the great-circle bearing (GCB). A positive value indicates a clockwise deviation; a negative value, a counterclockwise deviation.
- SP : The total azimuthal spread of the bearing data.
- SD : Standard deviation.

For analysis purposes, the reduced data from individual tests were grouped and further processed to obtain the following parameters:

- $\overline{\Delta\theta}$: The average of the averaged bearing deviations, $\Delta\theta$.
- $\overline{|\Delta\theta|}$: The average of the magnitudes of $\Delta\theta$, $|\Delta\theta|$.
- $\overline{SP}$: The average of the spreads.
- $\overline{SD}$: The average of the standard deviations.
- $\overline{RMS}$ Error: Defined as $\sqrt{\overline{(SD)}^2 + \overline{(\Delta\theta)}^2}$.

Comparison of Fade Crest Detector Modes

The initial operational tests compared the averaging and comparison technique (Mode 1) with the peak sample and hold technique (Mode 2). Comparisons were made by using both modes in sequence on the same transmission. Two series of tests were performed for a wide variety of transmission characteristics with the test results presented in Table I. Mode 1 test results are for fade margins providing smallest $\Delta\theta$. Table I shows that: (1) the average bearing deviation and standard deviation are about 10° for both modes; (2) the total spreads are restricted to less than one-half of a quadrant; (3) the peak sample and hold technique performs best in the presence of a low SNR; and (4) the performance of

both modes is essentially the same for both series of tests even though different transmissions and times were used. Also, the results show the peak sample and hold technique performance for a low SNR is essentially identical to that for a good SNR, implying that this mode operates independently of the average value of the signal.

Effectiveness of Averaging and Comparison Technique Fade Margin

The effect of fade margin increase on performance was also evaluated. Tests were performed on thirty-six transmissions having good SNR and essentially periodic fading using fade margins of 0, 3, 6, and 10 dB in sequence for each test. The reduced data are shown in Figure 17.

TABLE 1

Comparison of Fade Detector Modes

Test Series	No. Tests	Mode	Total No. of Bearings	$\lvert\overline{\Delta\theta}\rvert$ deg	$\overline{SP}$ deg	$\overline{SD}$ deg
1	15	1	456	9	33	9
	15	2	635	11	44	13
2	38*	1	1733	7	32	8
	38*	2	1813	12	42	10

*Mode 1 unusable on 5 of the 38 tests due to low SNR.
Mode 2 produced values of 13°, 43°, and 11° for $\lvert\overline{\Delta\theta}\rvert$, $\lvert\overline{SP}\rvert$, and $\lvert\overline{SD}\rvert$, respectively, for these five tests.

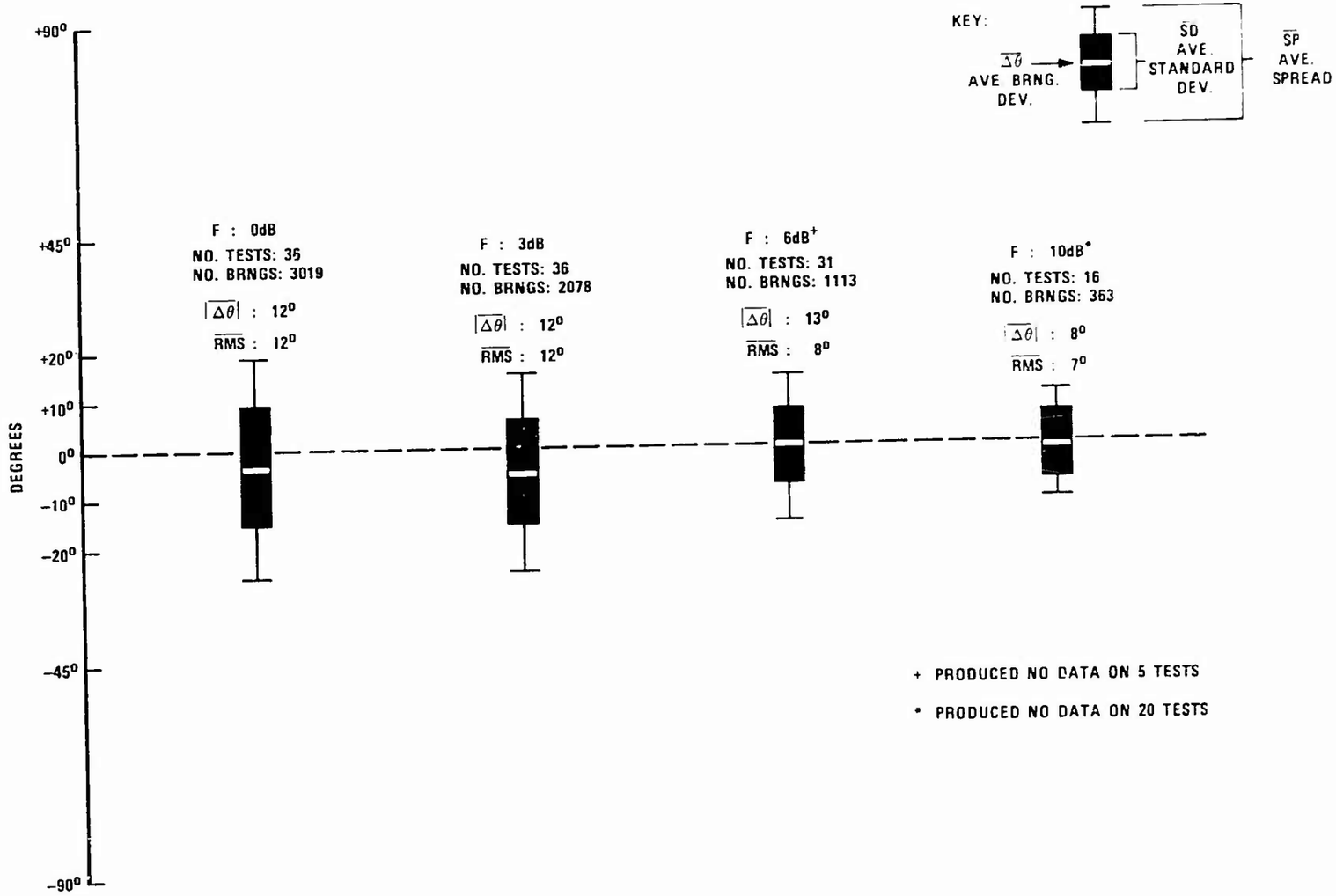

Figure 17. Test Results Depicting Effects of Fade Margin on Bearing Error and Dispersion.

Bearings were displayed at 0 and 3 dB fade margins on all tests; however, five tests and twenty tests produced no bearings at fade margins of 6 and 10 dB, respectively. Hence, it appears that a 3 dB fade margin is about the largest value that should be used in any given operational situation, especially if the observation time is limited. Figure 17 shows monotonic decreases in bearing spread, standard deviation, and RMS error with increasing fade margin and supports the contention that the more accurate bearings occur at the crests.

Comparisons between the 3 and 6 dB fade margins were further investigated by an additional series of twenty-two tests which produced essentially the same results as depicted in Figure 17 for these two fade margins.

Overall Exploratory Systems Test Results, Using Optimum Fade Crest Detector

A series of tests was performed using the optimum type of fade crest detector for the particular fading conditions. Mode 1 was selected for the transmission with polarization fading and a good SNR; Mode 2 was selected for the transmissions with multipath fading and/or a poor SNR. The results are depicted in Figure 18.

The Mode 1 data were obtained from eight separate transmitter locations in the North American continent; however, a majority of the tests were on VOA (Greenville, N.C.) transmission near the F2MUF. Most of the Mode 2 data were obtained using transmissions from Europe, Africa, and South America. North-South and East-West propagation paths were present during dawn, dusk, and daytime ionospheric conditions. Therefore,

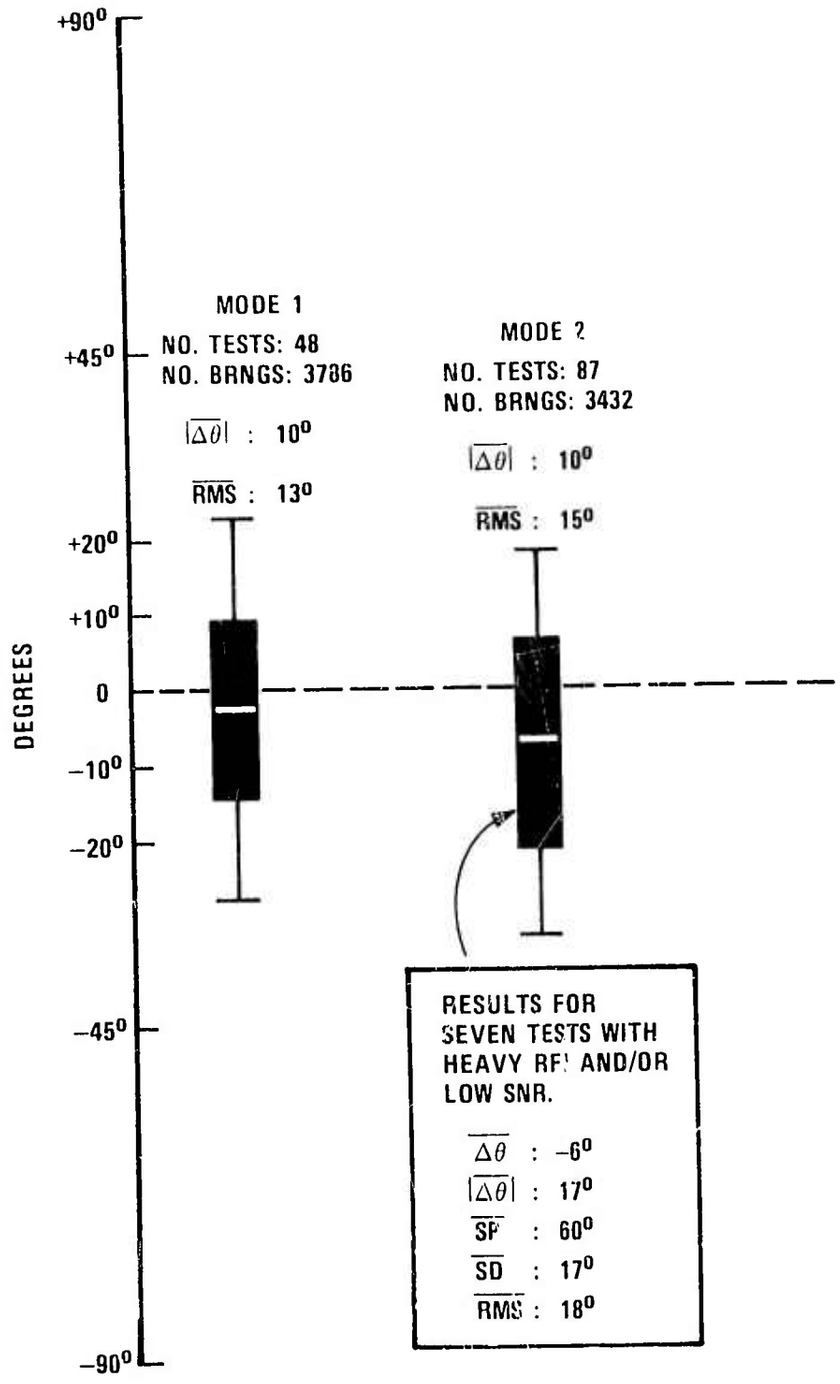

Figure 18. Overall Test Results Using Optimum Fade Crest Detector.

the test results represent a wide variety of signal and propagation conditions.

The results for both modes are very similar and show average bearing errors of 10° or less with a majority of the bearings restricted to within ± 15° of the GCB by the unblanking.

Data from seven tests with heavy RFI and/or very low SNR were included in the overall Mode 2 data. These data were also reduced separately and are shown under the Mode 2 data. As expected, these data exhibit larger dispersion and less accuracy than the tests with better signal conditions; however, these data indicate that it is possible to obtain fairly accurate bearing information using Mode 2 even for very poor signal conditions.

X. COMPARISON OF EXPLORATORY SYSTEM WITH THE AN/PRD-5 HF/DF SYSTEM

Fade Crest Detection

The exploratory system (ES) and the AN/PRD-5 system were compared by simultaneous, side-by-side testing.

The AN/PRD-5 operates from 0.5-20 MHz using a two-foot loop rotating at 1 rps. The display unit is a 3-inch CRT with P7 phospher that displays a completely symmetrical two-lobe propeller pattern for each detected null of the rotating loop (i.e., two complete displays are generated for a single 360° scan). The exploratory system produces only one-half of a propeller pattern for each null, i.e., only one display is generated for a single 360°. This type of display more clearly indicates the presence of accurate bearings through pattern symmetry.

Figure 19 shows the test results for both Modes 1 and 2. Essentially all of the Mode 1 data were obtained on single-hop transmissions at or near the F2MUF with polarization fading dominant. A 3 dB fade margin was used on a large majority of the Mode 1 tests. Mode 2 data were obtained on multiple-hop transmissions with a low SNR; in most cases, the signal was peaking-up out of the noise or interference.

Figure 19 illustrates the better performance of the exploratory system in that the bearing spread, RMS error, and standard deviation values for the AN/PRD-5 are 2 to 3 times greater than those for the exploratory system. For both systems, the bearing errors and spreads are larger in the presence of polarization fading (Mode 1). The field tests revealed that it is very difficult to obtain bearings using the PRD-5 in the presence of polarization fading. With constant polarization rotation, the PRD-5 bearing display rotates 360° continuously without any noticeable change in pattern or swing rate. In order to obtain data, a highly subjective operating technique using the sense antenna was devised for the PRD-5; however, this technique required preliminary procedures prior to each test. The exploratory system's automatic unblanking capability allows for immediate bearing data even for consistent polarization fading.

Operational Evaluation - Swing Rate Discriminator

The SRD was designed primarily as an error reducing technique for time-varying polarization errors; hence, a large majority of the field tests were performed using transmissions with consistent polarization fading. The SRD was used both alone and with Mode 1.

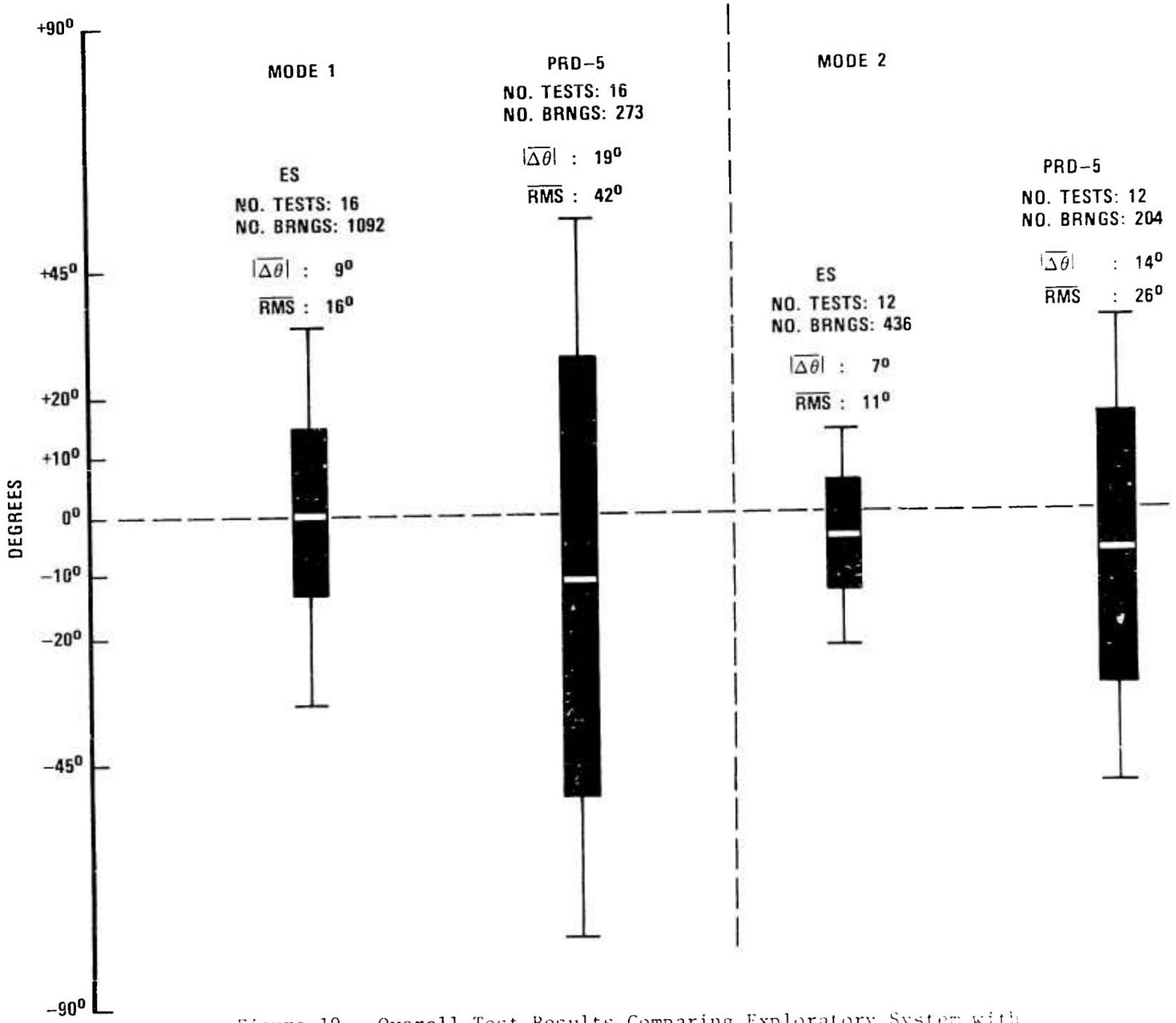

Figure 19. Overall Test Results Comparing Exploratory System with AN/PRD-5.

Table II presents the results for sixty-five separate tests. The AN/PRD-5 data were obtained during simultaneous, side-by-side testing. Table II shows slightly smaller $\overline{\Delta\theta}$ and $|\overline{\Delta\theta}|$ values for the exploratory system; however, the most significant improvement is in the standard deviation and RMS error values when the SRD is used with Mode 1. There is approximately a 3 to 1 difference between these parameters for the exploratory system, SRD with Mode 1, and the PRD-5.

Bearing Distribution Using SRD Data

The SRD provides a continuous DC analog of bearing positions versus time. Polarization fading produces a monotonic change in the analog level over one complete polarization relation. The DC analog data can be used to obtain histograms of bearing versus observed relative frequency. The number of bearings that lie in specified azimuth intervals is determined over the entire range of bearing indications for a number of complete polarization rotation periods. Figure 20 shows a histogram obtained from the analog data using 20° azimuth intervals.

If uniform polarization is assumed ($\Psi = Kt$) and the elevation angle-of-arrival known, (3) may be used to obtain a theoretical histogram. An example is shown in Figure 21 for an elevation angle of 57° - the value calculated for a set of DC analog data [18].

The calculated and observed histograms are very similar. Both show maxima in the interval containing the GCB and minima in the interval which differs from the GCB by 90°. Figure 20 shows that the angular rate-of-bearing-swing is lowest near the GCB since the largest number of bearings occurred in the interval containing the GCB.

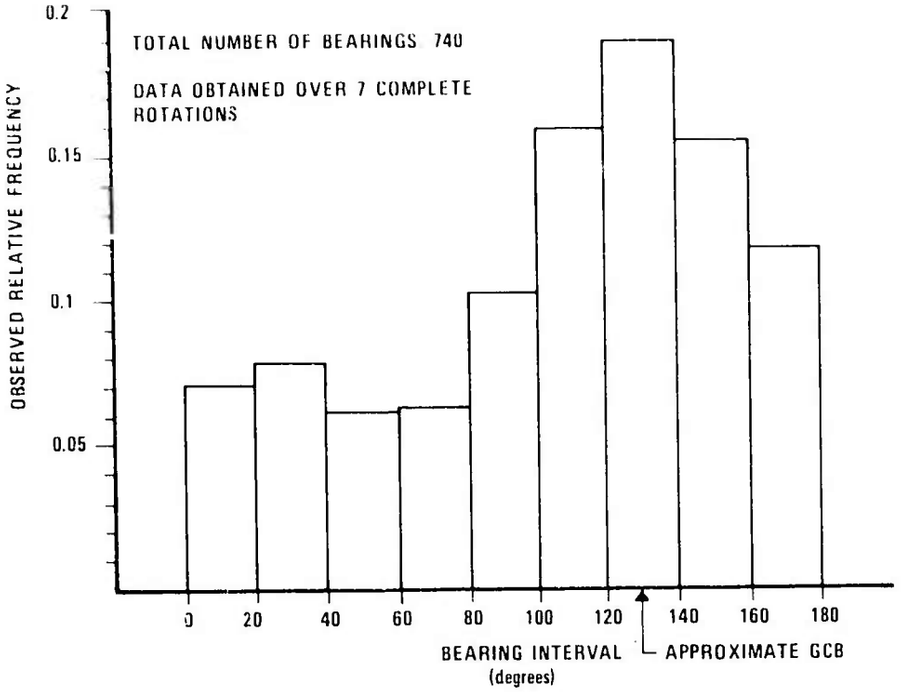

Figure 20. Observed Relative Frequency of Occurrence of Bearings.

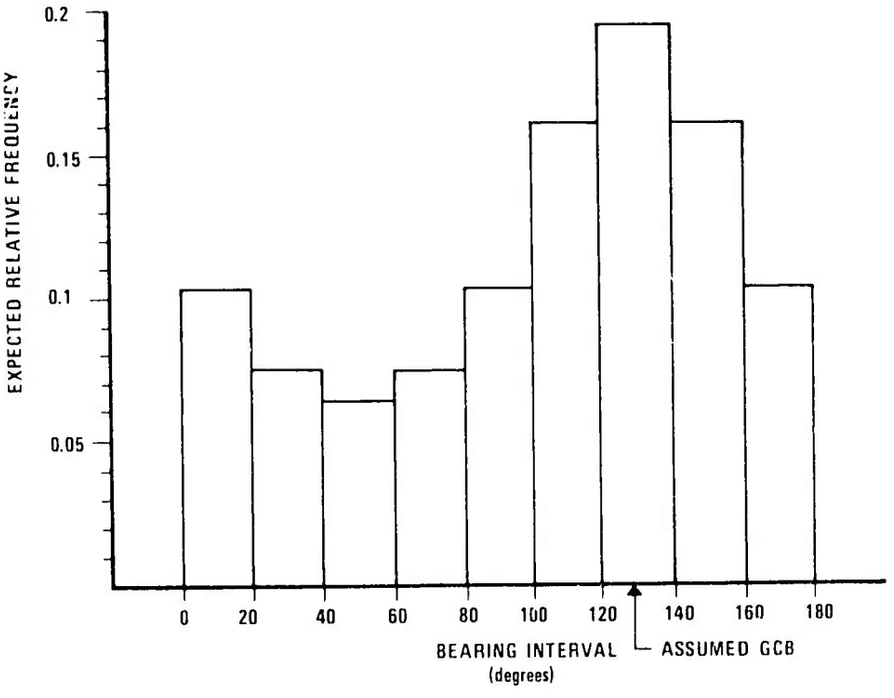

Figure 21. Theoretical Relative Frequency of Occurrence of Bearings.

The close similarities between the two histograms substantiate the validity of (3) as a model for describing bearing errors caused by polarization fading. Also, the measured histogram data could be used to determine elevation angle since each elevation angle produces a unique histogram. For example, if the elevation angle had been 90°, the histogram would have been flat across the 180° range whereas a 0° elevation angle would have a histogram with all bearings in the 120° - 140° interval.

TABLE II

Comparison of Exploratory System
Using SRD with the AN/PRD-5

	PRD-5	Exploratory with SRD Mode	Exploratory with SRD Mode and Mode 1
$\overline{\Delta\theta}$	-7°	0°	-3°
$\overline{\lvert\Delta\theta\rvert}$	11°	9°	9°
$\overline{SD}$	43°	25°	13°
RMS Error	44°	25°	13°
No. of Bearings	857	365	653

XI. OPERATIONAL EVALUATION - TILTED LOOP

Field tests were performed over a four-month period with emphasis on sky-wave signals originating from distances less than 600 km. A majority of the tests were on one-hop, high elevation angle (> 30°)

signals dominated by polarization fading due to Faraday rotation. The tests verified that the tilted loop response is essentially as predicted by theory. The experimental system was compared with the PRD-5 during side-by-side testing. Results show that the tilted loop technique can provide about 4 : 1 and 9 : 1 improvement in bearing accuracy and dispersion, respectively, on transmissions with polarization fading In some cases, the tilted loop system provided bearing information where none could be obtained using the conventional system. Significant improvements were also observed on lower elevation angle transmission dominated by multipath effects.

Figure 22 illustrates test results for the exploratory system A majority of the test transmissions were ICW signals with polarization fading -- a worst-case combination for loop DF systems. The instantaneous sensing significantly reduced the time required for bearing acquisition relative to the PRD-5. The average reduction was about 2 : 1; however, in some cases, no sense could be obtained with the PRD-5 even after tens of minutes. Typical test time was two minutes.

Measures of elevation angle obtained from the field tests showed good correlation with the expected angles, which were calculated assuming E - and F - layer propagation and predicted average layer heights. The measured angles occurred within the expected region on 53 of 60 tests. No ionogram data were available and the expected angles could not be accurately defined. However, the data imply a $\pm$ 10° accuracy. Under conditions of exceptionally good polarization fading, the elevation angle could be measured to within several degrees.

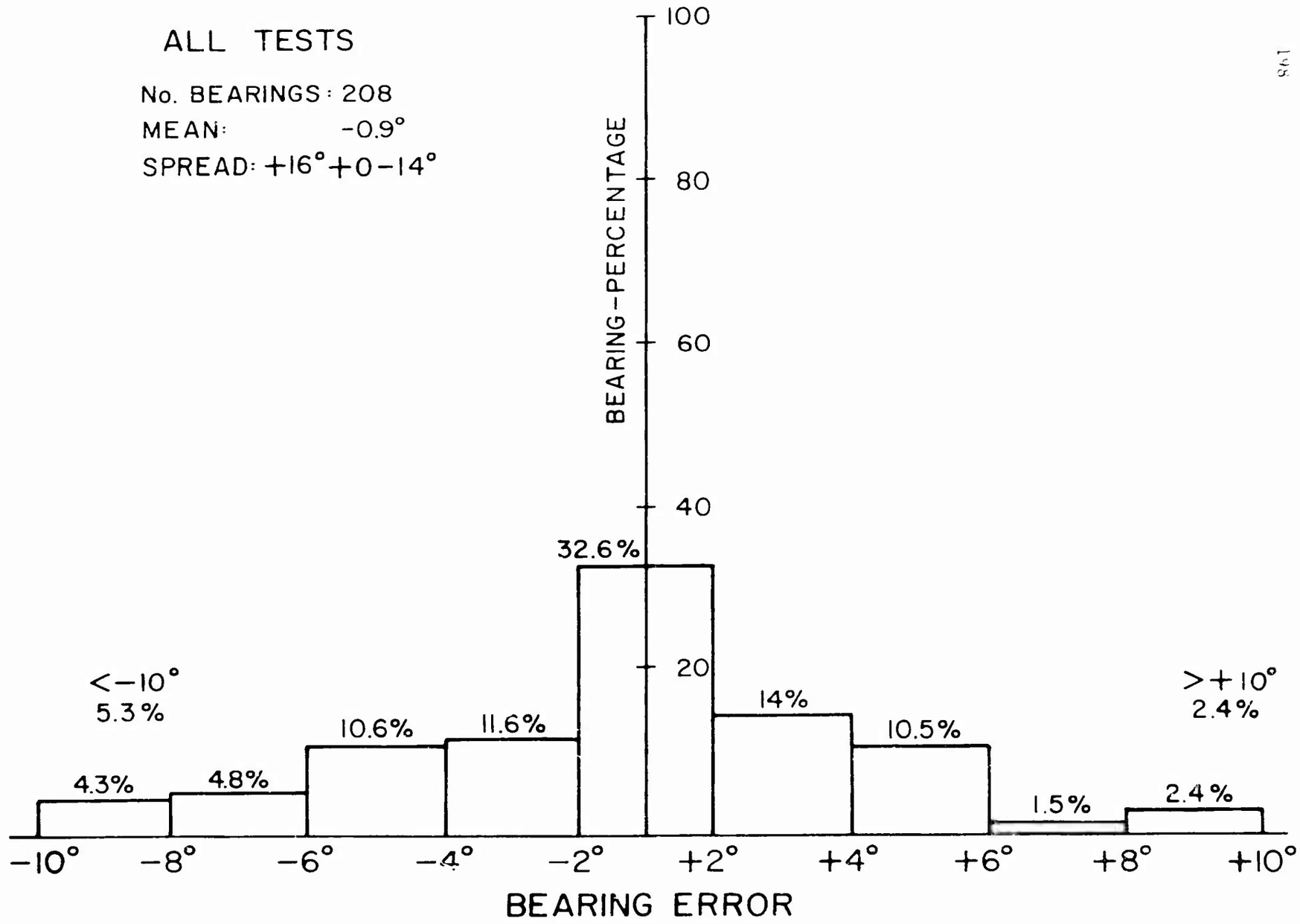

Figure 22. Test Results-Tilted Loop and ICW Signals.

XII. CONCLUSIONS

Techniques to improve simple loop HF/DF system performance on ionospherically-propagated signals have been developed, implemented in an exploratory HF/DF system, and proven effective by operational evaluation. Significant improvements in performance relative to a contemporary system have been obtained.

Bearing error reduction techniques include fade crest detection, swing rate discrimination, and the tilted loop technique. The latter two techniques provide for a measure of elevation angle-of-arrival. System improvements include clutter reduction and synchronous detection, which increases sensitivity and allows for instantaneous sensing. Bearing acquisition time has also been increased, and operation on continuous and interrupted carrier transmissions is possible.

Georgia Tech submits that many of these techniques can be applied to larger-aperture DF systems to both reduce bearing errors and improve over-all performance.

ACKNOWLEDGEMENT

The authors are especially grateful for the assistance and encouragement of Mr. Lawrence Scott, Technical Monitor, of the U. S. Army Electronics Command. His contributions have been invaluable in the conducting of these investigations.

REFERENCES

[1] A. D. Bailey, et al., "A study of HF directional propagation over a 450 km East to West path," University of Illinois, Radiolocation Research Laboratory, Urbana, Illinois, RRL No. 254, AD625413, November, 1965.

[2] F. S. Howard and F. M. Wood, "Note on the bearing error and sensitivity of a loop antenna in an abnormally polarized field," Proc. IRE, Vol. 32, pp. 231-233, April 1944.

[3] E. C. Hayden, "Some basic problems in the determination of the direction of arrival of radio waves," University of Illinois, Urbana, Illinois, Technical Report No. 11, Contract Nonr 1834 (02), September 1958.

[4] E. C. Hayden, "Correlation of DF errors with ionospheric radio propagation phenomena," University of Illinois, Urbana, Illinois, Report RADC-TDR-62-236, Contract AF 30(602)-2413, March 1962.

[5] D. N. Travers and S. M. Hixon, "Abstracts of the available literature on radio direction finding 1899-1965," Southwest Research Institute, San Antonio, Texas, Contracts NObsr-64585,85086 and 89167, July 1966.

[6] F. E. Terman and J. M. Pettit, "The compensated loop direction finder," Proc. IRE, Vol. 33, pp. 307-318, May 1945.

[7] D. P. Kanellakos, "Origin and location of ionospheric perturbations affecting the frequency and bearing of HF radio waves," Stanford University, Stanford, California, Technical Report No. 43, Contracts Nonr-226(33), Nr 088 003 and ARPA order 196-61, November 1962.

[8] D. A. Hedlund and L. C. Edwards, "Polarization fading over an oblique incidence path," IRE Trans. on Antennas and Propagation, Vol. AP-6, pp. 21-25, June 1958.

[9] R. Chapman, et al., "Dispersive characteristics of the ionosphere," General Electric Co., Syracuse, New York, Final Technical Report No. RADC-TR-66-211, Contract AF 30(602)-3360, August 1966.

[10] B. Goldberg, "MF/HF communications systems," IEEE Trans. on Communication Technology, "Vol. COM-14, No. 6, pp. 767-784, November-December 1963.

[11] J. C. Hancock and D. D. Weiner, "Channel characterization," Frequency, Vol. 1, No. 7, pp. 12-16, November-December 1963.

[12] H. A. Wale and L. M. Delves, "Some relations between the bearing and amplitude of a fading radio wave," Jour. Atmos. Terr. Phys., Vol. 43, pp. 72-85, 1958.

REFERENCES (Continued)

[13] R. K. Salamon, et al., "Fading multipath and direction of arrival studies for HF communications," National Bureau of Standards Report 7206, National Bureau of Standards Boulder Laboratories, Boulder, Colorado, 15 December 1961

[14] N. Burtnyk, "Performance of an interferometer direction finder for the HF band." Proc IEEE, Vol. 112, No. 11, pp 2055-2059, November 1965.

[15] K. Davies, "Ionospheric radio propagation." National Bureau of Standards Mono. 80, National bureau of Standards, April 1965

[16] J. D. Moore and M P. Castles, "HF spaced loop antenna," Southwest Research Institute, San Antonio, Texas, Final Report, Contract DA 28-043 AMC-01960(E), July 1967.

[17] P. C. Sandretto, Principles of Aeronautical Radio Engineering, New York: McGraw-Hill, 1942.

[18] H. H. Jenkins and R W. Moss, "Error reduction in loop direction finder," Georgia Institute of Technology, Atlanta Georgia, Final Report, Contract DA28-043 AMC-01207(E), September 1967.

[19] H. H. Jenkins, R. W. Moss, and L Scott, "Error reduction in HF loop DF systems," IEEE Transactions on Aerospace and Electronic Systems, Vol. AES-5, No. 3, May 1969, pp. 486-498.

[20] H. H. Jenkins and R. W. Moss, "Tiltable, rotating vertical loop antenna assembly," Engineering Experiment Station, Georgia Institute of Technology, Annual Report, Contract DAAB07-68-C0072, July 1968.

[21] H. H. Jenkins and R. W. Moss, "Tiltable, rotating, vertical loop DF system," Engineering Experiment Station, Georgia Institute of Technology, Quarterly reports 1, 2, and 3, Contract DAAB07-68-C0072, August 1968, through May 1969.

EDWARD W. ERNST

Department of Electrical Engineering
University of Florida, Gainesville, Florida

DIGITAL TECHNIQUES FOR RADIO DIRECTION FINDING

I. INTRODUCTION

The digital computer has had and is continuing to have a marked impact on the field of Radio Direction Finding. Although RDF was a relatively mature field of study and application by the time the digital computer made its appearance, the impact of the digital computer on this field is a considerable one. The influence of digital methods has been most pronounced in three facets of Radio Direction Finding:

1) Studies of RDF systems by means of digital simulation,

2) The acquisition and analysis of experimental data by digital methods,

3) Performing some of the functions of an RDF system by means of digital hardware.

Although these three facets have developed more or less together, they will be presented and discussed somewhat separately.

II. SIMULATION STUDIES

An essential requirement for a radio direction finding system to be studied by means of digital simulation is that it must be possible to describe the system under study, or the essential characteristics of the system under study, by means of a mathematical model. For purposes of developing the needed mathematical model, it is useful to divide the RDF system into six parts:

1) The signal which impinges upon the RDF system,

2) The antenna elements of the array (including any estimates that can be made of the effect of local site conditions),

3) The means by which the signals from the antenna elements are combined to give directional characteristics,

4) The receiver portion of the RDF system,

5) The detectors which extract information from the signal presented at the output of the receivers,

6) The display and data presentation portion of the RDF system.

The considerable amount of work that has been done in RDF makes it possible to write a mathematical description for most parts of the RDF system. In addition, the linear nature of the pertinent characteristics of the system (with the exception of the detector) simplifies considerably the model which must be constructed and the nature of the computation. In the simulation process, the values of the signal (or other variables) are determined for successive intervals of time. This allows one to determine any particular value at the output or other point in the RDF system as a function of time under conditions of fixed system parameters. It is then possible to allow one or more of the parameters in the system to assume new values and compute a new set of values for the variable under study. Once a digital simulation model of a system has been prepared, it is relatively easy to determine the behavior to be expected from the system under any specific combination of values of the various portions of the system. In one sense, the simulation model may be considered a means of answering several different types of questions concerning the RDF system. One type of question is, "What will happen with this particular RDF system if I have a particular (assumed) type of input signal condition?" A second type of question is, "What

will happen if the RDF system itself is made different than it is at present in some way?" So that some idea may be obtained of the usefulness of this means of studying RDF systems, let us consider several typical examples of simulation studies.

Several studies have been conducted to determine various characteristics of the circularly disposed antenna array (Wullenweber) which is used for experimental work at the University of Illinois. As part of the studies made by Broeker,[9] it was helpful to determine the response of the sum output of the scanner to a signal which consisted of two interfering waves. These studies showed that for interfering waves which arrived at azimuthal angles very close together, the result was a distorted and broadened azimuthal scan pattern; whereas for waves which arrived at angles separated by several degrees, the two signals were observed as separate on the azimuthal scan pattern. Typical output results determined by digital simulation are shown in Figures 1 and 2. Another means for determining direction of arrival with the Wullenweber system compares the output from the sum pattern and the output from the difference pattern. In the presence of a single signal, the phase difference between the right-bank signal and the left-bank signal, determined by using the sum and the difference, can be interpreted in terms of the deviation of the direction of arrival from the boresite of the array. As shown in Equation (1), the direction of arrival and the phase, δ, between the right bank and the left bank is related by a constant, k.

$$\alpha = \frac{\delta}{k} \quad . \tag{1}$$

Figures 3 and 4 are from the studies made by Rosenbaum[4] and show

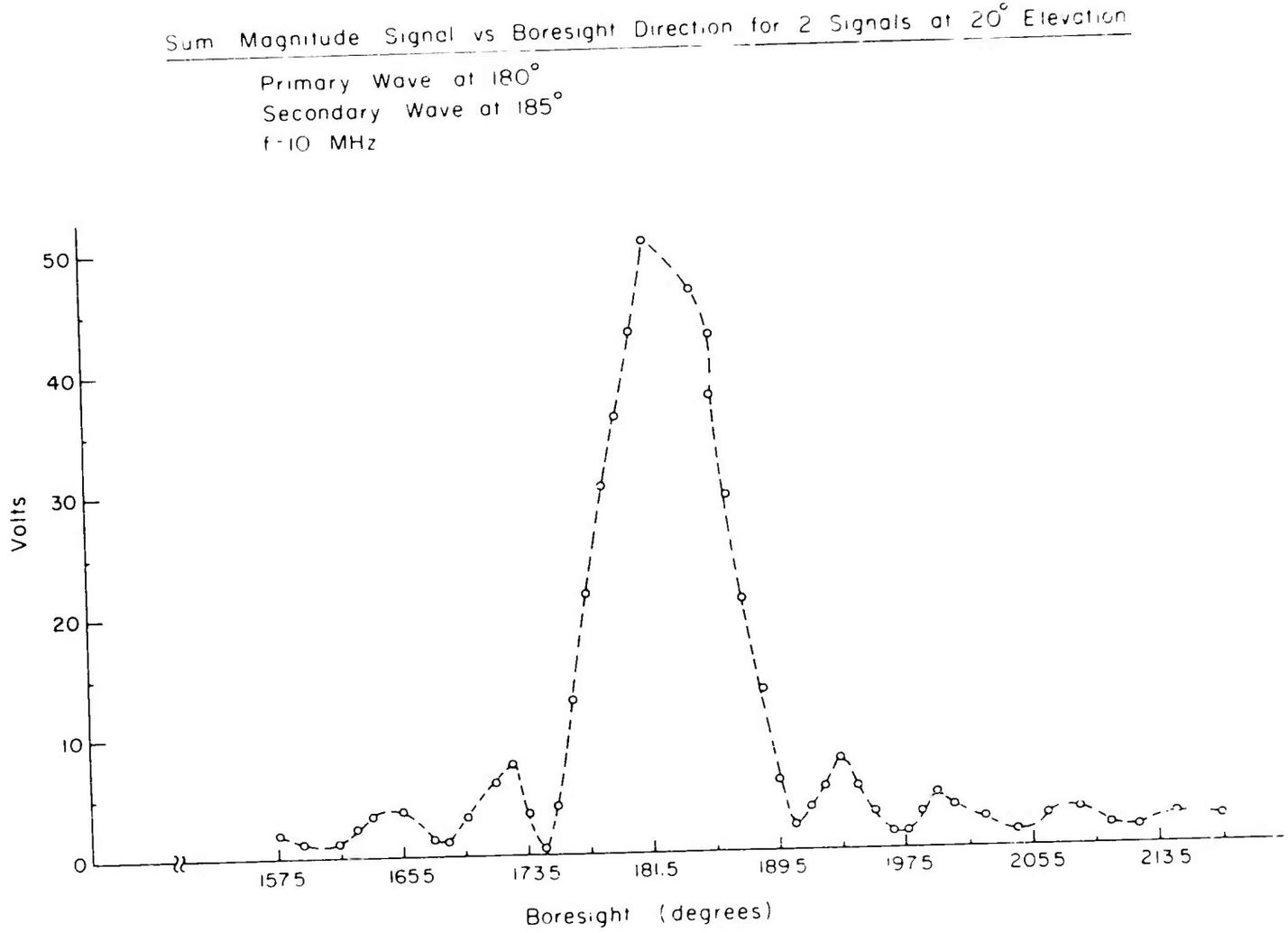

Figure 1. SUM Magnitude for Two Close Signals.

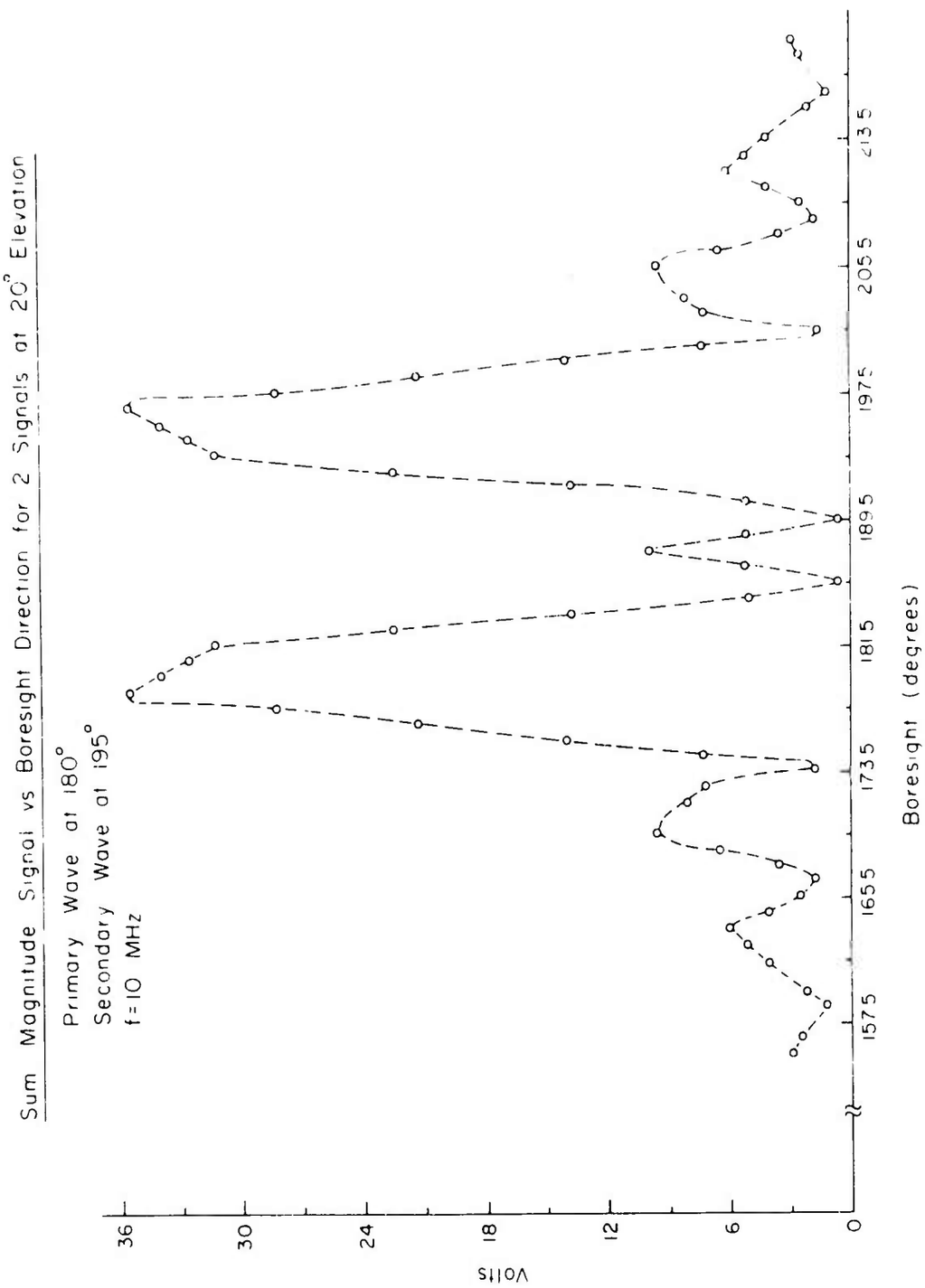

Figure 2. SUM Magnitude for Two Signals.

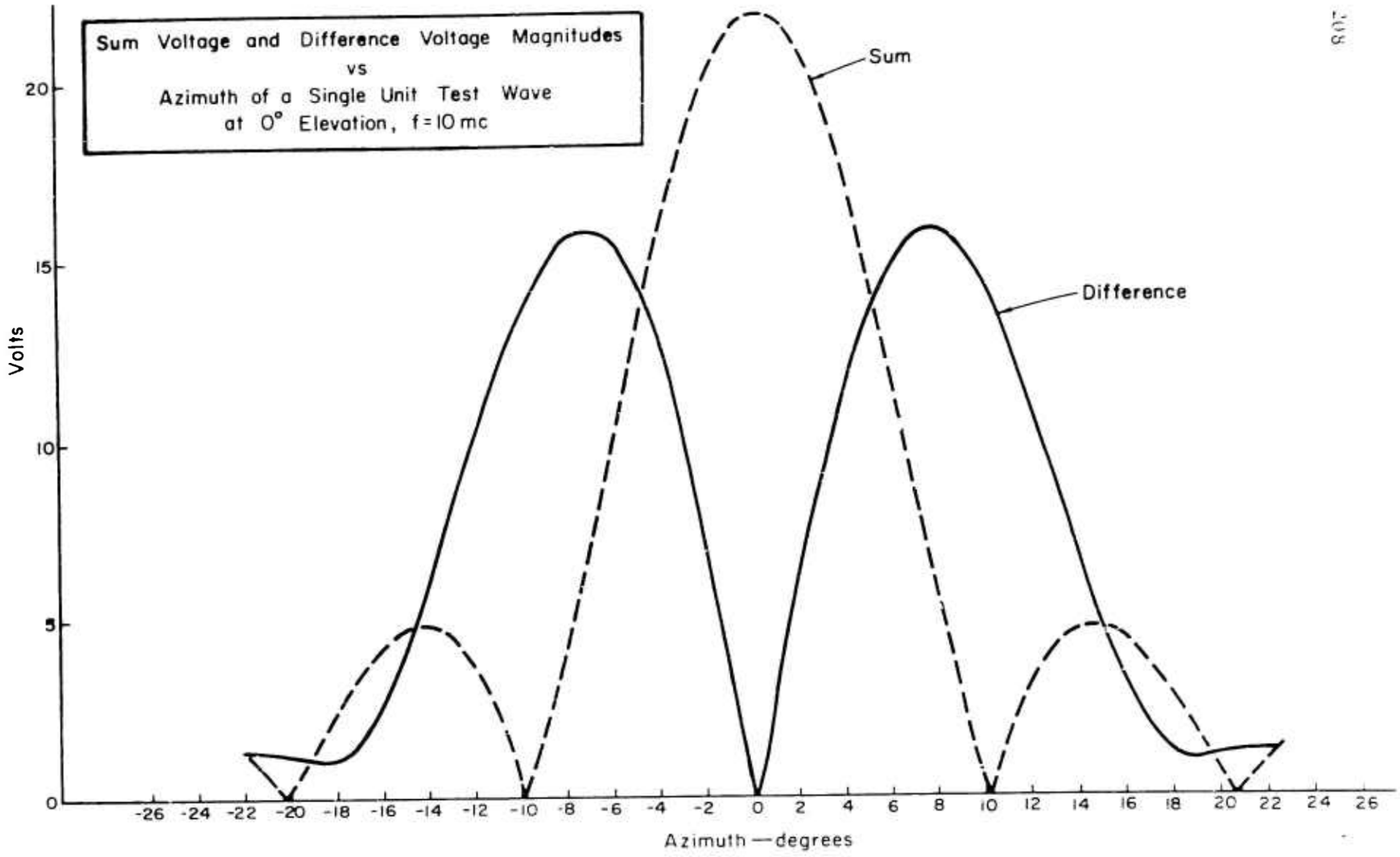

Figure 3. Σ and Δ Magnitude

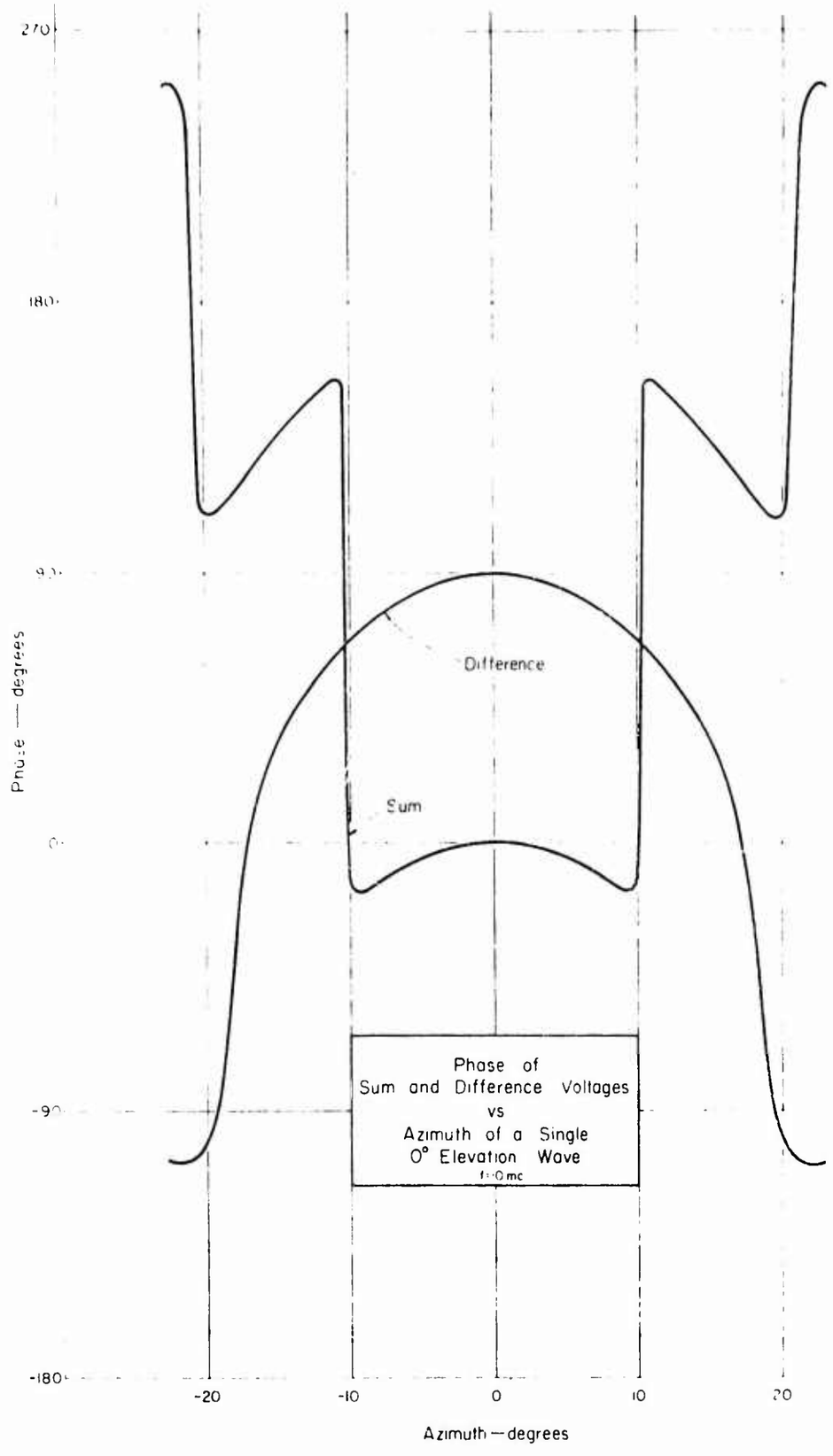

Figure 4. Σ and Δ Phase

certain characteristics of the sum and difference pattern as determined by simulation studies, while Figure 5 gives the value of the constant k in Equation (1) as a function of frequency for a fixed value of elevation angle of arrival. An added question concerning this particular type of system configuration is, "What does this indicate concerning the direction of arrival of the signal in the presence of wave interference?" Rosenbaum used digital simulation to study the question and some of his results are shown in Figures 6 and 7, which give the orientation of the ellipse axis as viewed on the cathode ray oscilloscope and the ellipticity of the pattern as a function of the azimuth and the relative magnitude of the interfering signal. It is of interest to note that strong interfering signals close (in azimuth) to the dominant or primary signal can cause large azimuthal errors. For example, a perturbing wave, separated by two degrees from the primary wave, could cause an apparent shift in the bearing by as much as six degrees, i.e., to a bearing completely away from either of the two signals. Figures 8 and 9 are from the studies of Medill[11] and give a comparison of the magnitude of the sum patterns and the differential phase as obtained from the right bank and left bank of the Wullenweber array. Additional studies of the differential phase, δ, as a function of frequency, produced the results shown in Figure 10. In an earlier work, Grush[2] showed that the apparent direction of arrival as determined by a Watson-Watt RDF system in the presence of wave interference could exhibit large variations in value, and that these depended upon the relative phase between the interfering signals. This is shown in Figure 11.

Display Calibration Constant, K
vs.
Frequency

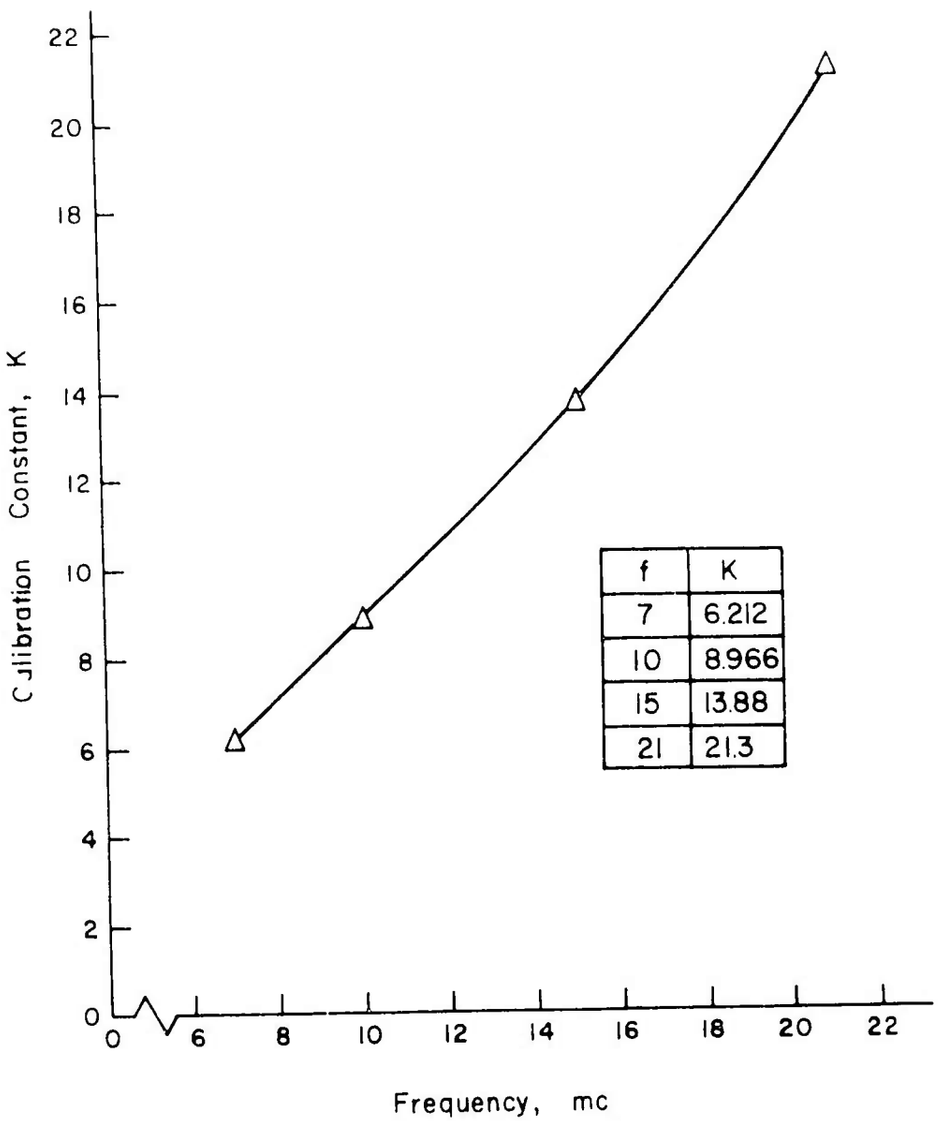

f	K
7	6.212
10	8.966
15	13.88
21	21.3

Figure 5. Frequency Calibration

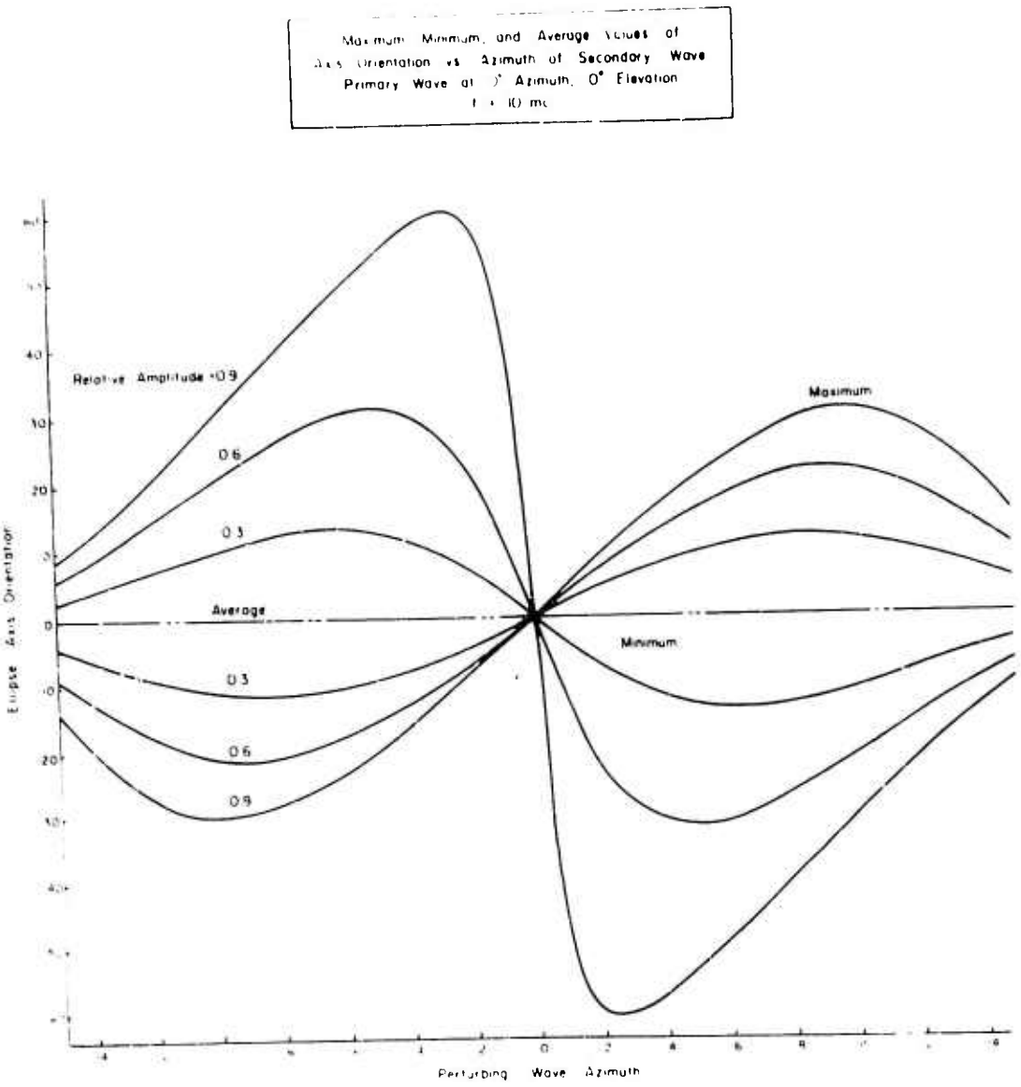

Figure 6. Ellipse Orientation

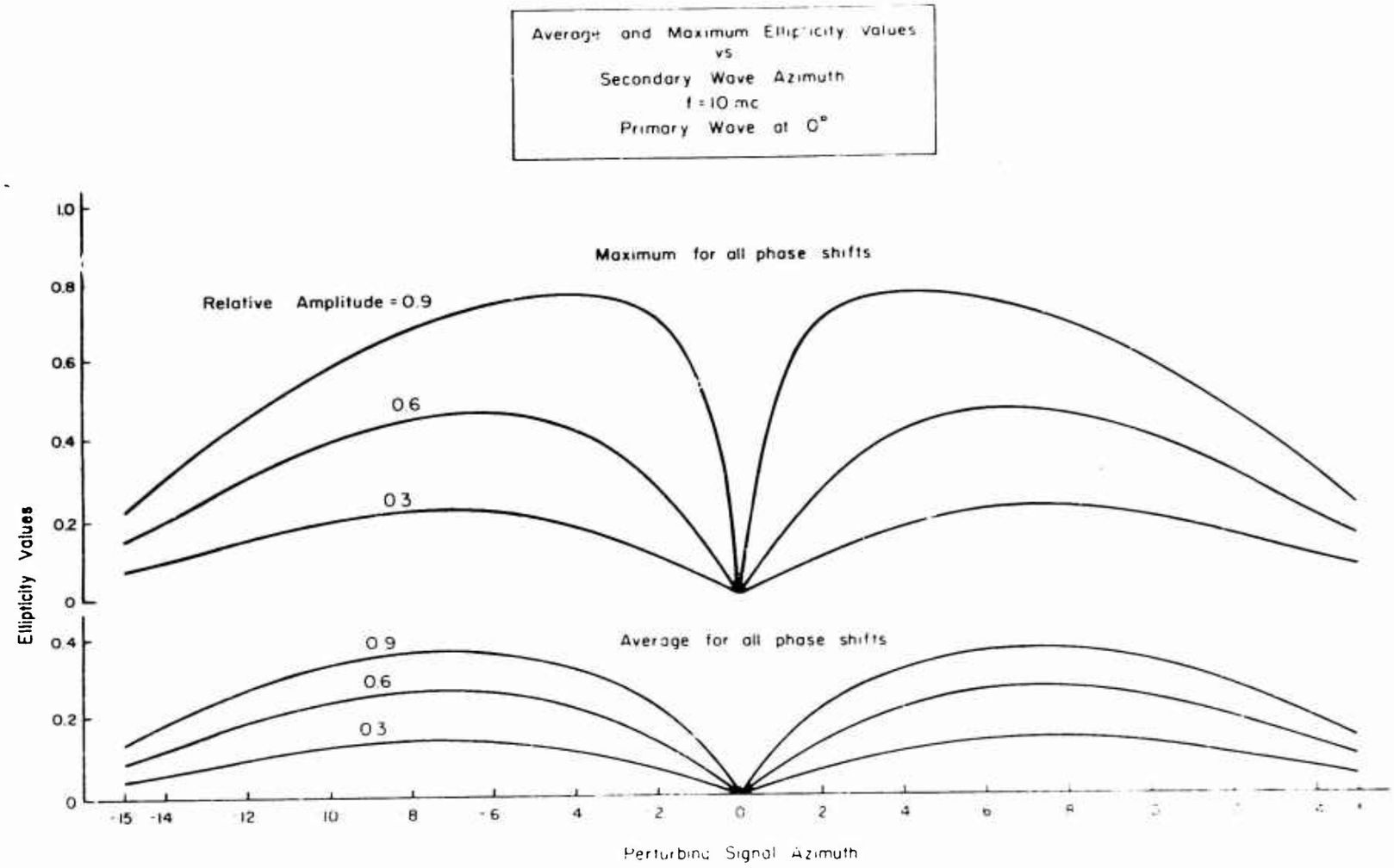
Average and Maximum Ellipticity Values
vs
Secondary Wave Azimuth
f = 10 mc
Primary Wave at 0°
Maximum for all phase shifts
Relative Amplitude = 0.9
0.6
0.3
Average for all phase shifts
0.9
0.6
0.3
Ellipticity Values
1.0
0.8
0.6
0.4
0.2
0
-15 -14 12 10 8 -6 4 2 0 2 4 6 8
Perturbing Signal Azimuth

Figure 7. E. [illegible]

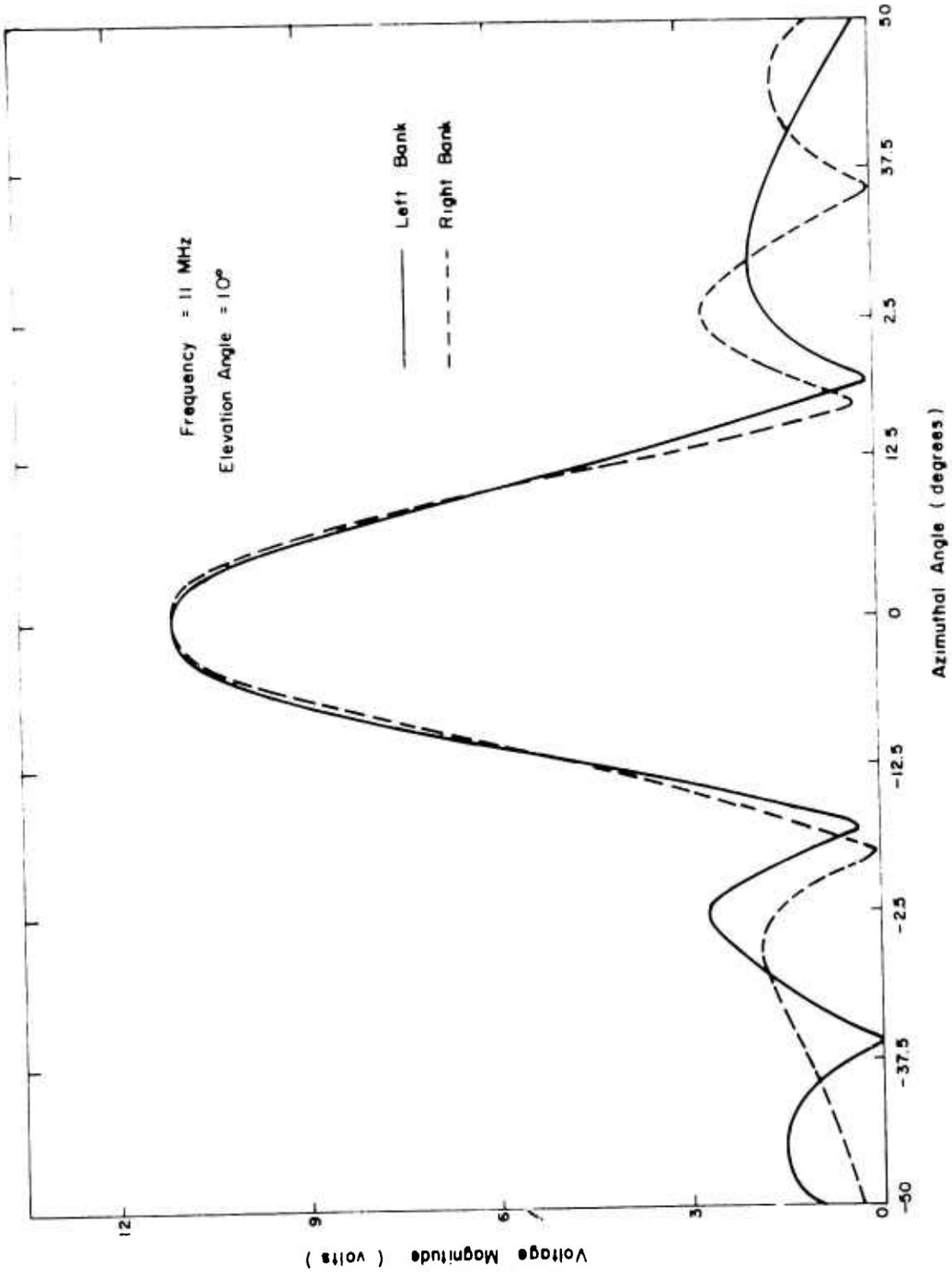

Figure 8. Amplitude pattern, single wire case

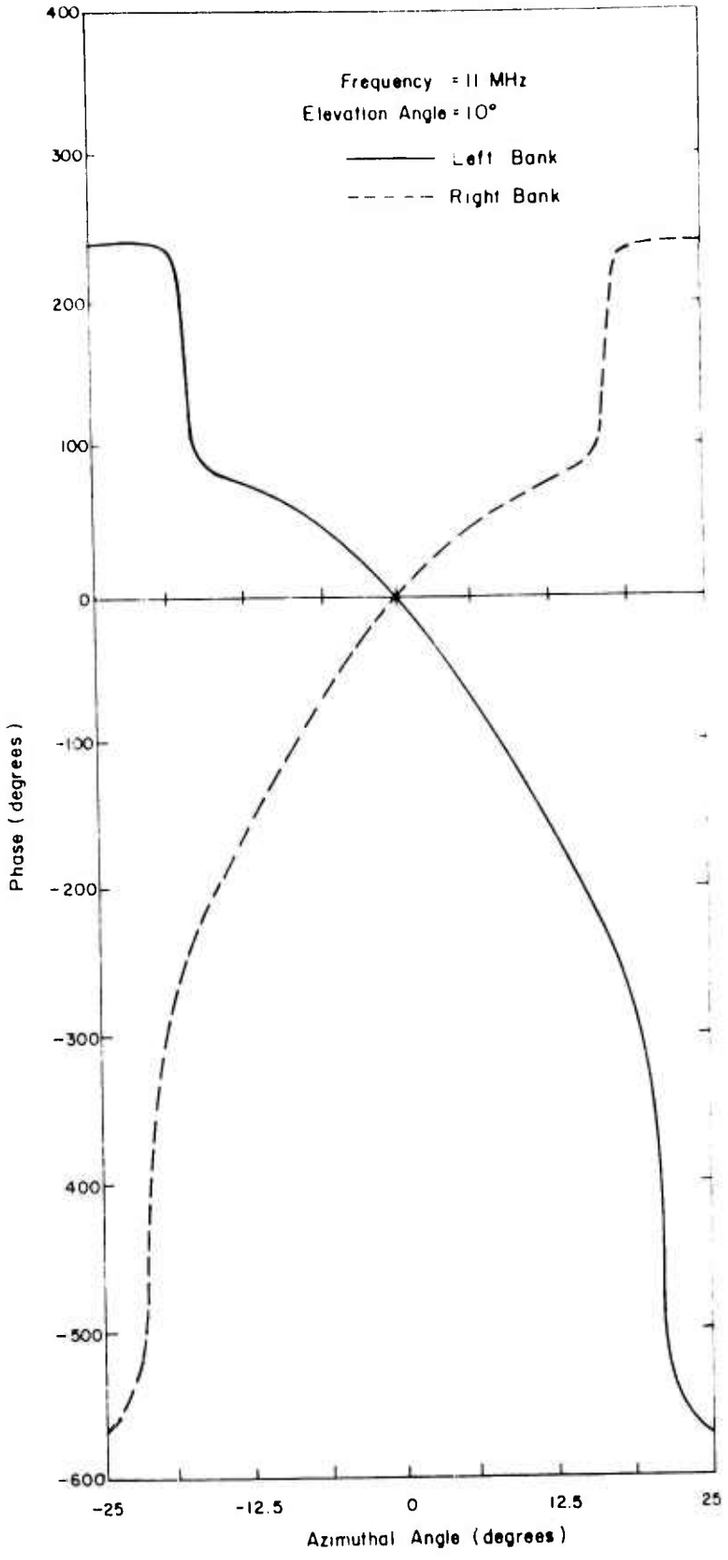

Figure 9. Phase pattern, single wave case.

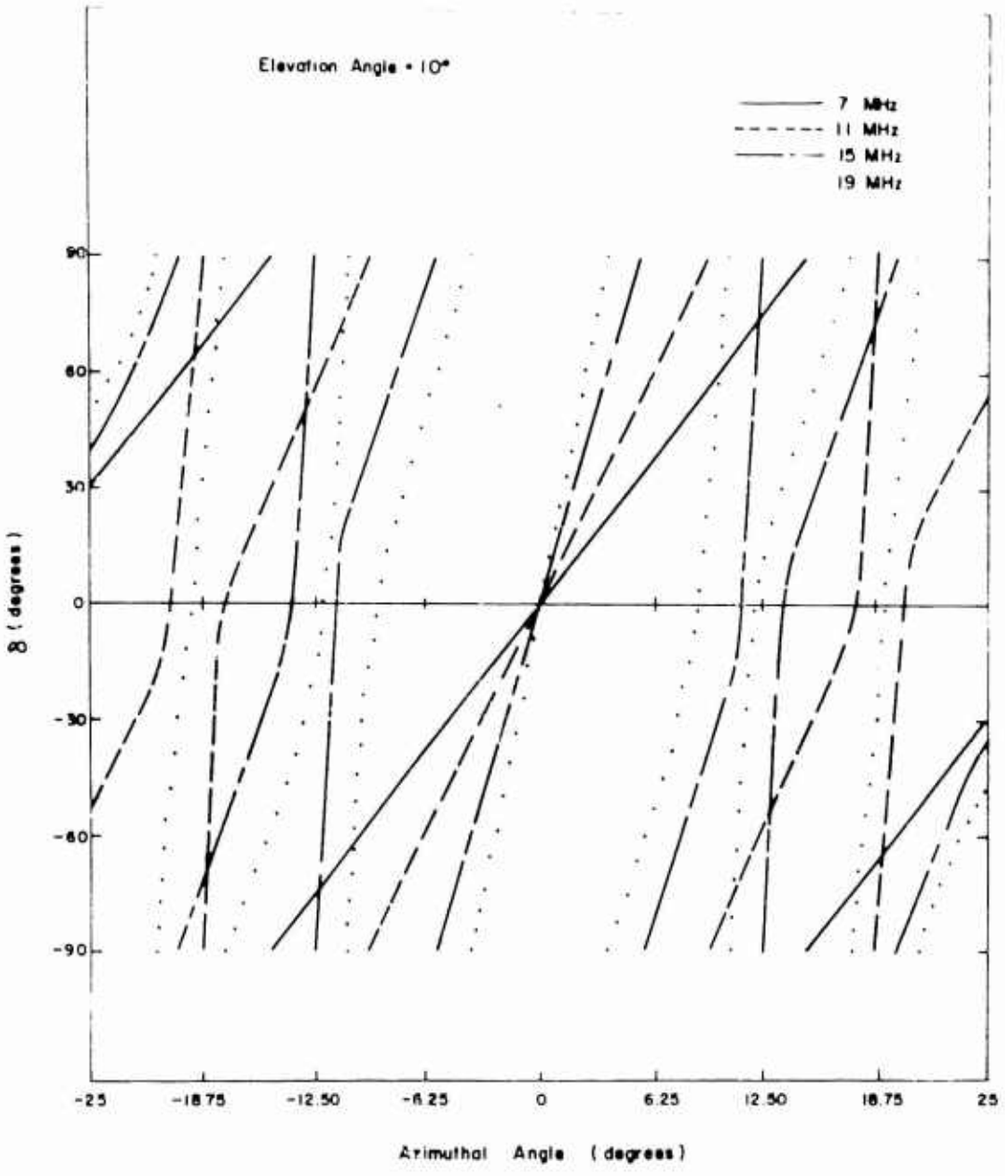

Figure 10. Delta as a function of azimuth, single wave case.

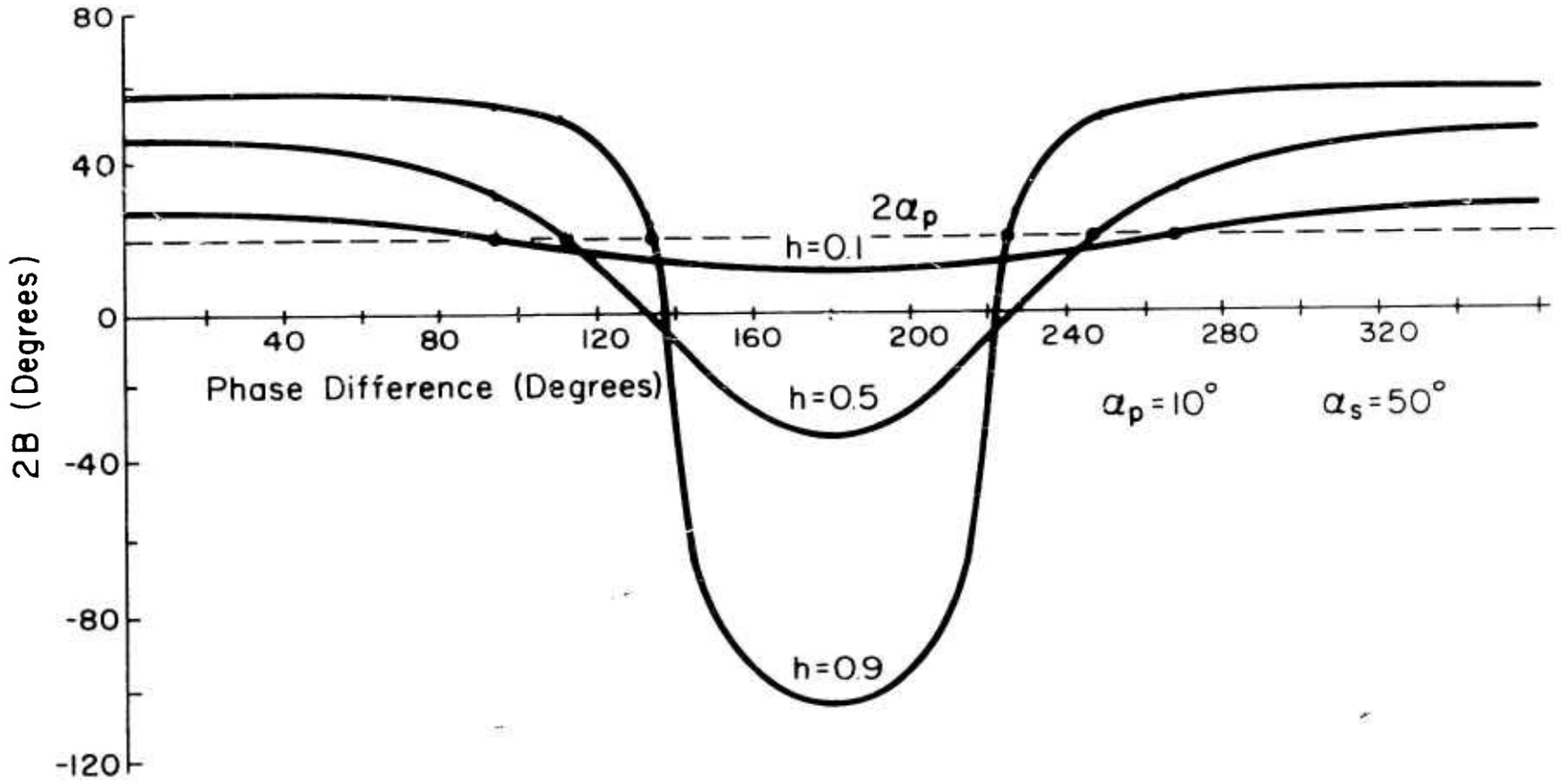

Figure 11. Plot of Twice the Instantaneous Bearing as a Function of Phase Difference ϕ.

Studies of the behavior to be expected from an RDF system which had been modified in some way (and which may best be described as a defective system) have been conducted by Jones,[5,15] in which he postulated that one of the antenna elements of the University of Illinois Wullenweber array had a 180° phase shift erroneously introduced. Figure 12, which shows part of the results from that study, indicates that at a frequency of 9.5 MHz the errors to be expected because of this defect are quite small at the cophasal angle for which the array was designed, but that they may become as large as 2 degrees for other elevation angles of arrival. Similarly, one may postulate that the cables connecting the antennas to the equipment building are not all the same electrical length, but vary in some pattern such as a sinusoidal variation over a portion of the cables with a random variation superimposed upon the systematic variation. It would be expected that this would be the cause of bearing error, at least for some directions of arrival.[6] More recently, studies have been made of the error in determining the direction of arrival when a large number of adjacent elements are assumed to be missing.[17] The plots of Figure 13 show the error in determining direction of arrival as a function of the difference in azimuth between the center of the defective portion of the array and the true direction of arrival. Of particular interest is the fact that for this large defect in the array, the error expected to occur does not appear to be large. Figure 14 shows the sum patterns expected under these conditions. Three sum patterns are shown: a) the sum pattern far away from the defect in the array; b) the sum pattern for the signal arriving from a direction corresponding to the center of the defect; c) the sum pattern corresponding to the signal arriving from the direction which yields the maximum error

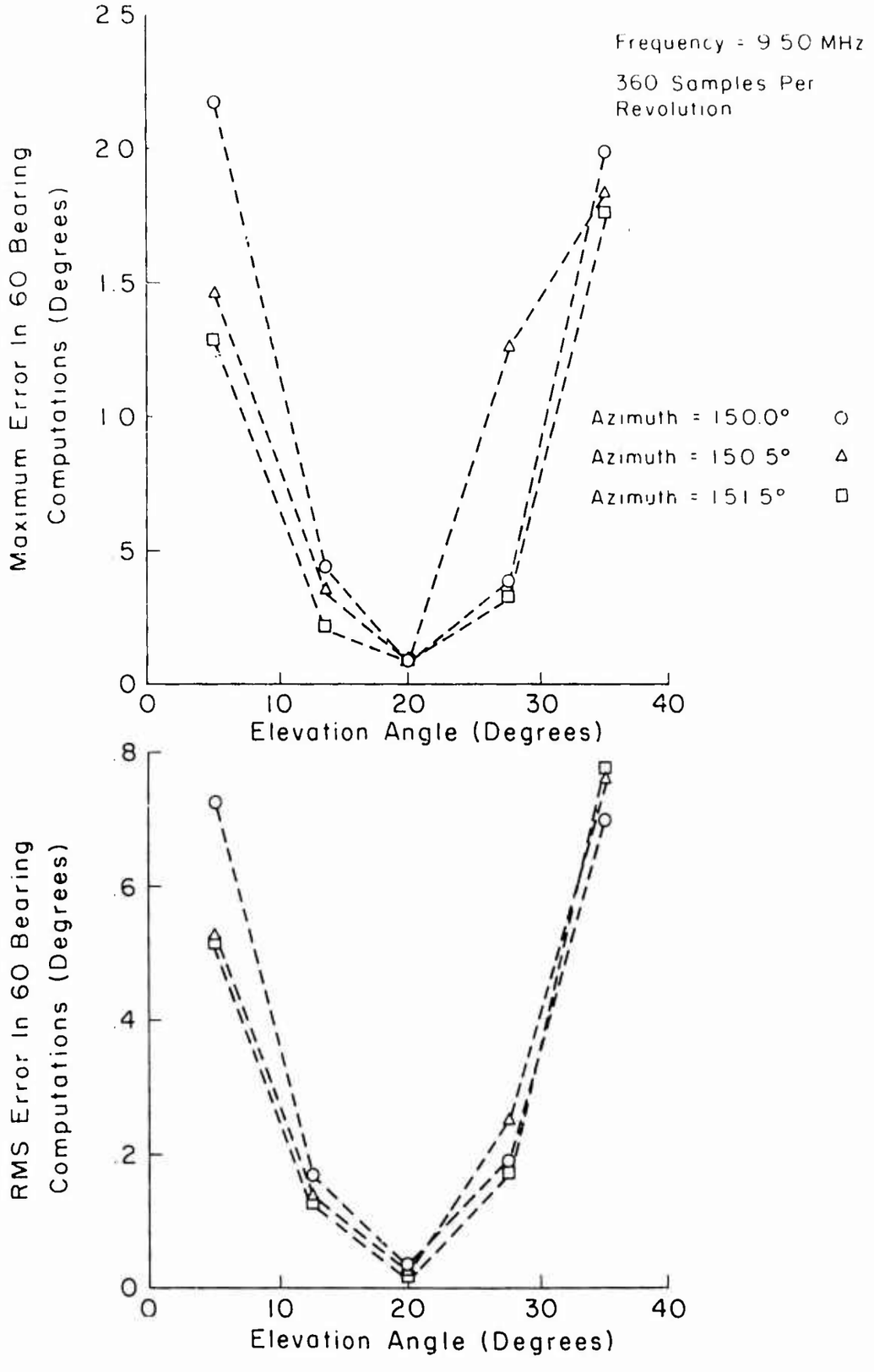

Figure 12. Effects of 180° Phase Shift in One Antenna

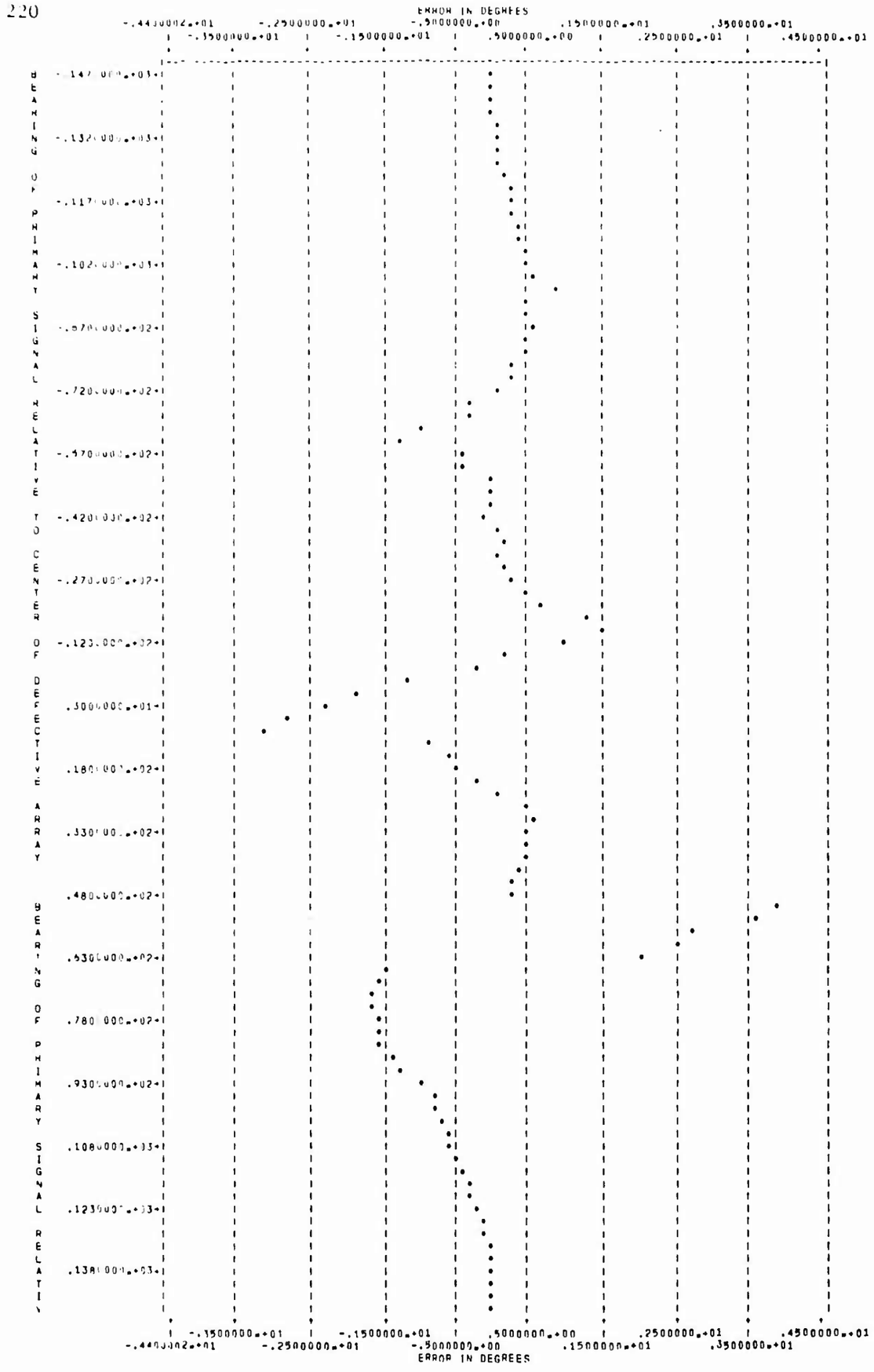

Figure 13. Error Pattern for the 39 Antenna Defect at 4 MHz

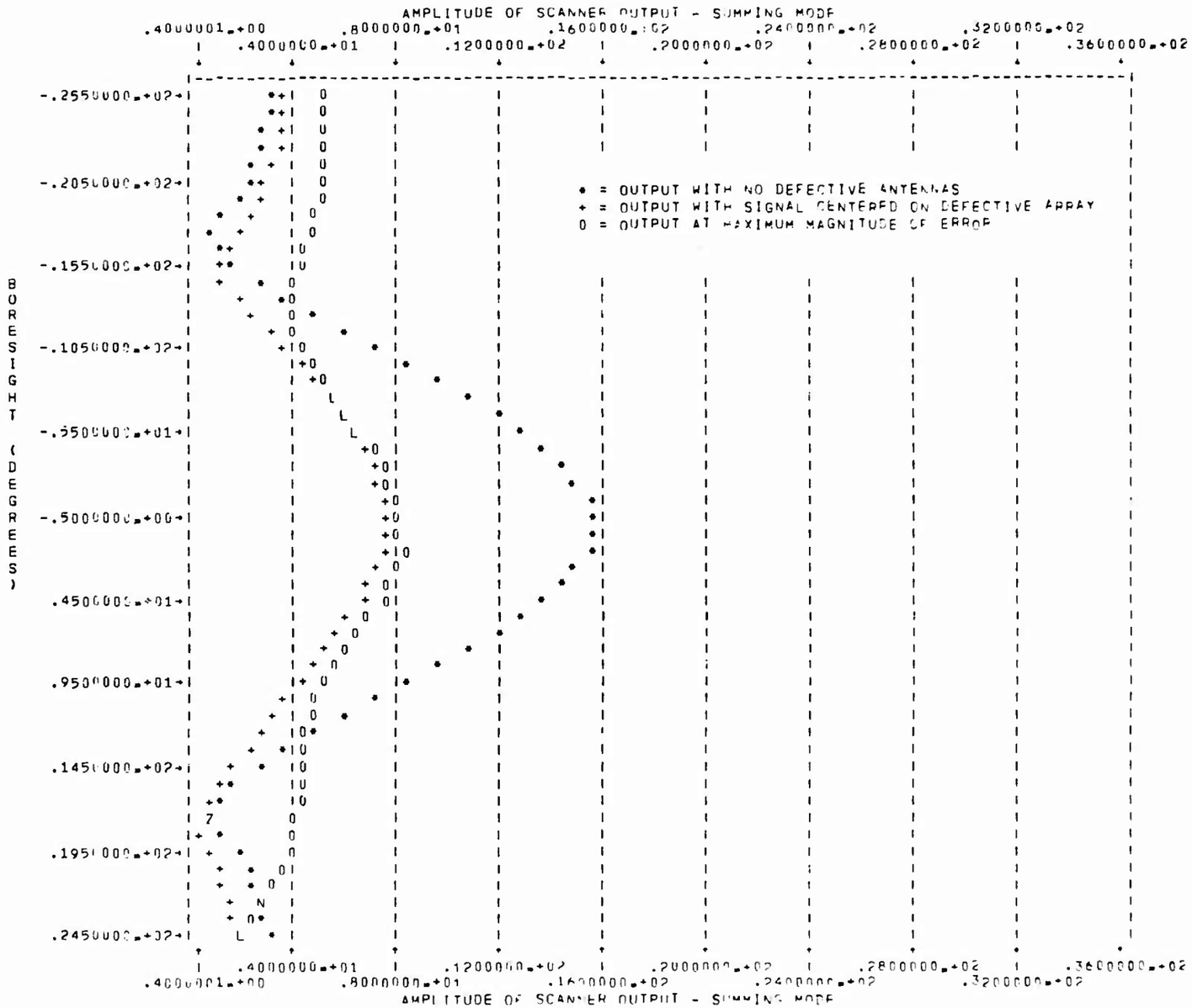

Figure 14. Scanner Output for the 39 Antenna Defect at 4 MHz

In any RDF system in which differential phase is to be measured, it is usually assumed that the receivers for the two channels are matched, i.e., the gain and phase shift through the two receiver channels are identical. As identical receivers are difficult to design and maintain, it is important to know the error that will be contributed if the two channels are not identical. Figures 15 and 16 from the work of Henderson[3] indicate the error that may be expected as a consequence of phase and gain mismatch of the two receiver channels of a Watson-Watt type RDF system.

Another modified system of interest is a system designed to yield improved performance.[3] One of the methods which has been postulated for reducing the effect of mismatch error, as discussed in the preceding paragraph, is to perform a channel interchange, i.e., exchange receiver channel A for receiver channel B and take as the correct value for the indicated bearing the average between the two values determined under the interchange and noninterchange conditions. Figure 17 shows the results of a study which inquired what the effect of such a process would be on errors in determining the direction of arrival with a Watson-Watt system. It can be seen that the error will be reduced considerably but will not be removed. It can also be seen that if one knew the difference in phase shift between the two receiver channels and the difference in gain, it would be possible to use a digital computer at the output to correct for this. One way by which this may be done is to connect a common signal to the two channel inputs at regular intervals. The relative magnitude of the output and the differential phase of the two outputs are, then, a direct measure of the imbalance of the two amplifiers. This

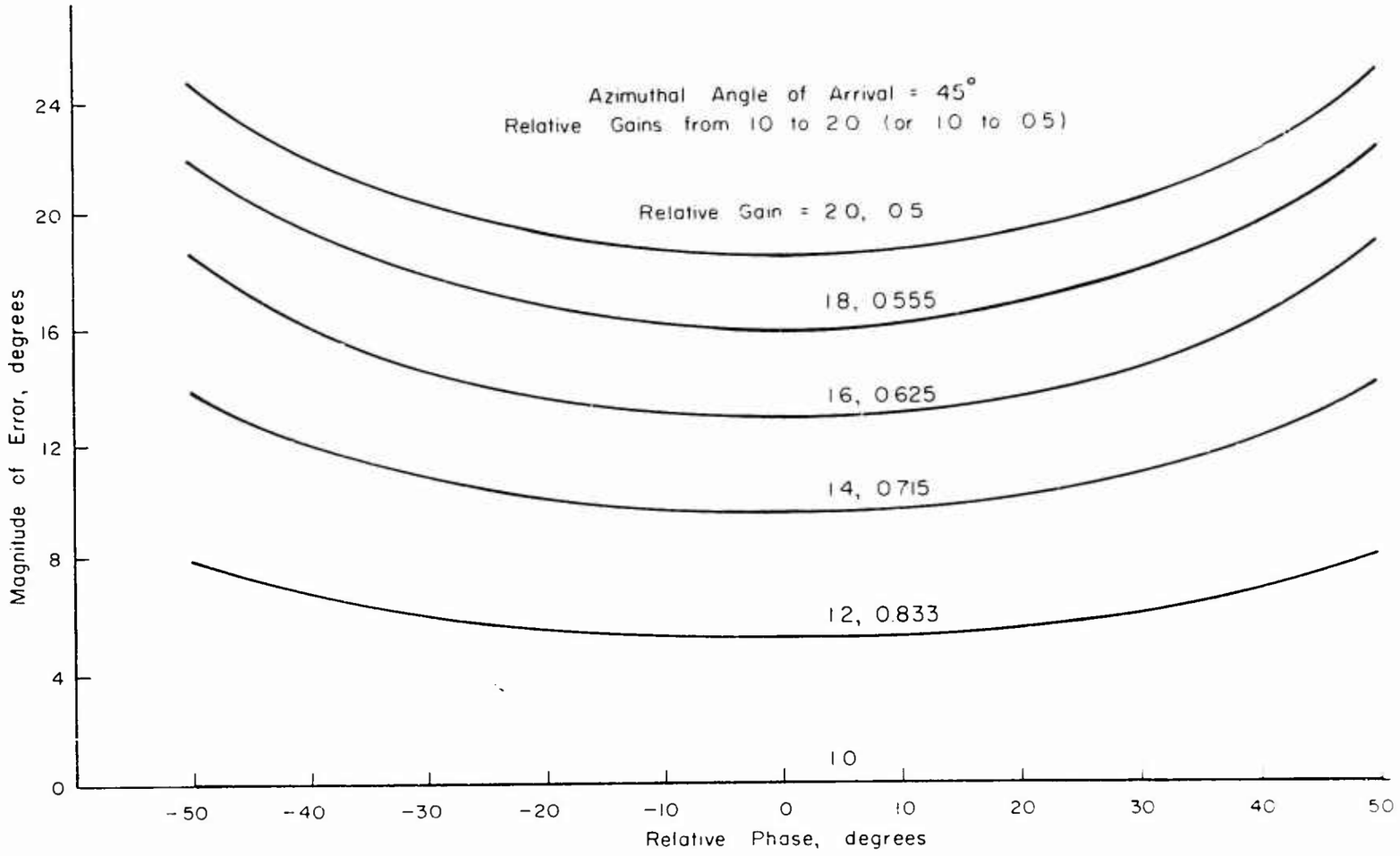

Figure 15. Magnitude of Bearing Error vs. Relative Phase Between Receivers.

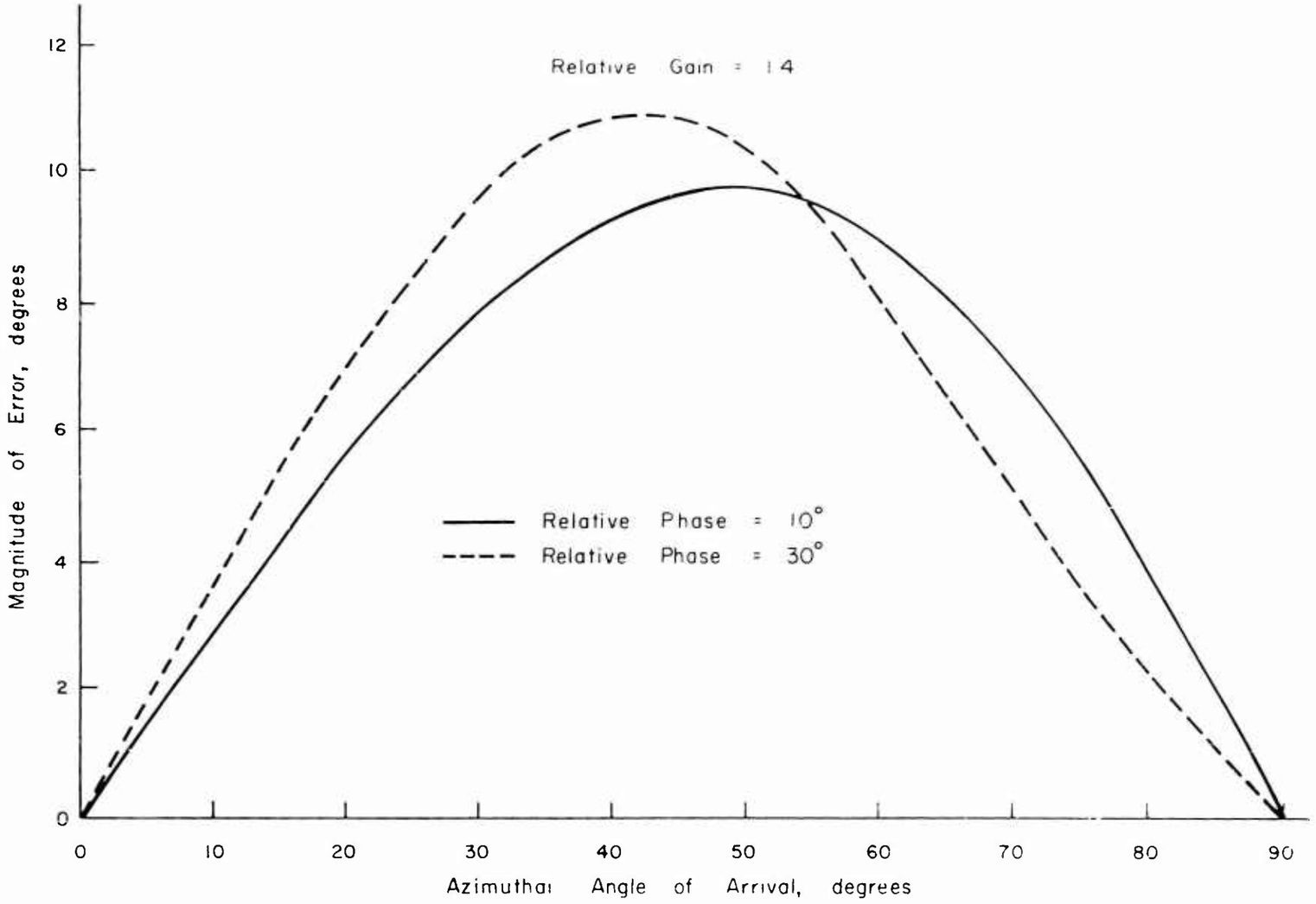

Figure 16. Magnitude of Bearing Error vs. Azimuthal Angle of Arrival.

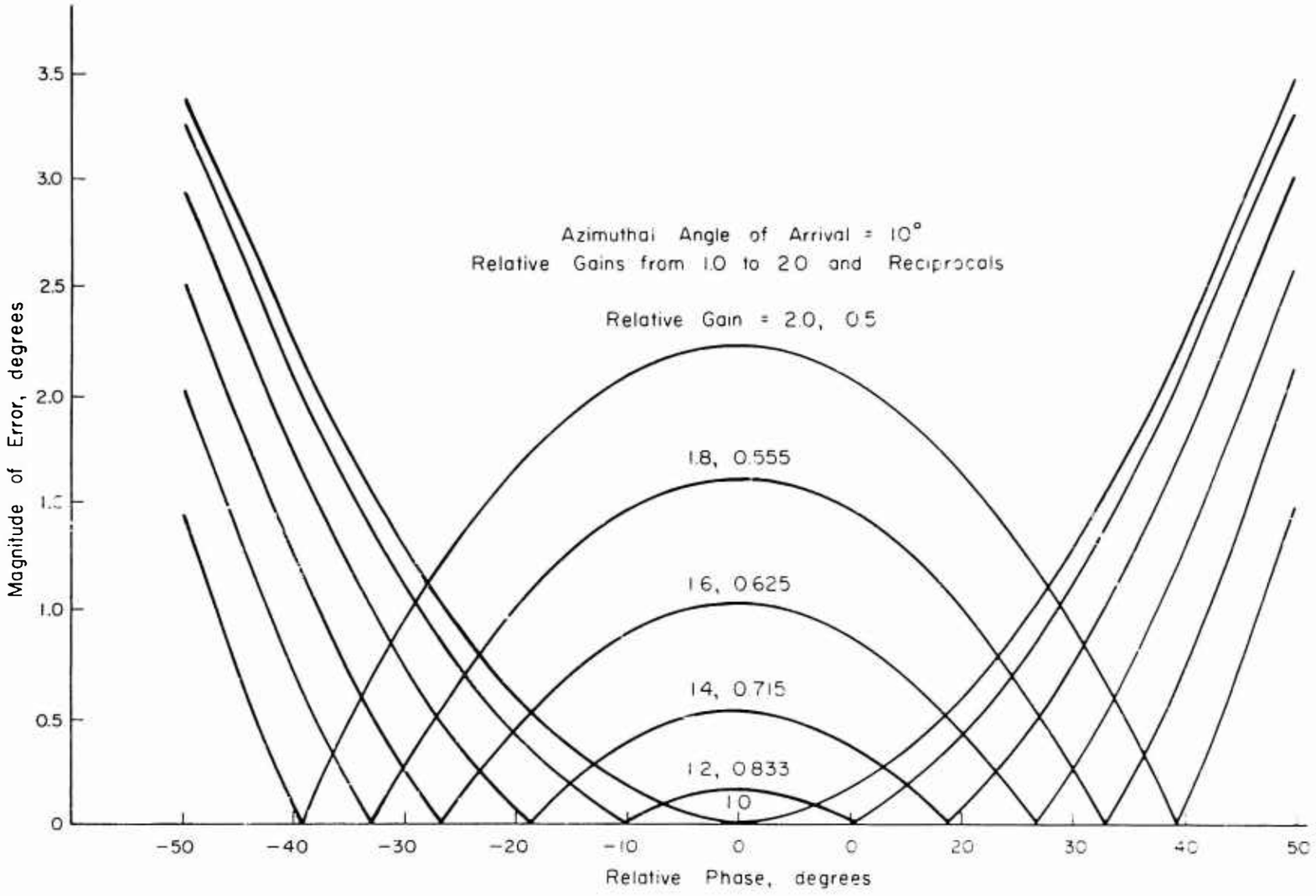

Figure 17. Interchanged Amplifier Technique - Magnitude of Bearing Error vs. Relative Phase Between Receivers.

information can then be used to correct the values of the direction of arrival which are determined with the nonideal unbalanced system. Figure 18 shows the error that would be expected under these conditions if the relative phase and relative gain between the two channels were allowed to drift as a function of time, and corrections were made at intervals of twenty successive readings. The drift is postulated as being more rapid at first than later. It is seen that even for large values of phase shift and gain imbalance, the magnitude of the error in determining the direction of arrival is relatively small.

One of the troublesome aspects of the cathode ray tube display in the Wullenweber system is that the pattern observed is considerably affected by the modulation and fading characteristics of the signal. One method postulated for reducing this difficulty was to utilize for the displayed quantity the ratio of two signals.[8] If the signals were modulated by the same value, then the ratio should be constant. Figures 19 and 20 are plots of the sum and difference patterns which have been determined by means of digital simulation studies for unmodulated signals and modulated signals, respectively. Figure 21 shows the results of dividing the sum pattern by the difference pattern and the difference pattern by the sum pattern, whereas Figure 22 indicates the sum and difference patterns which would be obtained if both were divided by the voltage on a fixed antenna which received the signal but did not contain any directional information which varied as a function of the scan. A system which utilized analog signal processing to carry out these functions was constructed at a later date and found to perform essentially as predicted.

Symbol	A	Relative Gain		Relative Phase	
		Start	End	Start	End
X	1	10	122124	00	9333
◊	101	122284	139948	9421	16316
Δ	201	139983	152632	16364	21207
θ	301	152719	160206	21216	24192
O	401	160261	162987	24200	25158
C	501	162988	162987	25159	25159

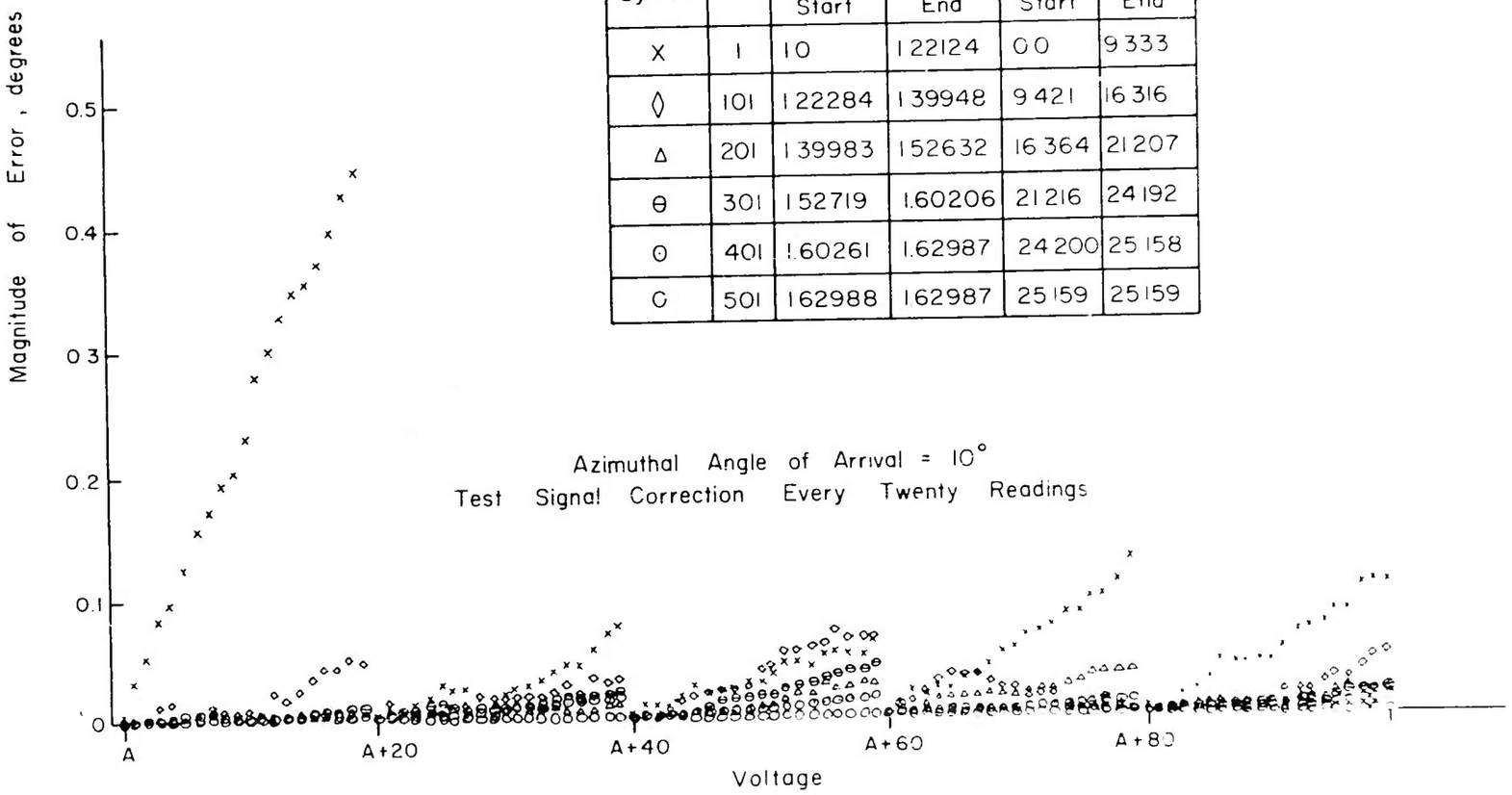

Figure 18. Magnitude of Bearing Error vs. Voltage Readings for Bearing Determination.

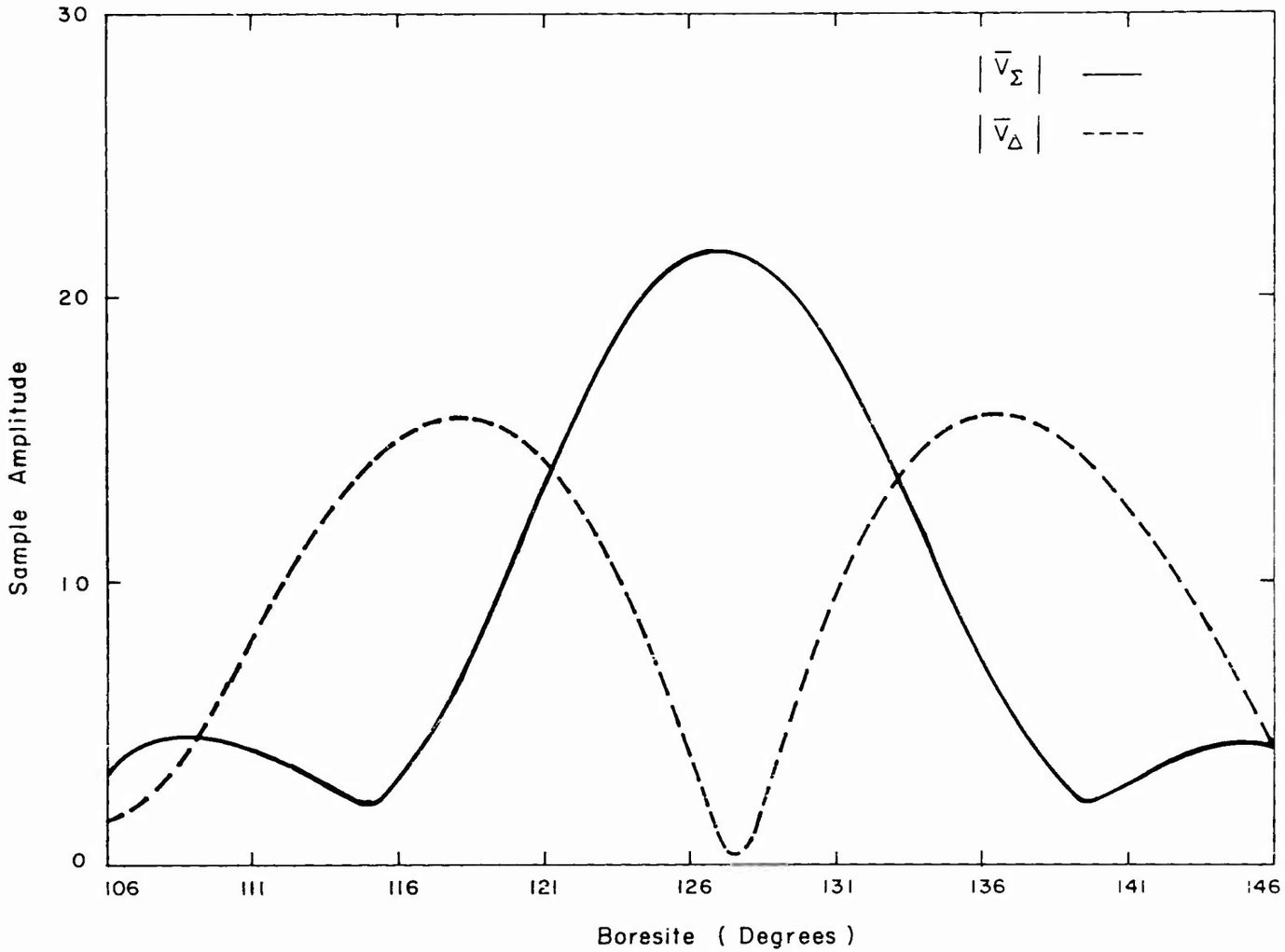

Figure 19. Sum Voltage Magnitude ($|\overline{V}_\Sigma|$) and Difference Voltage Magnitude ($|\overline{V}_\Delta|$) with no Modulation as a Function of Boresite

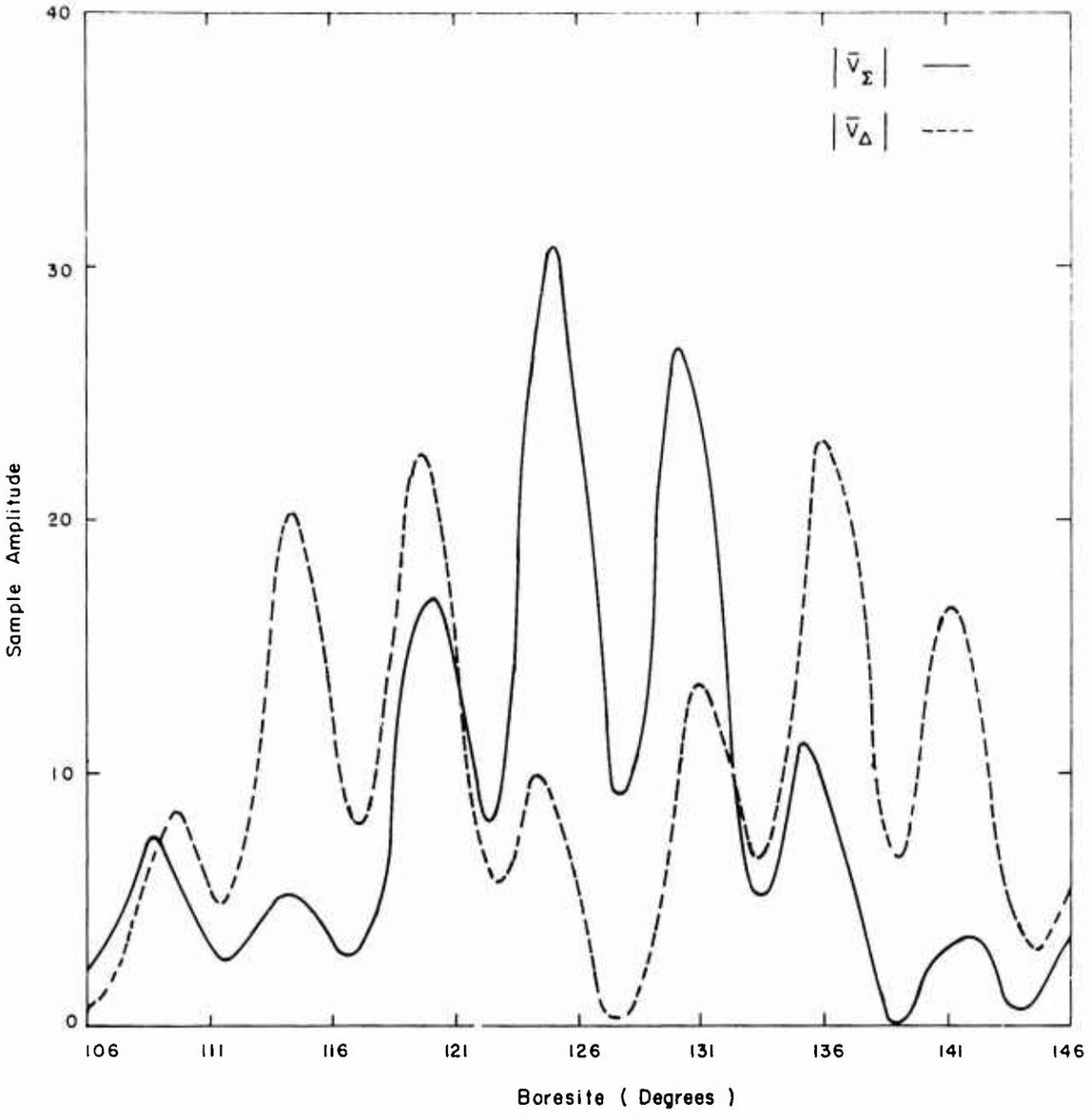

Figure 20. Sum Voltage Magnitude ($|\bar{V}_\Sigma|$) and Difference Voltage Magnitude ($|\bar{V}_\Delta|$) with Modulation as a Function of Boresite

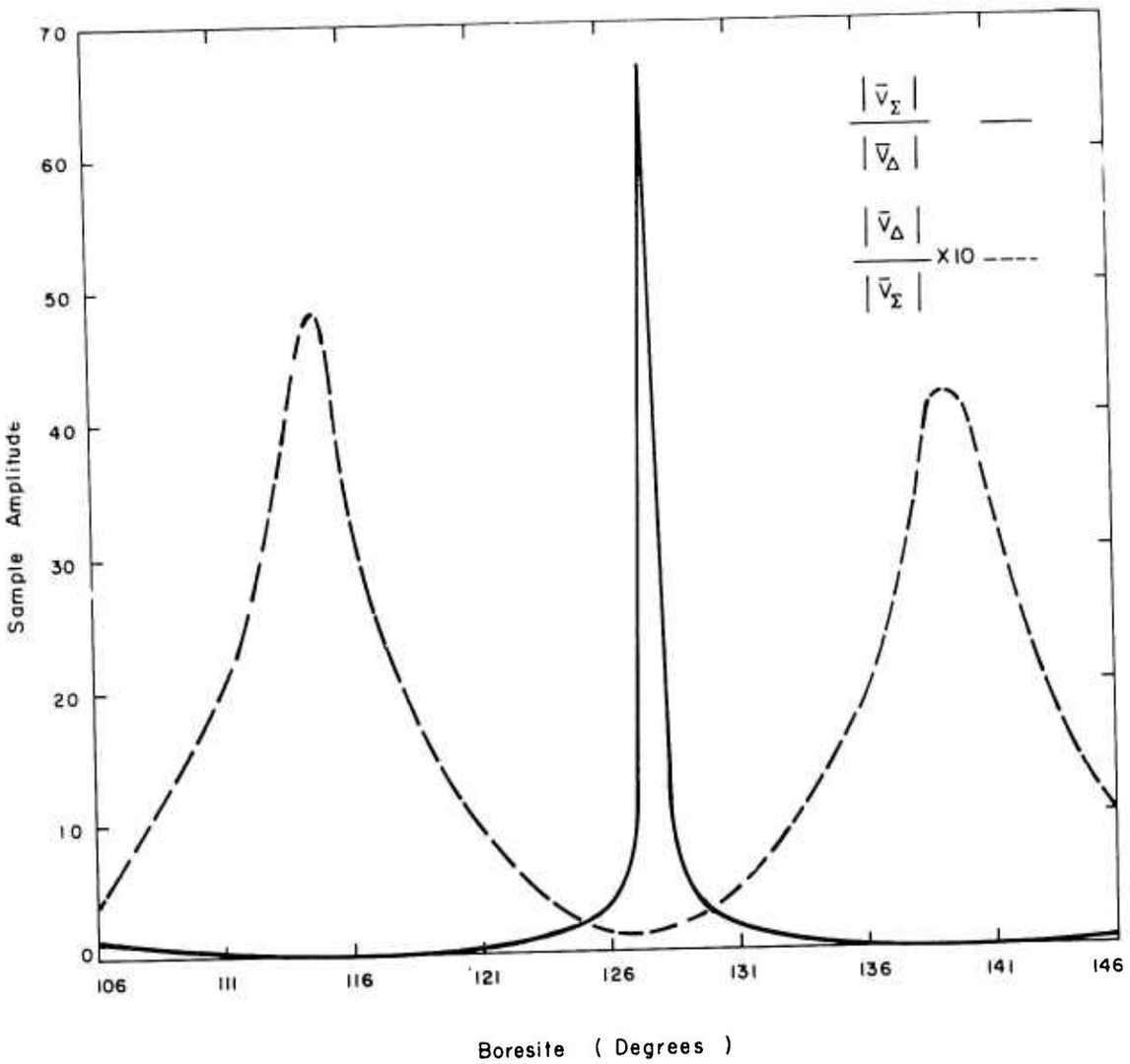

Figure 21. Sum Magnitude ($|\overline{V}_\Sigma|$) Divided by Difference Magnitude ($|\overline{V}_\Delta|$) and Difference Magnitude Divided by Sum Magnitude as a Function of Boresite

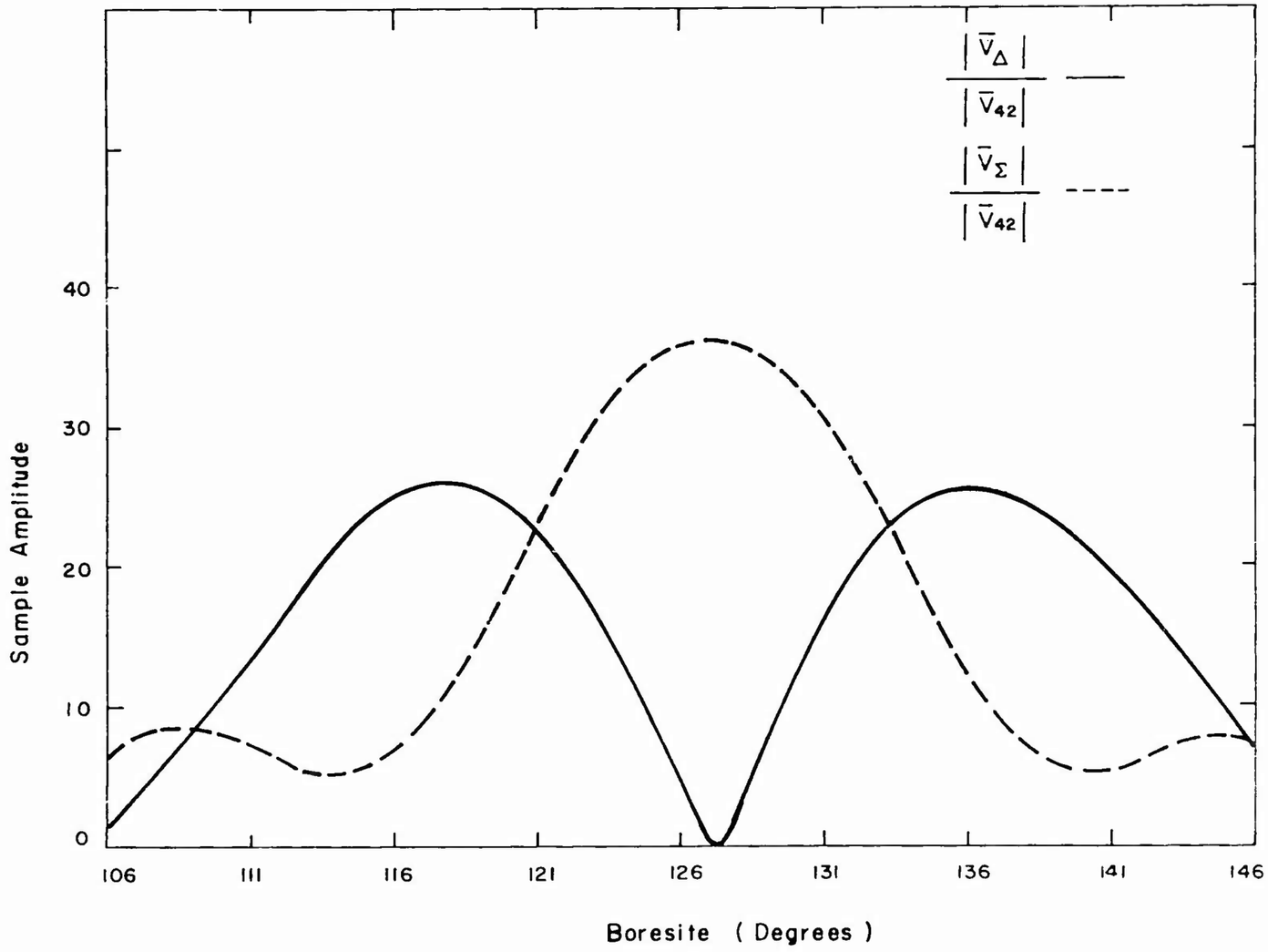

Figure 22. Sum Magnitude ($|\bar{V}_\Sigma|$) Divided by Magnitude of Antenna Number 42 ($|\bar{V}_{42}|$) and Difference Magnitude ($|\bar{V}_\Delta|$) Divided by Magnitude of Antenna Number 42 as a Function of Boresite

The University of Illinois Wullenweber array, as originally configured, did not yield information concerning elevation angle of arrival. One of the suggestions made for adding this capability to the system was to combine certain of the antenna elements so as to form phantom antennas aligned in the azimuthal direction toward the signal source[13] as shown in Figure 23. One of the difficulties that is expected with such a system is that errors may be produced as a consequence of the inability to precisely measure the relative differential phase of the phantom interferometer pair. One means of simulating such an error is to simply truncate the precision with which the differential phase is known. Figure 24 shows the error to be expected for various elevation angles of arrival for two frequencies (4 MHz and 6 MHz) if the differential phase is truncated to a precision of .1 degree. It can be seen that for low elevation angles (5 degrees or less) noticeable error may be expected, even for a relatively high precision differential phase measurement such as has been postulated.

One of the principal areas in which digital methods have had a pronounced impact on Radio Direction Finding is in the use of digital hardware to perform functions similar to those performed by analog methods either alone or with human operators. The most widely studied of these is the use of digital computation methods which can be translated into digital hardware for determining the direction of arrival. In this type of system modification, it is postulated that the voltages available at certain parts of the system are processed in some way such as determining the magnitude or the relative phase. These quantities are then used as input for a digital computation of the direction of arrival. One of

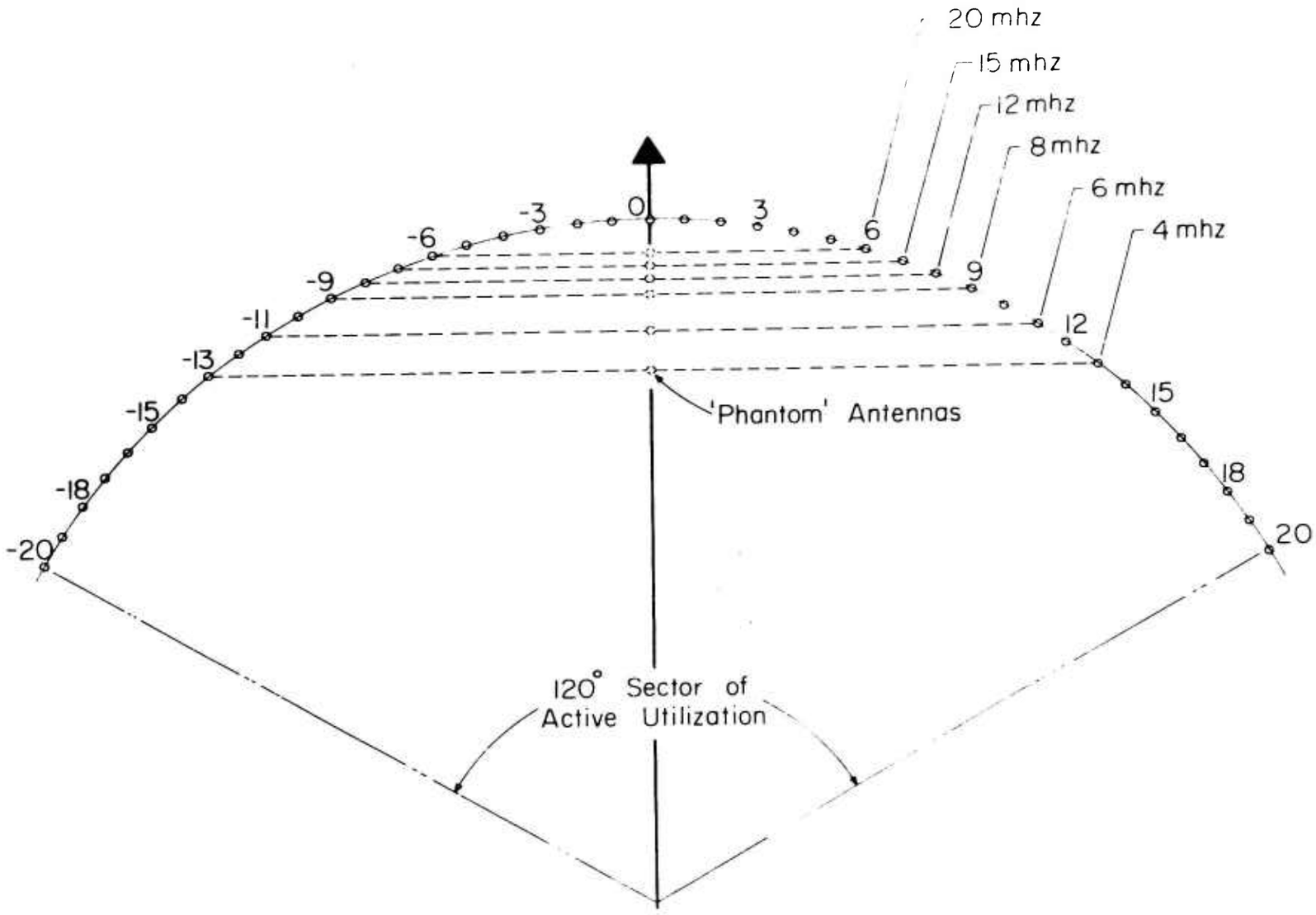

Figure 23. Phantom Antennas for Half-Wavelength Spacing.

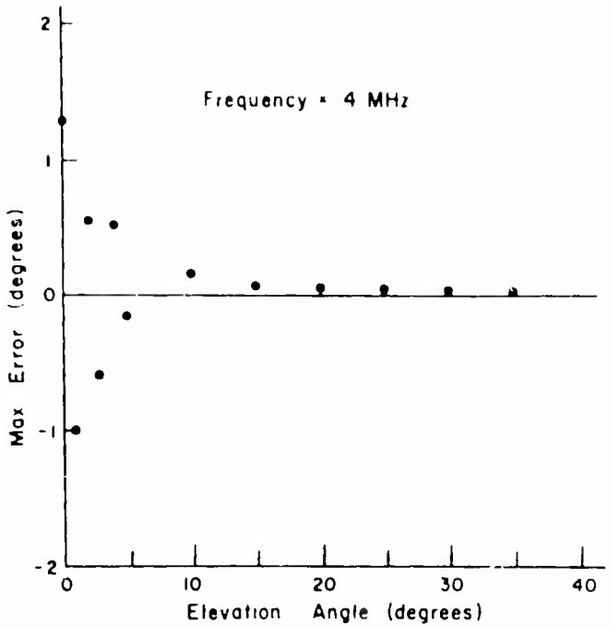

Figure 24(a). Maximum Errors in Elevation Angle Estimation at Any Azimuth; Frequency = 4 MHz.

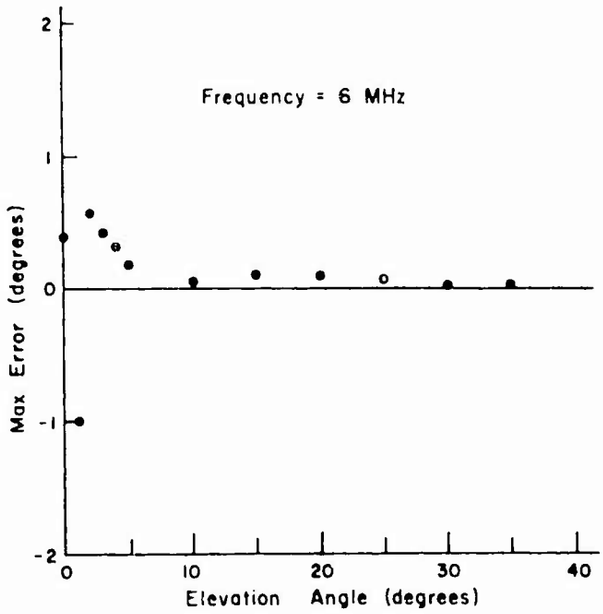

Figure 24(b). Maximum Errors in Elevation Angle Estimation at Any Azimuth; Frequency = 6 MHz.

the principal advantages offered by this method of operation is the removal of the operator from the direct line of observation. That is, it is possible to obtain estimates of the direction of arrival without requiring the judgment and interpretation of a human operator. The method which has been used for automatic bearing computation at the University of Illinois Wullenweber system is based on the work of Smith[1] and is known as the "Center of Gravity" method. The centroid ("Center of Gravity") of the major lobe of the array response as a function of azimuthal position of the scanner is determined. The displacement of the centroid, C, from an arbitrary reference is given by Equation (3) where x_i is the azimuthal displacement from the given reference where the

$$C = \frac{\sum_{i=1}^{n} x_i, F(x_i)}{\sum_{i=1}^{n} F(x_i)} \qquad (3)$$

values of the sum pattern, $F(x_i)$, are known. The principal problem in implementing this bearing computation procedure is to devise a means by which those points which are to be considered as the major lobe of the response can be determined. In the method currently used, the maximum signal level is first determined and the first point to the right and to the left of the maximum which falls below 10 per cent of the maximum is noted. (See Figure 25.) Those points between the 10 per cent level define the major lobe. If no point falls below the 10 per cent point before a minimum is reached, then the first minimum on either side of the maximum is used to define the limit for the major lobe. One of the errors

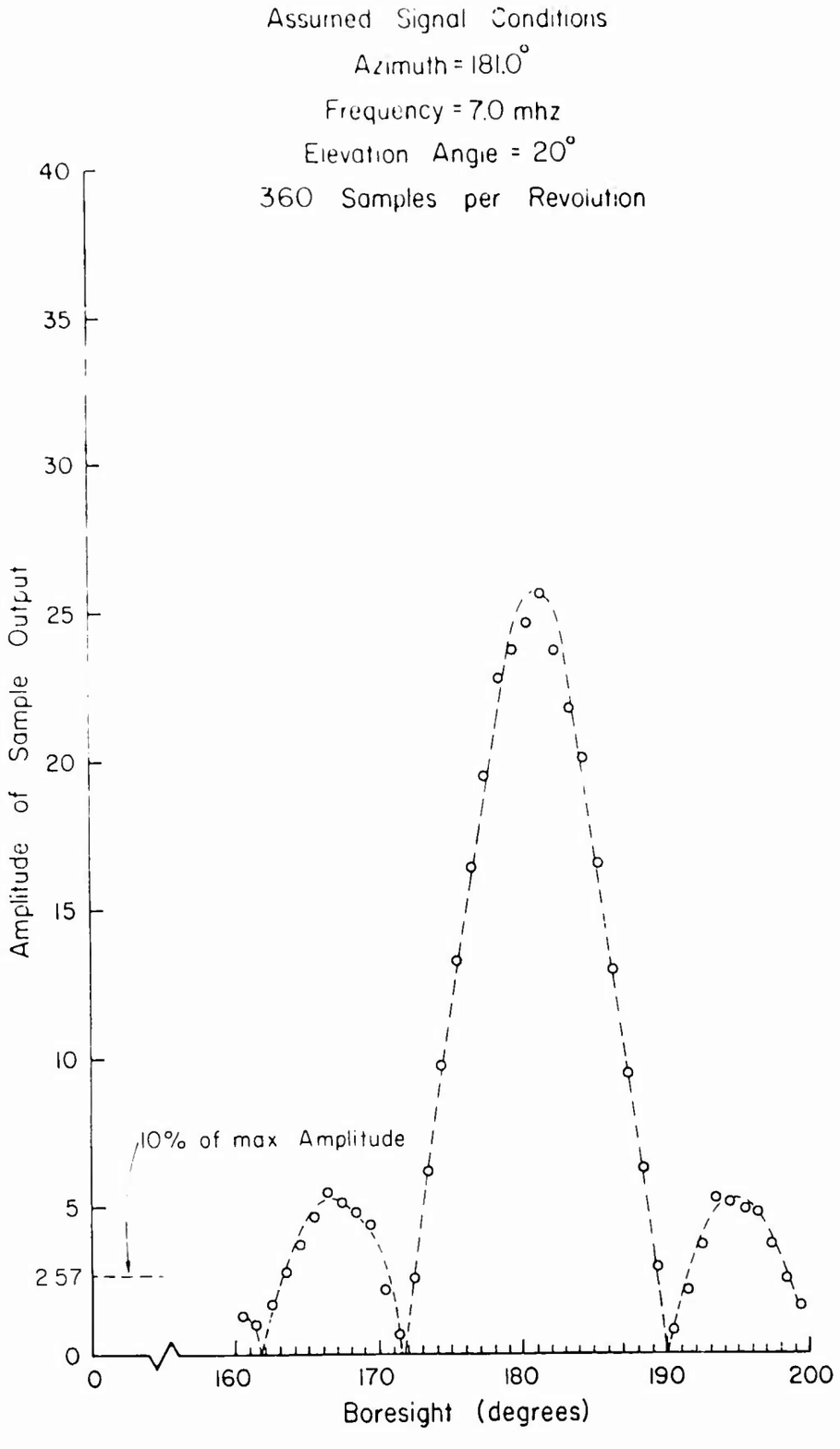

Figure 25. Simulated Antenna Scanner Output - Summing Mode

associated with this method of determining the direction of arrival is that the sum pattern is sampled at regular intervals. Thus an error may be found which depends upon the relative positions of the direction of arrival, and the sampling azimuths. Figure 26 is a plot of the errors determined through digital simulation studies of the center of gravity method of bearing computation.[5] Not shown here is the considerable error which comes about when the number of samples per revolution is small; or, what amounts to the same thing, the number of samples that is included within the major lobe is small. Digital simulation studies have shown that when the number of samples included in the major lobe becomes less than twelve, the error increases noticeably.

As was noted earlier, the difference between the azimuthal direction of signal arrival, α, and the boresite position of the scanner is related to the differential phase between the right-bank voltage and the left-bank voltage by Equation (4). This is shown in Figure 27.

$$\alpha = \frac{1}{k} (\gamma_R - \gamma_L) \quad . \tag{4}$$

For a fixed azimuthal direction of signal arrival, Equation (5) shows the relation between the differential phase and the scanner boresite azi-

$$(\gamma_R - \gamma_L) = k\ x + b \tag{5}$$

muthal position, x. As b is the differential phase for a zero value of azimuth, the scanner boresite position when the differential phase, $(\gamma_R - \gamma_L)$, is equal to 0 is the direction of arrival of the signal as given by Equation (6).

$$x = \frac{-b}{k} \quad . \tag{6}$$

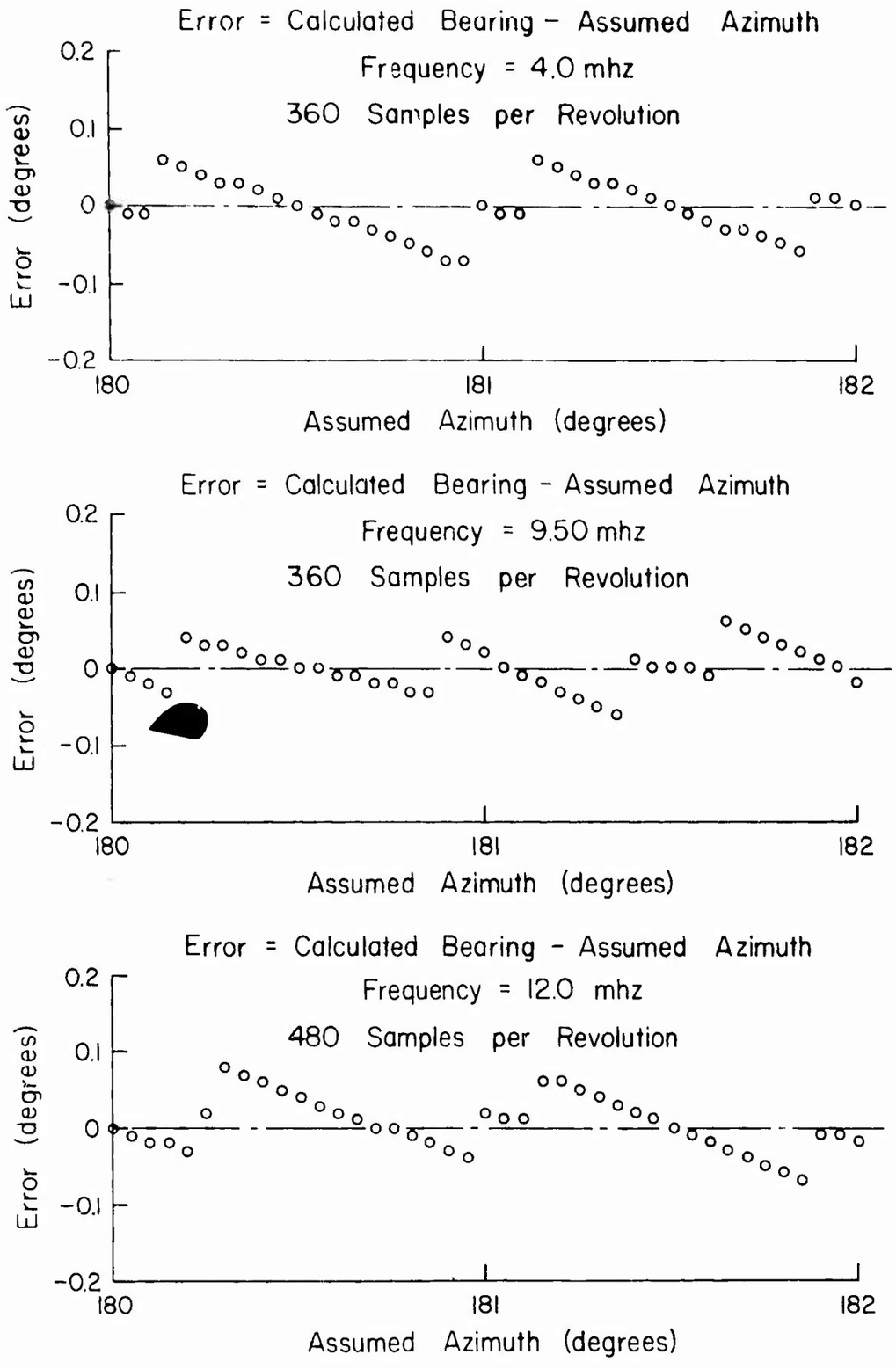

Figure 26. Errors in Automatic Bearing Computer

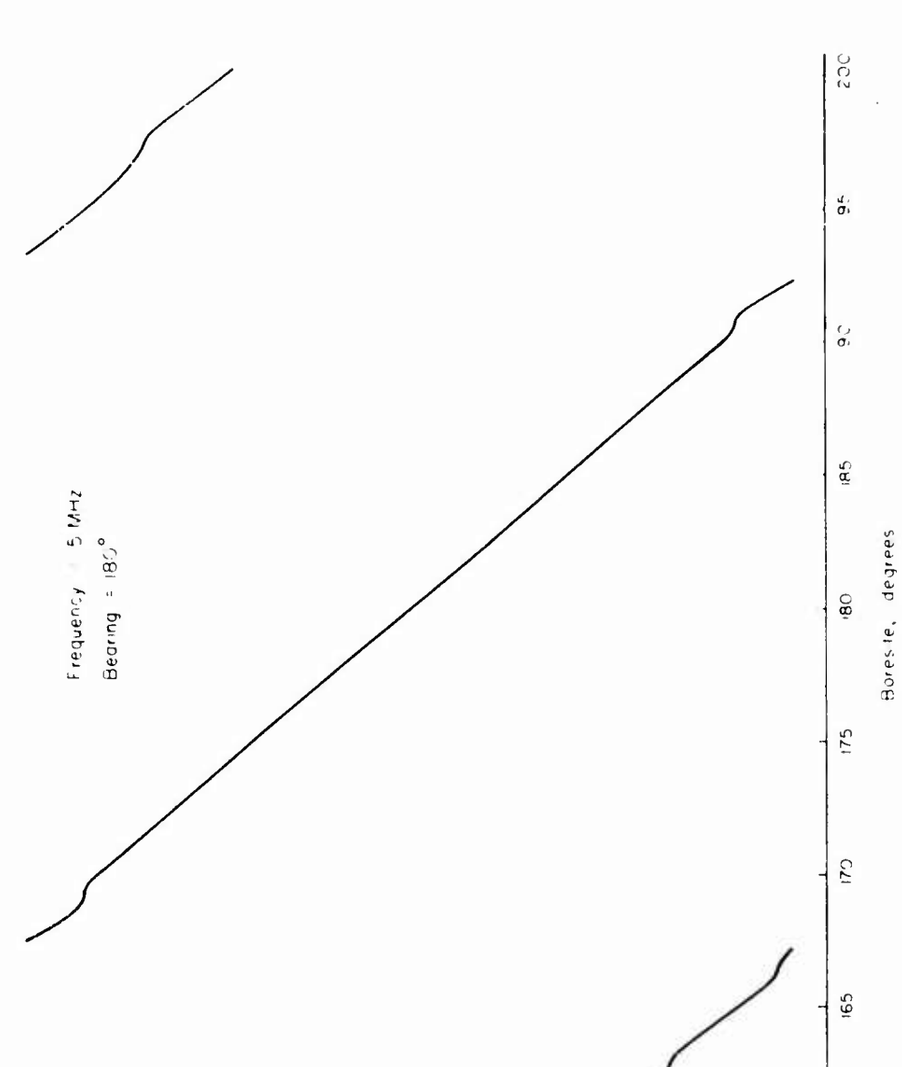

Figure 27. Value of δ as a function of boresite angle for constant signal condition.

The differential phase is measured at regular intervals of scanner boresite position and a least squares fit to a straight line made to these data. The slope and intercept for the straight line will correspond to the value of k and the value of b, respectively. From this, the direction of arrival of a signal may be readily determined.[7]

In an earlier work, Grush[2] showed that a digital computer could be used to determine the direction of arrival in a Watson-Watt RDF system by measuring the amplitude and relative phase of the two signals which are used to form the display. The algorithm for this computation is that of Equation (7) in which e_1 and e_2 are the magnitudes of the two voltages and θ is the differential phase between them.

$$B = \frac{1}{2} \operatorname{Tan}^{-1} \left[\frac{2e_1 e_2 \cos \theta}{e_1^2 - e_2^2} \right] . \qquad (7)$$

An alternate form is shown in Equation (8) in which e_s is the magnitude of the phasor sum of e_1 and e_2. Thus, if measurements of the magnitude of e_1, e_2, and e_s are available and used as input for the computational process, the direction of arrival may be readily determined.

$$B = \frac{1}{2} \operatorname{Tan}^{-1} \left[\frac{e_s^2 - (e_1^2 + e_2^2)}{e_1^2 - e_2^2} \right] . \qquad (8)$$

It should be clear that if one assumes the availability of a digital computer and the ability to determine by direct measurement the values of appropriate quantities in the RDF system, and uses these values as input for the digital computer, the digital computer can be made to function as a digital bearing computer and yield estimates of the direction of arrival on an automatic basis.

III. DATA ACQUISITION

In many areas of research, it has been found to be desirable to process the experimental data with a digital computer. One of the principal reasons for doing this is the speed and accuracy with which a large volume of experimental data can be processed. Studies in RDF and in other areas in which direction finding plays an important part are no exception. The large volume of data makes it extremely impractical to consider acquiring data by any other than automatic methods. Further, if the data are to be introduced to a digital computer for computation, it is quite desirable that the data be coded into a digital format suitable for direct input to a digital computer at the earliest possible stage.

Although a wide variety of data can be recorded for input to a computer, the experimental studies conducted by the Radiolocation Research Laboratory have tended to record those quantities which can be directly measured with somewhat conventional instrumentation. Thus, rather than perform a computation to determine the direction of arrival on an on-line basis and record the direction of arrival thus obtained, the voltages and differential phases which could be used to determine direction of arrival have been recorded and used as input to the computer from which the direction of arrival computation has been subsequently made. The subject of data acquisition for digital computer processing is a topic of its own. It is important to recognize that when using an automatic data acquisition system, one is bound by previous decisions that have been made concerning the data that are to be acquired. For

this reason, considerable thought should be given to the design of the data acquisition system and to the manner in which it is to be used before data taking starts [15] Some of the items to be considered include:

a) What data should be recorded,

b) What is the precision needed for the various data,

c) What is the format to be used for the recorded data,

d) How rapidly should the data be recorded.

If the two data acquisition systems used by the Radiolocation Research Laboratory are considered, the answers, for these two cases, may be seen.

The data acquisition system (DAS) used to acquire data from the interferometer RDF system[18] is shown in the block diagram of Figure 28. The data and the precision needed which were determined to be desirable for this system are as follows:

Three values of differential phase, 12 bits (0.1°) for each value;

Three values of signal amplitude, 12 bits for each value;

One value of calibration phase and one value of a calibration amplitude, 12 bits for each value;

Time (BCD) hours, minutes, seconds;

Frequency (BCD) Megahertz (to 39), Kilohertz .

The format for recording these data utilizes 8 channel punched paper tape. Six channels are used for data bits, one channel for a parity bit, one channel for control and possible expansion. Thus, each phase or amplitude measurement requires two characters and by squeezing the time and frequency data together, these data may be contained in 22 bits each, thus utilizing all but 2 bits of 4 characters. By proper encoding, these 2 bits can indicate whether the 4 character group is time datum, frequency data, or some other kind of data as indicated in Table 1. Thus,

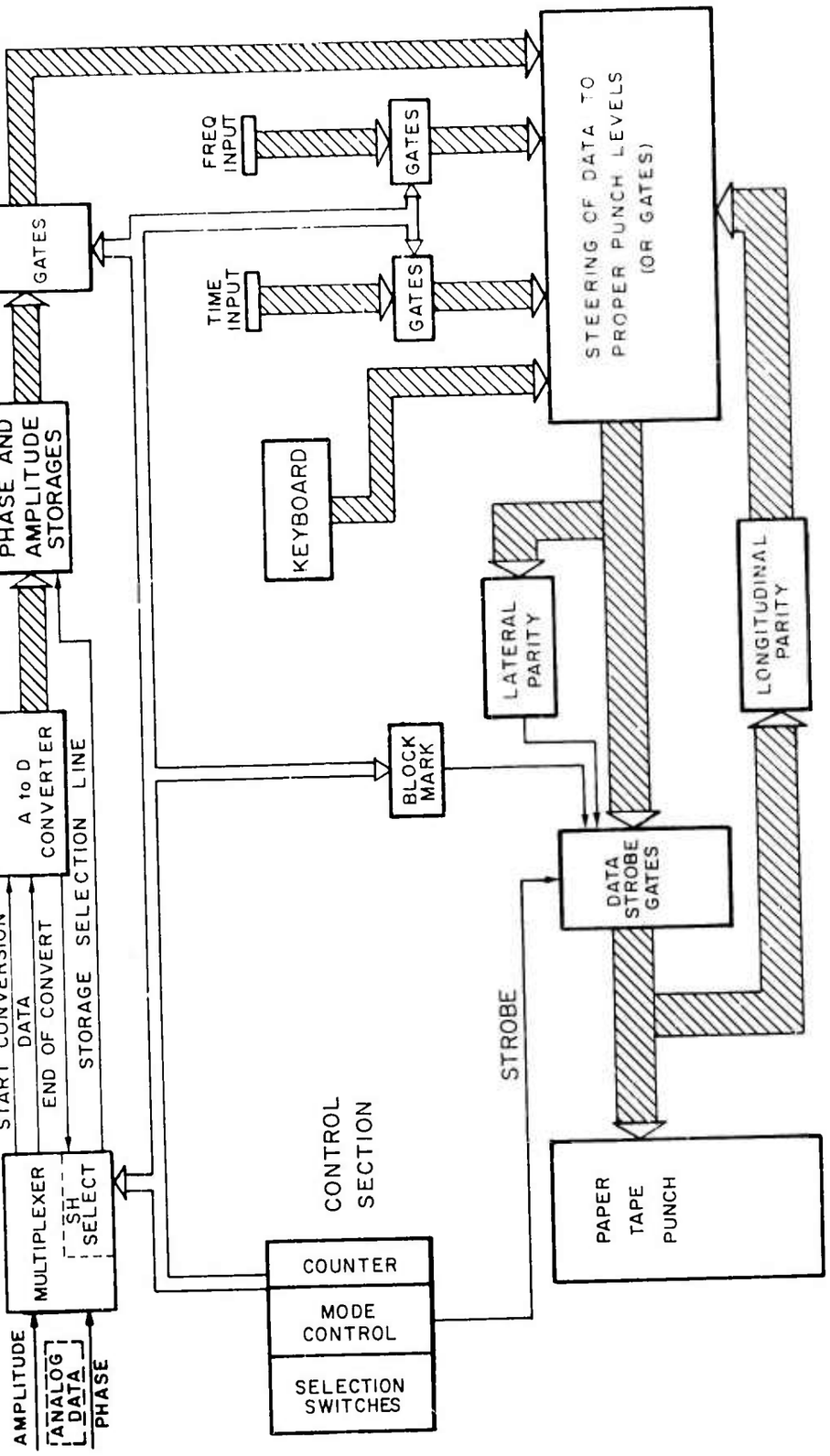

Figure 28. System block diagram.

Table 1

Encoding Pattern for Time and Frequency Data

Encoding Pattern, Time

Character No. \ Bit Position	1	2	3	4	5	6	7	8
1	0	0	H	H	h	h		
2	h	h	M	M	M	M		
3	m	m	m	m	S	S		
4	S	S	s	s	s	s		

HH - hours, tens (0, 1, 2)
hhhh - hours, units (0, 1,...,9)
MMMM - minutes, tens (0,1,...,6)
mmmm - minutes, units (0,1,2,...,9)
SSSS - seconds, tens (0,1,...,6)
ssss - seconds, units (0,1,...,9)

Encoding Pattern, Frequency

Character No. \ Bit Position	1	2	3	4	5	6	7	8
1	0	1						
2	M	M	m	m	m	m		
3	L	L	L	L	K	K		
4	K	K	k	k	k	k		

MM - Megahertz, tens (0,1,2,3)
mmmm - Megahertz, units
LLLL - Kilohertz, hundreds
KKKK - Kilohertz, tens
kkkk - Kilohertz, units

the total record of data consisting of time or frequency, plus the necessary phase and amplitude measurements, consists of 20 data characters plus an end of record character -- a total of 21 characters as shown in Table 2. The speed with which the data should be taken is determined by the rate of variation of the data sampled. However, the maximum speed or the maximum rate is determined by hardware limitations. For this system, the limitation is the speed of the paper tape punch which has a maximum of 240 punched characters per second. This implies a minimum time between data records of a little bit less than 90 milliseconds.

The other system for acquiring data for direct input to the computer is the high speed data system (HSDS), shown in Figure 29, located at the Bondville Road Field Station.[19] As this system is designed to acquire data from the Wullenweber RDF system, it is designed to take samples of the sum and difference amplitudes as well as the differential phase between the right and left bank voltages at the output of the scanner for several positions during rotation of the scanner. The number of positions at which these three quantities may be sampled per scan varies and may be as large as 90, although 30 points per scan (one sample per degree) have been used for most of the experimental work. In addition, values of eleven other quantities are sampled once per scan, making a total of 101 data samples for each rotation of the scanner. Each data sample has two parts: one part is a code to identify which of the pieces of data the second part (which is the value of the data) represents. As there are 16 possible channels of input data, the 4 bit code is used for encoding the channel number. A 14 bit binary code is used for encoding the value of the quantity recorded. Although the information is recorded on a nine track

Table 2

Format of Data Record

21-Character Block	Character No.	31-Character Block
	1	
Frequency or	2	
Time Data	3	
	4	
Phase (2,1)	5	
	6	
Amplitude (2)	7	
	8	
Phase (1,3)	9	Characters 1 to 20
	10	are the same as for
		the 21 Character Block
Amplitude (1)	11	
	12	
Phase (3,2)	13	
	14	
Amplitude (3)	15	
	16	
Phase (common)	17	
	18	
Amplitude (common)	19	
	20	
Longitudinal Parity and End of Block Marker	21	Phase (2,4)
	22	
	23	Amplitude (4)
	24	
	25	Phase (4,5)
	26	
	27	Amplitude (5)
	28	
	29	Phase (4,2)
	30	
	31	Longitudinal Parity and End of Block Marker

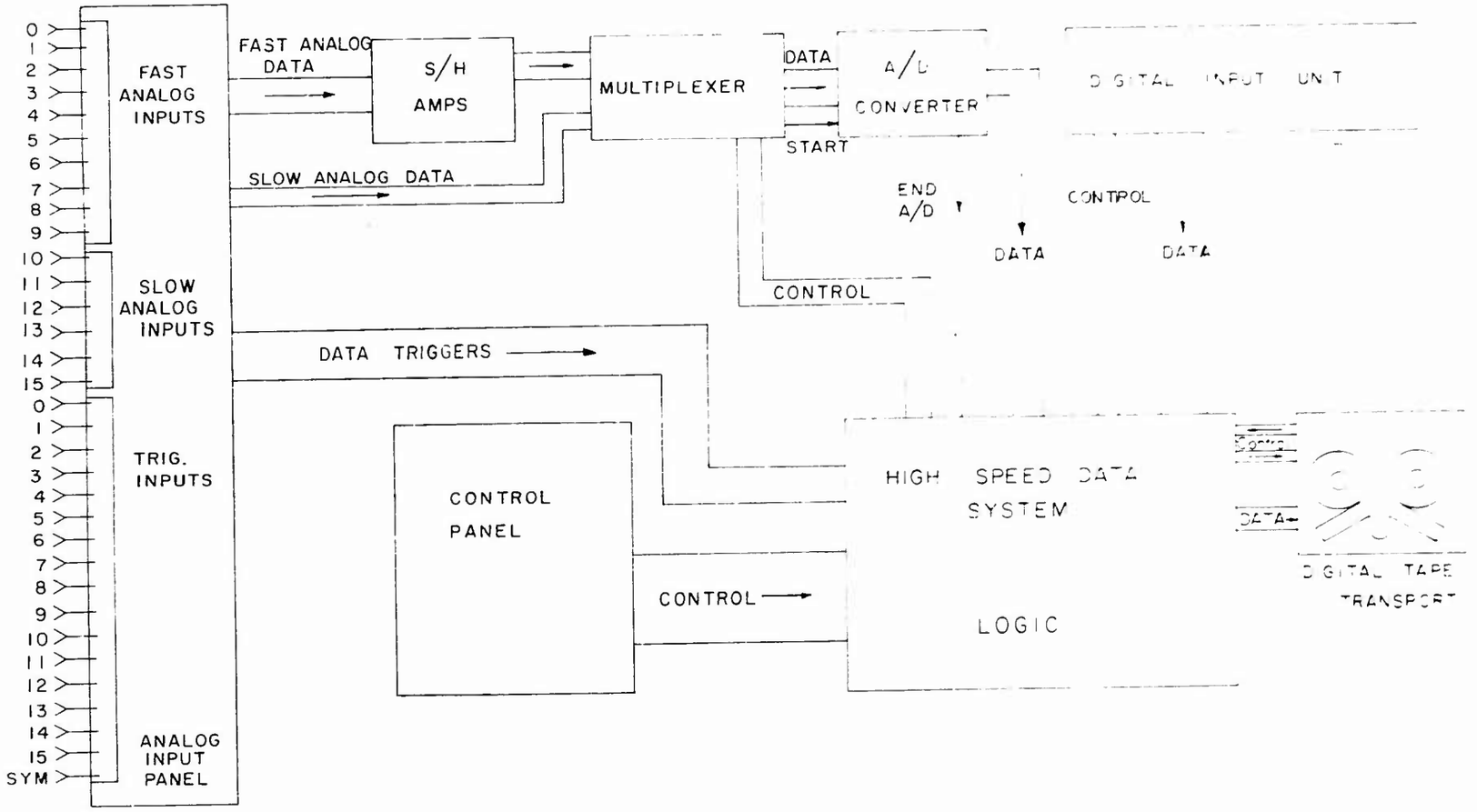

Figure 29. Simplified Block Diagram for HSDS

digital magnetic tape, only six tracks are used for recording data. Thus, three characters are needed to encode a single sample of data. This system is capable of recording at a much more rapid rate. A complete data sample may be recorded in between 100 and 200 microseconds. This allows the 101 data points per scan to be recorded in about 10 to 20 milliseconds.

Although the recorded data are in a format suitable for direct input to the computer, they are not used for direct computation. Rather, the data are edited, errors are eliminated, and the error-free data are stored in a revised format in a data file which may be more readily accessed for subsequent calculations than can the original data. All the data in a complete record (that needed for one calculation of direction of arrival of the interferometer or that for one scan with the Wullenweber system) are maintained in the file as a single data record. The data record has as identifying keys the date and time at which a record was made. If more than one data record has the same date and time, a sequence number is given to indicate the different times to be assigned to each of the records. Figure 30 shows three plots produced by a digital computer from the data recorded at the BRFS.[20]

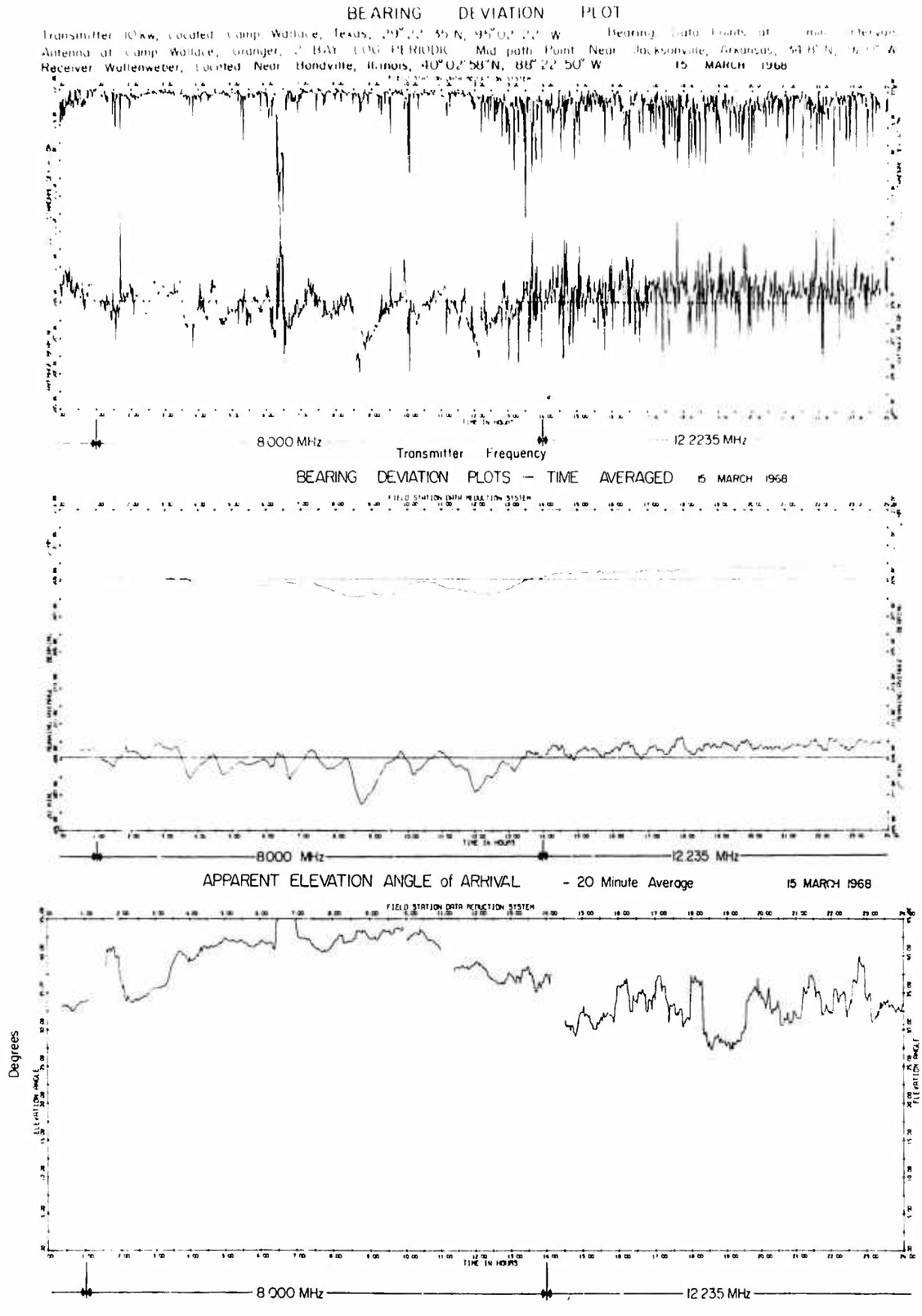
BEARING DEVIATION PLOT
Transmitter 10 kw, Located Camp Wallace, Texas, 29° 22' 35 N, 95° 02' 22" W
Antenna at Camp Wallace, Granger, 2 BAY LOG PERIODIC Mid path Point Near Jacksonville, Arkansas, 34 85 N,
Receiver Wallenweber, Located Near Bondville, Illinois, 40° 02' 58"N, 88° 22' 50" W
15 MARCH 1968
8000 MHz
Transmitter Frequency
12 2235 MHz
BEARING DEVIATION PLOTS — TIME AVERAGED 15 MARCH 1968
FIELD STATION DATA REDUCTION SYSTEM
TIME IN HOURS
8000 MHz
12.235 MHz
APPARENT ELEVATION ANGLE of ARRIVAL - 20 Minute Average
15 MARCH 1968
FIELD STATION DATA REDUCTION SYSTEM
Degrees
TIME IN HOURS
8 000 MHz
12 235 MHz

Figure 30.

LIST OF REFERENCES

(1) R. S. Smith, "Electronic observers for radio direction finding," Thesis 1962, RRL Publication 273, January 1965.

(2) H. Grush, "An investigation of a digital bearing computer for a small aperture radio direction finding system," RRL Publication 280, June 1965.

(3) J. Henderson, "Mismatch correction techniques for twin-channel receivers," RRL Publication 282, August 1965.

(4) S. Rosenbaum, "Characteristics of the monopulse mode display for the Wullenweber radio direction finding system," RRL Publication 291, August 1965.

(5) E. Jones, Jr., "A digital simulation of the Wullenweber direction finding system," RRL Publication 296, December 1965.

(6) E. Jones, Jr., "Effects of random phase errors in the Wullenweber direction finding system," RRL Publication 305, April 1966.

(7) E Ernst, E. Jones, Jr., R. Ledbetter, "A monopulse bearing computation method for use in the scanning mode," RRL Publication 307, April 1966.

(8) E Ernst, R. Ledbetter, W. McClurg, "Techniques of improving scanning RDF displays," RRL Publication 310, November 1966.

(9) B. Broeker, E. Ernst, E. Jones, Jr., "A study of wave interference in the Wullenweber RDF system," RRL Publication 311, June 1966.

(10) M. Glick, E. Ernst, E. Jones, Jr., "Studies in time averaging and wave interference in radio direction finding," RRL Publication 312, June 1966.

(11) D. Medill, E. Ernst, "A digital bearing computer for monopulse mode operation of the Wullenweber RDF system," RRL Publication 313, August 1966.

(12) L. Allen, E. Ernst, "Improved digital bearing computer techniques," RRL Publication 314, August 1966.

(13) E. Ernst, E. Jones, Jr., "Elevation angle of arrival determination in the Wullenweber RDF system," RRL Publication 315, August 1966.

(14) E. Ernst, E. Jones, Jr., "A study of the effects of systematic errors in the Wullenweber direction finding system," RRL Publication 318, October 1966.

(15) R. Ledbetter, E. Ernst, "The acquisition of data for digital bearing computation," RRL Publication 321, January 1967

(16) R. Vonderohe, E. Ernst, "The use of tapes for the storage of digital data," RRL Publication 323, January 1967

(17) E. W. Ernst, B. W. Rogers, "A simulation of a CDAA with large systematic defects," RRL Publication 357, June 1969.

(18) A. D. Bailey, J. D. Dyson, E. W. Ernst, "Studies and investigations leading to the design of a radio direction finder system for the MF-HF-VHF range," Final report, RRL Publication 353, March 1969 .

(19) W. C. McClurg, "HSDS: a high speed data system," RRL Publication 339, March 1968.

(20) A. D. Bailey, E. W. Ernst, L. J. Miller, W. W. Wood, "An atlas of reduced data obtained in a cooperative HF directional propagation experiment over a 1330 kilometer path " (March 1967 - March 1968), RRL Publication 344, September 1968.

W. M. SHERRILL, T. C. GREEN, R. LORENZ

Southwest Research Institute
San Antonio, Texas

DIGITAL DF APPLICATIONS

A growing segment of the DF community has begun to apply digital techniques to radiolocation problems. Computer processing and digital logic are applicable to receiver tuning, bearing calculations, remote direction finder operation, and other tasks requiring sophisticated data processing. In this report, we will describe digital DF experiments and hardware completed in our laboratory for special radiolocation problems.

Multichannel receivers are necessary for certain radiolocation applications. For fast response time or careful amplitude and phase measurements, at least two phase and gain matched receiver channels are used. Ultimately, as the demands for short response time and sophisticated processing increase, receivers with three channels or more will be used. The history of the development of twin channel receivers shows significant technical difficulties in achieving gain and phase match of the order of 1 dB and 10° over the HF band.

The conventional amplitude comparison twin channel direction finder or Watson-Watt system uses a CRT with the bearing given by the display ellipse major axis. Figure 1 shows the ellipse orientation equation. When the amplitude and phase difference between the two channels are measured, the major axis is readily computed, for example, using a digital computer without the need for CRT display. More

$$\theta = \frac{1}{2} \tan^{-1} \left\{ \frac{2E_1E_2 \cos \Phi_{12}}{E_1^2 - E_2^2} \right\}$$

$$[\ -90 \leq \theta \leq 90\ ]$$

FIGURE 1

$$R = \frac{E_1}{E_2} \qquad F = \frac{E_{sin}}{E_{cos}}$$

Bearing Computation

$$\theta = \frac{1}{2} \tan^{-1} \left\{ \frac{2\ RF \cos (\phi_{12} - \phi_{cal})}{(RF)^2 - 1} \right\}$$

$$\theta_{OB} = \frac{\theta}{2}, \frac{\theta}{2} + \frac{\pi}{2}, \frac{\theta}{2} + \pi, \frac{\theta}{2} + \frac{3\pi}{2}$$

FIGURE 2

important than this, however, is the capability for compensating for phase and gain mismatch between the channels using simple receiver calibration data. Figure 2 shows a simple formulation where the amplitude and phase mismatch is determined by the injection of equal in-phase signals. The mismatch ratios (R) are applied as compensating factors in the bearing equation. This simple approach offers the capability for tolerating receiver mismatch conditions when they are known. Figure 3 shows a block diagram of a simple verification of this compensation technique using a laboratory DVM and phase meter.

Figure 4 shows a comparison of calibration curves obtained using crossed spaced loop antennas for vertical polarization. The bearing is obtained by amplitude comparison of the sine-cosine related antenna response. The calibration curve at the bottom is the conventional analog calibration curve obtained reading the CRT ellipse. The calibration curve at the top was obtained using the major axis computation measured from the digitized amplitudes and phase difference. The difference between these curves is essentially determined by the residual precision of the two measurements, and amounts to approximately ±1 1/2°. Figure 5 shows an analog calibration curve at the bottom taken with 3 dB receiver gain mismatch and 30° phase mismatch. These mismatch values were deliberately set into the receiver and the resulting calibration curve shows ±8° octantal error as expected. The top calibration curve, however, is obtained after numerical compensation of the receiver channels. The bearing performance is essentially equivalent to that obtained previously with matched channels.

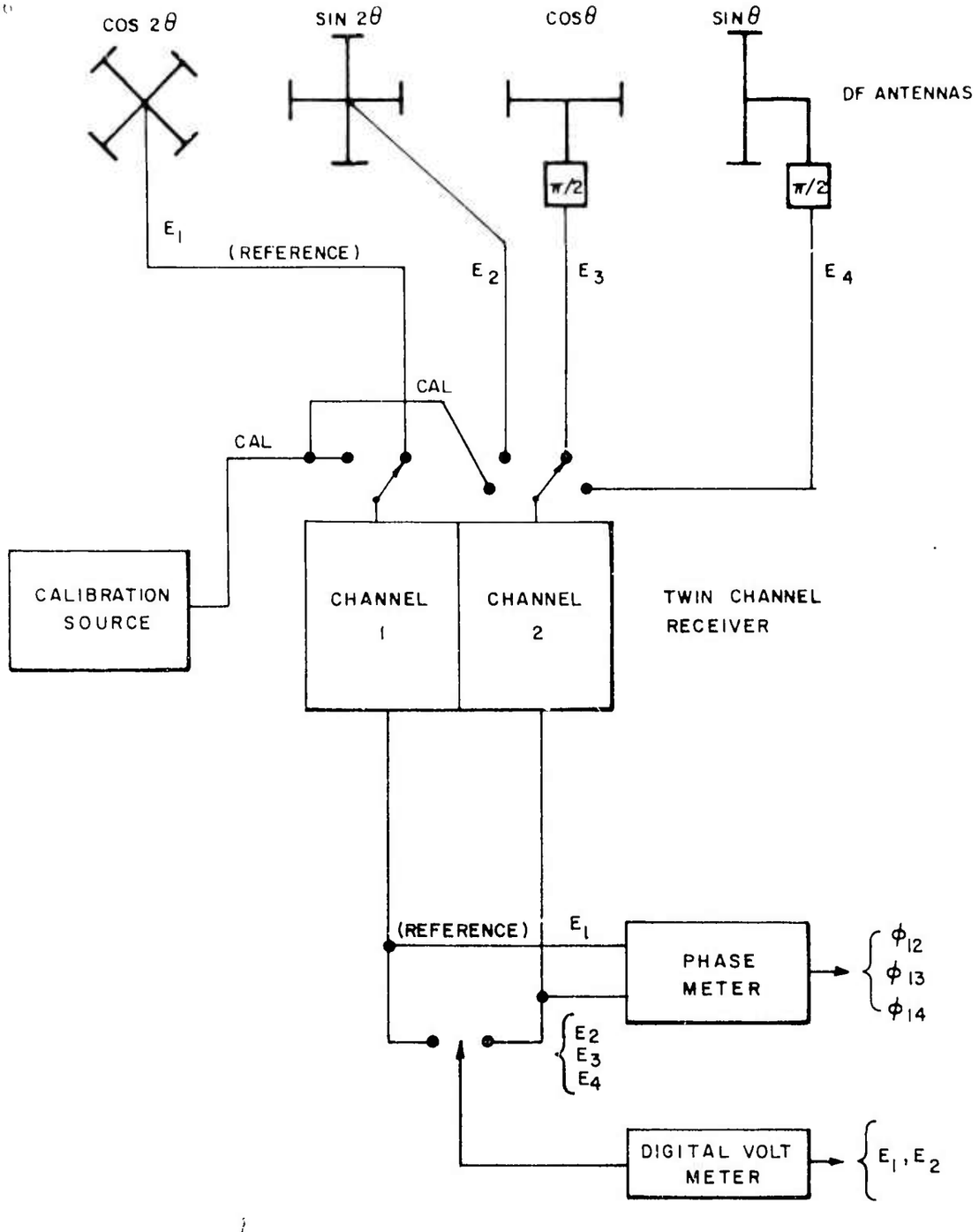
COS 2θ
SIN 2θ
COSθ
SINθ
DF ANTENNAS
π/2
π/2
E1
(REFERENCE)
E2
E3
E4
CAL
CAL
CALIBRATION SOURCE
CHANNEL 1
CHANNEL 2
TWIN CHANNEL RECEIVER
(REFERENCE)
E1
PHASE METER
φ12
φ13
φ14
E2
E3
E4
DIGITAL VOLT METER
E1, E2

FIGURE 3

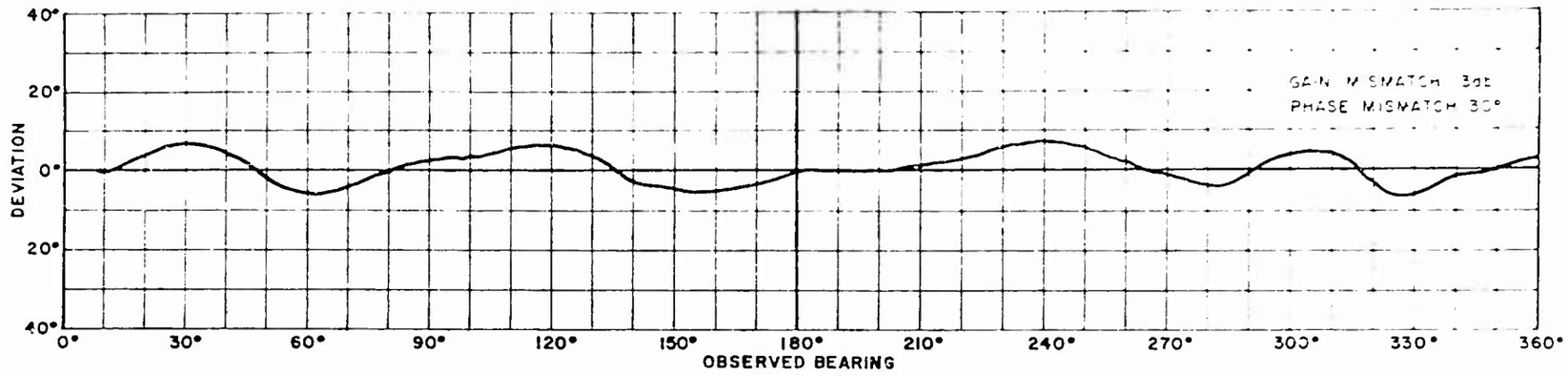

MISMATCH

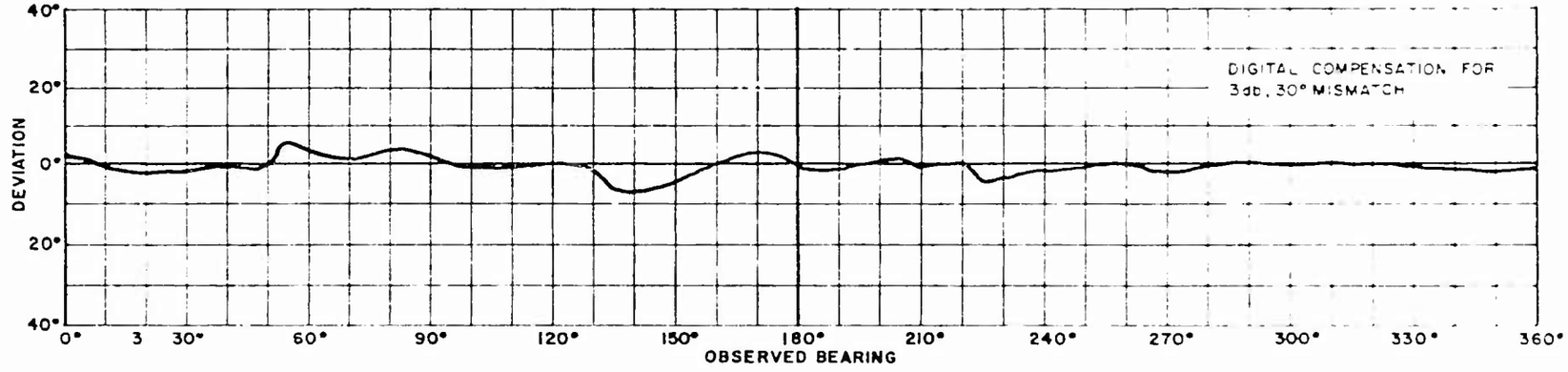

COMPENSATED

FIGURE 4

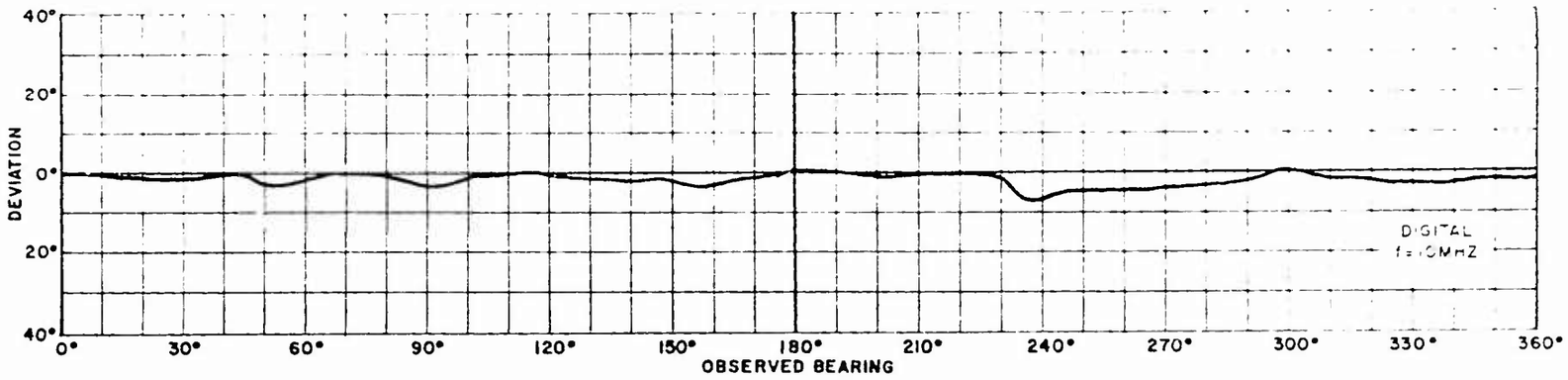

DIGITAL

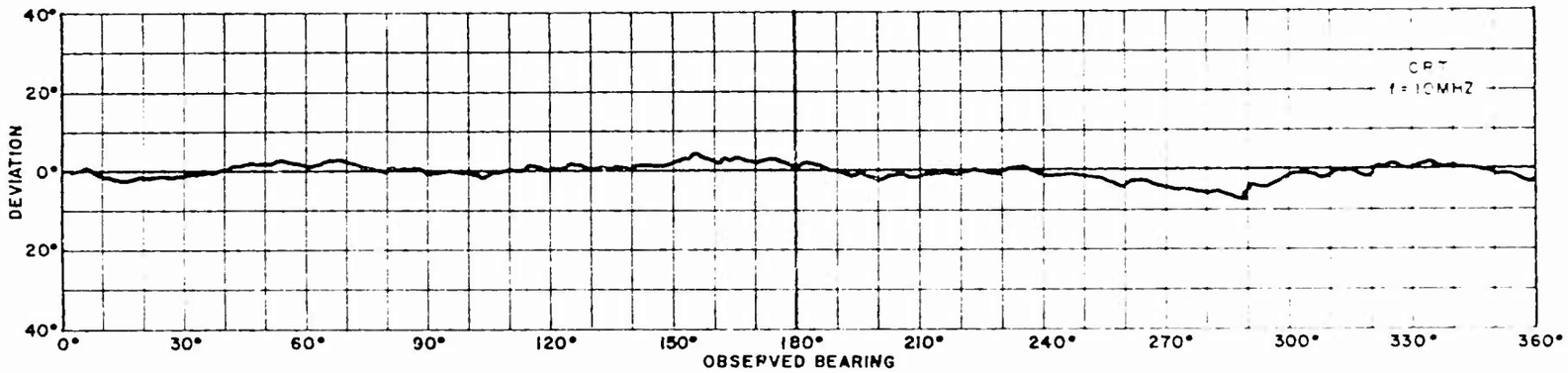

ANALOG

FIGURE 5

The most important implication of this technique is the clear possibility that multiple channel receivers with nominal phase and gain match can be compensated by digital calibration data updated as required in the DF computation. This digital compensation technique should be as tolerant as 6-10 dB mismatch, and may significantly increase the feasibility of multichannel receivers. A multiplicity of applications would immediately arise when they become available.

Figure 6 shows the phase relation between vertically polarized sine-cosine antennas for sense finding. For a system such as the spaced loop, the phase reverses in each octant correspond to the 26 amplitude response. At the bottom of Figure 6, the quadrant and phase data are summarized into a truth table where the (0) implies an in-phase condition and the (1) implies 180° phase. The sense function around the circle thus is given by binary words, each word corresponding to a different octant for the spaced loop or quadrant for the simple loop. Figure 7 shows a block diagram of a four-channel receiver system for determining octant sense by instantaneous phase comparison of the spaced loop and simple loop, DF and sense antennas. It should be emphasized that in sense finding, it is not necessary to make a precise phase measurement but rather to determine whether the DF and sense signals are more nearly in-phase than out-of-phase. The nominal tolerance is ±60°. Figure 8 shows a conceptual implementation of this technique where the sense logic lights the correct octant of the alidade. Figure 9 shows a digital sense block diagram of a circuit built and tested for a three-channel receiver (since the four channels were not available) where fast acting logic gates sense positive going or

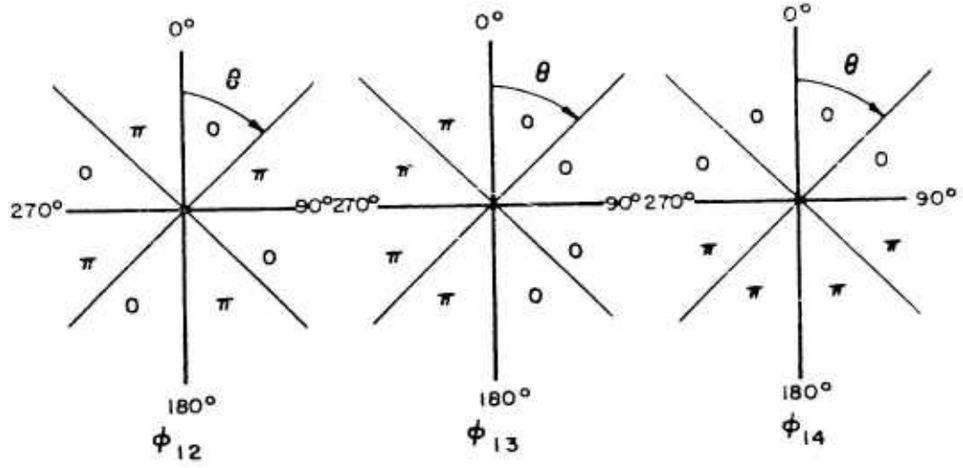

PHASE ANGLE			OCTANT	QUADRANT
ϕ_{12}	ϕ_{13}	ϕ_{14}		
1	1	1	1	1
0	1	1	2	
1	1	0	3	2
0	1	0	4	
1	0	0	5	3
0	0	0	6	
1	0	1	7	4
0	0	1	8	

FIGURE 4

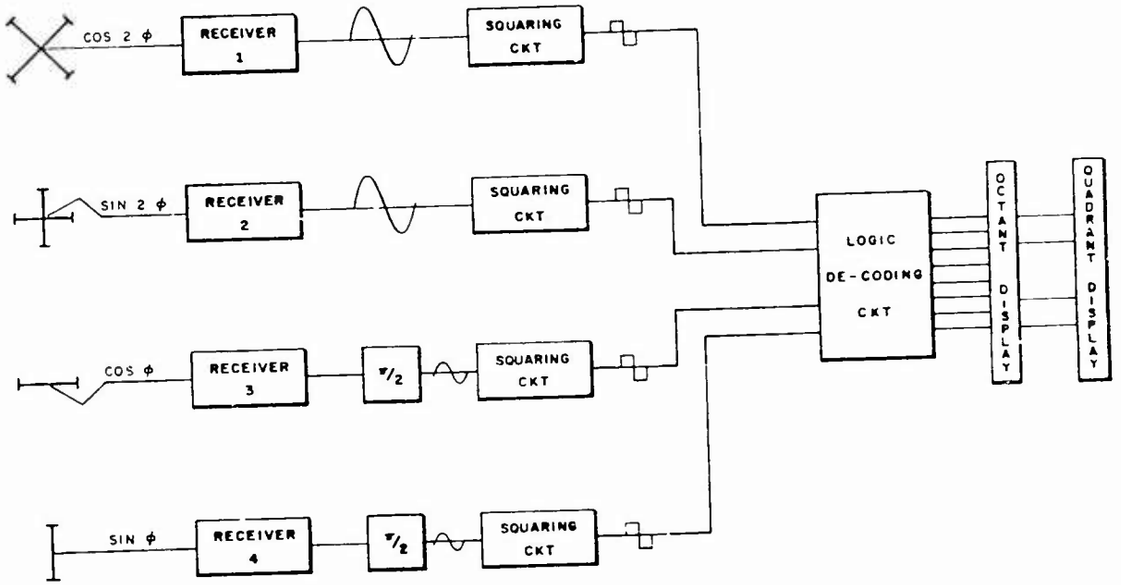
COS 2 ϕ
RECEIVER 1
SQUARING CKT
SIN 2 ϕ
RECEIVER 2
SQUARING CKT
LOGIC DE-CODING CKT
OCTANT DISPLAY
QUADRANT DISPLAY
COS ϕ
RECEIVER 3
π/2
SQUARING CKT
SIN ϕ
RECEIVER 4
π/2
SQUARING CKT

FIGURE 7

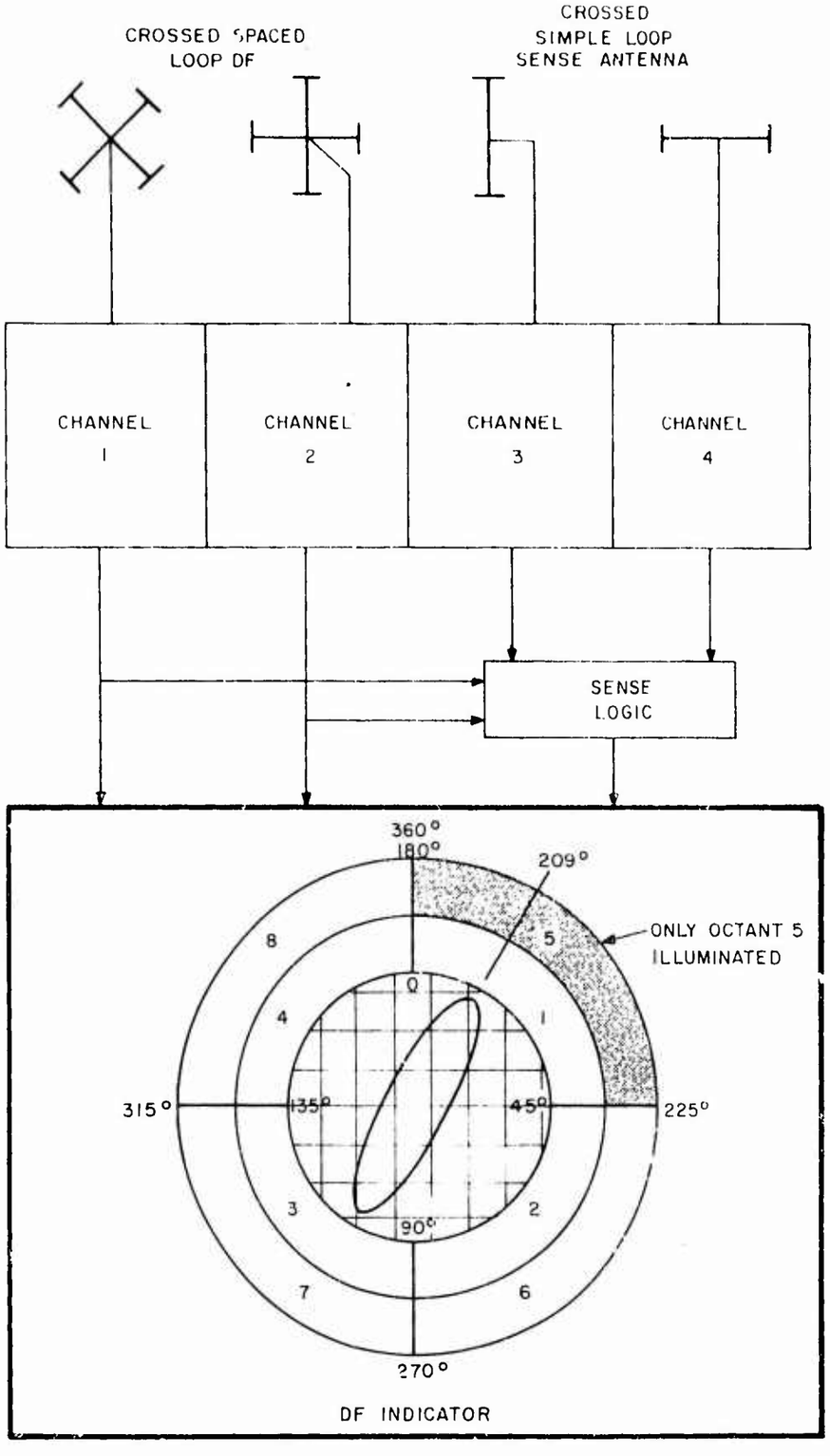
CROSSED SPACED
LOOP DF
CROSSED
SIMPLE LOOP
SENSE ANTENNA
CHANNEL
1
CHANNEL
2
CHANNEL
3
CHANNEL
4
SENSE
LOGIC
360°
180°
209°
ONLY OCTANT 5
ILLUMINATED
8
5
4
0
1
315°
135°
45°
225°
3
2
90°
7
6
270°
DF INDICATOR

FIGURE 8

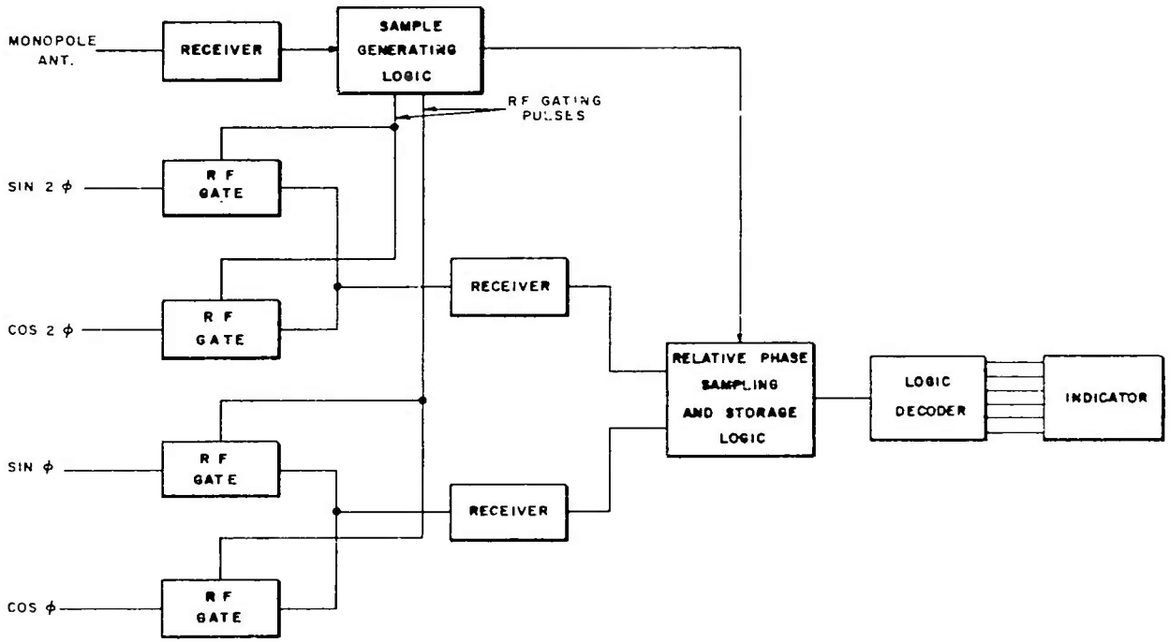
MONOPOLE ANT.
RECEIVER
SAMPLE GENERATING LOGIC
RF GATING PULSES
SIN 2 ϕ
R F GATE
COS 2 ϕ
R F GATE
RECEIVER
SIN ϕ
R F GATE
COS ϕ
R F GATE
RECEIVER
RELATIVE PHASE SAMPLING AND STORAGE LOGIC
LOGIC DECODER
INDICATOR

FIGURE 9

negative going slopes of the IF waveform to determine relative in-phase or out-of-phase conditions across the array. A pair of DF and sense antennas are sampled simultaneously thus requiring two steps to acquire a complete set of phase data. The sampling sequence is controlled by the monopole reference. One complete set of phase data can be obtained in less than 100 microseconds. This digital approach to sense finding eliminates the CRT sense display and permits sense finding simultaneous with the DF calculation.

Another application of digital control circuits is programmed azimuth scan of a DF array. Figure 10 shows an AN/FRD-10 System. Each of three racks in the center are 180 Stage Commutators which perform DF azimuth scan. Figure 11 shows typical DF displays obtained with the AN/FRD-10 DF system connected to a circular array of Beverage antennas. Sum and difference polar patterns are shown as well as the inverted difference. The thing to emphasize is that the azimuth scan is performed by a 180-stage solid state ring commutator which permits simultaneous digital selection of an arbitrary number of antennas at arbitrary locations in the array. The selected array is then sequenced in azimuth around the azimuth circle. Cogging and other pattern deteriorating characteristics are absent in this design. The scan rate is 10 cycles per second chosen equal to the conventional Wullenweber scan rate but is limited only by the receiver bandwidth. Figure 12 shows a photograph of the digital commutator and the azimuth readout strobe. The circular sweep is generated electronically without a mechanically rotating clock. Either the strobe or the DF pattern can be rotated to read out the bearing. Because the Beverage antenna elements are directive, simple summing was provided in the RF switch.

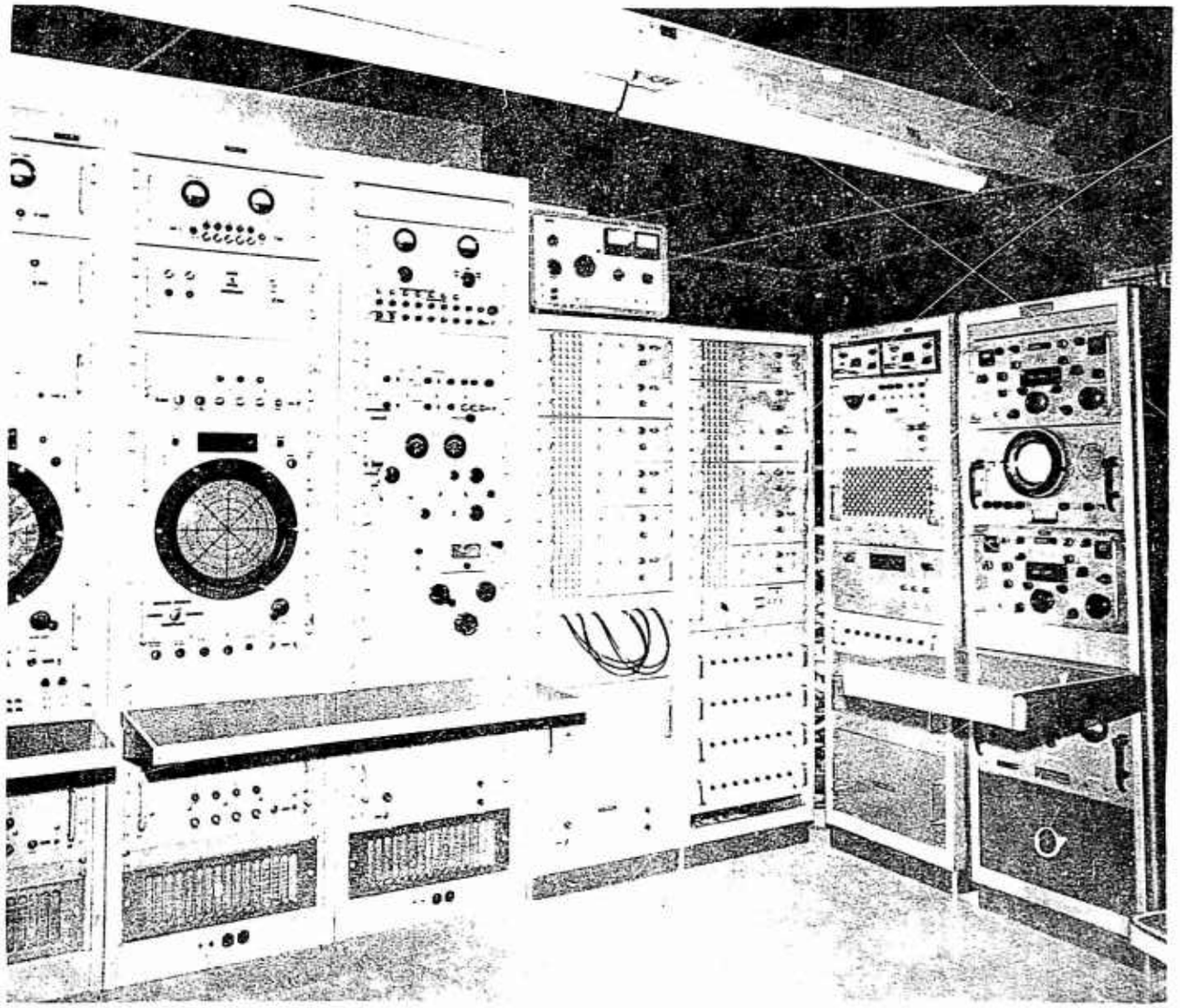

Figure [illegible]

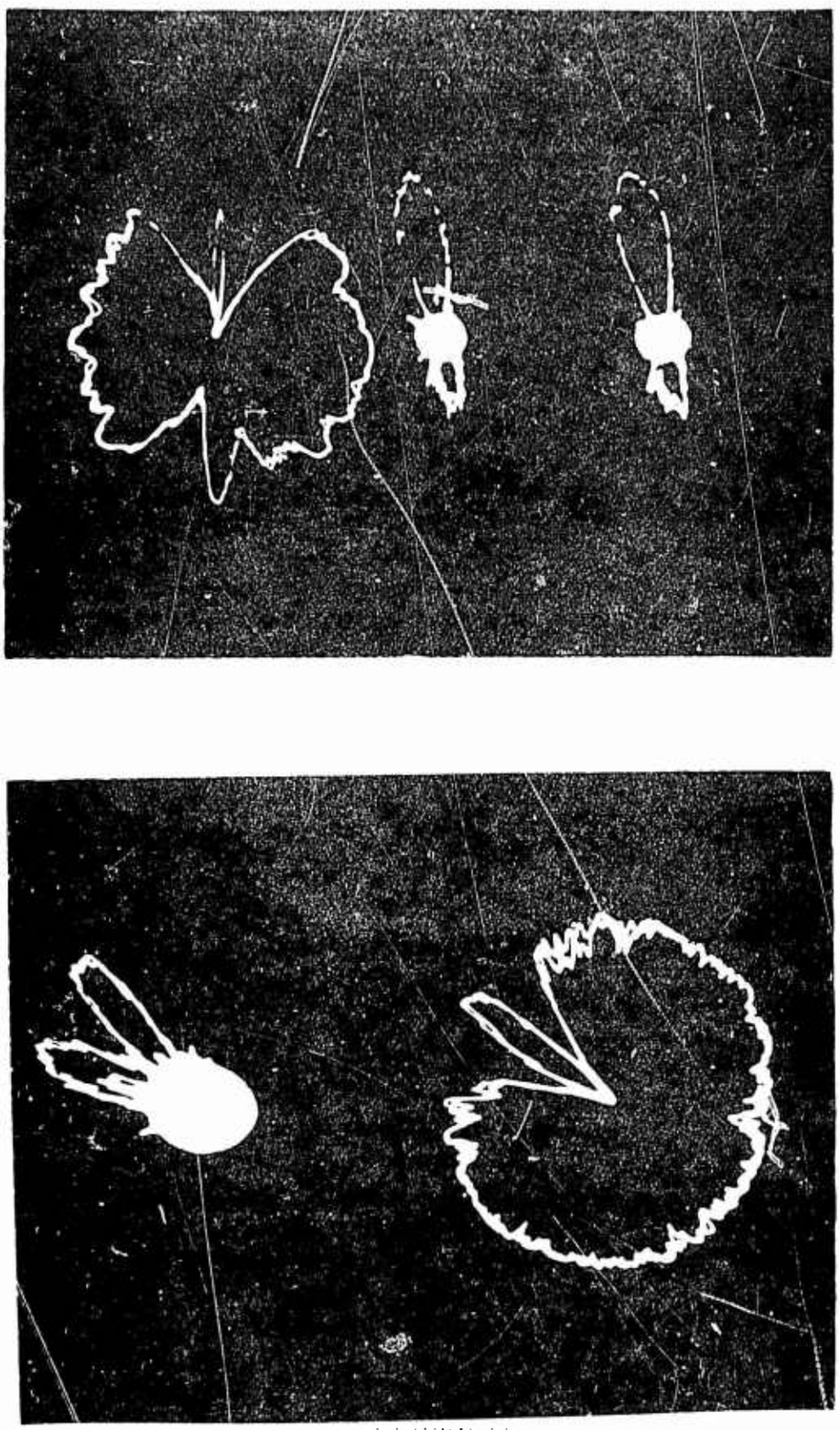

FIGURE 11
TYPICAL BEAM PACE ARRAY DE PATTERNS USING
THE A/C FRD 10 DISPLAY

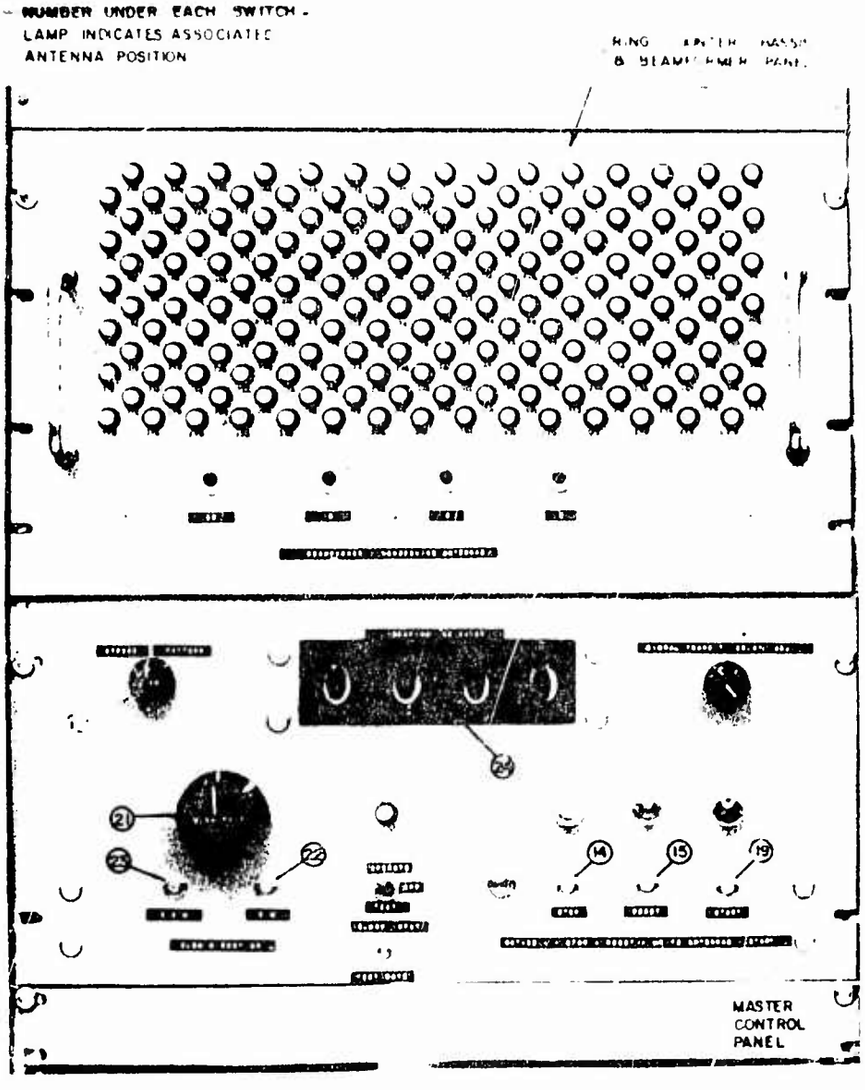
NUMBER UNDER EACH SWITCH -
LAMP INDICATES ASSOCIATED
ANTENNA POSITION
MASTER
CONTROL
PANEL

Figure 12

Figure 13 shows the circuit diagram and on-off ratio of the switch. Each of the 180 antennas is fed to a balanced transistor gate. Each gate provides 8 dB amplification matched to ±1 dB with phase match better than ±5°. The gate is turned on and off by application of a square wave to the switching signal input. The balanced design eliminates DC offset switching transients at the gate output. A 10 dB (S+N)/N ratio is obtained for an input of less than 1 volt RMS.

The use of digital switching permits very generalized computer control of the azimuth scan process for circular or other arrays. These techniques can be applied to the spatial filter type (Wullenweber) array or interference type direction finding arrays such as the interferometer. Figure 14 shows the block diagram of the Army interferometer system in operation in our laboratory emphasizing the use of digital circuits and an on-line, real-time digital computer for bearing calculation. The multiple phase cycle ambiguities in the long baselines are resolved by an appropriate algorithm using phase measurements from the short baselines. The 8K DDP 516 computer provides sufficient core storage for basic on-line direction finding and single site location programs with operator interactive features. In addition, the 98K disc file to be installed shortly with the computer will permit rapid access input and output of other computer programs and storage of up to 75K words of data for subsequent off-line processing.

Data editing is performed by digital logic in two ways. The threshold circuit inhibits the A/D converter except when a set

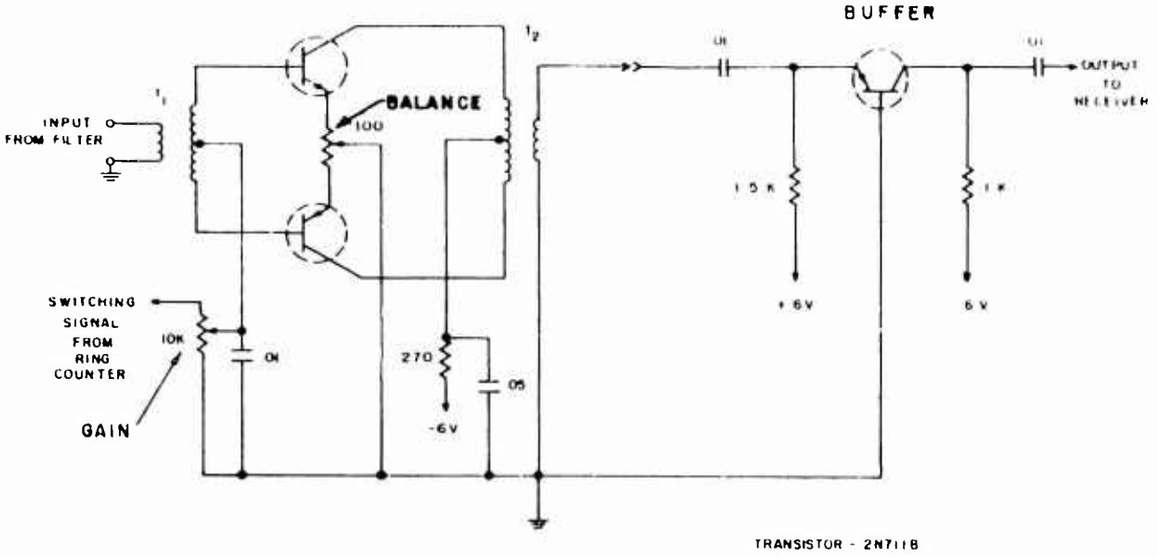

SCHEMATIC DIAGRAM, RF SWITCH

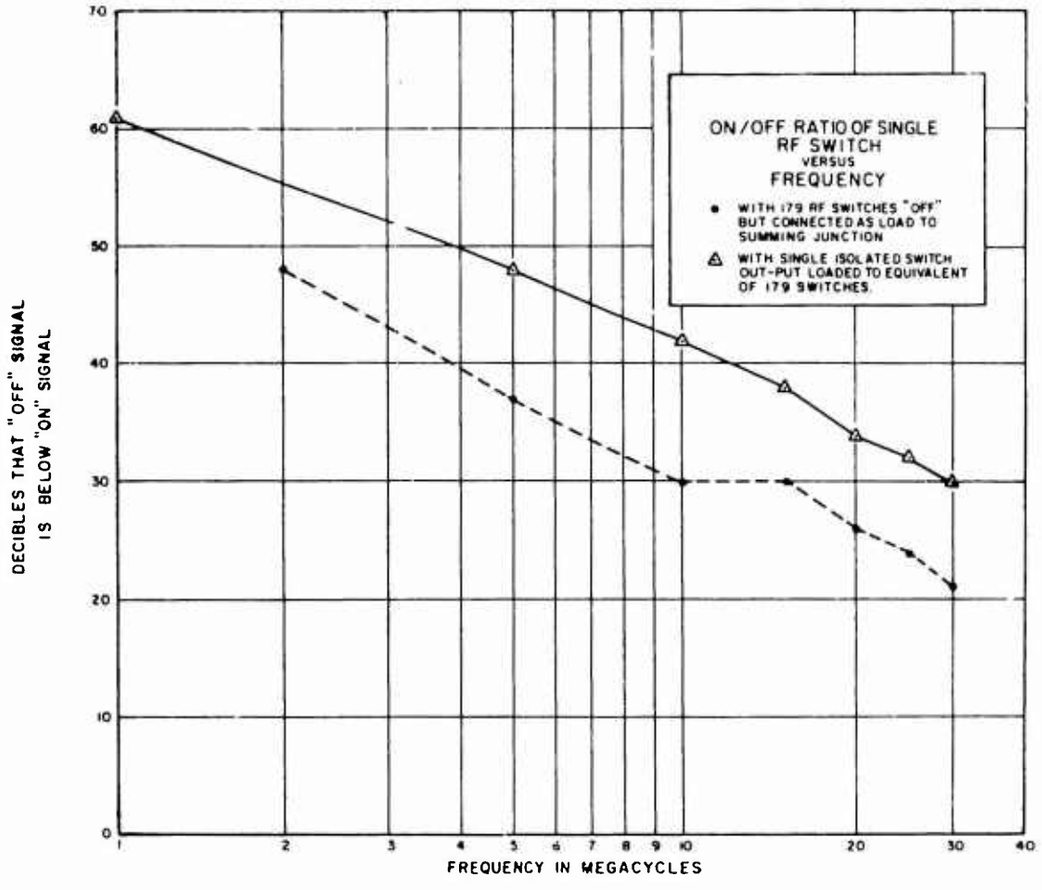

Figure 13

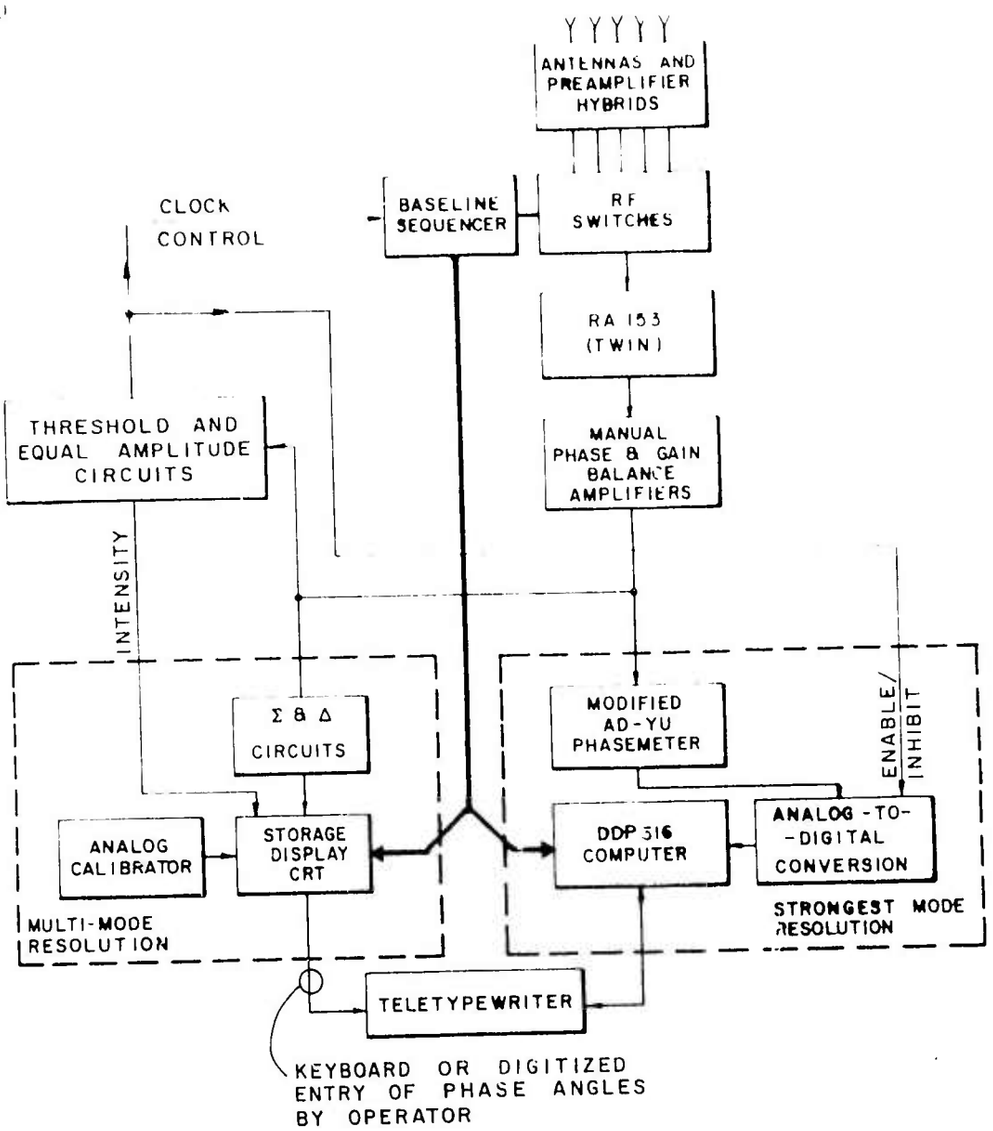

BASELINE EQUATIONS

NS SHORT $\quad \Phi_{ns} = \beta d_s \cos\phi \cos\Psi$

NS LONG $\quad \Phi_{nsl} + N_{ns}\,360^\circ = \beta d_l \cos\phi \cos\Psi$

EW SHORT $\quad \Phi_{ew} = \beta d_s \sin\phi \cos\Psi$

EW LONG $\quad \Phi_{ewl} + N_{ew}\,360^\circ = \beta d_l \sin\phi \cos\Psi$

OBSERVED AZIMUTH

$$\phi = 360^\circ - 180.5^\circ - \tan^{-1}\left[\frac{\Phi_{ewl} + N_{ew}\,360^\circ}{\Phi_{nsl} + N_{ns}\,360^\circ}\right]$$

OBSERVED ELEVATION

$$\cos\Psi = \frac{\sqrt{(\Phi_{ewl} + N_{ew}\,360^\circ)^2 + (\Phi_{nsl} + N_{ns}\,360^\circ)^2}}{\beta d_l}$$

FIGURE 14

threshold is exceeded. In this way, interrupted carrier, SSB, and other such modulations can be handled to eliminate A/D conversion when no signal is present. The plane wave test circuit provides an additional threshold criterion by requiring equal amplitudes within a set tolerance before the A/D converter samples the phase meter At present the tolerance is no more restrictive than 1dB.

Figure 15 shows the comparison of snap bearings obtained with and without data editing. Where signal fading and interrupted carrier occur, this data editing feature is indispensable. As currently designed, the threshold circuit permits the A/D converter to take phase samples (at the rate of 1 per 120 microseconds) for a 32 ms interval on each sequencer state. These phase readings are averaged for the phase angle. If the threshold continues to be satisfied after 32 ms, the sequencer switches to the next state and so on such that eight frames of DF data can be obtained per second. A specified number of azimuth and elevation frames is then averaged for a single answer typed out to the operator.

A similar five-element interferometer is being assembled for the Navy at the simulated ship site at our laboratory. The simulated ship at the center of the site is a full-scale electrical mock-up of a typical destroyer superstructure. Figure 16 shows a plan view of the simulated ship site and the interferometer arrangement for the first siting configuration.

315.0	84.0	15	150
310.7	84.3	15	150
311.2	84.8	15	150
305.7	85.0	15	150
313.4	84.4	15	150
311.3	84.6	15	150
307.2	84.8	15	150

With Plane Wave Editing
Elevation Spread - 1.0°
Azimuth Spread - 9.3°

318.2	83.7	15	150
309.5	84.7	15	150
311.2	83.6	15	150
300.0	84.9	15	150
307.9	84.5	15	150
301.6	84.5	15	150
306.3	84.5	15	150
304.2	85.2	15	150
308.3	84.7	15	150
300.6	84.7	15	150
302.1	84.9	15	150

Without Plane Wave Editing
Elevation Spread - 1.5°
Azimuth Spread - 18.2°

302.6	84.6	15	150
298.5	85.1	15	150
301.9	84.5	15	150
295.8	85.1	15	150
302.0	84.5	15	150
297.3	84.7	15	150
301.3	84.4	15	150
294.3	85.0	15	150
293.9	84.9	15	150
292.1	85.1	15	150:
			Y
			:N

With Plane Wave Editing
Elevation Spread - 0.7°
Azimuth Spread - 10.5°

READY:
READY:SY
SEQUENCE B:
FREQUENCY(MHZ) 8.500:6
RUN NO. 70 22MY69:

FIGURE 15

BANDERA TARGET, FREQUENCY 8.5 MHz, RANGE 55 km

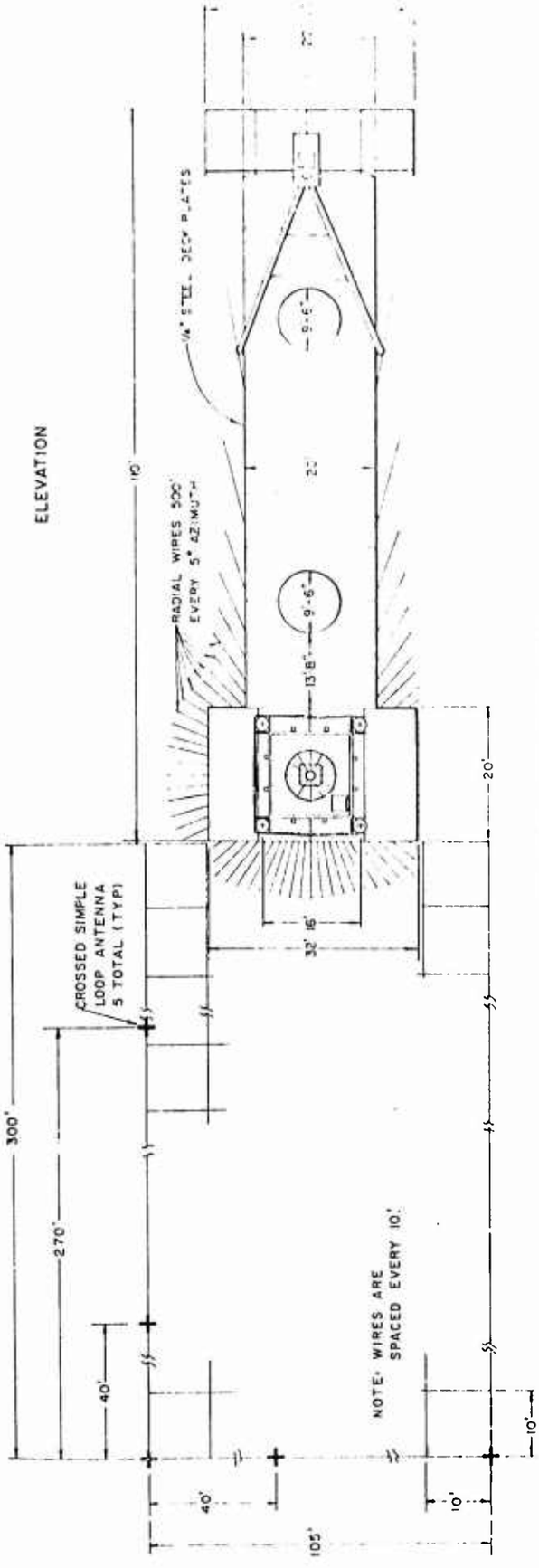

b. ARRAY DIMENSIONS

FIGURE 16

The long baseline spacings are 105 feet and 270 feet, respectively The receiver and phase meter are located in the laboratory area at the site. The interferometer computer is located approximately 3/4 mile northwest of the ship site. The remote DDP 516 computer is used to perform on-line remote processing of the ship site interferometer data. The standard telephone dial system was chosen as the most convenient medium for transmitting information to and from the computer and remote interferometer. In addition, these techniques provide a versatile approach for remote computer control and data processing at other sites.

Figure 17 shows a block diagram of the remote interferometer system. Four phase angles are measured using the antenna located at the apex of the L for reference. The equipment used here employs standard laboratory instruments to minimize set-up time for the system. The IF outputs of the twin receiver are fed to an analog phase meter. A commercial digital voltmeter performs the necessary A/D phase angle conversion with BCD output for three decimal digits. The sequencer assembly provides the sample and hold instructions to the DVM. After encoding the phase angle and state number, a standard shift-register converts the parallel input to serial output and feeds the acoustic telephone coupler. The Data Set at the remote computer converts the received tones to serial digital data for input to the 516 computer.

Interferometer control is provided from a teletype unit at the ship site. The TTY terminal operates at 10 characters per second; therefore, it requires approximately 1.7 seconds to complete a four-phase angle frame measurement. The time averaged azimuth and elevation

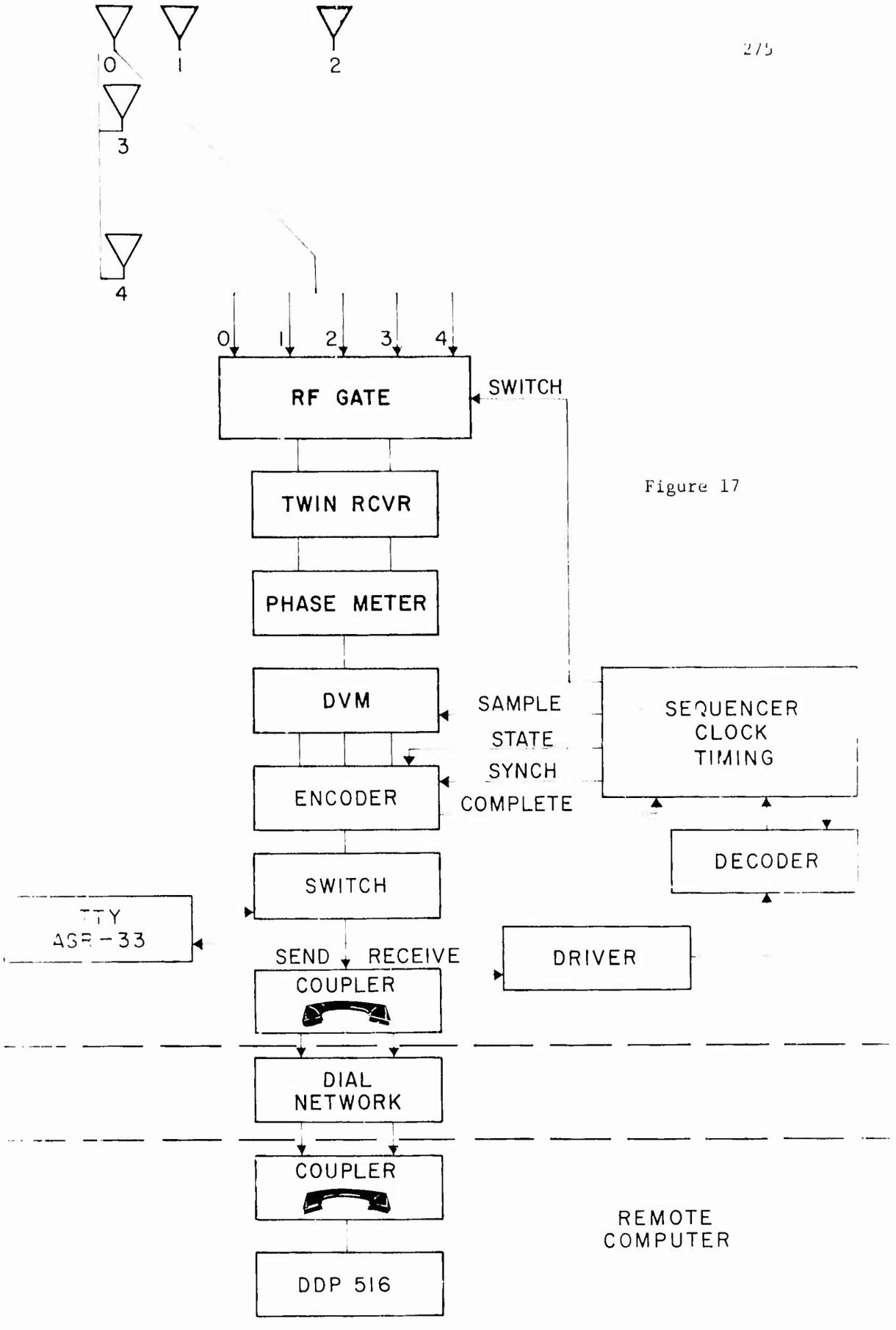
0
1
2
3
4
0
1
2
3
4
RF GATE
SWITCH
TWIN RCVR
PHASE METER
DVM
SAMPLE
STATE
SYNCH
COMPLETE
SEQUENCER
CLOCK
TIMING
ENCODER
DECODER
SWITCH
TTY
ASR-33
SEND
RECEIVE
DRIVER
COUPLER
DIAL
NETWORK
COUPLER
REMOTE
COMPUTER
DDP 516

Figure 17

answers are fed from the computer to the control TTY. This first system is designed for rudimentary skywave performance in the ship environment. The sophistication available in the Army system can be incorporated as desired; however, for the high speed data transfers required, a broadband 2400 bit/sec phone circuit is needed.

We have summarized a number of applications to radiolocation systems for digital computation and logic. Ultimately, time sharing software available with modern system computers makes possible the simultaneous operation of a number of remote DF systems and experiments. DF systems can be remoted not only across the campus but to any compatible computer using radio digital communication links or even the direct dial long distance telephone. Applications requiring this technology are sure to increase in the coming years.

L. J. MILLER

Department of Electrical Engineering
University of Illinois, Urbana, Illinois

ELEVATION ANGLE MEASUREMENTS ON THE UNIVERSITY OF ILLINOIS WULLENWEBER ANTENNA ARRAY

I. INTRODUCTION

In an attempt to measure elevation angles using the Wullenweber Antenna Array at the University of Illinois, two methods have been used. The first method was used by Westlund[1] to obtain elevation angle data while the second method is based upon a system proposed by Bailey.[2]

II. WESTLUND METHOD

The Westlund method of determining the elevation angle, as applied to the Wullenweber Antenna Array, is shown in Figure 1. This method is an application to the Wullenweber system of the Wilkins-Minnis[3] method of elevation angle determination. It consists of two vertically stacked, vertically polarized antennas positioned at heights z_1 and z_2 above the earth. The lower antenna, at height z_2, is one of the folded monopole antennas of the Wullenweber Antenna Array. The second antenna, at height z_1, is a dipole antenna which is supported off one of the poles used to support the reflecting screen. This dipole antenna is mounted directly over the folded monopole antenna.

For this configuration, it can be shown that for the ideal case the corresponding antenna terminal voltages are:

$$E_{zi} = -j4\eta H_i \cos\theta \cos\left(\frac{2\pi z_i}{\lambda} \sin\theta\right) \sin\left(\frac{2\pi y}{\lambda} \cos\theta\right) e^{jwt} \qquad (1)$$

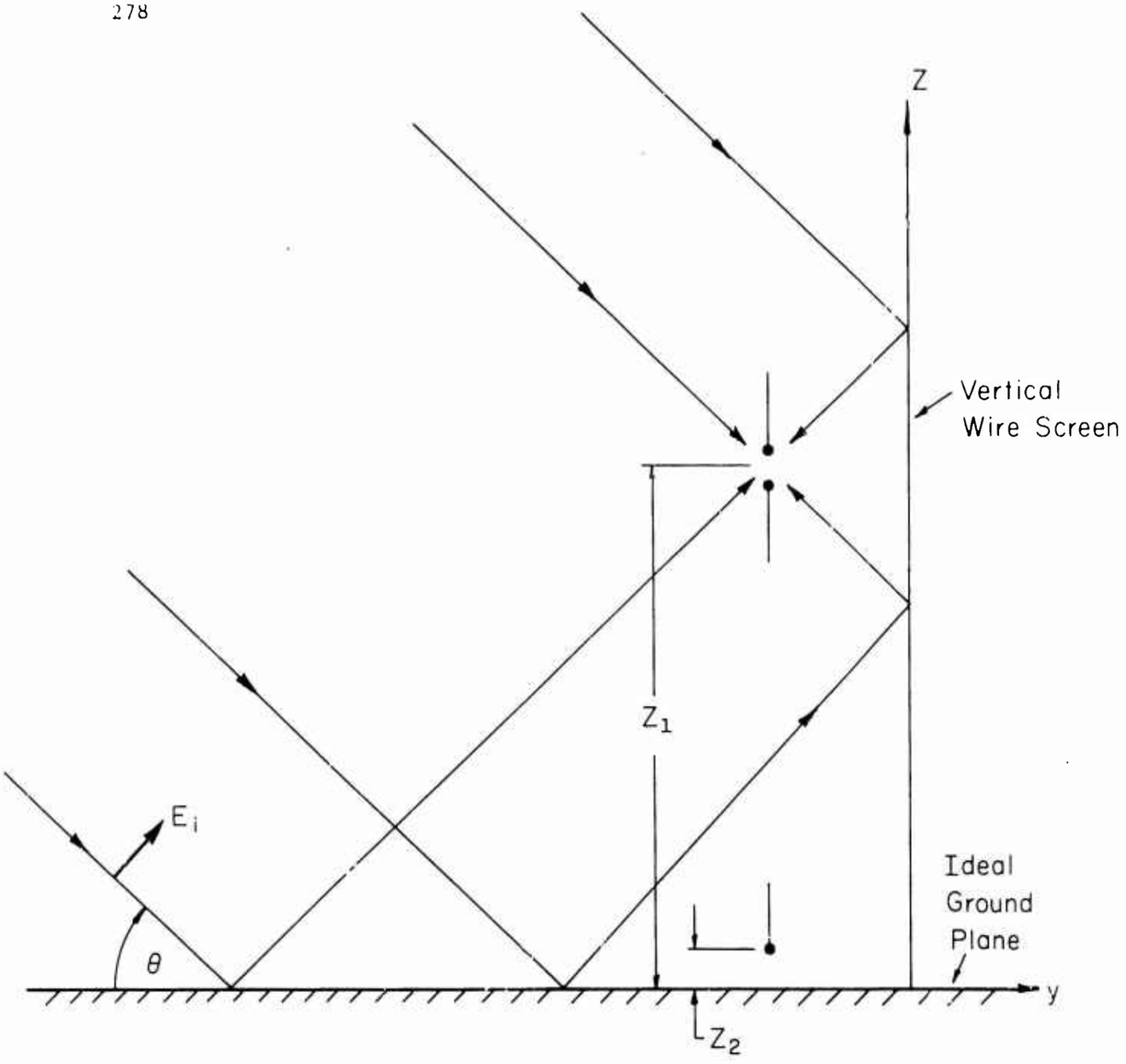

Figure 1.0 Geometry for Elevation Angle Measurements, Amplitude Ratio Method

$$E_{z2} = -j4\eta H_i \cos\theta \cos\left(\frac{2\pi z_2}{\lambda} \sin\theta\right) \sin\left(\frac{2\pi y}{\lambda} \cos\theta\right) e^{jwt} \qquad (2)$$

where H_i = incident magnetic field intensity

η = intrinsic impedance of free space

θ = elevation angle measured from the ground plane

λ = wavelength at the operating frequency

z_1, z_2 = vertical distance above the ground plane of the dipole and monopole, respectively

y = horizontal distance from the vertical-wire reflecting screen.

From these equations, it is seen that the antenna terminal voltages have the same time phase. It is further seen that the amplitude of the voltage at each of these antenna terminals is a function of the elevation angle of arrival, the frequency of operation, and the respective height of these antennas above ground. Since for any given elevation angle measurement, the frequency of operation and the height of each of these antennas above ground are known, then the amplitude of each of these antenna terminal voltages is dependent upon the elevation angle of arrival θ. Therefore, to determine the elevation angle of arrival by this method, some means of extracting this information from the two signal amplitudes is required.

One method of extracting this information is to apply the output of each antenna terminal to one channel of a matched twin-channel receiver. At the IF output of the receiver, prior to detection, these signals are then applied to a conventional X-Y display oscilloscope. This will give a line or ellipse on the display at an angle γ such that:

$$\gamma = \tan^{-1}\frac{E_{z1}}{E_{z2}} = \tan^{-1}\left[\frac{\cos(\frac{2\pi z_1}{\lambda}\sin\theta)}{\cos(\frac{2\pi z_2}{\lambda}\sin\theta)}\right] \quad . \qquad (3)$$

By measuring the angle γ from the display scope, the elevation angle θ may be determined. This is the method used by Westlund to obtain elevation angle data.

Displaying and determining elevation angle information in this manner is acceptable if rather infrequent or manual-type measurements are to be employed to record this information. However, if an automated data recording system is to be employed, such as the High-Speed Data System[4] (HSDS) which is normally used to record data obtained by use of the University of Illinois Wullenweber Antenna Array, then some other method of extracting this information from the signal amplitudes is required. To record these data using the HSDS, one approach is to detect the antenna voltages E_{z1} and E_{z2} at the output of the twin-channel receiver. These voltage amplitudes are then recorded by the HSDS and the elevation angle θ is determined by programming the G-20 computer to solve the equation:

$$\frac{E_{z1}}{E_{z2}} = \frac{\cos(\frac{2\pi z_1}{\lambda}\sin\theta)}{\cos(\frac{2\pi z_2}{\lambda}\sin\theta)} \quad . \qquad (4)$$

At the present time, work is in progress to reinstrument this method of elevation angle measurement. The data obtained will be recorded by the HSDS and processed by the G-20 to determine the elevation angle θ.

This method of determining elevation angle when used in conjunction with the U of I Wullenweber Array, or any other Wullenweber type

of antenna array, has two disadvantages. The first disadvantage is that in using this method it is not possible to obtain the required information by use of just those antennas which already make up the antenna array. Additional dipoles or other types of antenna elements are required. The second disadvantage is that for measuring elevation angles at different azimuths, these additional antenna elements must be located on the array at those azimuths of interest.

III. BAILEY METHOD

The Bailey method of determining elevation angle is directly applicable to the Wullenweber Antenna Array and is based upon the technique of measuring the differential phase between two horizontally displaced antenna elements. Theoretical studies of this method by Jones, Schlicht, and Ernst[5] introduced the concept of "Phantom Antennas" and this system is shown in Figure 2. This is the system which is presently being used to measure elevation angles on the University of Illinois Wullenweber Antenna Array.

Measurement of elevation angle by the Phantom Antenna concept is based upon the measurement of the differential phase between a Front Phantom and one or more Rear Phantoms. The Front Phantom is formed by selecting two adjacent antennas on the array such that the direction of arrival of the desired incoming signal passes between these two antennas. The output from each of these antennas is combined by an RF combiner to create the Front Phantom. By the phasor addition of voltages from other symmetrically disposed pairs of antennas, the Rear Phantoms are formed and they are located directly behind the Front Phantom. For elevation angle measurements so far conducted on the

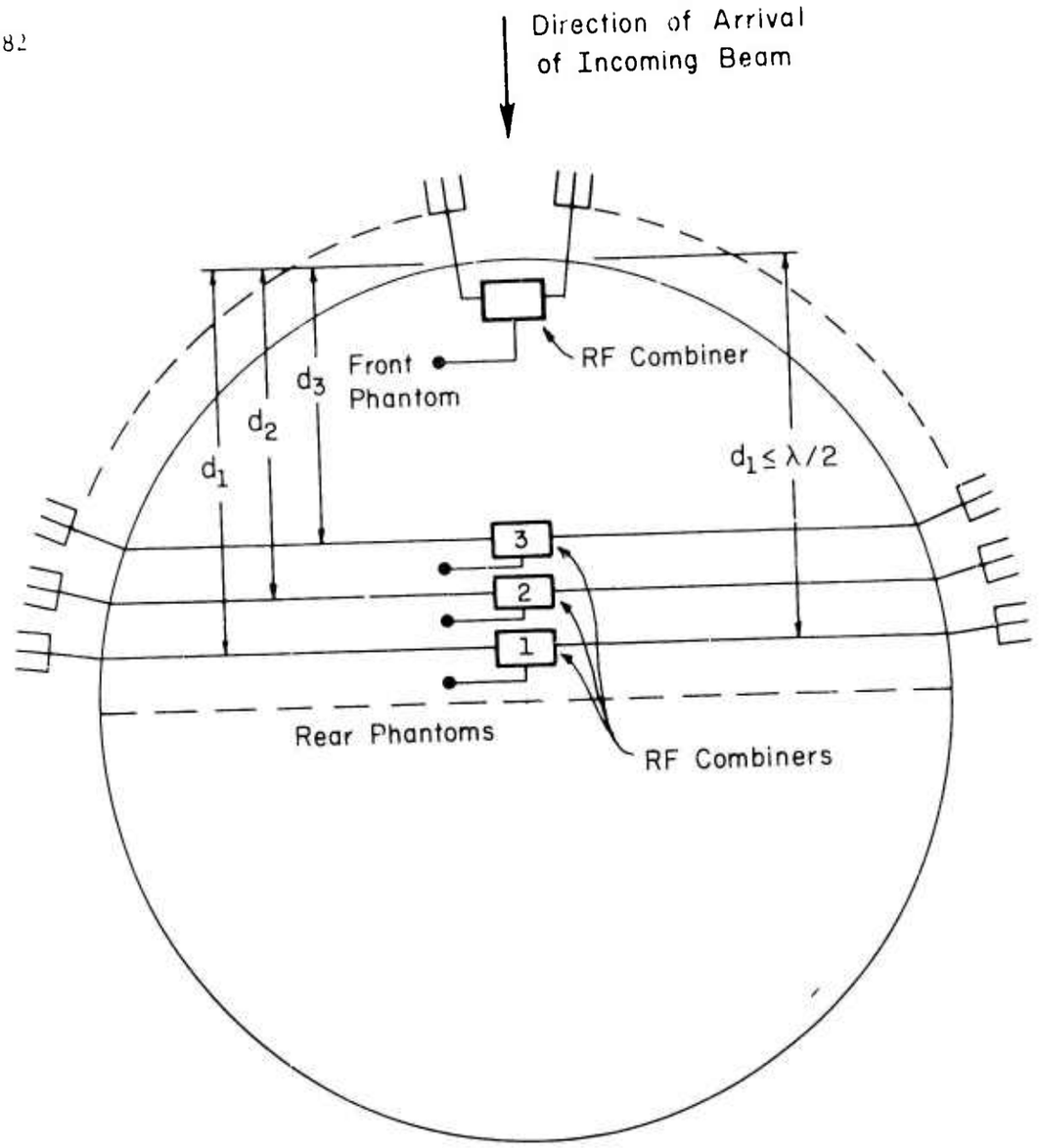

Figure 2.0 Geometry for Elevation Angle Measurements, Differential Phase Method

University of Illinois Wullenweber, at least two Rear Phantoms have been in use and sometimes three. To avoid ambiguity problems, the horizontal spacing between the Front and Rear Phantoms, d, is restricted to a distance of one-half wavelength or less for any given operating frequency.

For this configuration, the elevation angle, θ, can be determined by solving the equation:

$$\psi = \frac{2\pi d}{\lambda} \cos \theta \cos \alpha \qquad (5)$$

where d = horizontal spacing between respective Front and Rear Phantoms

λ = wavelength at the operating frequency

α = difference between the angle of arrival of signal and the azimuthal alignment of Phantom Antennas

ψ = differential phase angle measured between Phantom Antennas

θ = elevation angle measured from the ground plane

To determine the elevation angle θ, the differential phase between the Front and Rear Phantoms, ψ, is measured by a phasemeter. The output from the phasemeter, an analog voltage which is proportional to this phase difference, is recorded by the HSDS. By means of a G-20 computer program, the value of ψ for use in equation (5) is calculated, d and λ are already known for any given operating frequency, and the elevation angle θ can be determined. For the studies so far conducted[6], the value of α in the above equation has been zero or nearly zero degrees; therefore, this quantity has not been used in any of the elevation angle calculations which so far have been made.

IV. CONCLUSIONS

By means of these two methods which involve measurement techniques which are completely independent of each other, it is hoped that some

measure of elevation angle may be obtained. It is further hoped that these two methods of measurement will yield elevation angle values which are somewhat correlated. This has not necessarily been true for elevation angles obtained by use of different Phantom Antenna pairs and some adjustment of this method appears necessary.

Based upon the data so far obtained, it would appear that for elevation angles above 15 degrees, either or both of these methods will give some indication of elevation angle. However, for elevation angles from 15 degrees down to zero degrees, both methods of measurement become increasingly insensitive and the results of measurements in this range are suspect.

References

1. Westlund, C. D., "A Study of Radio Waves Scattered from Field-Aligned and Other Ionospheric Irregularities," Radiolocation Research Laboratory, Department of Electrical Engineering, University of Illinois, Urbana, Illinois, RRL Publication No. 185, Contract No. Nobsr 64723, June, 1961.

2. Bailey, A. D., "Some Notes on the Determination of the Vertical Angle of Arrival of HF Radio Waves and Implications in Circularly Disposed Arrays," Radiolocation Research Laboratory, Department of Electrical Engineering, University of Illinois, Urbana, Illinois, Technical Memorandum, RRL Publication No. 263, Contracts No. Nobsr 89229 and Nonr 1834(02), October, 1964.

3. Wilkins, A. F., and C. M. Minnis, "Angle of Arrival of H.F. Waves," Wireless Engineer, February, 1956.

4. McClurg, W. C., "A High-Speed Data System," Radiolocation Research Laboratory, Department of Electrical Engineering, University of Illinois, Urbana, Illinois, Technical Report No. 4, RRL Publication No. 339, Contract No. N00014-67-A-0305-0002, March, 1968.

5. Jones, E. C., H. C. Schlicht, and E. W. Ernst, "A Simulation Study of Elevation Angle of Arrival Measurements in the Wullenweber RDF System," Radiolocation Research Laboratory, Department of Electrical Engineering, University of Illinois, Urbana, Illinois, Technical Note No. 3, RRL Publication No. 306, Contract No. N00014-66-C0010A02, April, 1966.

6. Bailey, A. D., E. W. Ernst, L. J. Miller, and W. W. Wood, "An Atlas of Reduced Data Obtained in a Cooperative HF Directional Propagation Experiment Over a 1330 Kilometer Path," Radiolocation Research Laboratory, Department of Electrical Engineering, University of Illinois, Urbana, Illinois, Technical Report No. 7, RRL Publication No. 344, Contract No. N00014-67-A-0305-0002, September, 1968.

W. W. Wood

Department of Electrical Engineering
University of Illinois, Urbana, Illinois

OBLIQUE INCIDENCE IONOSONDE AMPLITUDE DATA

Engineering changes to the University of Illinois ionosonde equipment include the addition of the "A" scan data and automatic gain control (AGC).

The "A" scan data are recorded directly on the ionogram at the frequency of interest; the "A" scan is deflected at a 45° angle. The single line scope trace is then shifted to form a "gap"; the "gap" does not represent missing frequencies. The length of the line of the "A" scan trace is an indication of the relative signal strength from each mode of transmission. The 45° deflection (as shown in Figures 1 and 2) increases the resolution of the "A" scan trace length.

The ionosonde AGC adjusts for the difference in day-night signal-to-noise ratio. The AGC samples the background noise level and adjusts the gain to a preset optimum noise level. A complete report on the AGC system will be available in the near future.[1] Figures 3 and 4 are examples of ionograms obtained without (Fig. 3) and with (Fig. 4) AGC.

---

[1] "An AGC System for a Step Frequency Ionosonde Receiver," R. Baumgartner, E. W. Ernst, F. O. Fahlsing, W. W. Wood, RRL Publication No. 356, Technical Note No. 10, Radiolocation Research Laboratory, Dept. of Electrical Engineering, University of Illinois, Urbana, Illinois.

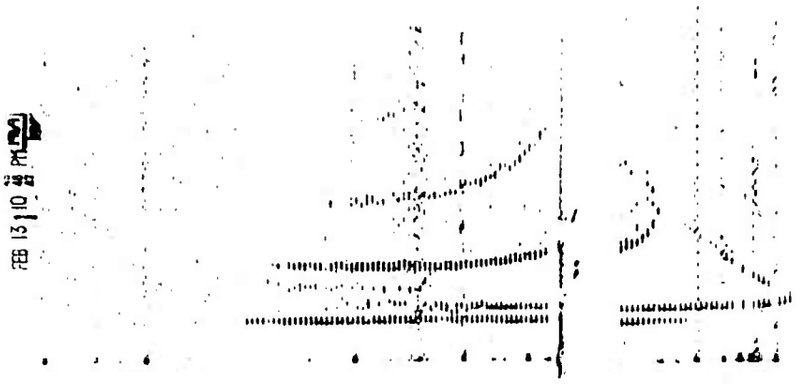

Figure 1.

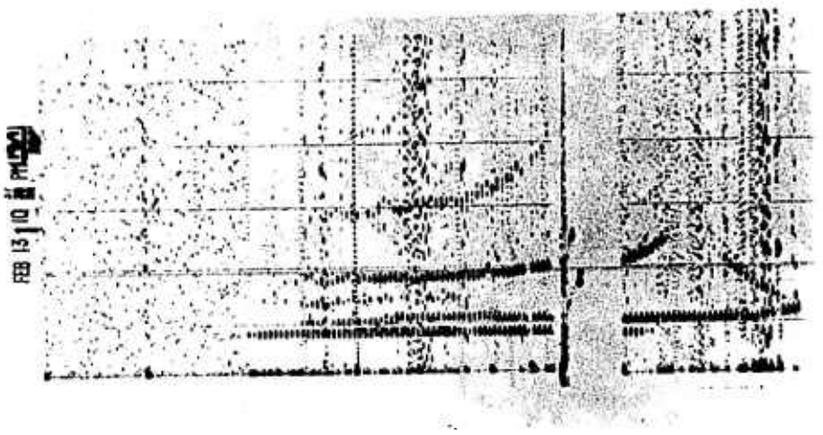

Figure 2.

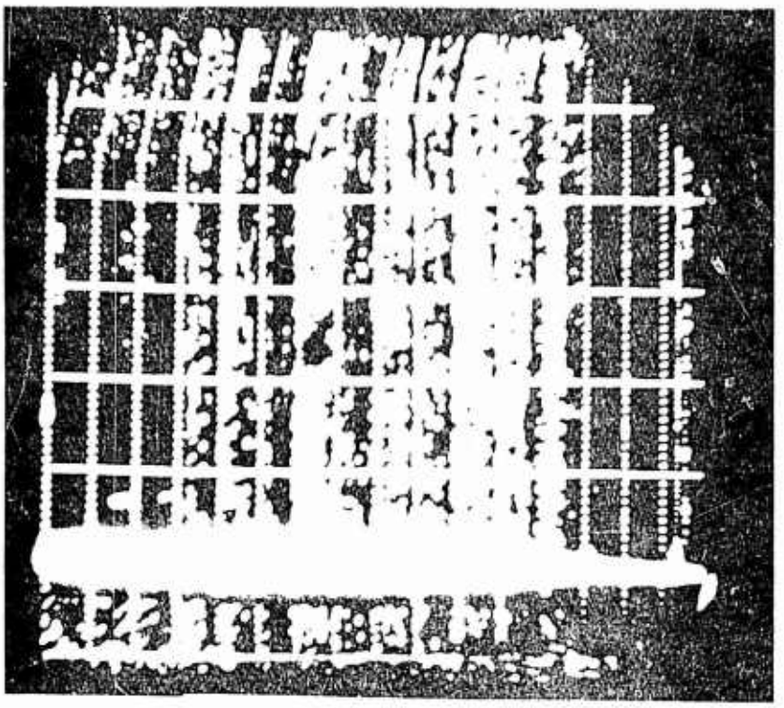

Figure 3.

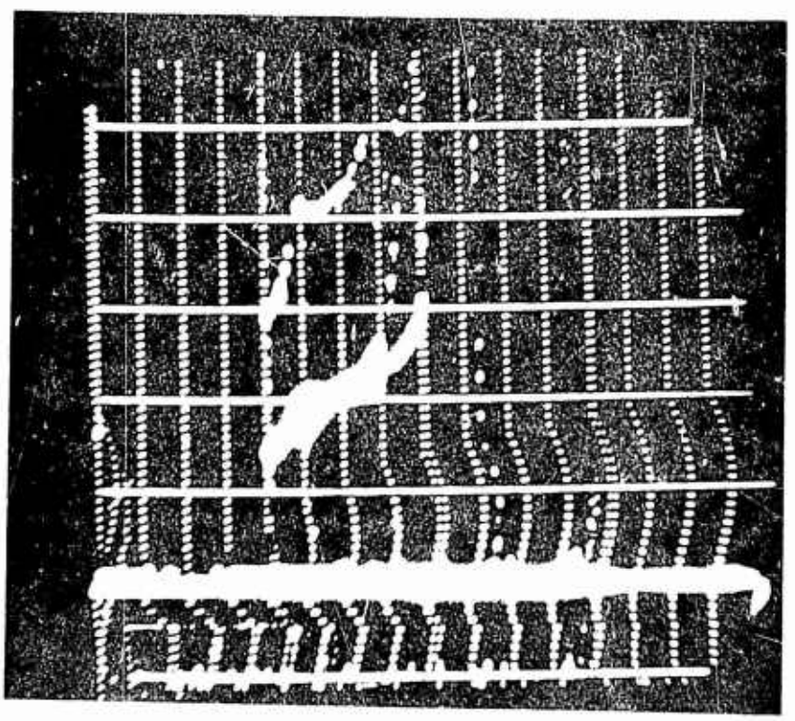

Figure 4.

GERALD A. SMITH

Department of Electrical Engineering
University of Illinois, Urbana, Illinois

WAVEFRONT TESTING AND ITS APPLICATIONS

The triple interferometer has been used for several years in radiolocation work. Its ability to resolve angle of arrival in elevation and azimuth is a great asset. However, due to the nature of the interferometer, it looks in all directions. This "open window" allows signals from all directions. One problem this brings is the inability to shut out unwanted signals. These unwanted signals can be placed in two categories. The first occurs when two transmitters are at the same frequency and at different locations. This does not pose too much of a problem because it is not likely the transmitters will be close enough in frequency (i.e. within one-half cycle per second) to prevent accurate determination of direction of arrival.

The unwanted signal that poses the greatest problem is the multipath propagated signal. This signal, transmitted from one source, travels via two paths to the receiver. This then appears as two signals, at slightly different frequencies at the receiver. The difference may be the order of one cycle per minute to one cycle per second The closer the two frequencies, the more difficult it is to resolve the incidence and azimuth of either.

The multipath propagation, referred to as modes, modifies the interferometer output in such a way as to render the angle of arrival measurements useless unless means for resolving the modes are used.

Assuming two modes are present, it has been proposed that one might find the correct angles of arrival if there were a way of knowing

at what instant in time the second path (or the first) were not present. It is known that for a single mode wave, the magnitude of the signal present at each antenna is equal. This suggests that each antenna should be checked and if the magnitude of the signals is indeed equal, (implying a single mode signal) then a measurement should be made.

One method of accomplishing this is to determine the magnitude of the signal at each antenna, compare these signals (three in the case of the triple interferometer) and if they are equal, display the outputs so that the answer might be computed.

A preliminary investigation at the University of Illinois has shown that logical circuits will perform the necessary functions required.

Some problems have been encountered; however, these are unique for our particular installation. First, we use a time-shared, twin-channel receiver to sample the phase difference and amplitude of three pairs of antennas. This would require a memory device to store the magnitude information and, after the complete cycle, make the magnitude comparison. This results in information from the previous cycle controlling the display for the present cycle. With a triple-channel receiver, the memory would be unnecessary.

Second, the storage oscilloscope that we use for the display requires AC unblanking; therefore, an additional circuit must be added to furnish the unblanking signal.

Wavefront testing, in our case, has been limited to testing the antenna pair being sampled and, if the magnitudes are equal, displaying the data. This method displays the results of only one antenna pair or two pairs, or all three. Should either of the first two occurrences

occur quickly, one would be led to believe that a valid solution was present when it was not. It has also been noted, in our case, that when the two modes are in-phase or 180 degrees out-of-phase, the magnitudes of antenna pairs can be equal, which leads again to a false belief that a valid solution is present. As a result, four solutions for the two mode cases are possible.

At present we have been able to record equal magnitude signals only when the two signals are in-phase or 180 degrees out-of-phase. This is not to say that the waves are never "single mode" during interference; it has been noted to happen but not recorded. It means that at the times pictures were taken, the double mode propagation did not disappear.

Only a limited amount of wavefront testing has been performed, and this on a highly restricted basis which prohibits any firm conclusions from being reached. Wavefront testing shows some promise and also some pitfalls. It may be necessary to wait 2 minutes for 5 seconds of display, for there is no assurance that one of the two modes will disappear completely or rapidly. Also, three or more modes may be present. One must then wait for all but one to disappear.

There is some thought that the "false solutions," when interference is in-phase or 180 degrees out-of-phase, will be removed when the decision to display data is based on all three antenna magnitudes rather than two. We do know that errors caused by displaying solutions when one or two pairs are displayed will be eliminated.

There may be value in the fact that the amplitudes are equal when we have interference at the in-phase and out-of-phase conditions

because this gives the major diagonals of the polygon described by the two modes. This information could cause the data acquisition system to record these diagonals and then the computer could reconstruct the polygon to extract useful information.

Unclassified

Security Classification

DOCUMENT CONTROL DATA - R&D

Security classification of title, body of abstract and indexing annotation must be entered when the overall report is classified

1 ORIGINATING ACTIVITY (Corporate author)

Department of Electrical Engineering
University of Illinois
Urbana, Illinois

2a. REPORT SECURITY CLASSIFICATION

2b. GROUP

3 REPORT TITLE

PROCEEDINGS OF A CONFERENCE ON HF RADIO PROPAGATION

4 DESCRIPTIVE NOTES (Type of report and inclusive dates)

Technical Report No. 16

5 AUTHOR(S) (Last name, first name, initial)

Edward W. Ernst, Editor

6 REPORT DATE	7a. TOTAL NO OF PAGES	7b. NO OF REFS
August 1970	300	

8a. CONTRACT OR GRANT NO	9a. ORIGINATOR'S REPORT NUMBER(S)
N00014-67-A-0305-0002	RRL Publication No. 375
b. PROJECT AND TASK NO.	
c.	9b. OTHER REPORT NO(S) (Any other numbers that may be assigned this report)
d.	UILU-ENG-70-311

10 AVAILABILITY LIMITATION NOTICES

EACH TRANSMITTAL OF THIS DOCUMENT OUTSIDE OF THE DEPARTMENT OF DEFENSE MUST HAVE PRIOR APPROVAL OF THE OFFICE OF NAVAL RESEARCH (CODE 427), WASHINGTON, D. C. 20360

11 SUPPLEMENTARY NOTES	12 SPONSORING MILITARY ACTIVITY
	Office of Naval Research Washington, D. C.

13 ABSTRACT

Of the 22 presentations made at the Conference, papers representing 16 of these are included in these Proceedings. These include papers on direction of arrival studies over medium range and long range paths, propagation studies using direction of arrival data, studies of RDF systems, RDF instrumentation, and digital methods for RDF.

DD FORM 1 JAN 64 1473

Unclassified

Security Classification

14 KEY WORDS	LINK A ROLE	LINK A WT	LINK B ROLE	LINK B WT	LINK C ROLE	LINK C WT
HF Radio Propagation						
Radio Direction Finding						
Interferometer RDF						
HF Direction Finding						
Digital Methods for DF						

INSTRUCTIONS

1. ORIGINATING ACTIVITY: Enter the name and address of the contractor, subcontractor, grantee, Department of Defense activity or other organization *(corporate author)* issuing the report.

2a. REPORT SECURITY CLASSIFICATION: Enter the overall security classification of the report. Indicate whether "Restricted Data" is included. Marking is to be in accordance with appropriate security regulations.

2b. GROUP: Automatic downgrading is specified in DoD Directive 5200.10 and Armed Forces Industrial Manual. Enter the group number. Also, when applicable, show that optional markings have been used for Group 3 and Group 4 as authorized.

3. REPORT TITLE: Enter the complete report title in all capital letters. Titles in all cases should be unclassified. If a meaningful title cannot be selected without classification, show title classification in all capitals in parenthesis immediately following the title.

4. DESCRIPTIVE NOTES: If appropriate, enter the type of report, e.g., interim, progress, summary, annual, or final. Give the inclusive dates when a specific reporting period is covered.

5. AUTHOR(S): Enter the name(s) of author(s) as shown on or in the report. Enter last name, first name, middle initial. If military, show rank and branch of service. The name of the principal author is an absolute minimum requirement.

6. REPORT DATE: Enter the date of the report as day, month, year, or month, year. If more than one date appears on the report, use date of publication.

7a. TOTAL NUMBER OF PAGES: The total page count should follow normal pagination procedures, i.e., enter the number of pages containing information.

7b. NUMBER OF REFERENCES: Enter the total number of references cited in the report.

8a. CONTRACT OR GRANT NUMBER: If appropriate, enter the applicable number of the contract or grant under which the report was written.

8b, 8c, & 8d. PROJECT NUMBER: Enter the appropriate military department identification, such as project number, subproject number, system numbers, task number, etc.

9a. ORIGINATOR'S REPORT NUMBER(S): Enter the official report number by which the document will be identified and controlled by the originating activity. This number must be unique to this report.

9b. OTHER REPORT NUMBER(S): If the report has been assigned any other report numbers *(either by the originator or by the sponsor)*, also enter this number(s).

10. AVAILABILITY/LIMITATION NOTICES: Enter any limitations on further dissemination of the report, other than those imposed by security classification, using standard statements such as:

(1) "Qualified requesters may obtain copies of this report from DDC."

(2) "Foreign announcement and dissemination of this report by DDC is not authorized."

(3) "U. S. Government agencies may obtain copies of this report directly from DDC. Other qualified DDC users shall request through

_____."

(4) "U. S. military agencies may obtain copies of this report directly from DDC. Other qualified users shall request through

_____."

(5) "All distribution of this report is controlled. Qualified DDC users shall request through

_____."

If the report has been furnished to the Office of Technical Services, Department of Commerce, for sale to the public, indicate this fact and enter the price, if known.

11. SUPPLEMENTARY NOTES: Use for additional explanatory notes.

12. SPONSORING MILITARY ACTIVITY: Enter the name of the departmental project office or laboratory sponsoring *(paying for)* the research and development. Include address.

13. ABSTRACT: Enter an abstract giving a brief and factual summary of the document indicative of the report, even though it may also appear elsewhere in the body of the technical report. If additional space is required, a continuation sheet shall be attached.

It is highly desirable that the abstract of classified reports be unclassified. Each paragraph of the abstract shall end with an indication of the military security classification of the information in the paragraph, represented as *(TS), (S), (C), or (U)*.

There is no limitation on the length of the abstract. However, the suggested length is from 150 to 225 words.

14. KEY WORDS: Key words are technically meaningful terms or short phrases that characterize a report and may be used as index entries for cataloging the report. Key words must be selected so that no security classification is required. Identifiers, such as equipment model designation, trade name, military project code name, geographic location, may be used as key words but will be followed by an indication of technical context. The assignment of links, rules, and weights is optional.